

Number: 28

Redalyc 3.0

ESCI Web of science

UNIVERSIDAD POLITÉCNICA SALESIANA ECUADOR

pISSN: 1390-650X

eISSN: 1390-860X

July / december 2020

INGENIUS

Revista de Ciencia y Tecnología



🇬🇧 Considerations in the design of electrical substations, including the effect of potential gradient on surrounding metallic structures
Pag. 9

🇬🇧 Passive Control Tolerant to Sensing Faults in dynamic compensation devices SVC through a hybrid strategy
Pag. 34

🇬🇧 Voltage stability and electronic compensation in electrical power systems using simulation models
Pag. 71

🇬🇧 Comparative analysis of thermal comfort of a single-family house in LSF and brick masonry
Pag. 100

INGENIUS

INGENIUS • Special Issue 28 • july/december 2022. Journal of Science and Tecnology of the Universidad Politécnica Salesiana of Ecuador. Publication dedicated to studies related to the Sciences of Mechanical Engineering, Electrical Engineering, Electronic Engineering, Mechatronic Engineering, Systems Engineering and Industrial Engineering.

Editors Board

RAFAEL ANTONIO BALART GIMENO, PHD, Universidad Politécnica de Valencia, España – Editor-in-chief.

JOHN IGNACIO CALLE SIGÜENCIA, PHD, Universidad Politécnica Salesiana, Ecuador – Editor-in-chief.

ESTEBAN MAURICIO INGA ORTEGA, PHD, Universidad Politécnica Salesiana, Ecuador – Associate Editor.

MARLON XAVIER QUINDE ABRIL, MSC, Universidad Politécnica Salesiana, Ecuador – Associate Editor.

TEODIANO FREIRE BASTOS FILHO, PHD, (Universidade Federal do Espírito Santo, Brasil – Associate Editor.

Scientific board

JUAN LÓPEZ MARTÍNEZ, PHD, Universidad Politécnica de Valencia, España.

ELENA FORTUNATI, PHD, Universidad de Perugia, Italia.

GUSTAVO ROVELO RUIZ, PHD, Hasselt University, Diepenbeek, Bélgica.

FRANKLIN GAVILANEZ ALVAREZ, PHD, American University, Estados Unidos.

PIEDAD GAÑAN ROJO, PHD, Universidad Pontificia Bolivariana, Colombia.

JOSÉ ALEX RESTREPO, PHD, Universidad Simón Bolívar, Venezuela.

SERGIO LUJAN MORA, PHD, Universidad de Alicante, España.

MARTHA ZEQUERA DÍAZ, PHD, Pontificia Universidad Javeriana, Colombia.

GROVER ZURITA, PHD, Universidad Privada Boliviana, Bolivia.

VLADIMIR ROBLES, PHD, Universidad Politécnica Salesiana, Ecuador.

GERMÁN ARÉVALO, PHD, Universidad Politécnica Salesiana, Ecuador.

WILBERT AGUILAR, PHD, Universidad de las Fuerzas Armadas, ESPE, Ecuador.

JACK BRAVO TORRES, PHD, Universidad Politécnica Salesiana, Ecuador.

WALTER OROZCO, PHD, Universidad Politécnica Salesiana, Ecuador.

MARIELA CERRADA, PHD, Universidad Politécnica Salesiana, Ecuador.

JULIO CÉSAR VIOLA, PHD, Universidad Politécnica Salesiana, Ecuador.

SERGIO GAMBOA SÁNCHEZ, PHD, Universidad Nacional Autónoma de México, México.

ROGER ABDÓN BUSTAMANTE PLAZA, PHD, Universidad de Chile, Chile.

CHRISTIAN BLUM, PHD, Consejo Superior de Investigaciones Científicas, España.

SILVIA NOEMI SCHIAFFINO, PHD, Universidad Nacional del Centro de la Provincia de Buenos Aires, Argentina.

ANALÍA ADRIANA AMANDI, PHD, Universidad Nacional del Centro de la Provincia de Buenos Aires, Argentina.

RUBÉN DE JESÚS MEDINA MOLINA, PHD,

Universidad de Los Andes, Venezuela.

JOHNNY JOSUÉ BULLÓN TORREALBA, PHD, Universidad de Los Andes, Venezuela.

RODRIGO PALMA HILLERNS, PHD, Universidad de Chile, Chile.

GERARDO ESPINOZA PÉREZ, PHD, Universidad Nacional Autónoma de México, México.

ALEXANDRE MENDES ABRÃO, PHD, Universidad Federal de Minas Gerais, Brasil.

KAMLA ABDEL RADI ISMAIL, PHD, Universidad Estatal de Campinas Unicamp, Brasil.

ARNALDO DA SILVA, PHD, Universidad Estatal de Campinas Unicamp, Brasil.

ÁLVARO ROCHA, PHD, Universidad de Coimbra, Portugal.

JOSÉ ANTENOR POMILIO, PHD, Universidad Estatal de Campinas Unicamp, Brasil.

LUIS PAULO REIS, PHD, Universidad de Minho, Portugal.

LUÍS FERNANDES, PHD, Escuela Superior Náutica Infante d. Henrique, Portugal.

ANÍBAL TRAÇA DE ALMEIDA, PHD, Universidad de Coimbra, Portugal.

JORGE SÁ SILVA, PHD, Universidad de Coimbra, Portugal.

PEDRO MANUEL SOARES MOURA, PHD, Universidad de Coimbra, Portugal.

SÉRGIO MANUEL RODRIGUES LOPES, PHD, Universidad de Coimbra, Portugal.

RICARDO MADEIRA SOARES BRANCO, PHD, Universidad de Coimbra, Portugal.

CARLOS ALEXANDRE BENTO CAPELA, PHD, Universidad de Coimbra, Portugal.

FILIFE ARAUJO, PHD, Universidad de Coimbra, Portugal.

LUIS MANUEL GUERRA SILVA ROSA, PHD, Universidad de Lisboa, Portugal.

HÉLDER DE JESUS FERNANDES, PUGA, PHD, Universidad de Minho, Portugal.

FILIFE SAMUEL, PEREIRA DA SILVA, PHD, Universidad de Minho, Portugal.

CÉSAR SEQUEIRA, PHD, Universidad de Lisboa, Portugal.

JOSÉ TEIXEIRA ESTÊVÃO FERREIRA, PHD,

Universidad de Coimbra, Portugal.

NUNO LARANJEIRO, PHD, Universidad de Coimbra, Portugal.

LUÍS AMARAL, PHD, Universidad de Lisboa, Portugal.

JORGE HENRIQUES, PHD, Universidad de Coimbra, Portugal.

WILLIAM IPANAQUE, PHD, Universidad de Piura, Perú.

LORENZO LEIJA SALAS, PHD, Centro de Investigación y Estudios Avanzados del Instituto Politécnico Nacional, México.

VALERI KONTOROVICH MAZOVER, PHD, Centro de Investigación y de Estudios Avanzados del Instituto Politécnico Nacional, México.

ALEJANDRO ÁVILA GARCÍA, PHD, Centro de Investigación y de Estudios Avanzados del Instituto Politécnico Nacional, México.

PAOLO BELLAVISTA, PHD, Universidad de Bologna, Italia.

CARLOS RUBIO, PhD, Centro de Ingeniería y Desarrollo Industrial, México.

FERNANDO HERNÁNDEZ SÁNCHEZ, PhD, Centro de Investigación Científica de Yucatán, México.

EMILIO MUÑOZ SANDOVAL, PhD, Instituto Potosino de Investigación Científica y Tecnológica, México.

YASUHIRO MATSUMOTO KUWABARA, PhD, Centro de Investigación y de Estudios Avanzados del Instituto Politécnico Nacional, México.

DAVID ZUMOFFEN, PhD, Centro Internacional Franco Argentino de Ciencias de la Información y de Sistemas, Argentina.

VICENTE RODRÍGUEZ GONZÁLEZ, PhD, Instituto Potosino de Investigación Científica y Tecnológica, México.

ALEJANDRO RODRÍGUEZ ÁNGELES, PhD, Centro de Investigación y de Estudios Avanzados del Instituto Politécnico Nacional, México.

ALISTAIR BORTHWICK, PhD, Universidad de Edimburgo, Reino Unido.

Reviewers board

FEDERICO DOMINGUEZ, PHD, Escuela Superior Politécnica del Litoral, Ecuador.

ENRIQUE CARRERA, PHD, Universidad de las Fuerzas Armadas, ESPE, Ecuador.

ANDRÉS TELLO, MSc, Universidad de Cuenca, Ecuador.

CRISTIAN GARCÍA BAUZA, PHD, Universidad Nacional del Centro de la Provincia de Buenos Aires, Argentina.

OSVALDO AÑÓ, PHD, Universidad Nacional de San Juan, Argentina.

THALÍA SAN ANTONIO, PHD, Universidad Técnica de Ambato, Ecuador.

VICTOR SAQUICELA, PHD, Universidad de Cuenca, Ecuador.

GONZALO OLMEDO, PHD, Universidad de las Fuerzas Armadas, ESPE, Ecuador.

ROMÁN LARA, PHD, Universidad de las Fuerzas Armadas, ESPE, Ecuador.

GUILLERMO SORIANO, PHD, Escuela Superior Politécnica del Litoral, Ecuador.

MARÍA FERNANDA GRANDA, PHD, Universidad de Cuenca, Ecuador.

RICARDO CAYSSIALS, PHD, Universidad Tecnológica Nacional, Argentina.

LEONARDO SOLAQUE GUZMAN, PHD, Universidad Militar Nueva Granada, Colombia.

JOSÉ DI PAOLO, PHD, Universidad Nacional de Entre Ríos, Argentina.

ASTRID RUBIANO FONSECA, PHD, Universidad Militar Nueva Granada, Colombia.

ROBINSON JIMÉNEZ, PHD, Universidad Militar Nueva Granada, Colombia.

ALFONSO ZOZAYA, PHD, Universidad de Carabobo, Venezuela.

MAURICIO MAULEDOUX, PHD, Universidad Militar Nueva Granada, Colombia.

LUIS MEDINA, PHD, Universidad Simón Bolívar, Venezuela.

ERNESTO CUADROS-VARGAS, PHD, Universidad Católica San Pablo, Perú.

SAMUEL SEPÚLVEDA CUEVAS, PHD, Universidad de la Frontera, Chile.

CARLOS CARES, PHD, Universidad de la Frontera, Chile.

RAFAEL SOTELO, PHD, Universidad de Montevideo, Uruguay.

OMAR LOPEZ, PHD, Universidad de Los Andes, Colombia.

JOB FLORES-GODOY, PHD, Universidad Católica del Uruguay, Uruguay.

LUIS MARIO MATEUS, PHD, Universidad de los Andes, Colombia.

AMADEO ARGÜELLES CRUZ, PHD, Instituto Politécnico Nacional, México.

SANTIAGO BENTANCOURT PARRA, PHD, Universidad Pontificia Bolivariana, Colombia.

GERMÁN ZAPATA, PHD, Universidad Nacio-

nal de Colombia, Colombia.

PEDRO GARCÍA, PHD, Universidad Autónoma de Barcelona, España.

ARTURO CONDE ENRÍQUEZ, PHD, Universidad Autónoma de Nuevo León, México.

ALBERTO CAVAZOS GONZÁLEZ, PHD, Universidad Autónoma de Nuevo León, México.

ERNESTO VÁZQUEZ MARTÍNEZ, PHD, Universidad Autónoma de Nuevo León, México.

MIGUEL DÍAZ RODRIGUEZ, PHD, Universidad de Los Andes, Venezuela.

EFRAÍN ALCORTA GARCÍA, PHD, Universidad Autónoma de Nuevo León, México.

LUIS CHIRINOS GARCIA, PHD, Pontificia Universidad Católica de Perú, Perú.

OSCAR AVILÉS, PHD, Universidad Militar Nueva Granada, Colombia.

DORA MARTÍNEZ DELGADO, PHD, Universidad Autónoma de Nuevo León, México.

DAVID OJEDA, PHD, Universidad Técnica del Norte, Ecuador.

IRENE BEATRÍZ STEINMANN, PHD, Universidad Tecnológica Nacional, Argentina.

MARIO SERRANO, Universidad Nacional de San Juan, Argentina.

CORNELIO POSADAS CASTILLO, PHD, Universidad Autónoma Nuevo León, México.

MARIO ALBERTO RIOS MESIAS, PHD, Universidad de Los Andes, Colombia.

YUDITH CARDINALE VILLARREAL, PHD, Universidad Simón Bolívar, Venezuela.

EDUARDO MATALANAS, PHD, Universidad Politécnica de Madrid, España.

JOSE EDUARDO OCHOA LUNA, PHD, Universidad Católica San Pablo, Perú.

DANTE ANGEL ELIAS GIORDANO, PHD, Pontificia Universidad Católica de Perú, Perú.

MANUEL PELAEZ SAMANIEGO, PHD, Universidad de Cuenca, Ecuador.

JUAN ESPINOZA ABAD, PHD, Universidad de Cuenca, Ecuador.

PIETRO CODARA, PHD, Universidad de Milan, Italia.

ALBERTO SORIA, PHD, Centro de Investigación y de Estudios Avanzados del Instituto Politécnico Nacional, México.

JOSÉ M. ALLER, PHD, Universidad Politécnica Salesiana, Ecuador.

FERNEY AMAYA F., PHD, Universidad Pontificia Bolivariana, Medellín, Colombia.

SANTIAGO ARANGO ARAMBURO, PHD, Universidad Nacional de Colombia, Colombia.

DIEGO ARCOS-AVILÉS, PHD, Universidad de las Fuerzas Armadas, ESPE, Ecuador.

PABLO AREVALO, PHD, Universidad Politécnica Salesiana, Ecuador.

ROBERTO BELTRAN, MSc, Universidad de las Fuerzas Armadas, ESPE, Ecuador.

LEONARDO BETANCUR, PHD, Universidad Pontificia Bolivariana, Medellín, Colombia.

ROBERTO GAMBOA, PHD, Universidad de Lisboa, Portugal.

PAULO LOPES DOS SANTOS, PHD, Universidad do Porto, Portugal.

PEDRO ANDRÉ DIAS PRATES, PHD, Universidad de Coimbra, Portugal.

JOSÉ MANUEL TORRES FARINHA, PHD, Universidad de Coimbra, Portugal.

CELSO DE ALMEIDA, PHD, Universidad Estatal de Campinas Unicamp, Brasil.

RAMON MOLINA VALLE, PHD, Universidad Federal de Minas Gerais, Brasil.

CRISTINA NADER VASCONCELOS, PHD, Universidad Federal Fluminense, Brasil.

JOÃO M. FERREIRA CALADO, PHD, Universidad de Lisboa, Portugal.

GUILHERME LUZ TORTORELLA, PHD, Universidad Federal de Santa Catarina, Brasil.

MAURO E. BENEDET, PHD, Universidad Federal de Santa Catarina, Brasil.

ARTEMIS MARTI CESCHIN, PHD, Universidade de Brasilia, Brasil.

GILMAR BARRETO, PHD, Universidad Estatal de Campinas Unicamp, Brasil.

RICARDO EMILIO F. QUEVEDO NOGUEIRA, PHD, Universidad Federal de Ceará, Brasil.

WESLEY LUIZ DA SILVA ASSIS, PHD, Universidad Federal Fluminense, Brasil.

ANA P. MARTINAZZO, PHD, Universidad Federal Fluminense, Brasil.

JORGE BERNARDINO, PHD, Universidad de Coimbra, Portugal.

LUIS GERALDO PEDROSO MELONI, PHD, Universidad Estatal de Campinas Unicamp, Brasil.

FACUNDO ALMERAYA CALDERÓN, PHD, Universidad Autónoma de Nuevo León, México.

FREDDY VILLAO QUEZADA, PHD, Escuela Superior Politécnica del Litoral, Ecuador.

JOSE MANRIQUE SILUPU, MSc, Universidad de Piura, Perú.

GERMÁN ARIEL SALAZAR, PHD, Instituto de Investigaciones en Energía no Convencional, Argentina.

JOSÉ MAHOMAR JANANIÁS, PHD, Universidad del BIOBIO, Chile.

ARNALDO JÉLVEZ CAAMAÑO, PHD, Universidad del BIOBIO, Chile.

JORGE ANDRÉS URIBE, MSc, Centro de Ingeniería y Desarrollo Industrial, México.

RICARDO BELTRAN, PHD, Centro de Investigación en Materiales Avanzados, México.

ADI CORRALES, MSc, Centro de Ingeniería y Desarrollo Industrial, México.

JORGE URIBE CALDERÓN, PHD, Centro de Investigación Científica de Yucatán, México

JOSÉ TRINIDAD HOLGUÍN MOMACA, MSc, Centro de Investigación en Materiales Avanzados, México.

JUAN MANUEL ALVARADO OROZCO, PhD, Centro de Ingeniería y Desarrollo Industrial, México.

ARNALDO JÉLVEZ CAAMAÑO, PhD, Universidad del BIOBIO, Chile.

JAVIER MURILLO, PhD, Centro Internacional Franco Argentino de Ciencias de la Información y de Sistemas, Argentina.

LUCAS DANIEL TERISSI, PhD, Universidad Nacional de Rosario, Argentina.

RENE VINICIO SANCHEZ LOJA, MSc, Universidad Politécnica Salesiana, Ecuador.

FREDDY LEONARDO BUENO PALOMEQUE, MSc, Universidad Politécnica Salesiana, Ecuador.

DIEGO CABRERA MENDIETA, MSc, Universidad Politécnica Salesiana, Ecuador.

EDWUIN JESUS CARRASQUERO, PhD, Universidad Técnica de Machala, Ecuador.

CARLOS MAURICIO CARRILLO ROSERO, MSc, Universidad Técnica de Ambato, Ecuador.

DIEGO CARRION GALARZA, MSc, Universidad Politécnica Salesiana, Ecuador.

CARMEN CELI SANCHEZ, MSc, Universidad Politécnica Salesiana, Ecuador.

DIEGO CHACON TROYA, MSc, Universidad Politécnica Salesiana, Ecuador.

PAUL CHASI, MSc, Universidad Politécnica Salesiana, Ecuador.

JUAN CHICA, MSc, Universidad Politécnica Salesiana, Ecuador.

DIEGO MARCELO CORDERO GUZMÁN, MSc, Universidad Católica de Cuenca, Ecuador.

LUIS JAVIER CRUZ, PhD, Universidad Pontificia Bolivariana, Medellín, Colombia.

FABRICIO ESTEBAN ESPINOZA MOLINA, MSc, Universidad Politécnica Salesiana, Ecuador.

JORGE FAJARDO SEMINARIO, MSc, Universidad Politécnica Salesiana, Ecuador.

PATRICIA FERNANDEZ MORALES, PhD, Universidad Pontificia Bolivariana, Medellín, Colombia.

MARCELO FLORES VAZQUEZ, MSc, Universidad Politécnica Salesiana, Ecuador.

CARLOS FLORES VÁZQUEZ, MSc, Universidad Católica de Cuenca, Ecuador.

CARLOS FRANCO CARDONA, PhD, Universidad Nacional de Colombia, Colombia.

CRISTIAN GARCÍA GARCÍA, MSc, Universidad Politécnica Salesiana, Ecuador.

TEONILA GARCÍA ZAPATA, PhD, Universidad Nacional Mayor de San Marcos, Perú.

LUIS GARZÓN MÑOZ, PhD, Universidad Politécnica Salesiana, Ecuador.

NATALIA GONZALEZ ALVAREZ, MSc, Universidad Politécnica Salesiana, Ecuador.

ERNESTO GRANADO, PhD, Universidad Simón Bolívar, Venezuela.

ADRIANA DEL PILAR GUAMAN, MSc, Universidad Politécnica Salesiana, Ecuador.

JUAN INGA ORTEGA, MSc, Universidad Politécnica Salesiana, Ecuador.

ESTEBAN INGA ORTEGA, PhD, Universidad Politécnica Salesiana, Ecuador.

PAOLA INGAVÉLEZ, MSc, Universidad Politécnica Salesiana, Ecuador.

CESAR ISAZA ROLDAN, PhD, Universidad Pontificia Bolivariana.

NELSON JARA COBOS, MSc, Universidad Politécnica Salesiana, Ecuador.

RUBEN JERVES, MSc, Universidad Politécnica Salesiana, Ecuador.

VICTOR RAMON LEAL, PhD, Investigador de PDVSA, Venezuela

GABRIEL LEON, MSc, Universidad Politécnica Salesiana, Ecuador.

EDILBERTO LLANES, PhD, Universidad Internacional SEK, Ecuador.

LUIS LÓPEZ, MSc, Universidad Politécnica Salesiana, Ecuador.

CARLOS MAFLA YÉPEZ, MSc, Universidad Técnica del Norte, Ecuador.

HADER MARTÍNEZ, PhD, Universidad Pontificia Bolivariana, Medellín, Colombia

JAVIER MARTÍNEZ, PhD, Instituto Nacional de Eficiencia Energética y Energías Renovables, Ecuador.

ALEX MAYORGA, MSc, Universidad Técnica de Ambato, Ecuador.

JIMMY MOLINA, MSc, Universidad Técnica de Machala, Ecuador.

ANDRES MONTERO, PhD, Universidad de Cuenca, Ecuador.

VICENTE MORALES, MSc, Universidad Técnica de Ambato, Ecuador.

FABIÁN MORALES, MSc, Universidad Técnica de Ambato, Ecuador.

DIEGO MORALES, MSc, Ministerio de Electricidad y Energías Renovables del Ecuador.

YOANDRYS MORALES TAMAYO, PhD, Universidad Técnica de Cotopaxi, Cotopaxi

OLENA LEONIDIVNA NAIDIUK, MSc, Universidad Politécnica Salesiana, Ecuador.

OSCAR NARANJO, MSc, Universidad del Azuay, Ecuador.

PAUL NARVAEZ, MSc, Universidad Politécnica Salesiana, Ecuador.

HERNÁN NAVAS OLMEDO, MSc, Universidad Técnica de Cotopaxi, Ecuador.

CESAR NIETO, PhD, Universidad Pontificia Bolivariana, Medellín, Colombia

FABIO OBANDO, MSc, Universidad Politécnica Salesiana, Ecuador.

LUIS ORTIZ FERNANDEZ, MSc, Universidade Federal de Rio Grande del Norte, Brasil

PABLO PARRA, MSc, Universidad Politécnica Salesiana, Ecuador.

PAULO PEÑA TORO, PhD, Ministerio de Productividad, Ecuador.

PATSY PRIETO VELEZ, MSc, Universidad Politécnica Salesiana, Ecuador.

DIEGO QUINDE FALCONI, MSc, Universidad Politécnica Salesiana, Ecuador.

DIANA QUINTANA ESPINOZA, MSc, Universidad Politécnica Salesiana, Ecuador.

WILLIAM QUITIAQUEZ SARZOSA, MSc, Universidad Politécnica Salesiana, Ecuador.

FLAVIO QUIZHPI PALOMEQUE, MSc, Universidad Politécnica Salesiana, Ecuador.

WASHINGTON RAMIREZ MONTALVAN, MSc, Universidad Politécnica Salesiana, Ecuador.

FRAN REINOSO AVECILLAS, MSc, Universidad Politécnica Salesiana, Ecuador.

NÉSTOR RIVERA CAMPOVERDE, MSc, Universidad Politécnica Salesiana, Ecuador.

JORGE ROMERO CONTRERAS, MSc, Universidad de Carabobo, Venezuela

FABIAN SAENZ ENDERICA, MSc, Universidad de las Fuerzas Armadas, ESPE, Ecuador.

LUISA SALAZAR GIL, PhD, Universidad Simón Bolívar, Venezuela

GUSTAVO SALGADO ENRÍQUEZ, MSc, Universidad Central del Ecuador., Ecuador.

JUAN CARLOS SANTILLÁN LIMA, MSc, Universidad Nacional de Chimborazo

JONNATHAN SANTOS BENÍTEZ, MSc, Universidad Politécnica Salesiana, Ecuador.

ANDRÉS SARMIENTO CAJAMARCA, MSc, Universidad Federal de Santa Catarina, Brasil

LUIS SERPA ANDRADE, MSc, Universidad Politécnica Salesiana, Ecuador.

CRISTIAN TIMBI SISALIMA, MSc, Universidad Politécnica Salesiana, Ecuador.

MILTON TIPAN SIMBAÑA, MSc, Universidad Politécnica Salesiana, Ecuador.

PAUL TORRES JARA, MSc, Universidad Politécnica Salesiana, Ecuador.

RODRIGO TUFÍÑO CÁRDENAS, MSc, Universidad Politécnica Salesiana, Ecuador.

FERNANDO URGILES ORTÍZ, MSc, Universidad Politécnica Salesiana, Ecuador.

JUAN VALLADOLID QUITOISACA, MSc, Universidad Politécnica Salesiana, Ecuador.

EFRÉN VÁZQUEZ SILVA, PhD, Universidad Politécnica Salesiana, Ecuador.

JULIO VERDUGO, MSc, Universidad Politécnica Salesiana, Ecuador.

MARY VERGARA PAREDES, PhD, Universidad de los Andes, Merida, Venezuela

JENNIFER YEPEZ ALULEMA, MSc, Universidad Politécnica Salesiana, Ecuador.

JULIO ZAMBRANO ABAD, MSc, Universidad Politécnica Salesiana, Ecuador.

PATRICIA ZAPATA MOLINA, MSc, Universidad Politécnica Salesiana, Ecuador.

Publications board

JUAN CÁRDENAS TAPIA, SDB, PHD
JAVIER HERRÁN GÓMEZ, SDB, PHD
JOSÉ JUNCOSA BLASCO, PHD
JUAN PABLO SALGADO GUERRERO, PHD
ANGLE TORRES TOUKOUMIDIS, PHD
JAIME PADILLA VERDUGO, PHD
SHEILA SERRANO VINCENTI, MSC
JORGE CUEVA ESTRADA, MSC
JOHN CALLE SIGÜENCIA, PHD
FLORALBA AGUILAR GORDÓN, PHD
BETTY RODAS SOTO, MSC
MÓNICA RUIZ VÁSQUEZ, MSC
JORGE ALTAMIRANO SÁNCHEZ, MSC
DAVID ARMENDÁRIZ GONZÁLEZ, MSC
LUIS ÁLVAREZ RODAS, PHD

General Editor

LUIS ÁLVAREZ-RODAS, PHD

Technical board

ÁNGEL TORRES-TOUKOUMIDIS, PHD
DRA. MARCIA PEÑA, Style Reviewer,
Centro Gráfico Salesiano - Editorial Don Bosco
MARLON QUINDE ABRIL, MSC, Diagramming and layout
DANIELA TORRES CARRERA

Publications Service

HERNÁN HERMOSA (General Coordination)
MARCO GUTIÉRREZ (OJS Layout)
PAULINA TORRES (Style Editing)
RAYSA ANDRADE (Layout)
MARTHA VINUEZA (Layout)
ADRIANA CURIEL AVILA, (Translation)

Editorial

Editorial Abya Yala (Quito-Ecuador),
Av. 12 de octubre N422 y Wilson,
Bloque A, UPS Quito, Ecuador.
Casilla 17-12-719 Teléfonos: (593-2) 3962800 ext. 2638
email: editorial@abyayala.org

Printing: 800 copies

Typographic system used in the composition of this document L^AT_EX.

INGENIUS

REVISTA DE CIENCIA Y TECNOLOGIA

Special Issue 28: Electric Networks and Smart Cities

july – december 2022

ISSN impreso 1390-650X / ISSN electrónico 1390-860X

The administration of the journal is done through the following parameters:

The journal uses the academic anti-plagiarism system  

The articles have an identification code (Digital Object Identifier) 

The editorial process is managed through the Open Journal System 

It is an open access publication (Open Access) licensed Creative Commons



The politics copyright of use postprint, are published in the Self-Archive Policy Repository

Sherpa/Romeo. 

The articles of the present edition can be consulted in

<http://revistas.ups.edu.ec/index.php/ingenius>



UNIVERSIDAD POLITÉCNICA SALESIANA DEL ECUADOR

INGENIUS Journal, is indexed in the following Databases and scientific information systems:

SELECTIVE DATABASES



REVIEWS EVALUATION PLATFORMS



SELECTIVE DIRECTORIES



SELECTIVE SERIAL LIBRARY



SCIENTIFIC LITERATURE SEARCHERS OPEN ACCESS



OTHER BIBLIOGRAPHICAL DATABASES



CATALOG OF INTERNATIONAL UNIVERSITY LIBRARIES



UNIVERSITÄT BAMBERG



Dear readers:

As a result of the constant growth of cities and the need of users to improve their quality of life, energy consumption has increased due to the electronic devices incorporated in homes (indoor) and in public use applications (outdoor).

Within the stages of a smart grid, stages as a response to demand, the smart metering infrastructure presented in the article "Electricity consumption meter to promote savings in residential consumers"; in addition, the inclusion of renewable energy in photovoltaic systems, wind, and that may be incorporated into the network from micro-generation including distributed generation should be contemplated. The massive deployment of charging centers for electric vehicles and an increase in the use of induction stoves in homes should be considered.

Consequently, the customer demands an electrical grid that supports new services, many of which give birth to a smart city capable of providing services in favor of society. Many contemplate intelligent household waste management and innovative park systems, among others.

Electrical substations must require robust grounding systems to ensure the quality and reliability of the system that is incorporated into an internet of things as it is called to applications that relate to telematics which involves a heterogeneous wireless network that will allow the connection of sensors or smart meters in micro-grids based on clean energy systems. It is essential to demonstrate in the article, "Methodology for design of electrical substations considering the effect of the potential gradient in surrounding metallic structures."

A fault-tolerant control system that evaluates in the article "Fault-Tolerant Passive Control of sensing in dynamic compensation devices - SVC

through a hybrid strategy" will be involved because each intelligent device may present contingencies that should, in most cases, be self-controlled, which involves artificial intelligence techniques and robust control that includes algorithms developed in the web system.

Additionally, the different applications involving sensors require platforms developed and integrated into embedded systems and non-licensed software to achieve a more significant deployment of solutions with reduced costs because the number of devices depending on the outdoor application could reach a hundred of these devices. Such impact is evaluated in the article "Remote learning platform for micro-controllers and internet of things."

Thus, smart grids and smart cities are in continuous change and advancement, which warns new research fields in which georeferencing aspects must be incorporated for the exact location of a sensor. Such a sensor can be the electric energy meter or the device to locate the waste container of a neighborhood or sector, in addition to other implications that are evaluated in the article "Design and validation of IoT measurement system for a photovoltaic generation."

Electrical grids, telecommunication networks, water networks, gas networks, and mass public transport networks may incorporate georeferenced deployments that facilitate and reduce deployment time and subsequent maintenance through graph theory and heuristic techniques.

A city solution incorporates several resources that must be optimized to minimize the impact on the investment. A better lifestyle implies planning and an opportunity for the technological solution to be scalable over time, not just a momentary solution.

Esteban Inga Ortega, PhD

Associate Editor

TABLE OF CONTENTS

Considerations in the design of electrical substations, including the effect of potential gradient on surrounding metallic structures	9
Consideraciones en el diseño de subestaciones eléctricas, incluyendo el efecto del gradiente de potencial en las estructuras metálicas circundantes Wilo Chiliquina, Pablo Robles	
Location of distributed resources in rural-urban marginal power grids considering the voltage collapse prediction index	25
Localización de recursos distribuidos en redes eléctricas rurales-urbanas marginales considerando el índice de predicción de colapso de tensión Anabel Lemus, Diego Carrión, Eduar Aguirre, Jorge W. González	
Passive Control Tolerant to Sensing Faults in dynamic compensation devices SVC through a hybrid strategy	34
Control Pasivo Tolerante a Fallos de sensado en dispositivos de compensación dinámicos - SVC mediante una estrategia híbrida Jessica Ramírez, Leony Ortiz, Alexander Aguila	
Design and validation of IoT measurement system for photovoltaic generation	44
Diseño IoT y validación de sistema de medida para generación fotovoltaica Thiago Angelino dos Santos, Filipe Gomes de Freitas, Diego Lima Carvalho Gonçalves, Luis Miguel Fernández-Ramírez	
Platform for Distance Learning of Microcontrollers and Internet of Things	53
Plataforma de enseñanza a distancia de microcontroladores e internet de las cosas Renata Pereira, Cleonilson de Souza, Darwin Patino, Juan Lata	
Structural Analysis of a Long-distance Double-decker Bus During Crashes	63
Análisis estructural de un bus de dos pisos de larga distancia durante colisiones Jimmy Brito Morocho, Marco Amaya Pinos, Luis López López, Fabricio Espinoza Molina	
Improvement of the lactose grinding process for a company manufacturing dairy products	71
Mejora del proceso de molienda de lactosa para una empresa fabricante de productos lácteos Darío J. Pinguil Loja, Víctor R. Lojano Pillco, Nelson G. Jara Cobos, Fran Z. Reinoso AVECILLAS	
Mathematical model of a resistive oven for thermoforming polypropylene sheets	80
Modelo matemático de un horno resistivo para termoformado de láminas de polipropileno Lidia Castro-Cepeda, José Cortés-Llanganate	
Structural and Modal Analysis Of Adapter Plates For Hydraulic Hammers And Skid Steers Under Real Work Condition	92
Análisis estructural y modal de las placas adaptación para martillos hidráulicos y minicargadores en condiciones reales de operación Yuri Villa, Trevor Vook, Jorge L. Villa, Pablo Carbajal, Leonardo Barrera, Max Florez	
Comparative analysis of thermal comfort of a single-family house in LSF and brick masonry	100
Análisis comparativo de confort térmico de vivienda unifamiliar en LSF frente a mampostería Rodrigo Brito-Peña, Daniel Villa-Enderica, Esteban Zalamea-León	
Guidelines	125
Normas editoriales	



CONSIDERATIONS IN THE DESIGN OF ELECTRICAL SUBSTATIONS, INCLUDING THE EFFECT OF POTENTIAL GRADIENT ON SURROUNDING METALLIC STRUCTURES

CONSIDERACIONES EN EL DISEÑO DE SUBESTACIONES ELÉCTRICAS, INCLUYENDO EL EFECTO DEL GRADIENTE DE POTENCIAL EN LAS ESTRUCTURAS METÁLICAS CIRCUNDANTES

Wilo Chilingua¹ , Pablo Robles^{2,*} 

Received: 23-05-2022, Received after review: 13-06-2022, Accepted: 22-06-2022, Published: 01-07-2022

Abstract

For designing and studying an electrical substation grounding system (GS), a simple remote substation is considered according to the safety procedures indicated in the IEEE 80 Standard. Buried metallic materials or nearby metallic structures permanently endanger human life when electrical faults occur. Scenarios related to the design of electrical substations that consider the transfer of electrical potentials that can occur between the GS and buried metallic materials in their vicinity are presented, the behavior of potential transfer is evaluated, values of transferred voltages are calculated, and the main variables that influence the transferred voltage levels are identified. The simulations are performed with the CYMGRD software specific for GS calculations. Its analysis generates real results in the potential transfer that must be considered by the GS design engineer, which enables to avoid designing isolated substations without taking into account existing elements that may affect the substation surroundings.

Keywords: Electrical substation, grounding systems, ground grid, potential transfer, step and touch voltage, buried metal structures

Resumen

Para el diseño y el estudio de un sistema de puesta a tierra de una subestación eléctrica (*Grounding Systems, GS*, en inglés), se considera una subestación remota simple según los procedimientos de seguridad indicados en la norma IEEE 80. Los materiales metálicos enterrados o las estructuras metálicas cercanas ponen en peligro permanente la vida humana cuando se producen fallas eléctricas. Se presentan escenarios relacionados con el diseño de subestaciones eléctricas que consideran la transferencia de potenciales eléctricos que pueden producirse entre la GS y los materiales metálicos enterrados en sus proximidades. Se evalúa el comportamiento de la transferencia de potencial, se calculan los valores de las tensiones transferidas y se identifican las principales variables que influyen en los niveles de tensión transferidos. Las simulaciones se realizan con el programa CYMGRD específico para el cálculo de GS. Su análisis genera resultados reales en la transferencia de potencial que deben ser considerados por el ingeniero de diseño de GS, lo que permite evitar el diseño de subestaciones aisladas sin tener en cuenta los elementos existentes que pueden afectar al entorno de la subestación.

Palabras clave: subestación eléctrica, sistemas de puesta a tierra, red de tierra, transferencia de potencial, tensión de paso y de contacto, estructuras metálicas enterradas

¹Master of Electricity Program, Universidad Politécnica Salesiana, Quito, Ecuador.

^{2,*}Research Group on Smart Grids GIREI, IUS-RECI Electricity Grids and Smart Cities, Universidad Politécnica Salesiana, Cuenca, Ecuador. Corresponding author ✉: pablo121075@icloud.com

Suggested citation: Chilingua, W. and Robles, P. "Considerations in the design of electrical substations, including the effect of potential gradient on surrounding metallic structures". *Ingenius, Revista de Ciencia y Tecnología*. N.º 28, (july-december). pp. 9-24. 2022. DOI: <https://doi.org/10.17163/ings.n28.2022.01>.

1. Introduction

The GS is an essential factor in human safety and maintenance of electrical inputs that make up a substation, considering its cost and durability [1]. In GS, ground fault currents must safely dissipate to return the ground to their sources; so that the protection devices can quickly disconnect the supply and eliminate the fault. However, fault currents flowing through the ground grid also flow through other buried metallic objects, including grounding systems connected to other facilities not affected by the faults [2], [3], [4], [5].

Although the GS may be physically isolated from each other, they are electrically linked through unwanted coupling, transferring dangerous electrical potentials from the meshes with fault currents to the non-energized passive meshes of other GS with a risk of electrocution for the personnel present. In those areas [6], [7], [8], [9]. Poor grounding in the oil and gas industry contributes to unnecessary downtime, but lack of good grounding is also dangerous and increases the risk of equipment failure leading to instrumentation errors, problems harmonic distortion, and power factor problems [10], [11,12].

Oil and gas pipelines are large and sophisticated structures protecting against electrical discharge, especially corrosion. For the design of the GS, cathodic protection [CP] must be included, in addition to the electrical effects that can occur when these two systems are together GS, and CP [13], [14], [15], [16], [17].

This article aims to present case studies on the problems introduced by the presence of metallic structures and adjoining protection systems, among others, in the transfer of potential gradients [GPG] in passive GS.

The design procedures described in the standards related to GS of electrical substations in urban areas and oil stations allow the calculation of safe levels of step and touch voltages within the substation area, but adjacent GPG is not taken into account [18], [19], [20], [21], [22], [23], [24].

The type of material used can be a decisive factor in human electrocution. Inside the substations, the touch voltage [MTV] and step voltage [MSV] are less dangerous due to the high resistivity surface layer [25]. However, this layer does not extend outside the substations, where the transferred touch and step voltages can be harmful and much more if there are adjoining buried metallic structures not connected to the GS [26], [27], [28]; [29].

1.1. Related Works

The potential gradient generated [30], [31] in oil refining complexes in the event of a failure in an electrical substation causes its transfer to the process areas, causing damage to the instrumentation system, [32,33].

Metallic parts such as water and gas pipes, rails, and building foundations can modify the distribution of electrical potential in the area, depending on the structural topology, which triggers the effect of the GPG, [8].

The GS must consider the conductors directly involved in the protected installation, and any other, connected or not, can interact with the whole GS (Figure 1).

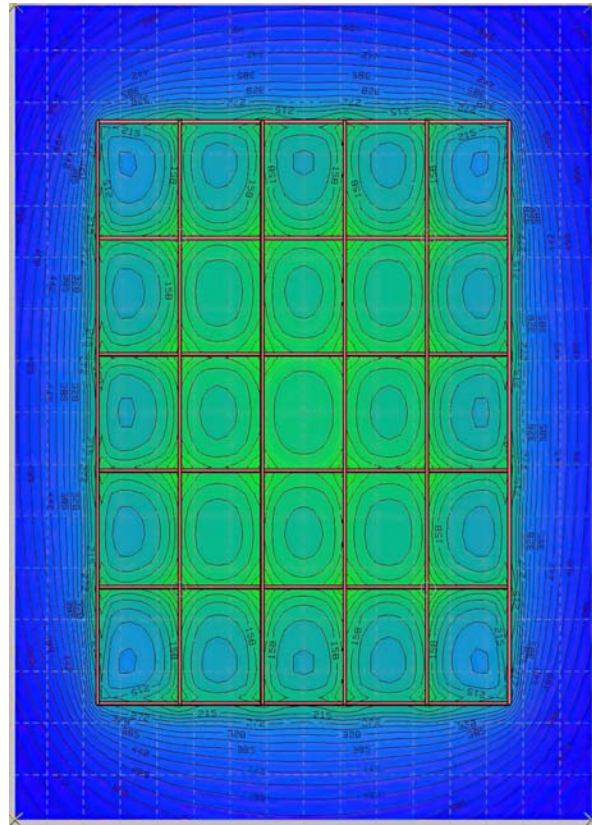


Figure 1. Equipotential contour of a mesh of one GS

The pipelines carrying harmful products are protected against corrosion, usually by layers of coating materials integrated with active cathodic protection systems [34,35]. The current flow, typically adopted for large or long structures, force the pipe to behave as a cathode, thus providing corrosion protection of its exposed parts when the coating fails. However, buried lines with cathodic protection, close to the grounding networks of electrical substations, allow the possibility of bonding and reduce the risk of metal-to-metal contact voltages. This bonding connection, necessary for the safety of operating personnel, can compromise the CP's effectiveness. To avoid corrosion of the CP and bonding with the mesh, mineral salts, which ionize, forming a solid electrolyte with a pH varying from 8 to 10, must be considered.

In electrical substations in urban areas, metal parts that can modify potential electrical distribution are

2. Materials and methods

2.1. Problem Formulation

Figure 2 presents a flow chart of the electrical substation design methodology, including the effect of the potential gradient on the surrounding metallic structures, where the designer's expertise allows obtaining results according to the threshold contact voltages and the threshold step voltage.

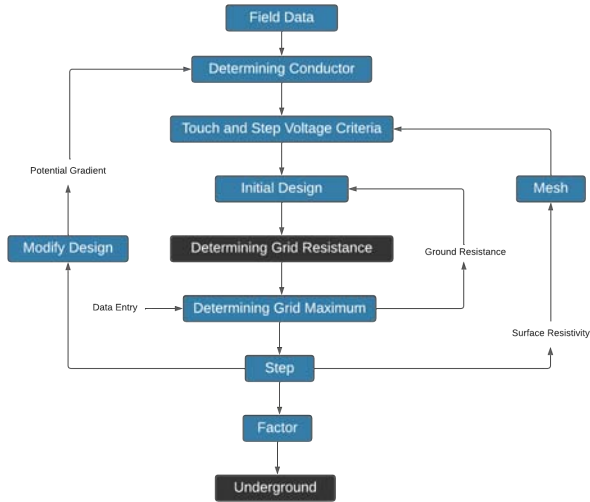


Figure 2. Methodology used for the design

Case studies are presented, which will allow analyzing the transfer of potential. The simulation of the scenarios is carried out with specialized CYMGRD software using the finite element method (FEM) developed by EATON; it allows the interpretation of soil resistivity measurements, elevation of earth potential, and evaluation of dangerous points in any area of additional interest, generates a visual representation of the results of the analysis on the potential of the mesh. The proposed scenarios are according to the type of surface layer used and the potential transfer analysis; the input data presented correspond to the following:

Table 3. General Notation & Descriptions

Nomenclature	Description
<i>Uniform</i>	Terran Model
ρ 50 Ω - m	Upper layer resistivity
40°C	Ambient temperature
0.15 μ m	Surface layer thickness
ρ_s -200 Ω -m - concrete	Surface layer resistivity
ρ_s - 5000 Ω -m - gravel	Surface layer resistivity
ρ_s -10000 Ω -m - asphalt	Surface layer resistivity
0.1sec	Fault duration time
10kA	Fault current
50kg	Human body mass
Sf100V	Current division factor
Cp100V	Growth factor
1m	Mesh depth
Cu4 - 0AWG	Conductor Cu

The present study focuses on the variation of the surface layer, the physical location of the mesh, and the different locations of the surrounding metallic structures.

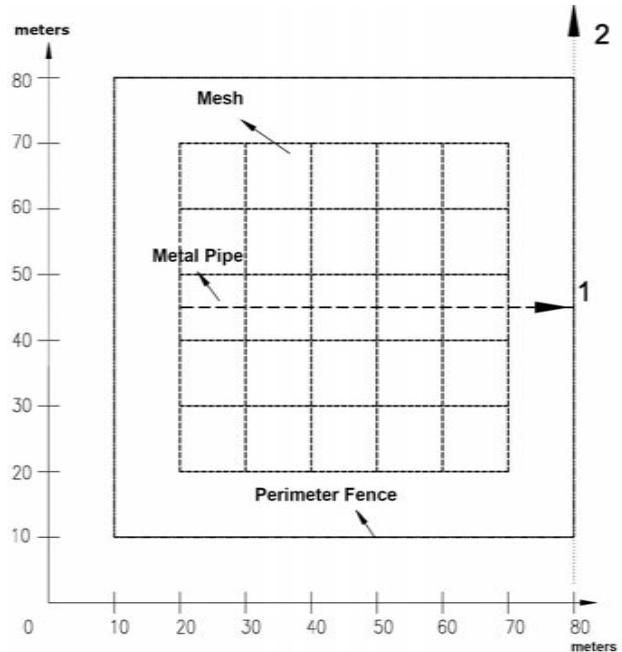


Figure 3. Top view of GS case study 1

In the case of asymmetric grids, the analysis study is similar; taking the stratigraphy of the terrain, the exposed potential gradients transfer study metric is applied for any grid configuration.

Parameter values of the GS are taken based on the mesh indicated in figure 3 so that the importance of step and touch voltage does not exceed the maximum allowed values; the use of copper rods or electrodes is not considered for these simulations.

For the design and simulation of the scenarios, the bodyweight of a 50kg person is taken.

Assuming the most sensitive case that can occur, the optimal mesh conductor for this configuration is a copper conductor of 20.3776 mm², equivalent to 2/0 AWG for the simulations of the scenarios, a 4/0 AWG copper conductor is taken up, where the IEEE 80 standard suggests considering the effects of corrosion present by the PH of the soil stratigraphy, [22].

2.1.1. Case Study 1

Figure 3 shows a substation grounding mesh; its dimensions correspond to 50×50 meters with 10-meter grids; the perimeter conductor GS at 1 m depth in uniform soil with a straight metallic cylindrical tube at 2 m depth.

It is analyzed such as a) effects are produced by the transfer of potentials in the mesh when having the presence of an underground metal perimeter fence, and b) the effects are due to potential transfers caused

by the presence of a metallic pipe buried under the GS.

For the analysis, different configurations of the GS and the underground pipeline.

Potentials are analyzed in an asymmetric mesh; a case presented depending on the topology and the facilities offered by its on-site construction.

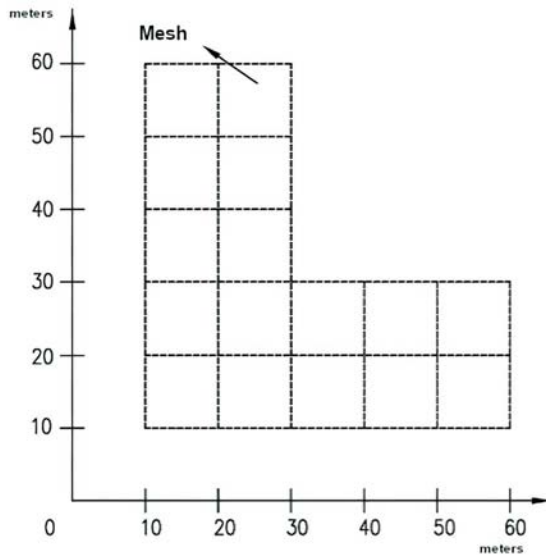


Figure 4. Top view of asymmetrical L-type mesh

2.1.2. Case Study 2

In Figure 5, rails located at a distance "d" from the mesh are added; for study case 2, the transfer of potential is reflected in changes of touch, step, GPG, and R_g voltages that occur in the directions will be analyzed indicated.

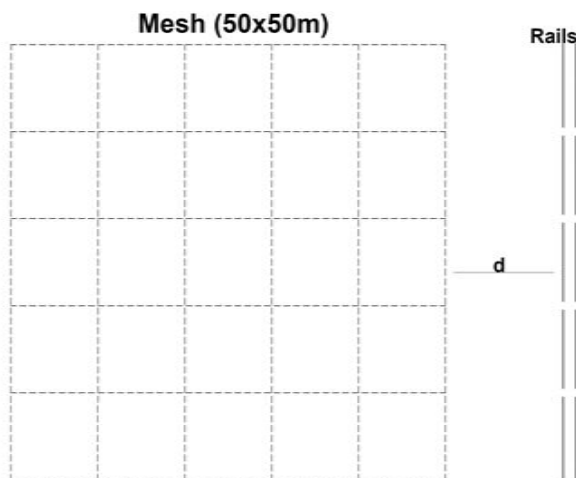


Figure 5. Top view Mesh - Rails

2.1.3. Case Study 3

The mutual interference of nearby ground grids is analyzed to assess the potentially dangerous circumstances in sites protected by the primary grid, including proximity to an adjoining one that dissipates the ground fault current in the surrounding ground, mainly in urban areas, a) mesh 1 Main and Mesh 2 Offline, b) mesh one primary and mesh two connected, c) mesh one primary and Mesh 2 are connected to other GS.

Two meshes of the grounding system are considered, with similar topology and technical parameters. Adjacent edges of the meshes are spaced a distance d meters apart.

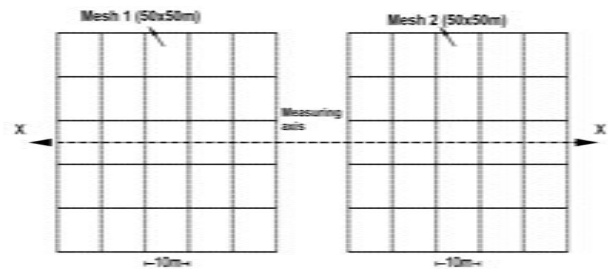


Figure 6. Nearby grounding grids

2.2. Interferences between GS and cathodic protection.

The standards and recommended practices for the design of cathodic protection systems establish the need to interconnect metallic structures with each other. However, this equipotential bonding can compromise cathodic protection and safety effectiveness. GS traditionally built with copper electrodes, due to their stability characteristics over time, present problems concerning cathodic protection: a copper ground mesh connected to the structure under cathodic protection can drain a considerable amount of the protection current. It may be impossible to polarize the steel structure correctly in specific scenarios. If the cathodic protection is no longer adequate, corrosion is at risk due to a galvanic coupling between copper and steel.

2.3. Impact of ground faults on pipelines and possible solutions.

Destructive electrical arcs can be prevented by bonding the GS to the pipe. However, such a connection would cause the cathodic protection system to drain; this is solved by inserting an ISP or a polarization cell in said connection. The fault current impressed on the pipe must be safely dissipated to earth employing uncoupled intentional sacrificial anodes, e.g., magnesium or zinc materials, connected and installed along the pipe with a low resistivity. These sacrificial anodes would also facilitate the dissipation to the ground of currents

conducted to the pipeline from locations remote from the substation area.

Instead of bonding conductors, installing decoupling devices, such as insulator surge protectors between grounding electrodes and pipelines, is the best compromise to safeguard safety and functionality during ground faults. Decouplers minimize the impact of ground faults on channels while preserving the effectiveness of the cathodic protection.

Human safety depends on the energy absorbed before the fault is cleared and the system is deactivated; it is suggested to establish step voltage and touch voltage limits which are called thresholds, depending on the material used as the surface layer and its reduction factor, Dalziel and Lee set constants related to the electrical discharge energy tolerated.

3. Results and discussion

3.1. Analysis of Results

3.1.1. Effects of perimeter mesh earth conductor

The underground metallic pipe is not considered; the contour and profile graphs of the potential gradient of the cases are made, considering the finished floor as the asphalt $\rho_s = 10000\Omega - m$.

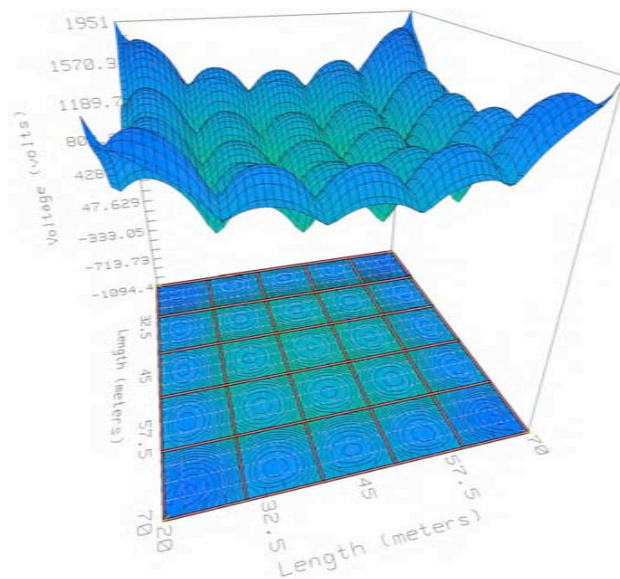


Figure 7. Touch voltage, insulated mesh- ρ_s asphalt

The underground metallic pipe is not considered; the contour and profile graphs of the potential gradient of the cases are made, considering the finished floor as the asphalt (Figure 7 and 8). Ground mesh and perimeter fence without connection see (Figure 9 and 10).

A summary of the simulations with the conditions set out for study case 1, with surface layers of concrete, gravel, and asphalt is presented.

At $\rho_s = 200\Omega - m$ concrete, the touch and step threshold voltages correspond to 457.82 V and 730.83 V.

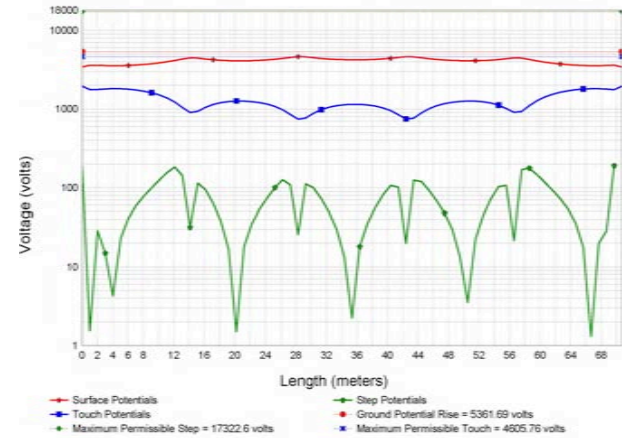


Figure 8. Insulated mesh potential profile - ρ_s asphalt

Table 4. Mesh and perimeter fence without connection

Cases	$\rho_s = 200\Omega - m$ concrete		
	MTV_{max}	MSV_{max}	GPG
Insulated mesh IM	1951.02	190.26	5361.69
Profile address 1 PA1	1455.92	119.73	5361.69
Profile address 2 PA2	3599.08	35.53	5361.69
Mesh-Net without connection MNWC	1015.99	89.43	3932.32
Profile address 1 no connection PA1NC	873.31	57.63	3932.32
Profile address 2 no connection PA2NC	1392.32	92.61	3932.32

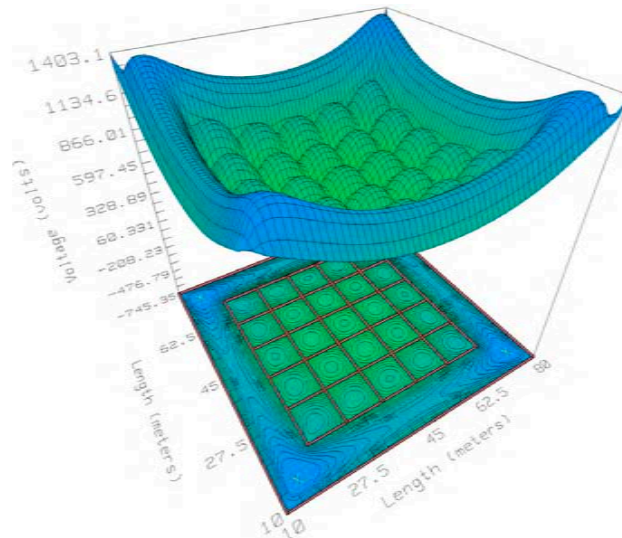


Figure 9. Touch voltage, mesh and fence without asphalt- ρ_s connection

Changing for a finished gravel floor, $\rho_s = 5000\Omega - m$, the threshold voltages of touch and step vary to

2489.47 V and 8857.39 V, with the change to asphalt $\rho_s = 10000\Omega - m$, touch and step voltages thresholds are 4605.76 V and 17322.6 V. The material used as surface layer allows to have a mesh resistance R_g at 0.476 Ω and for an isolated mesh with near no connection at a value of 0.35 Ω . The maximum touch voltages [MTV], maximum step voltage [MSV], and GPG see the Table 4.

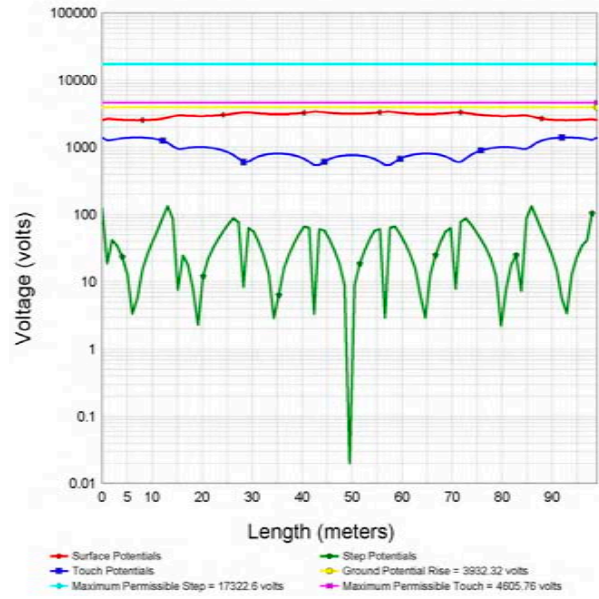


Figure 10. Potential mesh and fence profile without asphalt- ρ_s connection

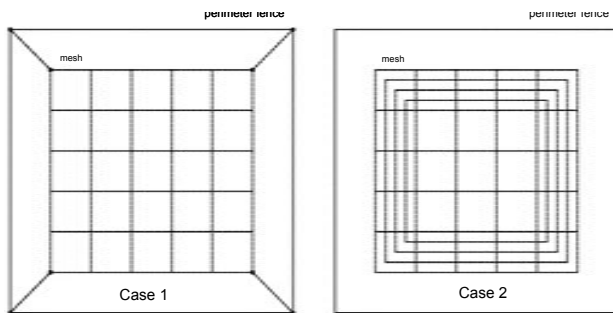


Figure 11. Modified mesh and mesh connected to fence

According to the simulations carried out with different values of the surface layer, the threshold touch voltages [TTV] and threshold step voltage [TSV] are directly related to the surface layer's resistivity. The change of material in the surface layer to gravel or asphalt allows the touch voltages, step voltage, GS, and R_g to vary in favor of the safety of the human being when the perimeter fence is implanted. The surface layer of concrete allows the MTV to exceed the values of TTV and TSV, which suggests improving the architecture of the mesh. Based on the mesh and perimeter fence indicated in figure 3, the modifications

made to the architecture of the mesh to reduce the MTV and MSV when there is a surface $\rho_s = 200 \Omega\text{-m}$, suggest a) attach the mesh to the perimeter fence, b) modify the mesh, increasing more loops on the outer parts. See figure 11. In case 1, with the architecture change, the TTV and TSV correspond to 457.82V and 730.83V, the $R_g = 0.34\Omega$ does not vary, and the MTV and MSV, as well as the GS, are shown in Table 5.

Table 5. Mesh and Perimeter Mint

$\rho_s = 200\Omega - m$ [concrete]			
Cases	MTV	MSV	GPG
Mesh and fence connected [MFC]	936,7	83,54	3858,7
Modified mesh without connection [MMWC]	851,86	150,73	3836,26

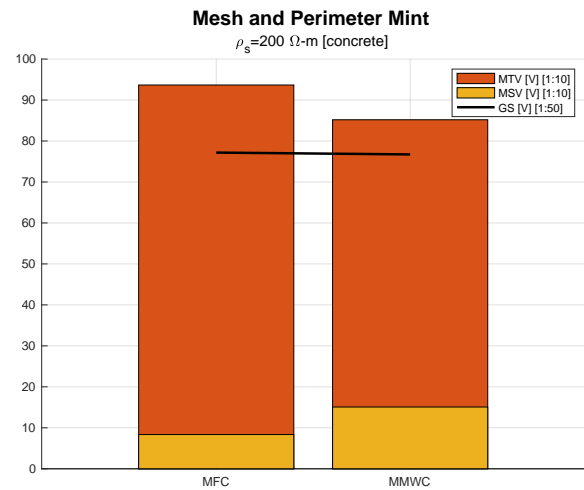


Figure 12. Metric with mesh architecture change

3.1.2. Influence of the perimeter mesh

The results allow us to observe the effects of the perimeter fence on the MTV, MSV, GPG, and R_g : If the earth conductor of the perimeter fence encloses the substation mesh, its effects on the MTV of the mesh decrease up to 48%, and the GS and R_g decrease by 27%. The most typical configurations used to decrease the touch voltage are observed in figure 11; in table 5, the MTV and MSV decrease in case 1. In case 2, with the modified mesh, the MTV decreases, and MSV increases concerning the values indicated in table 3 when there is a mesh and fence without a connection. If the GS increases, the R_g increases; this is logical since the GS is proportional to R_g , according to its formula, $GPG = I_g \cdot R_g$. When the GS increases, the peak touch voltage decreases. In case 1, mesh and fence connected, the maximum voltage value decreases by 8%, especially where the mesh and rail are not connected. In case 2, modified mesh, the maximum touch voltage decreases by 16% for the case in which the mesh is present and the fence is offline.

3.1.3. The buried metal pipe effects

For the analysis of the effects of the pipe on the ground grid, the fence indicated in figure 2 is not taken into account; the touch, step, and GS voltage simulations are carried out on the grid and direction 1. Metal pipe of a fixed diameter, buried at different depths. See Table 5. A metal pipe is buried at a fixed depth and variable diameters. See Table 6. An example of item a is simulated, with a surface layer of asphalt for the case of a 400 mm Ø pipe case and a depth of 2m, Table 6.

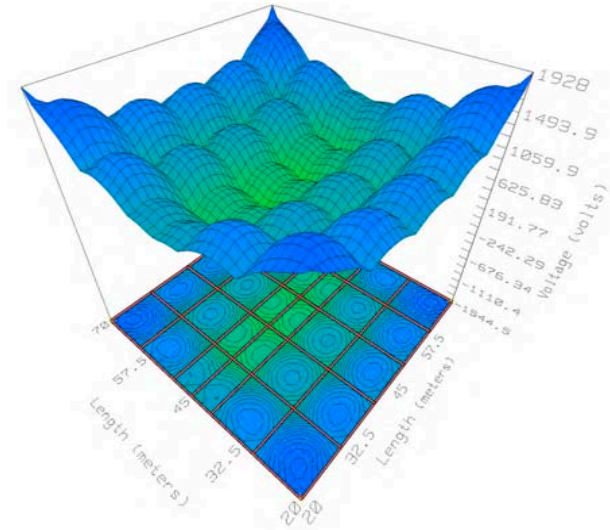


Figure 13. Touch voltage, mesh and asphalt- ρ_s pipe

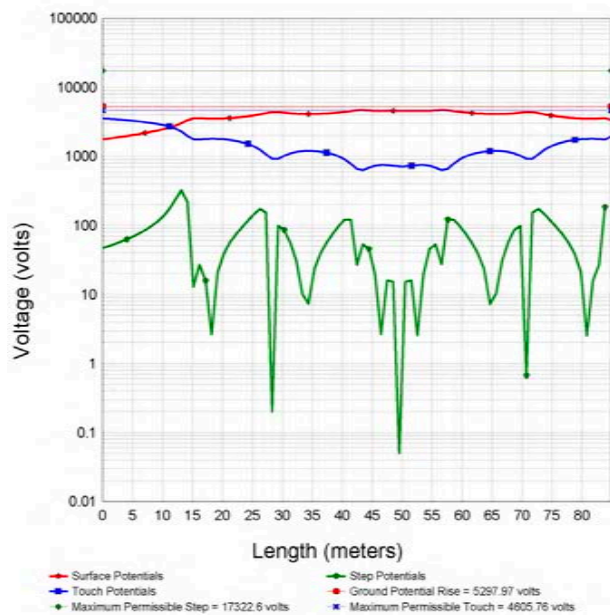


Figure 14. Potential direction profile 1 - mesh and pipe - ρ_s asphalt

A summary of the simulations carried out with pipes of different diameters, depths, and surface

layers of concrete, gravel, and asphalt are present. $\rho_s = 200\Omega - m$ [concrete], constant diameter pipe, and underground metallic line at depths of 2, 3, 4, and 5 m, TTV, and TSV correspond to 457.82 V and 730.83 V when changing the scenario For the surface layer of gravel [$\rho_s = 5000\Omega - m$], the TTV and TSV vary between 2489.47 V and 8857.39 V, for the case of asphalt as a surface layer being its $\rho_s = 10000\Omega - m$, the TTV. TSV equal 4605.76 V and 17322.6 V, R_g is set to 0.47 Ω . The maximum touch, step, and PG voltages present a variation presented in Table.

Table 6. Constant pipe diameter and variable depth

Mesh and underground piping (diameter 400 mm)

$\rho_s = 200\Omega - m$ [concrete]

$\rho_s = 5000\Omega - m$ [gravel]

$\rho_s = 10000\Omega - m$ [asphalt]

Mesh - Pipe 2m [MP2]	1924.62	186	5288.62
Profile Address 11 [PD11]	1053.52	113.23	5288.62
Mesh - Pipe 3m [MP3]	1911.75	184.93	5263.10
Profile Address 12 [PD12]	1090.21	112.56	5263.10
Mesh - Pipe 4m [MP4]	1897.24	183.78	5235.02
Profile Address 13 [PD13]	1114.58	111.75	5235.02
Mesh - Pipe 5m [MP5]	1881.5	182.56	5204.92
Profile Address 14 [PD14]	1131.21	110.75	5204.92

$\rho_s = 200\Omega - m$ [concrete], pipe diameter variation at 0.8, 0.6, 0.4, 0.2m at constant depth, TTV and TSV at 457.82V and 730.83V, yes gravel with $\rho_s = 5000\Omega - m$ is used as a surface layer, TTV and TSV indicate values in 2489.47 V and 8857.39V. For the scenario of using asphalt as the surface layer, knowing that its $\rho_s = 10000\Omega - m$, the result corresponds to 4505.76 V and 17322.6 V, indicating that $R_g = 0.47\Omega$. The MTV, MSV, and PG present a variation presented in Table 7.

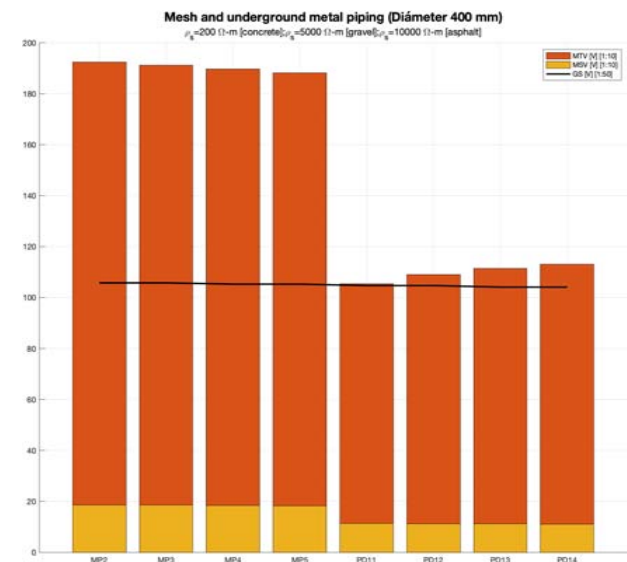


Figure 15. Metric mesh and underground metallic pipe

Table 7. Variable diameter and constant depth pipe - ρ concrete

Mesh and underground metal piping (2m)
 $\rho_s = 200\Omega - m$ [concrete]
 $\rho_s = 5000\Omega - m$ [gravel]
 $\rho_s = 10000\Omega - m$ [asphalt]

Cases	MTV	MSV	GPG
Mesh - Pipe \varnothing 0.8m [MP0.8]	1920.08	185.26	5276.08.62
Profile Address 11 [PD11]	998.72	112.12	5276.08
Mesh - Pipe \varnothing 0.6m [MP0.6]	1922.13	185.59	5261.76
Profile Address 12 [PD12]	1018.71	112.62	5261.76
Mesh - Pipe \varnothing 0.4m [MP0.4]	1924.62	186	5288.62
Profile Address 13 [PD13]	1053.62	113.23	5288.62
Mesh - Pipe \varnothing 0.2m [MP0.2]	1927.98	186.54	5297.97
Profile Address 14 [PD14]	1104.79	114.06	5297.97

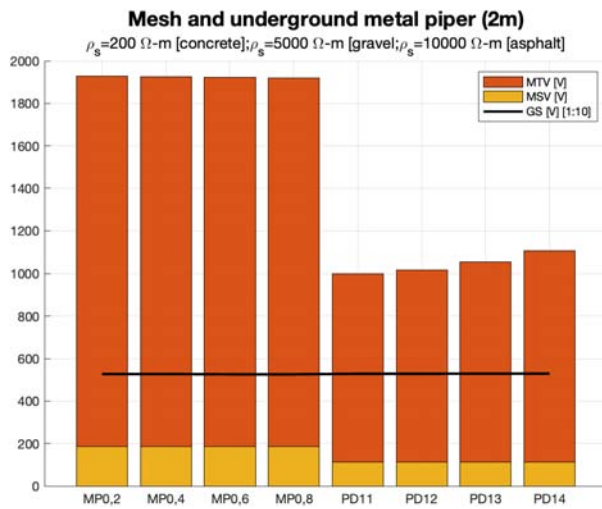


Figure 16. Display of values Table 8

In the presence of an underground metal pipe that crosses under the mesh, with a constant diameter and variable depth, the MTV and MSV decrease the deeper it is, while the R_g and GS do so on a smaller scale. If its diameter is variable and its depth constant, the MTV and MSV increase when the pipe diameter decreases, and the R_g and GS increase to a lesser extent. In figure 3, different scenarios are proposed, keeping constant the parameters of the mesh, diameter, and variable depth, the objective of these configurations allows to determine which strategy is more favorable for the decrease of TTV and TSV that can be generated on the surface area of the pipeline when a fault occurs in the electrical system.

3.1.4. Analysis of results of underground metallic pipelines

The voltages MTV [457.82 V] and MSV [730.83 V] of case 1 indicated in table 1 are taken as reference, where it is recommended to install more ground mesh conductors parallel to the underground pipe that passes below; this helps to decrease the TTV and TSV in the

mesh, due to the increase in electromagnetic fields. Another way to reduce TTV and TSV is to make the pipe cross diagonally as much as possible. An exhaustive analysis suggests underground pipes leave an electrical substation area because voltage-transfer generates GPG and TTV values higher than those admissible for its configuration. In these cases, installing copper weld rods attached to the beginning and end of the pipe is recommended. According to the studies carried out on the metallic pipe, it is possible to observe that this affects the potential of the mesh.

When inside the grid area, the buried metal pipe decreases the TTV and TSV; in real situations, this does not happen because the pipes always enter and leave the grid area. When a metal pipe leaves or is outside the mesh area, it causes elevation of TTV and GPG in regions outside the mesh; this is logical since by increasing the length of the pipe, the increase in potential will approach the rise in network potential. When a fault occurs in the electrical system, a current is generated in the pipe; this increases when the pipe is further away. The scenarios presented with underground metallic pipes clearly show the danger of transferred potentials. For GS designs in electrical substations, corrective measures must be taken when metallic structures are nearby; the designer must know their influence with acceptable precision; otherwise, they may apply erroneous or unjustified measures.

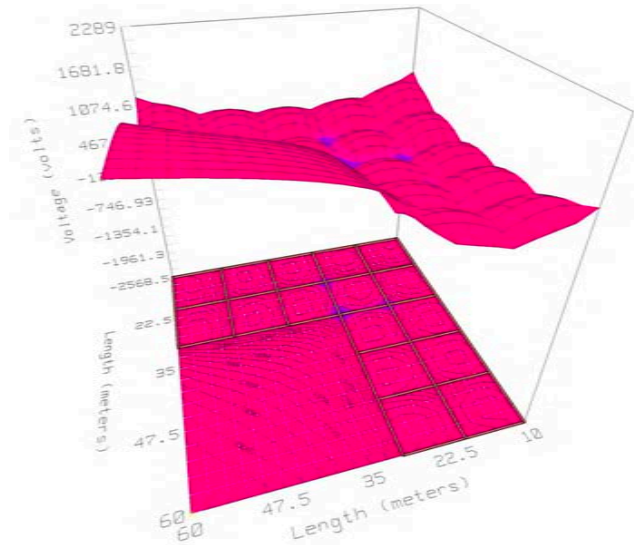


Figure 17. Asymmetrical mesh touch voltage - ρ_s concrete

According to sound engineering practices, corrective procedures are in place to minimize the transfer of potential when metallic structures are buried. Joining the metallic structure to the main mesh, however, the consequences of the said procedure is carefully verified due to the possible transfer of the increase in the potential of the networks [reverse situation]. Provide denser meshes for the grid over the buried pipe. These

meshes can, in some cases, act as a protective mesh by reducing the magnitude of the touch voltage. Install insulating flanges on underground metal piping at suitable locations. The optimal solution in the corrective methods to be used will depend on several factors, such as the properties of the soil, the location of the metallic structure, and the fault current, among others.

3.1.5. Mesh Type L

An GS study of an asymmetric mesh is presented, see figure 4, for this case, a surface layer of resistivity $\rho_s = 200\Omega - m$ [concrete] is considered, obtaining the values shown in Table 8.

Table 8. Asymmetric mesh type L

Cases	Asymmetric mesh type L $\rho_s = 200\Omega - m$ [concrete]					GPG [V]
	MTV	MSV	TTV	TSV	$R_g\Omega$	
Insulated mesh	457,82	2288,99	730,83	132,11	0,56	3168

In the exposed case, it is observed that with the surface layer of concrete, the MTV exceeds the MSV; in figure 16, the procedures to improve the TTV are the same as those exposed in symmetric or asymmetric meshes.

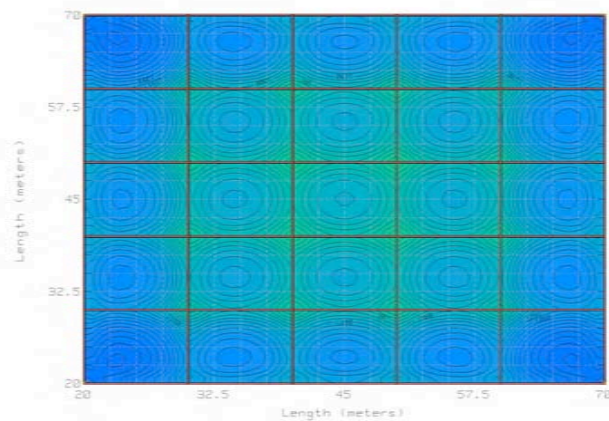


Figure 18. Mesh potential contour - without rails

3.1.6. Analysis of results Scenario 2

A mesh and nearby rails are considered, the configuration of the mesh indicated in figure 3 is used, the study is made based on what is shown in figure 5, and a surface layer of asphalt is considered.

3.1.7. Case 2.1 Ground grid without considering nearby rails

An analysis of the potential contour of the ground grid is made without considering the rails; figure 18 shows the potential distribution on the ground surface when a fault condition occurs.

3.1.8. Case 2.2 Ground Grid considers rails without connection to the grid

It is proposed to analyze the potential contour of the ground grid considering the rails at a distance $[d=30m]$ without connection; this is a common situation in electrical substations and power plants, the simulation of the rails is done through steel conductors 90 mm diameter aluminum-clad separated at a distance of 1.5 m and a length of 50 m. Figure 19.

3.1.9. Case 2.3 Earth grid considering the rails connected to the grid

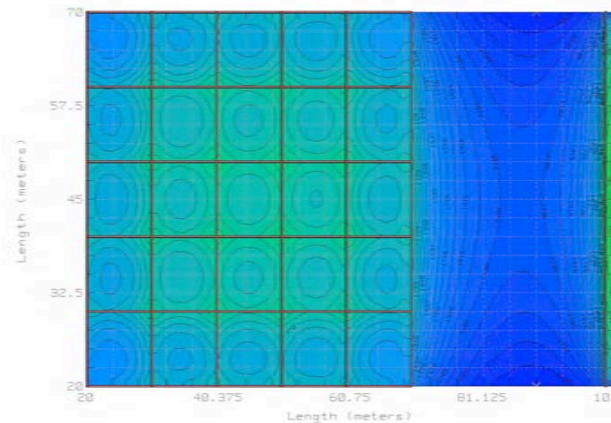


Figure 19. Mesh potential contour - with rails

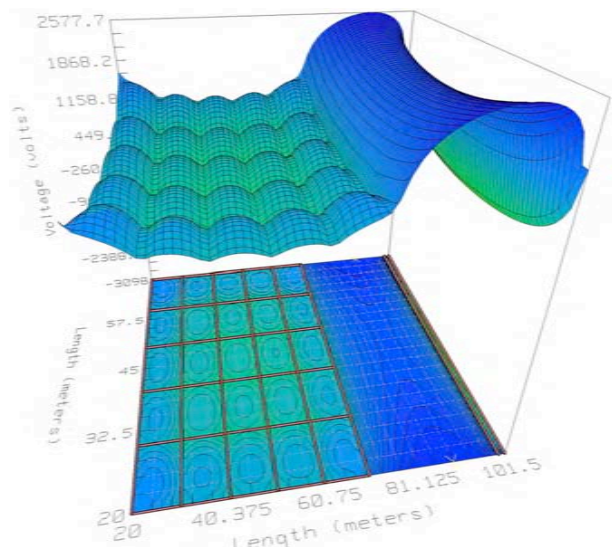


Figure 20. Touch voltage mesh and rails without connection

The potential contour of the ground grid, considering the rails connected to the ground grid employing 4/0 AWG copper cables at 5 points uniformly distributed on the rails, is presented as a case study. See figure 20. Figures 17, 18, and 19 show the change in potential curves when the rails are installed; the most

important differences can be seen in the distribution of potentials in the surroundings since high GS are generated to be considered. Figures 19 and 20 show that the TTV values increase in the area between the rails and the mesh when they are not connected; they are joined with the mesh to reduce these potentials. Figures 21 and 22.

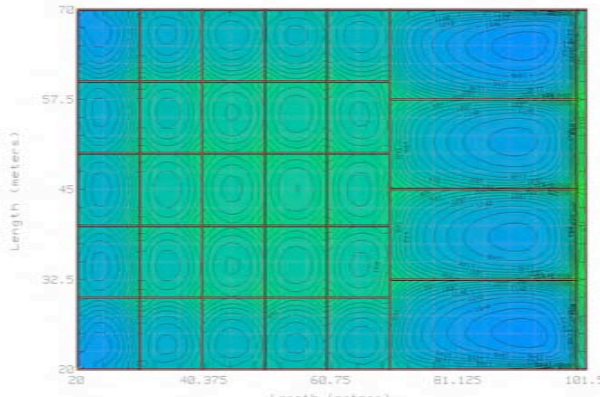


Figure 21. Mesh potential contour with rail connection

Table 9. Variable diameter and constant depth pipe - ρ concrete

Mesh and Rails (Rail Diameter 90mm, Depth 10mm)				
$\rho_s = 10000\Omega - m$ [asphalt]				
Idem	Cases	MTV	MSV	GPG
1	Insulated Mesh [IM]	1951.02	190.26	5361.69
2	Potential Rails [PR1]	3984.13	9.57	5361.69
3	Mesh and Rails without Connection 1 [MRWC1]	1651.47	152.99	4606.32
4	Rail Potentials [PR2]	1739.38	576.69	4606.32
5	Mesh - Pipe \varnothing 0,4m [MP0,4]	1924.62	186	5288.62
6	Potential Rails [PR3]	717.73	227.69	4201.47
7	Mesh and Rails without Connection 2 [MRWC2]	1671.74	155.12	4657.38
8	Isolated Potential Rails [PRA]	1606.9	756.61	4657.38

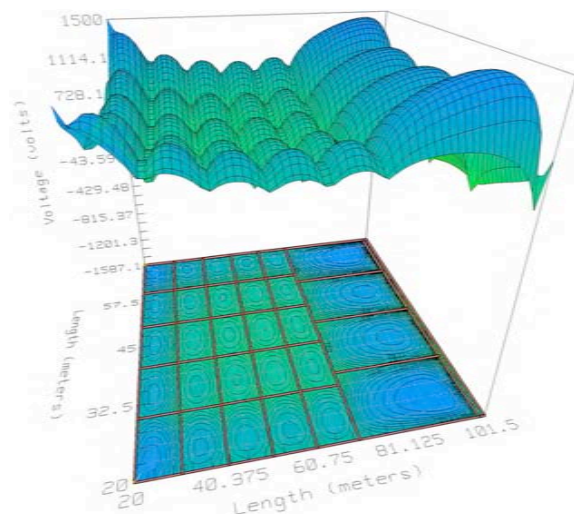


Figure 22. Voltage of touch screen and connected rails

If the rails are not connected to the mesh, the TTV and TSV values are high, see Table 9, item 2, if they

are connected to the mesh, they decrease, and the GP and R_g values. Another way to reduce the potentials in the rails when they are not connected to the mesh is to insulate the union joints, see Table 9, item 8; in the same way, the rails can be grounded using metal rods or copper-weld.

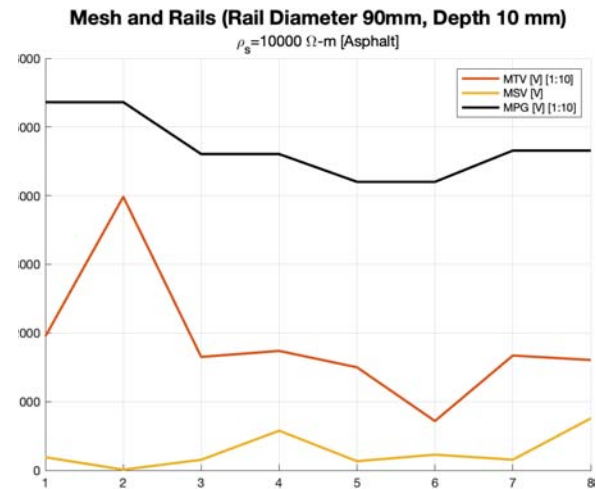


Figure 23. Display of values table 6

3.1.10. Analysis of Results Scenario 3

Mesh 1 and mesh two are considered; Figure 6, the mesh configuration indicated in figure 3 is used with a surface layer of gravel and a short-circuit current of 10 kA.

3.1.11. Mesh 1 and Mesh 2 No Connection

When an electrical fault occurs in mesh 1, it affects mesh two due to the difference between the potentials of the ground surface and the potential in mesh 2; the simulation for the two meshes is done by varying their distance, starting from 10 up to 120 meters; obtaining TTV= 2489.47 V and TSV=8857.39 V.

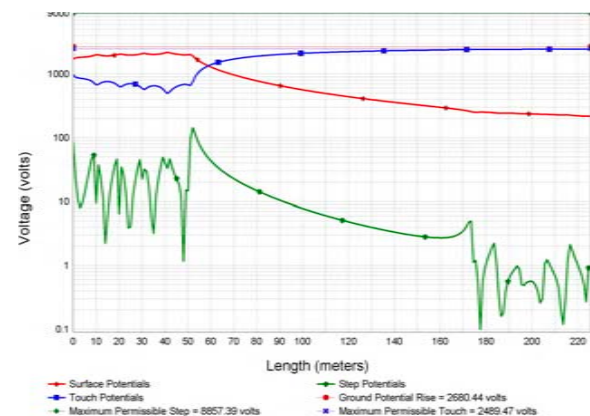


Figure 24. Touch and step voltage on the measuring axis of the meshes. Mesh 1 and Mesh 2 without connection

Table 10. Voltages touch step R_g GPG – Insulated mesh

d(m)	Mesh 1				Mesh 2			
	Maximum Voltage		$R_g\Omega$	GPG	Maximum Voltage		$R_g\Omega$	GPG
	Touch	Step	V	Touch	Step	V	V	
10	980.754	96.58	0.468	2636.63	2054.55	22.64	0.468	734.951
20	978.146	95.8	0.473	2661.43	2165.5	14.71	0.473	607.649
30	976.994	95.49	0.474	2670.57	2234.7	10.86	0.474	522.136
40	976.354	95.33	0.475	2674.82	2284.7	8.44	0.475	409.968
50	976.009	95.26	0.476	2677.06	2323.38	6.77	0.476	409.968
60	975.806	95.21	0.476	2678.34	2354.56	5.56	0.476	370.686
70	975.693	95.18	0.476	2679.11	2380.38	5.64	0.476	382.68
80	975.629	95.17	0.476	2679.61	2420.21	3.93	0.476	311.425
90	975.588	95.16	0.476	2679.94	2420.96	3.41	0.476	288.475
100	975.554	95.14	0.476	2680.16	2437.25	3.99	0.476	268.717
110	975.543	95.14	0.476	2680.32	2451.58	2.65	0.476	251.521
120	975.528	95.14	0.476	2680.4	2464.27	2.36	0.476	236.414

The MTV generated by mesh 1 in mesh 2 grow as they move away, reaching their maximum value of 2464.27 V at a distance of 120m; otherwise, the MSV decreases as they move away. In meshes 1 and 2, the R_g values are maintained at all separation distances, while in Mesh 2, the GPG decreases as they move away. On the line of the measurement axis, a graph of the touch and step voltage is plotted for insulated grids 1 and 2, for a distance $d=30m$, Figure 24.

3.1.12. Mesh 1 and Mesh 2 are Connected.

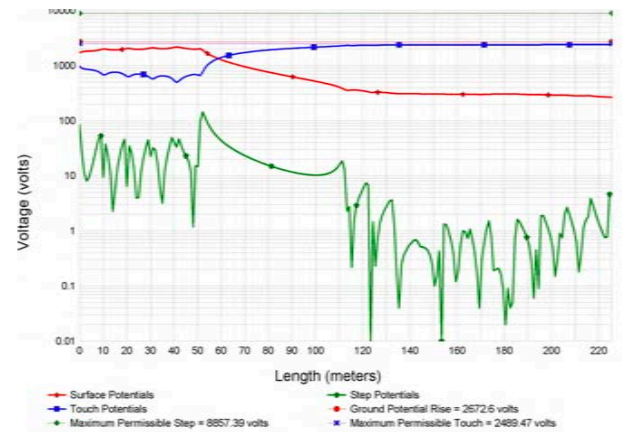
If meshes 1 and 2 are connected, the leak fault currents are the same, and the potentially dangerous voltages are generated due to their geometric symmetry. The meshes may be intentionally or unintentionally attached through various metal installations such as cables, pipes, or metal rails.

Table 11. Voltages touch, step, R_g , GPG.Mesh 1 and 2 joined

d(m)	Mesh 1				Mesh 2			
	Maximum Voltage		$R_g\Omega$	GPG	Maximum Voltage		$R_g\Omega$	GPG
	Touch	Step	V	Touch	Step	V	V	
10	600.808	52.99	0.307	1731.01	600.808	54.4	0.307	1731.01
20	576.057	51.15	0.296	1668.63	576.057	53.41	0.296	1668.63
30	557.325	49.72	0.287	1619.07	557.325	51.84	0.287	1619.07
40	542.037	48.53	0.28	1577.25	542.037	50.55	0.28	1577.25
50	526.901	47.48	0.273	1540.53	526.901	49.42	0.273	1540.53
60	517.206	46.51	0.268	1507.44	517.206	48.38	0.268	1507.44
70	506.565	45.63	0.262	1477.04	506.565	47.44	0.262	1477.04
80	496.696	44.79	0.257	1448.7	496.696	46.54	0.257	1448.7
90	487.437	43.99	0.252	1422.2	487.437	45.7	0.252	1422.2
100	478.677	43.22	0.248	1397.06	478.677	44.89	0.248	1397.06
110	514.775	47.22	0.263	1481.65	514.775	48.88	0.263	1481.65
120	462.371	41.78	0.24	1350.29	462.371	43.37	0.24	1350.29

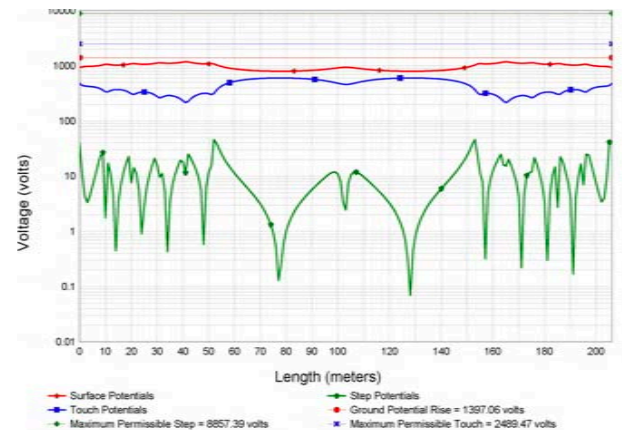
The union of the two meshes is considered using an isolated cable with the same characteristics as those that make up the respective meshes, obtaining similarity between MTV and MSV in both meshes, see table 10. In an electrical failure, the voltage values are reflected in mesh 2. It indicates the need for an exhaustive analysis; before intentionally connecting mesh 1 with mesh 2, it is necessary to check if the security measures applied in the Mesh 2 installations can build up to dangerous voltages and ground currents. On the other hand, the parallel connection of the grounding system meshes decreases the ground currents and the TTV associated with mesh 1. The

TTV and TSV metrics at a distance $d=30m$ are shown in Figure 25.

**Figure 25.** Voltages touch and step - on the measuring axis of mesh 1 and mesh 2 connected

3.1.13. Mesh 1 and Mesh 2 without Connection - Mesh 2 Underground.

Distribution source transformer stations are often located close to surrounding buildings in urban areas. On the other hand, GS's are often intentionally or unintentionally interconnected; therefore, they tend to have a very low R_g . It is essential to assess potentially dangerous voltages that may appear on the ground grid of an adjacent building closest to the substation.

**Figure 26.** Touch and step voltages on the measuring axis - Mesh 1 and Mesh 2 isolated - Mesh 2 grounded**Table 12.** Voltages touch, step, R_g , GPG Mesh 1 - Mesh 2 grounded

d(m)	Mesh 1			Mesh 2				
	Maximum Voltage		GPG	Maximum Voltage		GPG		
	Touch	Step	V	Touch	Step	V		
10	989.093	98.77	0.46	2589.35	2101.29	31.52	0.46	549.539
20	981.739	96.67	0.46	2638.14	2202.31	20.62	0.46	483.27
30	978.94	95.97	0.474	2656	2268.01	15.1	0.474	423.433
40	977.658	95.68	0.474	2663.49	2320.62	12.7	0.474	367.376
50	976.7981	95.47	0.474	2669.13	2355.08	10.32	0.474	333.388
60	976.309	95.36	0.474	2672.6	2382.59	8.57	0.474	305.593

The potential distribution on the ground surface of grid 1, where the source distribution substation is located, and grid 2, which represents the ground grid of the building closest to the substation, is calculated. The calculations are made assuming that the ground mesh of the building is connected to the ground meshes of the surrounding buildings; it is assumed that the meshes of the structures have the same characteristics and technical parameters equal to mesh 1. The simulation for the two meshes is done by varying their distance, starting from 10 to 60 meters, obtaining $TTV=2489.47$ V and $TSV=8857.39$ V. In the situation in urban areas, the MTV in the neighboring building for $d = 30$ presents high values; however, the stepped voltages in the space between the substation and the adjoining installation are higher voltages for the grids connected. The transfer of dangerous potentials and the technical parameters of the mesh and the ground depend mainly on the value of the fault current. A considerable distance between nearby meshes does not guarantee a decrease in the transfer of dangerous potentials. In electrical substations, the resistivity value of the surface layer is an important parameter to take into account; its value directly influences the TTV and TSV values of the substation and, therefore, the transferred potential gradients.

4. Conclusions

Based on the scenarios presented in this study with variables of resistivity of the surface layer and different configurations, the variation of the GPG has been determined against several strategies. Technical parameters that appear in GS designs have been related and evaluated, observing how these influence the GPG.

This article presents the simulation and analysis of real potential transfer scenarios between electrical substations and metallic structures. Based on them, results have been obtained that reflect the values of dangerous transfer voltages to metallic structures near a substation, exceeding the TTV and TSV allowed in a GS. Measures and procedures taken into account to reduce transfer voltages in the design and construction of GS are indicated.

The values of short-circuit currents, soil resistivity, distances, and location between nearby metal structures, among other design parameters, influence the transfers of electrical potentials between a substation and adjoining metal structures. It is essential to consider the GPG generated in a GS outside the substation area, the interference effects of potentials generated by the existence of metal structures, and the GS close to the substation.

In nearby grids, an analysis is made of the potentially dangerous situations that may appear when transferring the potentials generated by the ground

fault currents to the grids and nearby ground equipment and the personnel protected by them. In designs of cathodic protection systems for pipelines in oil stations, interferences between GS's connected to the substation grid with cathodic protection systems are avoided as much as possible. Otherwise, the problem should be deepened, proposing suitable solutions to this interference, which would prevent compromising the effectiveness of the cathodic protection system.

Detailed scenario analysis is performed when the nearby grid is with other grounded objects; these circumstances are necessary for installing substations in urban areas. The analysis carried out in the document has shown that in case of ground faults in an unintentional connection of ground networks, it can cause high TTV and TSV in nearby meshes, which can lead to severe risks for the human being who transmits them.

References

- [1] J. Nahman and D. Salamon, "Mutual interference of neighboring grounding systems and approximate formulation," *Electric Power Systems Research*, vol. 151, pp. 166–173, 2017. [Online]. Available: <https://doi.org/10.1016/j.epsr.2017.05.029>
- [2] L. Fu, "The influence of Urban Substation on Neighbouring Metal Grounding System," *Journal of Physics: Conference Series*, vol. 1176, no. 4, 2019. [Online]. Available: <https://doi.org/10.1088/1742-6596/1176/4/042051>
- [3] L. Neamt, H. Balan, O. Chiver, and A. Hotea, "Considerations about Substation Grounding System Design," in *Proceedings of 2019 8th International Conference on Modern Power Systems, MPS 2019*. Institute of Electrical and Electronics Engineers Inc., 2019. [Online]. Available: <https://doi.org/10.1109/MPS.2019.8759737>
- [4] M. L. Di Silvestre, L. Dusonchet, S. Favuzza, S. Mangione, L. Mineo, M. Mitolo, E. R. Sanseverino, and G. Zizzo, "On the Interconnections of HV-MV Stations to Global Grounding Systems," *IEEE Transactions on Industry Applications*, vol. 55, no. 2, pp. 1126–1134, 2019. [Online]. Available: <https://doi.org/10.1109/TIA.2018.2875383>
- [5] G. Aiello, S. A. Rizzo, S. Alfonzetti, and N. Salerno, "Computation of Transferred Potentials from Grounding Grids by Means of Hybrid Methods," in *Proceedings - 2018 IEEE International Conference on Environment and Electrical Engineering and 2018 IEEE Industrial and Commercial Power Systems Europe, IEEEIC/I and CPS Europe 2018*. Institute of Electrical and Electronics Engineers Inc., 2018. [Online]. Available: <https://doi.org/10.1109/IEEEIC.2018.8493916>

- [6] L. Popović, “Preliminary testing and assessment of safety conditions of HV substations located in urban areas,” *Electric Power Systems Research*, vol. 195, 2021. [Online]. Available: <https://doi.org/10.1016/j.epsr.2021.107111>
- [7] C. Martineac and R. N. Hasanah, “Influence of soil resistivity on substations earth grounding system,” in *Proceedings of 2019 8th International Conference on Modern Power Systems, MPS 2019*. Institute of Electrical and Electronics Engineers Inc., 2019. [Online]. Available: <https://doi.org/10.1109/MPS.2019.8759796>
- [8] G. Cafaro, P. Colella, P. Montegiglio, E. Pons, R. Tommasini, F. Torelli, and G. Valtorta, “Ground Resistance of Buried Metallic Parts in Urban Areas: An Extensive Measurement Campaign,” *IEEE Transactions on Industry Applications*, vol. 53, no. 6, pp. 5209–5216, 2017. [Online]. Available: <https://doi.org/10.1109/TIA.2017.2748502>
- [9] W. A. Byrd, “Below Grade Coated Direct Imbedded Steel Pole Corrosion Failures With Solutions,” *IEEE Power and Energy Technology Systems Journal*, vol. 6, no. 1, pp. 41–46, 2018. [Online]. Available: <https://doi.org/10.1109/JPETS.2018.2884974>
- [10] Q. Lv, Z. Xiang, X. Li, J. Ai, S. Liu, and C. Zhang, “Research on overvoltage protection strategy of oil-gas pipeline based on non-metallic grounding material,” in *2019 4th International Conference on Intelligent Green Building and Smart Grid, IGBSG 2019*. Institute of Electrical and Electronics Engineers Inc., 2019, pp. 97–102. [Online]. Available: <https://doi.org/10.1109/IGBSG.2019.8886338>
- [11] S. A. H. Mohammed and I. M. Abdulbaqi, “Numerical Study and Design of an Impressed Current Cathodic Protection System for Buried Metallic Pipes,” in *2018 3rd Scientific Conference of Electrical Engineering, SCEE 2018*. Institute of Electrical and Electronics Engineers Inc., 2018, pp. 95–100. [Online]. Available: <https://doi.org/10.1109/SCEE.2018.8684076>
- [12] E. Inga and R. Hincapié, “Creación de artículos académicos basados en minería de datos y Web 2.0 para incrementar la producción científica en ingeniería,” *Revista Educación en Ingeniería*, vol. 10, no. 20, pp. 65–74, 2015. [Online]. Available: <https://bit.ly/3MX1Woz>
- [13] T. H. Shabangu, P. Shrivastava, B. T. Abe, K. B. Adedeji, and P. A. Olubambi, “Influence of AC interference on the cathodic protection potentials of pipelines: Towards a comprehensive picture,” in *2017 IEEE AFRICON: Science, Technology and Innovation for Africa, AFRICON 2017*. Institute of Electrical and Electronics Engineers Inc., 2017, pp. 597–602. [Online]. Available: <https://doi.org/10.1109/AFRCON.2017.8095549>
- [14] G. Liu, G. Jiang, Z. Zhang, D. Mei, and Y. Zheng, “Research on the influence of DC current overflowing on grounding electrode corrosion,” in *Proceedings of 2017 IEEE 3rd Information Technology and Mechatronics Engineering Conference, ITOEC 2017*, vol. 2017-Janua. Institute of Electrical and Electronics Engineers Inc., 2017, pp. 291–295. [Online]. Available: <https://doi.org/10.1109/ITOEC.2017.8122438>
- [15] M. G. Mahlobo, P. Mjwana, M. N. Tladi, B. A. Obadele, P. A. Olubambi, and P. Refait, “Evaluation of cathodic protection performance of carbon steel pipeline buried in soil: A review,” in *2018 IEEE 9th International Conference on Mechanical and Intelligent Manufacturing Technologies, ICMIMT 2018*, vol. 2018-Janua. Institute of Electrical and Electronics Engineers Inc., 2018, pp. 37–43. [Online]. Available: <https://doi.org/10.1109/ICMIMT.2018.8340417>
- [16] B. Zhang, F. Cao, X. Meng, Y. Liao, and R. Li, “Numerical approach of impressed potential on buried pipelines near high-voltage DC grounding electrodes,” *IET Generation, Transmission and Distribution*, vol. 12, no. 5, pp. 1177–1182, 2018. [Online]. Available: <https://doi.org/10.1049/iet-gtd.2017.1436>
- [17] F. Babaghayou, B. Zegnini, and T. Seghier, “Experimental model investigation of the corrosion of buried steel pipelines with cathodic protection near high voltage power lines,” *Proceedings of 2016 International Conference on Electrical Sciences and Technologies in Maghreb, CISTEM 2016*, pp. 1–6, 2017. [Online]. Available: <https://doi.org/10.1109/CISTEM.2016.8066812>
- [18] H. Xuedong, Y. Wei, L. Xinghua, S. Xiangping, and H. Xuyin, “Analysis of grounding status of substation secondary system and improvement measures,” in *China International Conference on Electricity Distribution, CICED, 2018*, pp. 1479–1483. [Online]. Available: <https://doi.org/10.1109/CICED.2018.8592194>
- [19] M. Di Silvestre, L. Dusonchet, S. Favuzza, S. Mangione, L. Mineo, M. Mitolo, E. Sanseverino, and G. Zizzo, “Interconnections criteria of grounding grids in global grounding systems,” in *Conference Record - Industrial and Commercial Power Systems Technical Conference*, vol.

- 2018-May, 2018, pp. 1–8. [Online]. Available: <https://doi.org/10.1109/ICPS.2018.8369974>
- [20] R. Pereira Sodre, B. Lopes Pereira, L. Leite Sidrim, J. F. Almeida, and C. L. S. Souza Sobrinho, “Optimization of Grounding Grids Design for a Square-Shaped Mesh,” *IEEE Latin America Transactions*, vol. 16, no. 1, pp. 135–139, 2018. [Online]. Available: <https://doi.org/10.1109/TLA.2018.8291465>
- [21] C. Payshetti, H. Jadhav, and S. Kulkarani, “Analysis of grounding grid of substation,” in *Proceedings of IEEE International Conference on Circuit, Power and Computing Technologies, ICCPCT 2017*, 2017. [Online]. Available: <https://doi.org/10.1109/ICPCT.2017.8074259>
- [22] I. Kasim, S. Abduh, and N. Fitryah, “Grounding system design optimization on 275 KV betung substation based on IEEE standard 80-2000,” in *QiR 2017 - 2017 15th International Conference on Quality in Research (QiR): International Symposium on Electrical and Computer Engineering*, vol. 2017-Decem. Institute of Electrical and Electronics Engineers Inc., 2017, pp. 400–407. [Online]. Available: <https://doi.org/10.1109/QIR.2017.8168519>
- [23] M. D. Kavimandan and A. M. Silva, “Impacts of Existing Infrastructure on Soil Resistivity,” *Proceedings of the IEEE Power Engineering Society Transmission and Distribution Conference*, vol. 2020-October, pp. 20–23, 2020. [Online]. Available: <https://doi.org/10.1109/TD39804.2020.9299899>
- [24] A. Raizer, W. Valente, and V. L. Coelho, “Development of a new methodology for measurements of earth resistance, touch and step voltages within urban substations,” *Electric Power Systems Research*, vol. 153, pp. 111–118, 2017. [Online]. Available: <https://doi.org/10.1016/j.epsr.2017.01.025>
- [25] M. Abdaldaim, P. Wang, and L. Li, “The design of 110kV substation grounding grid with high resistivity soil,” in *2017 IEEE 6th Asia-Pacific Conference on Antennas and Propagation, APCAP 2017-Proceeding*. Institute of Electrical and Electronics Engineers Inc., 2018, pp. 1–3. [Online]. Available: <https://doi.org/10.1109/APCAP.2017.8420847>
- [26] X. Wu, V. Simha, R. J. Wellman, M. Thakur, and S. S. Dimpfl, “Substation Grounding Study Input Parameter Sensitivity Analysis and Simulation Strategies,” in *IEEE Transactions on Industry Applications*, vol. 55, no. 3. Institute of Electrical and Electronics Engineers Inc., 2019, pp. 2272–2280. [Online]. Available: <https://doi.org/10.1109/TIA.2018.2885475>
- [27] D. S. Gazzana, A. B. Tronchoni, R. C. Leborgne, M. Telló, and A. S. Bretas, “Numerical Technique to the Evaluation of Multiple Grounding Electrodes Coupled by the Soil in High Voltage Substations,” in *Proceedings - 2019 IEEE International Conference on Environment and Electrical Engineering and 2019 IEEE Industrial and Commercial Power Systems Europe, EEEIC/I and CPS Europe 2019*. Institute of Electrical and Electronics Engineers Inc., 2019. [Online]. Available: <https://doi.org/10.1109/EEEIC.2019.8783554>
- [28] C. Gomes and M. Izadi, “Electrical Isolation of Two Earthing Systems under Lightning Conditions with TiO₂ Nano Fluid Barrier,” *2019 15th International Symposium on Lightning Protection, SIPDA 2019*, no. October, pp. 1–5, 2019. [Online]. Available: <https://doi.org/10.1109/SIPDA47030.2019.8951640>
- [29] P. R. Bonda and M. K. Mishra, “Optimized Design of Earthing System for Substations with High Soil Resistivity and Limited Plot Area,” in *2018 20th National Power Systems Conference, NPSC 2018*. Institute of Electrical and Electronics Engineers Inc., 2018. [Online]. Available: <https://doi.org/10.1109/NPSC.2018.8771780>
- [30] M. Salam, Q. Rahman, S. Ang, and F. Wen, “Soil resistivity and ground resistance for dry and wet soil,” *Journal of Modern Power Systems and Clean Energy*, vol. 5, no. 2, pp. 290–297, 2017. [Online]. Available: <https://doi.org/10.1007/s40565-015-0153-8>
- [31] C. Cardoso, L. Rocha, A. Leiria, and P. Teixeira, “Validation of an integrated methodology for design of grounding systems through field measurements,” in *CIREd - Open Access Proceedings Journal*, vol. 2017, no. 1, 2017, pp. 897–901. [Online]. Available: <https://doi.org/10.1049/oap-cired.2017.0452>
- [32] K. P. Sengar and K. Chandrasekaran, “Designing of cost minimum substation grounding grid system using DE, SCA, and HDESCA techniques,” *IET SCIENCE MEASUREMENT & TECHNOLOGY*, vol. 13, no. 9, pp. 1260–1267, 2019. [Online]. Available: <https://doi.org/10.1049/iet-smt.2019.0021>
- [33] M. Campaña, P. Masache, E. Inga, and D. Carrión, “Estabilidad de tensión y compensación electrónica en sistemas eléctricos de potencia usando herramientas de simulación,” *Ingenius*, vol. 2, no. 1, 2022. [Online]. Available: <https://doi.org/10.17163/ings.n28.2022.07>
- [34] M. H. Elmashtoly, H. I. Anis, and A. Emam, “Mitigating Hazardous Potentials Near Pipelines Using

- Passive Grounding Grids,” *IEEE Access*, vol. 9, pp. 121 957–121 963, 2021. [Online]. Available: <https://doi.org/10.1109/ACCESS.2021.3109309>
- [35] L. Amaya and E. Inga, “Location of Harmonic Distortions in Electrical Systems using Compressed Sensing,” *Ingeniería y Competitividad*, vol. 24, no. 1, p. 15, 2022. [Online]. Available: <https://bit.ly/3xA4zqI>
- [36] N. Permal, M. Osman, A. M. Ariffin, and M. Z. Abidin Ab Kadir, “Effect of non-homogeneous soil characteristics on substation grounding-grid performances: A review,” *Applied Sciences (Switzerland)*, vol. 11, no. 16, 2021. [Online]. Available: <https://doi.org/10.3390/app11167468>
- [37] P. Musil, P. Mlynek, J. Slacik, and J. Pokorny, “Simulation-based evaluation of the performance of broadband over power lines with multiple repeaters in linear topology of distribution substations,” *Applied Sciences (Switzerland)*, vol. 10, no. 19, pp. 1–24, 2020. [Online]. Available: <https://doi.org/10.3390/app10196879>
- [38] B. Anggoro, R. S. Utami, and L. Handayani, “Optimal Design of Grounding System Substation, Case Study : 275/150 kV Sigli Substation,” *Proceedings of the 2nd International Conference on High Voltage Engineering and Power Systems: Towards Sustainable and Reliable Power Delivery, ICHVEPS 2019*, vol. 1, 2019. [Online]. Available: <https://doi.org/10.1109/ICHVEPS47643.2019.9011064>
- [39] X. Tian, Z. Lan, F. Huo, Z. Huang, S. Huang, Y. Ding, J. Geng, X. Yan, and Y. Liu, “Calculation of electric field on substation equipment considering AC Ion flow field,” *Mathematical Problems in Engineering*, vol. 2020, 2020. [Online]. Available: <https://doi.org/10.1155/2020/3914872>
- [40] Z. G. Datsios and P. N. Mikropoulos, “Safety performance evaluation of typical grounding configurations of MV/LV distribution substations,” *Electric Power Systems Research*, vol. 150, pp. 36–44, 2017. [Online]. Available: <https://doi.org/10.1016/j.epsr.2017.04.016>
- [41] Z. Liu, W. Shi, and B. Zhang, “Numerical analysis of transient performance of grounding grid with lightning rod installed on multi-grounded frame,” *Energies*, vol. 14, no. 12, pp. 1–13, 2021. [Online]. Available: <https://doi.org/10.3390/en14123392>
- [42] V. P. Androvitsaneas, K. D. Damianaki, C. A. Christodoulou, and I. F. Gonos, “Effect of soil resistivity measurement on the safe design of grounding systems,” *Energies*, vol. 13, no. 12, 2020. [Online]. Available: <https://doi.org/10.3390/en13123170>
- [43] B. KÜchler, U. Schmidt, and J. Hänsch, “Harmonic current distribution in grounding systems of cabled medium voltage grids during single-pole ground fault,” *Energies*, vol. 14, no. 4, 2021. [Online]. Available: <https://doi.org/10.3390/en14041110>
- [44] F. Sinchi-sinchi, C. Coronel-naranjo, A. Barragán-escandón, and F. Quizhpi-palomeque, “Soil Treatment to Reduce Grounding Resistance by Applying Low-Resistivity Material (LRM) Implemented in Different Grounding Systems Configurations and in Soils with Different Resistivities,” *Applied Sciences*, vol. 12, 2022. [Online]. Available: <https://doi.org/10.3390/app12094788>
- [45] F. Holik, L. H. Flå, M. G. Jaatun, S. Y. Yayilgan, and J. Foros, “Threat Modeling of a Smart Grid Secondary Substation,” *Electronics (Switzerland)*, vol. 11, no. 6, pp. 1–21, 2022. [Online]. Available: <https://doi.org/10.3390/electronics11060850>



LOCATION OF DISTRIBUTED RESOURCES IN RURAL-URBAN MARGINAL POWER GRIDS CONSIDERING THE VOLTAGE COLLAPSE PREDICTION INDEX

LOCALIZACIÓN DE RECURSOS DISTRIBUIDOS EN REDES ELÉCTRICAS RURALES-URBANAS MARGINALES CONSIDERANDO EL ÍNDICE DE PREDICCIÓN DE COLAPSO DE TENSIÓN

Anabel Lemus¹ , Diego Carrión^{2,*} , Eduar Aguirre³ , Jorge W. González⁴ 

Received: 01-06-2022, Received after review: 20-06-2022, Accepted: 22-06-2022, Published: 01-07-2022

Abstract

This research focuses on the georeferenced location of distributed resources, specifically the injection of active power through distributed generation. A rural-urban marginal feeder of a distribution company in Ecuador with georeferenced information was taken as a case study, which has a three-phase primary link at a medium voltage and several single-phase branches at a medium voltage of great length to supply users who are far away from the local company's network. Consequently, to analyze the behavior of the electrical network, the Cymdist software was used to perform simulations in a steady state without and with the insertion of distributed generation. For the location of the distributed generation, the voltage collapse prediction index was used as a technique for quantifying and identifying problems in the network nodes. Moreover, based on the proposed methodology, the suitable georeferencing of the sites where it is necessary to inject active power to improve the voltage profiles and reduce the voltage collapse prediction index was obtained.

Keywords: Distributed generation, Distributed generation, Voltage collapse prediction index, Distributed resources, Electric power systems

Resumen

Esta investigación se centra en la localización georeferenciada de los recursos distribuidos, concretamente en la inyección de potencia activa a través de la generación distribuida. Se tomó como caso de estudio un alimentador marginal rural-urbano de una empresa distribuidora de Ecuador con información georeferenciada, que cuenta con un enlace primario trifásico a media tensión y varios ramales monofásicos a media tensión de gran longitud para abastecer a usuarios alejados de la red de la empresa local. En consecuencia, para analizar el comportamiento de la red eléctrica, se utilizó el software Cymdist para realizar simulaciones en estado estacionario sin y con la inserción de generación distribuida. Para la ubicación de la generación distribuida, se utilizó el índice de predicción de colapso de tensión como técnica para cuantificar e identificar problemas en los nodos de la red. Además, a partir de la metodología propuesta, se obtuvo la georeferenciación idónea de los sitios donde es necesario inyectar potencia activa para mejorar los perfiles de tensión y reducir el índice de predicción de colapso de tensión.

Palabras clave: Generación distribuida, Índice de predicción de colapso de voltaje, Recursos distribuidos, Sistemas eléctricos de potencia

¹ Master program of business administrator, Indiana Tech University, Fort Wayne - Indiana - USA.

^{2,*} Electrical Engineering Department, Universidad Politécnica Salesiana, Quito - Ecuador.
Corresponding author ✉: dcarrion@ups.edu.ec

³ Electrical Engineering Department, Universidad Don Bosco, San Salvador - El Salvador.

⁴ Electrical Engineering Department, Universidad Pontificia Bolivariana, Medellín - Colombia.

Suggested citation: Lemus, A.; Carrión, D.; Aguirre, E. and González, J. W. "Location of distributed resources in rural-urban marginal power grids considering the voltage collapse prediction index," *Ingenius, Revista de Ciencia y Tecnología*, N.º 28, pp. 25-33, 2022, DOI: <https://doi.org/10.17163/ings.n28.2022.02>.

1. Introduction

Electric power systems (EPS) are currently seeking to optimize non-conventional renewable resources, and that is why many of them have begun to change their energy matrix, betting on solar photovoltaic, low and high enthalpy solar thermal, on-shore and off-shore wind, and geothermal power plants. These generation plants have incorporated new variables in the decision and optimization processes in operation and dispatch of energy [1, 2].

The advantage of this type of solution is that it is possible to reduce the losses in the electric transmission systems, and therefore, it can be assured that the power system is efficient. The presence of DG poses new challenges in the management and operation of electricity grids. To date, it represents about 20% of the total generation of some power systems, and this figure is gradually increasing based on the energy policies of each region. An example of this change can be seen in Europe, where an energy system with less dependence on non-renewable resources, with the introduction of emission reduction policies that significantly impact electricity markets [3–6].

Another solution to this problem is the insertion of distributed energy resources (DER), which have also increased on the planet, thus seeking a sustainable energy system with fewer environmental problems and greater energy efficiency. Thus, DER management concepts have been generated, and virtual power plants (VPP) have been created. A VPP is a single actor in the electricity market and comprises several DERs. Within this new concept, the owners of the VPPs can access the electricity market while compensating for the power deficit due to intermittency in the wind and solar energy sources, accompanied by uncertainty in the behavior of demand [7–9].

With the increased penetration of DER in the electric grid, more flexibility is required on the consumption side. The flexibility in DER deployed on a distribution grid can become an attractive asset for trading in electricity markets. A VPP can provide a demand response to an aggregator operating in the market. However, this flexibility may be subject to user behavior, and local regulations in the residential sector [10].

Currently, the principle of operation of VPPs is based on demand response (DR), the most widely used and researched technique. Thus commercial and industrial load management and distributed generation are the main focus of these studies. Several factors define

the business models under which VPPs operate, such as financing method (market or incentives), target market (system services, imbalance management, a day ahead, during the day, balancing market), motivation factor (pricing structure, environmental aspect, system aspect), customer type (residential, commercial, industrial and street lighting), consumption characteristics (responsiveness, capacity, reliability, frequency, duration), DG characteristics (primary resource, responsiveness, capacity, reliability, frequency, duration), activation type (response time, duration, changes, capacity) and control mode (manual, semi-automatic or automatic) [11, 12].

Generally speaking, VPPs can respond to two types of markets: marginal markets where all generators receive the same price at the highest marginal dispatch price and pay-per-bid markets where VPPs receive the price bid by them. The operational management of the EPS depends on power flow studies using optimization and simulation techniques. The optimal DC (OPF-AC) and AC (OPF-AC) flows are the most commonly used techniques for power flow optimization. On the other hand, specialized software such as Digsilent power factory and Cymdist is used for simulation, which allows the implementation of georeferenced power flow studies, from which the different electrical parameters such as node voltage, angle, active and reactive power flows, generation dispatch and power factor can be obtained [13, 14].

Most studies have focused on studying DER in urban distribution networks, where the load is concentrated, and the benefits are achieved by establishing a technical-economic balance. However, the studies are scarce for rural and marginal urban distribution networks, so this research focuses on identifying the DER connection point based on simulation techniques in a rural georeferenced distribution system [15–17].

Through the results obtained from the simulation, the voltage collapse prediction index is determined in each node. In the nodes where the index is close to 1, it becomes a candidate node to locate a DER so that the DER connection points are determined later through the proposed heuristic methodology. For this purpose, the voltage profile, the loss reduction, and the power factor improvement are verified. Figure 1 shows the conceptualization of ideas raised in this research.

The article is organized as follows: section 2 refers to the concepts related to distributed resources, section 3 defines the problem and the case studies, section 4 analyzes the results, and section 5 shows the main conclusions.

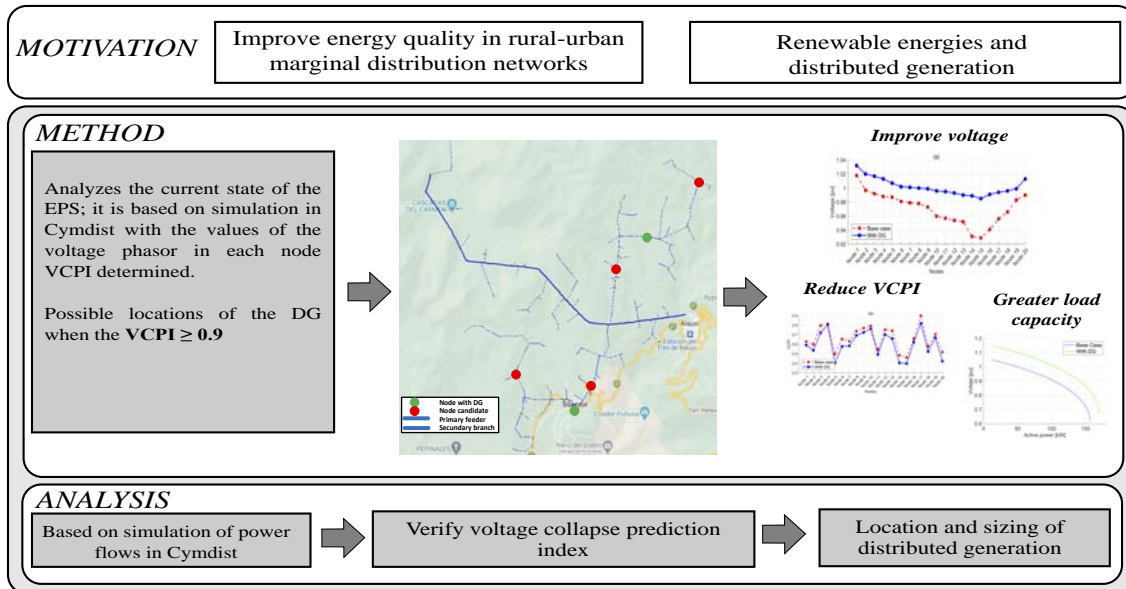


Figure 1. Research conceptualization

1.1. Related Works

One of the alternatives available in current EPS to alleviate congestion in the distribution and transmission networks is distributed energy resources (DER), a set of technologies that can be deployed in the electric grid. Among these is distributed generation, which seeks to generate electricity very close to the consumption points. Other technologies used are the Battery Energy Storage Systems (BESS), which seek to store the energy that is not used during low-demand hours so that it can be used during peak hours, thus reducing the demand for a centralized generation.

1.1.1. Distributed generation

Distributed generation has become one of the primary sources of non-conventional natural resources for electricity generation at sites very close to the load. Thus, DG is connected to distribution networks at medium or low voltage levels, depending on the type of contract and its power. The leading primary energy used for electricity generation in DG is solar, specifically solar photovoltaic, which can be implemented from small plants located on the terraces of residences to generation complexes that can reach up to MW of installed power [18–20].

The DG has made it necessary for distribution systems to become bi-directional networks, thereby reducing congestion in transmission networks and losses in power systems. Now users can be part of the electricity market, producing their energy and injecting the surplus into the public grid, [21, 22]. The energy management of the DG is carried out through the VPPs that allow an optimal dispatch of resources

based on measurement and monitoring systems of the DG, the BESS, and controllable load resources. The control strategy of VPPs can be divided into three different patterns: centralized control, distributed control, and fully distributed control; according to their structure and information, depending on the roles and responsibility, VPP is distinguished as commercial VPP (CVPP), technical VPP (TVPP) and combined VPP [7, 23].

Communications play a fundamental role in the operation and management of the VPP. It is possible to have an online measurement in time of the primary energy resources that are used for electricity generation, the necessary demand in each time interval, imbalances in the networks, and uncovered energy needs that must be imported from public networks for adequate demand management [24, 25].

1.1.2. Voltage collapse prediction index

In the operation of power systems, many parameters define the behavior of EPS, such as power quality indexes, stability indexes, reliability indexes, voltage profile, and line chargeability, among others. Power flow studies allow quantifying each of the electrical parameters in the EPS steady-state operation and are the mathematical tool used by simulators to show the behavior of power systems under different generation and demand scenarios.

There are different reliability and stability indexes to verify the state of power systems. For example, the EPS are analyzed under the N-1 contingency state to study reliability. For this purpose, the contingency ranking index is used to determine the degree of contingency affectation, thus obtaining information that

will help plan the expansion and improvement of the EPS. On the other hand, different indexes have been proposed to identify voltage, angle, frequency, charge-ability, and load fluctuation failures [26–29].

The identification of the operative limits allows determining nodes with a deficiency in which the power system must be improved so that through the VCPI, it is possible to locate problem nodes in which, before any change in the load the power system can collapse, the VCPI is determined through (1) [30]. VCPI is based on the electrical network's voltage phasors and admittance characteristics and calculated for each node of the EPS. The VCPI values are between 0 and 1, and the closer it is to 1, the higher the probability of voltage collapse at that node.

$$VCPI_k = \left| 1 - \frac{\sum_{m \neq k}^n V'_m}{V_k} \right| \quad (1)$$

$$V'_m = \frac{Y_{km}}{\sum_{j \neq k}^n Y_{kj}} V_m \quad (2)$$

Where:

- V_m is the voltage phasor at node m,
- V_k is the voltage phasor at node k,
- Y_{km} is the admittance between nodes k and m,
- Y_{kj} is the admittance between nodes k and j.

The VCPI is a global technique that considers the effects of the loads in the other nodes on a particular node, which can be linked to the voltage stability studies achieved by analyzing the P-V curves; therefore, it can be said that the VCPI can predict a node in which voltage instability may occur in power systems.

Table 1 shows significant contributions in planning electrical distribution systems, which in recent years have focused on topics such as renewable energies, distributed resources, distributed generation, virtual power plants, and demand management. The principal electrical parameters analyzing by other authors are voltage, congestion, power factor, and Geo-referenced.

Table 1. Summary of related works

Author	Year	Objetives	Parameters considered				Thematic		
			Voltage	Congestion	Stability	Geo-referenced	Distributed generation	Virtual power plant	Planning
Sena [20]	2022	Electrical network evaluation	✓	✓	-	-	✓	-	✓
Heang [18]	2022	Reduces active power losses	✓	-	-	-	-	-	✓
Quinteros [13]	2022	Power system restoration	✓	✓	✓	-	-	-	✓
Carrión [28]	2021	Improve electrical power systems	✓	✓	✓	✓	-	-	✓
Aderibigbe [19]	2021	Optimal placement of distributed generators	✓	✓	-	-	✓	✓	✓
Mosquera [3]	2020	Optimal virtual power plant location	✓	-	-	-	-	✓	✓
Valenzuela [23]	2019	Management of electrical distribution networks	✓	-	-	✓	-	-	✓
Valenzuela [25]	2019	Planning underground distribution networks	-	✓	-	✓	-	-	✓
Danish [26]	2019	Voltage stability index	✓	✓	-	✓	-	-	-
Inga [22]	2018	Planning electrical distribution network	✓	✓	-	✓	-	-	✓
Present work		Planning and sizing of electrical distribution network	✓	✓	✓	✓	✓	-	✓

2. Materials and methods

2.1. Problem and Methodology

Feeder 1500090T01 of the Riobamba electric company (EERSA S.A.) has been taken as a case of analysis since the concession area of the distribution company corresponds to rural and marginal urban networks in its more significant percentage. Feeder 1500090T01 is shown in figure 2, in which it can be seen that it has two (2) links to the sub-transmission ring and two single-phase derivations to the users; as can be seen, the coverage of this feeder is 100% rural, where its users are far away from each other, and there are service quality problems. As it is a marginal urban, rural network, only the primary link is three-phase, and all the branches are single-phase, which generates an additional problem about the power balance, so it is assumed that the location of the proposed DG will be adapted to the voltage profiles and several phases existing at the connection point.

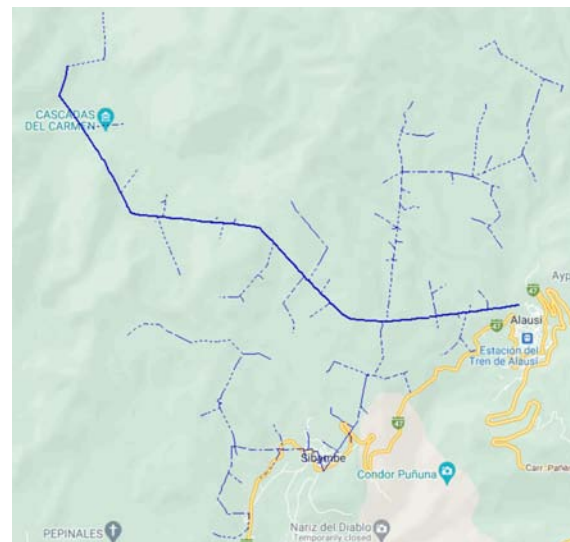


Figure 2. Feeder 1500090T01 of EERSA S.A. Source: Cymdist

Figure 3 shows the equivalent single-line diagram of the power system considered for the analysis, in which the two secondary branches can be distinguished. The nodes of the secondary branches are identified by the letter U for the upper branch. And by the letter D for the lower branch. The upper branch comprises 20 nodes connected by the end-users, and the lower branch has 26 nodes.

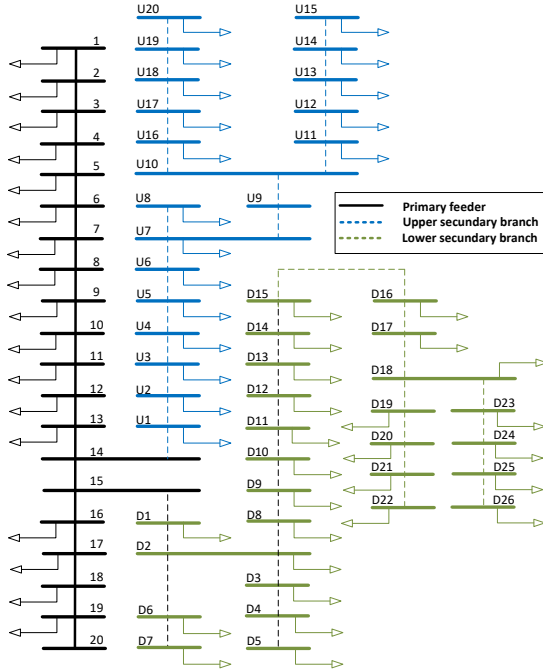


Figure 3. Feeder 1500090T01 of EERSA S.A. Source: Cymdist

The analysis of the power flows performed through simulation in Cymdist, with which the current state of the network is obtained, data that are the starting point for the location of distributed resources in the network; with these values, we proceed to determine the VCPI. Since there are different voltage profiles, the studies will be carried out in p.u., values whose base is referred to as the main three-phase link, in such a way that the different electrical variables are unified. Algorithm 1 defines the methodology for DG insertion in the nodes that present a VCPI very close to 1, assuming the existence of the primary resource, physical space, and without generating a more significant environmental impact.

Table 2. Variables related to the mathematical model

Symbol	Description
V_i	Voltage at node i .
$P_{i,j}$	Active power flow between nodes i and j .
$Q_{i,j}$	Reactive power flow between nodes i and j .
Pd_i	Active power demand at node i .
Qd_i	Reactive power demand at node i .
n	Number of EPS nodes.
Pot_{DG_i}	DG active power.

Algorithm 1 DG location based on VCPI

Step: 1 Input data

Electrical Power System Parameterization
 Generators, lines, transformers, loads, connectivity matrix
 Steady state simulation by Cymdist
 Save $[V_i, P_{i,j}, Q_{i,j}, Pd_i, Qd_i]$.

Step: 2 VCPI determination

for $i = 1 : n$
 $VCPI_i = VCPI_k$
 end for

Step: 3 Possible nodes for DG

Sort VCPI
 for $i = 1 : n$
 $VCPI_i \geq 0.9$
 Select node $can_{d_i} = i$
 end for

Step: 4 DG location and sizing

Locate DG in $node_i$
 $Pot_{DG} = 1$
If $VCPI \geq 0.9$
 Discard node
else
 for $i = 1 : length(can_{d_i})$
 while $VCPI_i \geq 0.9$
 $Pot_{DG_i} = Pot_{DG_i} + 1$
 end while
 end for
end if

Step: 5 Show results

$can_{d_i}, Pot_{DG_i}, P_{i,j}, Q_{i,j}, V_i$

The methodology to ideal deploy DG in power systems is shown in Algorithm 1, in which VCPI is considered the primary constraint; in Step 1, the EPS steady-state simulation in Cymdist is considered, and the different electrical parameters are stored. In Step 2, the steady-state of the power system is analyzed, and the VCPI at each node is determined. In Step 3, the VCPI comparison is performed, and the highest VCPI values are taken as possible DG locations. In Step 4, the location and sizing of the DG are performed. Finally, in Step 5, the results of the proposed methodology applied in the simulation in Cymdist are shown. For the sizing of the DG, 1 kW steps were considered, comparing the previous VCPI with the new one, as well as voltage profiles and line congestion. Table 2 shows the notation of variables used in Algorithm 1.

The proposed methodology analyzes the current state of the EPS; it is based on simulation in Cymdist,

with the values of the voltage phasor in each node VCPI determined. This index is the decision parameter for the possible locations of the DG when the $VCPI \geq 0.9$, each node which, after implementing DG, reduces its $VCPI \leq 0.9$ is considered like nodes in which DG should be implemented. In this way, once it has the possible locations, place the DG in those nodes, and if it does not reduce the VCPI, the node is discarded. For DG sizing, incremental steps of 1kW were performed until the EPS obtains a VCPI value of ≤ 0.9 at all nodes. Once the nodes in which DG should be implemented and its power capacity are determined, the current state is analyzed, and it is verified if it improved the voltage profile and stability by analyzing the P-V crossovers.

3. Results and discussions

3.1. Analysis of Results

This index identified the possible nodes where DG can be located to improve the indicator above without affecting the other electrical parameters. Based on the simulation in the Cymdist software, the EPS steady-state power flows were obtained, and with this, applying algorithm one and based on the voltage phasors, the VCPI at each node was determined. The location of the possible nodes and the final location of the DG can be seen in Figure 2.

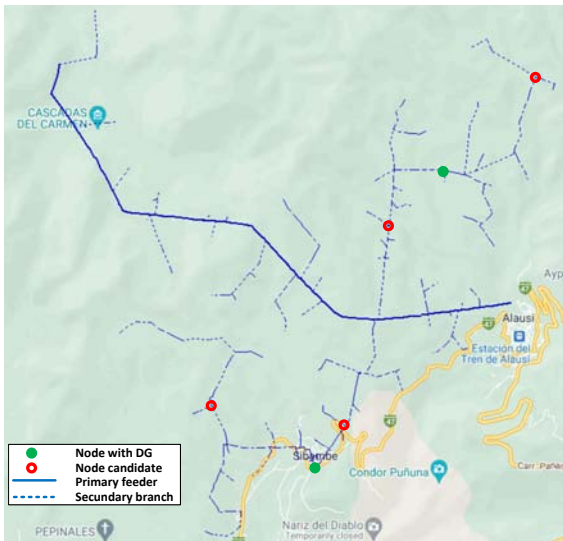


Figure 4. DG georeferenced location

As shown in Figure 4, the location of the DG is not in the three-phase network but in two of the single-phase branches, which is why the DG systems must also be single-phase. The DG system in the upper branch is sized with a value of 17 kW at node U8, whose coordinates are Lat.: -2.1669009, Long.: -78.8633971. The value includes the VCPI improved in all the nodes of

that branch. On the other hand, in the lower branch, the DG power was 32 kW at node D12, whose coordinates are Lat.: -2.2292529, Long.: -78.8900419, which, as in the lower branch, improves the VCPI of the entire branch.

The voltage profile in the main feeder can be seen in Figure 5 (a) and in the upper branch Figure 5 (b) and lower Figure 5 (c); in the three cases, it can be seen how the voltage improves after the DG enters the points selected by the proposed methodology. On the other hand, Figure 6 shows the comparison of the VCPI before and after DG insertion, both for the main feeder (a) and the upper (b) and lower (c) branches.

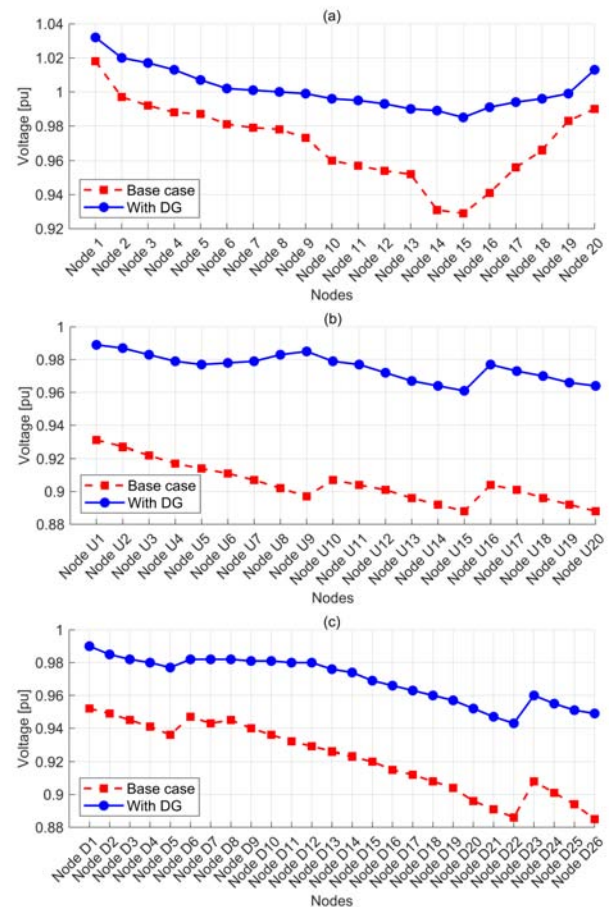


Figure 5. Voltage profile at nodes

VCPI try to reduce their original values, so it can be asserted that the quality of electrical service improves in these branches, which is undoubtedly one of the electrical parameters that power system planners are looking for nowadays.

Considering that modifications have been made to the EPS compared to its initial state, it is necessary to verify the overall operation of the distribution network, and one way to do this is to analyze the system's stability. For the proposed case based on the VCPI, it is necessary to study the voltage stability, which is done

through the P - V curves. Consequently, the nodes of the main feeder where the secondary branches are connected, nodes 14 and 15, have been considered.

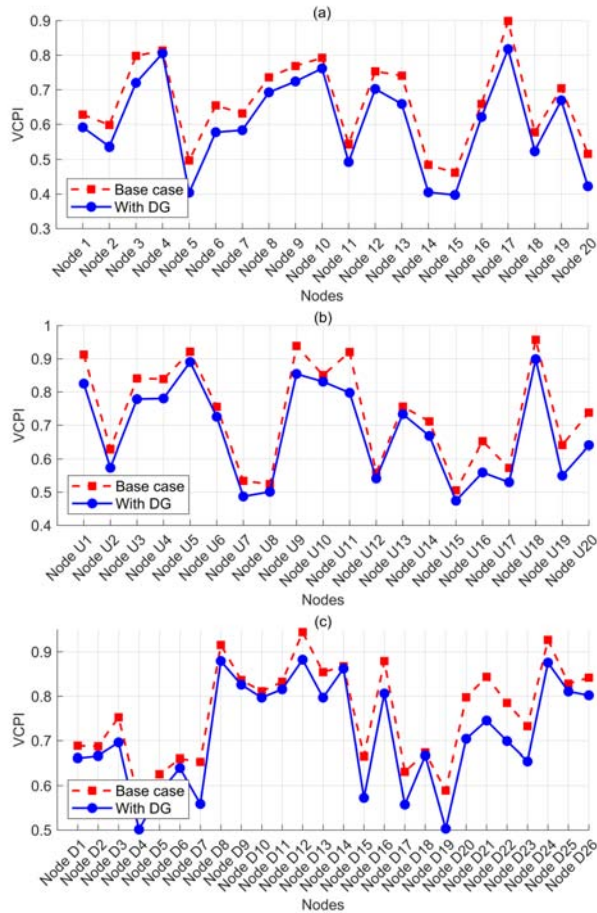
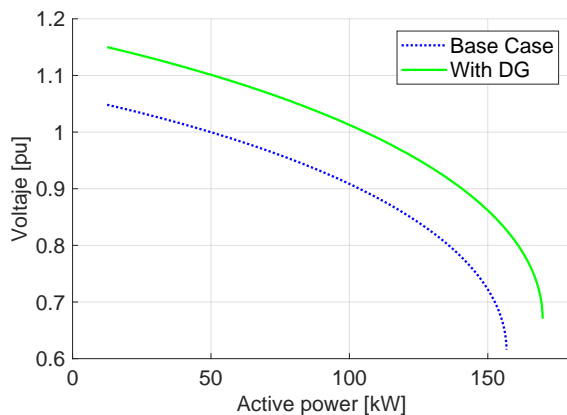
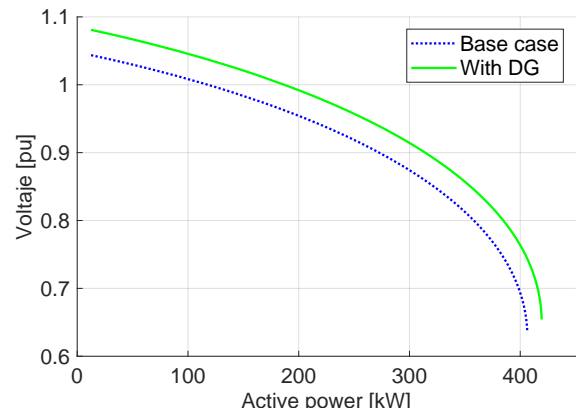


Figure 6. VCPI at nodes

Figure 7 (a) shows the P-V curve for node 14. It can be seen how the voltage increases with the fluctuation of the total load of the upper branch, similar to the Hopf bifurcation shifts to the right. A similar situation can be seen in Figure 7 (b), showing the results at node 15, which feeds the lower branch.



(a) P-V curve in node 14



(b) P-V curve in node 15

Figure 7. P - V curves (a) Node 14. (b) Node 15

4. Conclusions

The different studies that can be achieved through simulation techniques are innumerable. They are often despised due to the lack of interface or knowledge to extract their parameters and use them in modeling programs such as Matlab or Phyton. For the case study presented, the databases of the results were extracted. Through Matlab, the proposed methodology was implemented based on the results, thus ideal locating the possible points at which power can be injected from a DG. The location and sizing of the DG improved the voltage profiles of the entire EPS, contrary to what happens when reactive compensation is performed, which only improves the voltage profile in the vicinity of the reactive injection point.

It was possible to demonstrate that through the VCPI, it is possible to detect nodes with weaknesses in the power system, and this can be used for different studies; for the case proposed through the analysis of this parameter, it was possible to locate and dimension two active power injection points in a distribution network.

It is possible to analyze georeferenced power systems with georeferenced data and not only have the examples stipulated in the literature, such as the CIGRÉ and IEEE models. It is now possible to access the databases of distribution companies and provide real solutions to their problems. It is essential to highlight that through Cymdist.

The georeferencing of the active power injection point is very useful to contrast with the existing primary resources at the site and determine what type of primary energy can be used to solve the drawbacks of the power grid.

References

- [1] P. Del Río and P. Mir-Artigues, “Combinations of support instruments for renewable electricity in Europe: A review,” *Renewable and Sustainable Energy Reviews*, vol. 40, pp. 287–295, 2014. [Online]. Available: <https://doi.org/10.1016/j.rser.2014.07.039>
- [2] M. A. Salmani, A. Anzalchi, and S. Salmani, “Virtual Power Plant: New Solution for Managing Distributed Generations in Decentralized Power Systems,” in *2010 International Conference on Management and Service Science*, 2010, pp. 1–6. [Online]. Available: <https://doi.org/10.1109/ICMSS.2010.5577383>
- [3] F. Mosquera, “Localización óptima de plantas virtuales de generación en sistemas eléctricos de potencia basados en flujos óptimos de potencia,” *I+D Tecnológico*, vol. 16, no. 2, 2020. [Online]. Available: <https://doi.org/10.33412/idt.v16.2.2827>
- [4] A. Riofrio and D. Carrión, “Approach and Deployment of Distributed Generation. State-of-art Based on Induction Cooker System,” in *ANDESCON 2014*, 2014. [Online]. Available: <https://doi.org/10.1109/ANDESCON.2014.7098544>
- [5] S. Singh, A. R. Gautam, and D. Fulwani, “Constant power loads and their effects in DC distributed power systems: A review,” *Renewable and Sustainable Energy Reviews*, vol. 72, no. December 2015, pp. 407–421, 2017. [Online]. Available: <https://doi.org/10.1016/j.rser.2017.01.027>
- [6] Z. Ren, W. Yan, C. Ding, J. Yu, and X. Zhao, “Probabilistic optimal power flow analysis of virtual power plant containing photovoltaic generation,” *Asia-Pacific Power and Energy Engineering Conference, APPEEC*, vol. 2015-March, no. March, 2014. [Online]. Available: <https://doi.org/10.1109/APPEEC.2014.7066012>
- [7] H. Saboori, M. Mohammadi, and R. Taghe, “Virtual power plant (VPP), definition, concept, components and types,” *Asia-Pacific Power and Energy Engineering Conference, APPEEC*, 2011. [Online]. Available: <https://doi.org/10.1109/APPEEC.2011.5749026>
- [8] P. Nezamabadi and G. Gharehpetian, “Electrical energy management of virtual power plants in distribution networks with renewable energy resources and energy storage systems,” *16th Electrical Power Distribution Networks Conference*, pp. 1–5, 2011. [Online]. Available: <https://bit.ly/3yqQznn>
- [9] M. Peikherfeh, H. Seifi, and M. K. Sheikh-El-Eslami, “Optimal dispatch of distributed energy resources included in a virtual power plant for participating in a day-ahead market,” *3rd International Conference on Clean Electrical Power: Renewable Energy Resources Impact, ICCEP 2011*, pp. 204–210, 2011. [Online]. Available: <https://doi.org/10.1109/ICCEP.2011.6036275>
- [10] L. Exel and G. Frey, “Toward a decentralized forecast system for distributed power generation,” *ENERGYCON 2014 - IEEE International Energy Conference*, pp. 1210–1217, 2014. [Online]. Available: <https://doi.org/10.1109/ENERGYCON.2014.6850577>
- [11] L. Hernandez, C. Baladron, J. Aguiar, B. Carro, A. Sanchez-Esguevillas, J. Lloret, and J. Masana, “A Survey on Electric Power Demand Forecasting: Future Trends in Smart Grids, Microgrids and Smart Buildings,” *Communications Surveys & Tutorials, IEEE*, no. 99, pp. 1–36, 2014. [Online]. Available: <https://doi.org/10.1109/SURV.2014.032014.00094>
- [12] P. Asmus, “Microgrids, Virtual Power Plants and Our Distributed Energy Future,” *The Electricity Journal*, vol. 23, no. 10, pp. 72–82, 2010. [Online]. Available: <https://doi.org/10.1016/j.tej.2010.11.001>
- [13] F. Quinteros, D. Carrión, and M. Jaramillo, “Optimal Power Systems Restoration Based on Energy Quality and Stability Criteria,” *Energies*, vol. 15, no. 6, 2022. [Online]. Available: <https://doi.org/10.3390/en15062062>
- [14] T. Kishore and S. Singal, “Optimal economic planning of power transmission lines: A review,” *Renewable and Sustainable Energy Reviews*, vol. 39, pp. 949–974, 2014. [Online]. Available: <https://doi.org/10.1016/j.rser.2014.07.125>
- [15] V. C. Güngör, D. Sahin, T. Kocak, S. Ergüt, C. Buccella, S. Member, C. Cecati, and G. P. Hancke, “Smart Grid Technologies : Communication Technologies and Standards,” *IEEE Transactions on Industrial Informatics*, vol. 7, no. 4, pp. 529–539, 2011. [Online]. Available: <https://doi.org/10.1109/TII.2011.2166794>
- [16] U. Akpan, M. Essien, and S. Isihak, “The impact of rural electrification on rural micro-enterprises in niger delta, nigeria,” *Energy for Sustainable Development*, vol. 17, no. 5, pp. 504–509, 2013. [Online]. Available: <http://dx.doi.org/10.1016/j.esd.2013.06.004>
- [17] D. Carrion, E. García, J. Gonzalez, I. Isaac, G. Lopez, and R. Hincapie, “Método Heurístico de Ubicación Óptima de Centros de Transformación

- y Enrutamiento de Redes Eléctricas de Distribución,” *Revista Técnica "Energía"*, vol. 4, no. 2, p. 20, 2015. [Online]. Available: <https://doi.org/10.37116/REVISTAENERGIA.V13.N1.2017.11>
- [18] S. Heang and V. Vai, “Optimal Network Reconfiguration with DGs Placement and Sizing in a Distribution System Using Hybrid SOE and GA,” in *2022 19th International Conference on Electrical Engineering/Electronics, Computer, Telecommunications and Information Technology (ECTI-CON)*, no. 1. IEEE, 2022, pp. 2–5. [Online]. Available: <https://doi.org/10.1109/ECTI-CON54298.2022.9795530>
- [19] M. A. Aderibigbe, A. U. Adoghe, F. Agbetuyi, and A. E. Airoboman, “A review on optimal placement of distributed generators for reliability improvement on distribution network,” *2021 IEEE PES/IAS PowerAfrica, PowerAfrica 2021*, 2021. [Online]. Available: <https://doi.org/10.1109/PowerAfrica52236.2021.9543266>
- [20] S. K. Sena, “An Approach to Detect Islanding in Photovoltaic Based Distributed Generation Systems using Sequence Components of Voltage,” in *2022 IEEE International Conference on Distributed Computing and Electrical Circuits and Electronics (ICDCECE)*. IEEE, 2022, pp. 1–6. [Online]. Available: <https://doi.org/10.1109/ICDCECE53908.2022.9792918>
- [21] W. Pavón, E. Inga, and S. Simani, “Optimal routing an ungrounded electrical distribution system based on heuristic method with micro grids integration,” *Sustainability*, vol. 11, no. 6, pp. 1–18, 2019. [Online]. Available: <https://doi.org/10.3390/su11061607>
- [22] E. Inga, M. Campaña, and R. Hincapié, “Optimal Sizing of Electrical Distribution Networks considering Scalable Demand and Voltage,” *2018 IEEE 1st Colombian Conference on Applications in Computational Intelligence, ColCACI 2018 - Proceedings*, vol. 1, no. 1, pp. 1–6, 2018. [Online]. Available: <https://doi.org/10.1109/ColCACI.2018.8484859>
- [23] A. Valenzuela, I. Montalvo, and E. Inga, “A decision-making tool for electric distribution network planning based on heuristics and georeferenced data,” *Energies*, vol. 12, no. 21, 2019. [Online]. Available: <https://doi.org/10.3390/en12214065>
- [24] F. Heimgaertner and M. Menth, “Distributed Controller Communication in Virtual Power Plants Using Smart Meter Gateways,” *2018 IEEE International Conference on Engineering, Technology and Innovation, ICE/ITMC 2018 - Proceedings*, pp. 1–6, 2018. [Online]. Available: <https://doi.org/10.1109/ICE.2018.8436311>
- [25] A. Valenzuela, E. Inga, and S. Simani, “Planning of a Resilient Underground Distribution Network Using Georeferenced Data,” *Energies*, vol. 12, no. 4, p. 644, 2019. [Online]. Available: <http://www.mdpi.com/1996-1073/12/4/644>
- [26] M. S. S. Danish, T. Senjyu, S. M. S. Danish, N. R. Sabory, K. Narayanan, and P. Mandal, “A recap of voltage stability indices in the past three decades,” *Energies*, vol. 12, no. 8, pp. 1–18, 2019. [Online]. Available: <https://doi.org/10.3390/en12081544>
- [27] R. Mahanty and P. Gupta, “Voltage stability analysis in unbalanced power systems by optimal power flow,” *IEE Proceedings - Generation, Transmission and Distribution*, vol. 151, no. 3, pp. 201–212, 2004. [Online]. Available: <https://doi.org/10.1049/ip-gtd:20050011>
- [28] D. Carrión, E. García, M. Jaramillo, and J. W. González, “A Novel Methodology for Optimal SVC Location Considering N-1 Contingencies and Reactive Power Flows Reconfiguration,” *Energies*, vol. 14, no. 20, pp. 1–17, 2021. [Online]. Available: <https://doi.org/10.3390/en14206652>
- [29] D. Carrión, J. Palacios, M. Espinel, and J. W. González, “Transmission Expansion Planning Considering Grid Topology Changes and N-1 Contingencies Criteria,” in *Recent Advances in Electrical Engineering, Electronics and Energy*, Springer, Ed. Springer, pp. 266–279. [Online]. Available: https://doi.org/10.1007/978-3-030-72208-1_20
- [30] I. A. Samuel, J. Katende, C. O. Awosope, and A. A. Awelewa, “Prediction of voltage collapse in electrical power system networks using a new voltage stability index,” *International Journal of Applied Engineering Research*, vol. 12, no. 2, pp. 190–199, 2017. [Online]. Available: <https://bit.ly/39Orhn8>



PASSIVE CONTROL TOLERANT TO SENSING FAULTS IN DYNAMIC COMPENSATION DEVICES - SVC THROUGH A HYBRID STRATEGY

CONTROL PASIVO TOLERANTE A FALLOS DE SENSADO EN DISPOSITIVOS DE COMPENSACIÓN DINÁMICOS - SVC MEDIANTE UNA ESTRATEGIA HÍBRIDA

Jessica Ramírez ^{1,*} , Leony Ortiz ¹ , Alexander Aguila ¹ 

Received: 15-05-2022, Received after review: 13-06-2022, Accepted: 17-06-2022, Published: 01-07-2022

Abstract

For this research, a passive fault tolerant control system is developed for a static reactive compensator coupled to a microgrid in connected mode, oriented to those faults that result as a consequence of common damages in their sensing systems. The proposed method uses a robust optimal controller by H_∞ and artificial neural networks as a nonlinear estimation method. Simulations, validation, plant identification and controller design are carried out using a microgrid Benchmark system, programmed in Matlab/Simulink. The research shows valuable results such as: the improvement in the reliability and resilience of static compensators against sensing failures, improvements in the behavior of the output signal of the static compensator controller exposed to sensing failures and the decrease in error with respect to classic controller.

Keywords: DSTATCOM, FTC, H_∞ , Microgrids, NARX, Robust control

Resumen

Para esta investigación se desarrolla un sistema de control tolerante a fallos pasivos para un compensador reactivo estático acoplado a una micro-red en modo conectado, orientado a aquellos fallos que resultan como consecuencia de daños comunes en sus sistemas de sensado. El método planteado utiliza un controlador óptimo robusto por H_∞ y redes neuronales artificiales como método de estimación no lineal. Las simulaciones, la validación, la identificación de la planta y el diseño del controlador se llevan a cabo por medio de un sistema Benchmark de una micro-red, programado en Matlab/Simulink. La investigación muestra valiosos resultados como: el mejoramiento en la confiabilidad y resiliencia de los compensadores estáticos ante fallas de sensado, mejoras en el comportamiento de la señal de salida del controlador del compensador estático expuesto a los fallos de sensado, disminución el error con respecto al controlador clásico.

Palabras clave: Control robusto, DSTATCOM, FTC, H_∞ , Micro-red, NARX

^{1,*}Ingeniería Eléctrica, Universidad Politécnica Salesiana, Quito - Ecuador.
Corresponding author ✉: jramirezg4@est.ups.edu.ec

Suggested citation: Ramírez, J.; Ortiz, L. and Aguila, A. "Passive Control Tolerant to Sensing Faults in dynamic compensation devices - SVC through a hybrid strategy," *Ingenius, Revista de Ciencia y Tecnología*, N.º 28, pp. 34-43, 2022, DOI: <https://doi.org/10.17163/ings.n28.2022.03>.

1. Introduction

The energy needs in the earth continue to increase especially due to the rise of industries and the needs related to transportation. In this way, such requirements have led to the emergence of new forms of electricity generation through renewable energy resources and the use of networks smaller than the traditional ones called Microgrids (MG) [1–3]. MG can be understood as an small-scale electrical systems containing several distributed generators, loads, and energy storage systems [1, 4–6].

Due to the emergence of new types of loads such as electric vehicles and storage systems that work with direct current, which are connected together with alternating current loads that are the most recurrent in home networks [4]. Mixed or hybrid AC/DC type MGs have taken on special relevance for researchers, due to the feasibility offered by each type of MG, with the only need to include energy conversion devices that work with power electronics elements [7–13].

Due to their characteristics, MGs must be able to function both in connected network mode and independently, and for each mode there must be a correct operation and control, which should even be able to withstand certain problems and failures [1, 4, 13, 14]. The operations control should also consider characteristic features of certain type of generation such as wind and solar, where variability and intermittency are common; and they are aspects that should consider for an continuous, stable, safe and resilient operation of the Hybrid MR. There are differences and significant changes to a traditional electrical network, compared to features offered by MG, in especially those that operate in AC and DC. In matters related to control and the problems that could occur in the operation, such changes are directly related to the existence of distributed control operations and the existence of power flows that they are bidirectional [15, 16].

As previously indicated, one of the most relevant aspects of proper functioning of the MG is the presence of robust control; the same that should be able to withstand the existence of failures in various components of the control system and the MG.

During fault events and sensor and actuators malfunction of the various subsystems of the MG, the control systems with more traditional feedback may not be able to guarantee the system stability or performance of all components.

Therefore, there are new strategies for the management of this type of network as we can mention the fault tolerant controls (FTC) [1, 13, 14, 17]. Such strategies allow the emergence of fault-tolerant control systems (FTCS), which can overcome the aforementioned deficiencies. [18].

Fault-tolerant controls can be divided into two groups: active controls (AFTCS), which are those that

contain diagnostic strategies and fault detection in real time through the use of information. Active control systems also contain reconfiguration mechanisms that allow the MG to be maintained stable and with acceptable performance even when there are failures in various system components. [1, 18, 19].

Fault-tolerant controls that are passive are instead designed to have a single robust structure, that is, they have no way of being automatically reconfigured during fault events. Another difference is that they do not consider the information that a fault detection and diagnosis system (FDD) may have. [1, 18].

Fault tolerant control systems have been studied extensively and there are several proposals that work in connected network mode and also when MG operates independently. The operation in connected mode to the conventional network is supported in the parameters of the main network and most of the proposals that have been previously established are related to the use of capacitor banks and flexible AC transmission systems (FACTS). In the case of advanced control strategies, voltage regulations are also used in the generation zones, although the controllers can be directly in the element to be controlled, as shown in Figure 1. [1], [20].

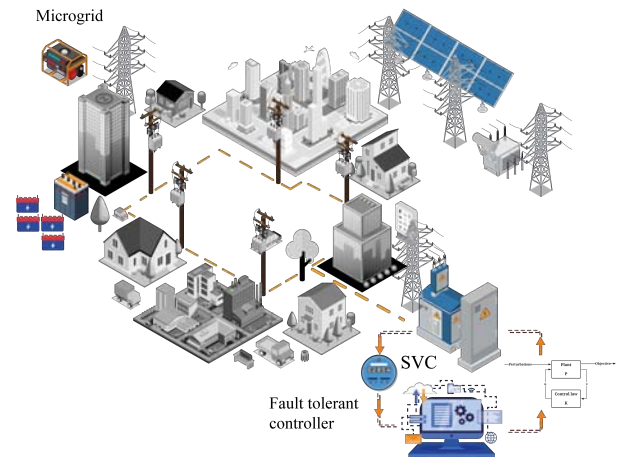


Figure 1. Fault tolerant control

On the other hand, in isolated operation, the researchers have determined that there are other needs, such as the correct choice of the generator system that becomes the frequency leader. [20].

Mainly when there is a high penetration of generation sources with renewable energies in which the inherent characteristics of intermittence and discontinuity and complicate the use of traditional MG control strategies [20].

In [20] an FTC system is presented that allows fault tolerance based on an adaptive controller based on the model through a PID control tuned by genetic algorithm and a structure with intelligence, it is stated that this structure guarantees monitoring of the conditions of the MR, which allows regulation of frequency,

voltage amplitude. The existence of fault scenarios including actuator failures, sudden load connection, as well as short duration faults is proposed; which allows testing the performance of the proposed method.

In [21] an FTC strategy is presented to deal with loss of effectiveness and lock-in-place faults that occur on an SVC, the strategy used in that document use an adaptive backstepping technique with a dynamic surface control (DSC). The results of the investigation shows that the strategy can produce a good performance over signals in the closed-loop system under the occurrence of the described faults.

Other investigations center their attention on fault-tolerant controllers for a wide area control systems but doesn't center on an SVC. The controller generally finds a way to deal with faults over communications of signals to control de whole system while other investigations use static or dynamic compensations systems to control the angle of synchronous machines where robust control try to maintain the machine in good operational conditions [22].

2. Materials and methods

2.1. Microgrids

MGs are in general a revolutionary set of elements that work together to generate, transport and supply power to a set of loads in a certain geographical area that can operate in isolated or with an interconnection link with a conventional network. This implies that a MG must have generation elements and loads that seek a constant balance based on the available resources at a technological and environmental level. In general, MGs make use of generation systems that take advantage of renewable resources such as water, wind, heat or radiation from the sun. [23,24].

Generation systems and consumption points are linked by distribution systems that can be AC or DC, as shown in figure 1, with the corresponding need to have AC/DC or DC/AC conversion elements. On the other hand, and due to the need to cover deficiencies that could arise from the implications of a complete system but with limited resources, reactive compensation systems and even storage systems can be made available, which in the long term can improve the quality of service. [25–27].

2.2. Neuronal network

A fairly simple abstract model of the functioning of an artificial neuron can be conceived, which can be seen in Figure 2.

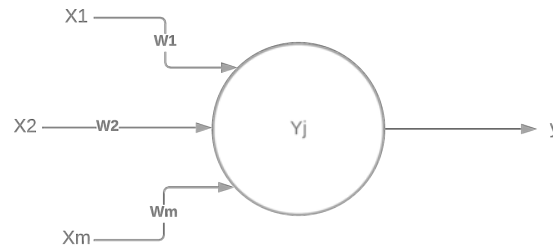


Figure 2. Artificial neuron

The artificial neuron is composed of a set of weights represented in the values W_1 , W_2 , W_m and that represents the synaptic connections of a real neuron, a vector x that composes the inputs and finally an output of the unit represented by y which is the result of an activation function.

An artificial neural network is the computational composition of multiple elementary processors composed of an adaptive system that, through an algorithm, is capable of adjusting its weights in order to improve performance with the use of samples. One of the main advantages of the use of artificial neural networks is the ease of use of training data through supervised or unsupervised processes. The supervised process occurs by making use of well-known input and output data, expecting that the output data of the neural network is as similar as possible to the output data that is available. Unsupervised learning makes use of a set of patterns that are valid to find structures or configurations that are present in the data [28].

2.3. Static VAR compensator (SVC)

Within the FACT type devices, the static reactive compensator falls into the category of those that have a bypass connection. The device in question consists of an inductor controlled by means of power electronics called thyristors and which receives the name of TCR [29]. Through the correct control of the TCR tripping, a variation of the reactance is achieved which, in the long term, implies a change in the consumption of reactive power at the connection point of the compensator, then it is possible to improve the power factor at said point. In this point the bus voltage is also checked [29–32].

The device is controlled by modifying the firing angle of the power elements that make up the SVC. This logic control is issued by control loops that may contain PI, PID controllers or even more robust options such as the one that will be implemented in the present investigation. [33–37]. The reactive compensation devices are used in the MR in order to compensate the power factor that is outside normal parameters [29–37]. Due to the effects of the loads connected to the system, an alteration in the power factor results in the affectation of the system voltage in the system bars [29–37].

On the other hand, it is usual that in the MG the generation systems require consumption or due to their own generation principles cause modifications in the reactive values which can cause a drop in the output voltage of the units and therefore a drop in power. The problem can be solved with the installation of an SVC [29–37].

2.4. H-infinite (H_∞)

It is used to achieve controllers with guaranteed performance and that are stable, the use of these models is presented as an optimization problem through which a model that meets the objective is found. One of the main advantages of the method is that it is widely applicable in multivariable systems, while part of the disadvantages include a high level of mathematical knowledge and an understanding of the system to be controlled.

The name of the method is based on the fact that the optimization is carried out on the so-called Hardy space in the positive half of the complex plane and represents the maximum value on the mentioned space, being understood as the maximum gain in any direction and at any frequency for a SISO system. It is the maximum magnitude of the frequency response. Among its uses is the reduction of the impact of a disturbance in a closed loop that can be observed as stability or performance.

The plant has inputs composed of an exogenous input that includes a reference signal, disturbances and manipulated signals. On the other hand, there are outputs between which there is an error signal that must be minimized and the measured variables that will be used as control signals in the system. By means of the measured signals and the value of K , the manipulated variables can be calculated. Expression (1) is used to formulate the problem in matrix form [17, 38, 39].

$$\begin{bmatrix} z \\ v \end{bmatrix} = P(s) \times \begin{bmatrix} w \end{bmatrix} = \begin{bmatrix} P_{11}(s) & P_{12}(s) \\ P_{21}(s) & P_{22}(s) \end{bmatrix} \times \begin{bmatrix} w \end{bmatrix} \quad (1)$$

It is possible to calculate the dependence of z on w by means of the lower linear fractional transformation (LFT) which is shown in expression (2), where $F_l \times (P, K)$ represents the result of the LFT that can be used to find the relation between z and w .

$$\begin{aligned} z &= F_l \times (P, K) \times w \\ F_l \times (P, K) &= P_{11} + P_{12} \times K \times \\ & (I - P_{22} \times K)^{-1} \times P_{21} \end{aligned} \quad (2)$$

According to the aforementioned, it is known that the objective of the method in question requires finding

a controller K such that $F_l \times (P, K)$ is minimized according to the norm H_∞ being the same applicable to the design carried out by means of H_2 . There are some techniques to achieve the objective, among which the Youla-Kucera parameterization that leads to very high order controllers, methods based on the resolution of 2 Riccati equations requiring many simplifications and finally the method based on optimization with a reformulation of Riccati using linear matrices of inequalities, a method that requires few assumptions [17].

2.5. Fault tolerant controller design

The control signal is manipulated directly by the controller, which replaces a traditional PI type controller that was part of the control system and whose performance will be compared with the H_∞ controller.

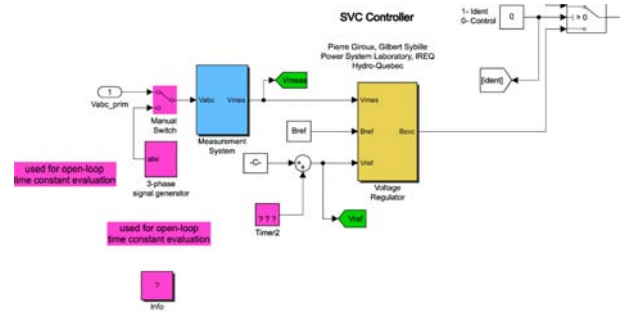


Figure 3. Controller zone

Figure 3 illustrates the area of the controller into which the robust controller is inserted. It can be seen that the variables that are measured are those that correspond to voltage signals in addition to having values that correspond to references necessary to generate adequate control signals.

On the other hand, figure 4 shows the way in which the designed controller is placed inside the voltage regulator considering the need to reduce the error to 0. The error corresponds to those values that result from the difference between the voltage measured and the reference voltage in addition to subtracting the value corresponding to the control signal in this case represented by the B_{svc} . It is understood that the controller acts directly on the control signal.

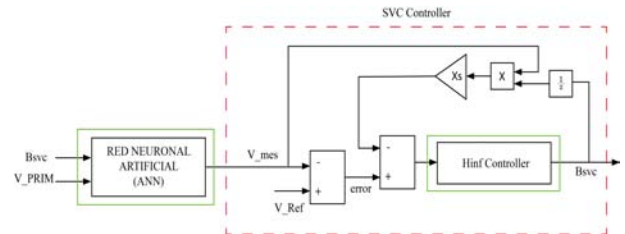


Figure 4. Voltage regulator design

2.6. Problem formulation

A controller is said to be fault tolerant when this controller is capable of maintaining the control objectives despite the fact that it is subject to the occurrence of faults, the faults in question can be additive or non-additive faults depending on the alteration that they cause. These alterations to the measurements that in the long term create modifications in the equations of the space of states. While non-additive or multiplicative faults cause changes in the terms of the state space.

Fault tolerance can be achieved by passive or active strategies, in some cases being able to maintain the controller with changes in its parameters, while in other cases the control laws can be reconfigured [1, 13].

3. Results and Discussion

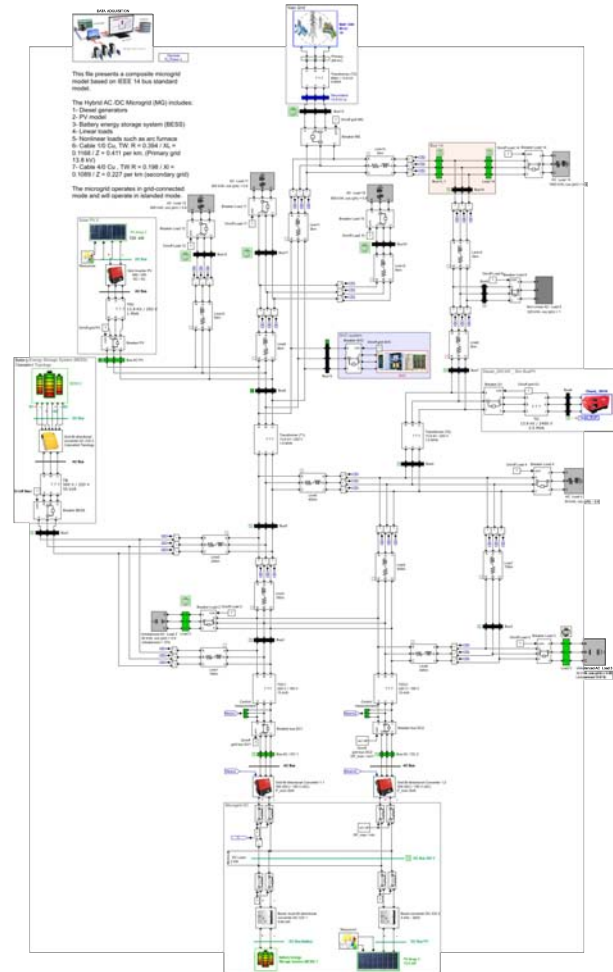


Figure 5. Microgrid Diagram

3.1. Study case

For the present study, the use of a benchmark-type test system is proposed, which represents an MG of

14 bars composed of 2 energy storage systems, 2 photovoltaic generation plants, 1 diesel generator, an one interconnection point with a conventional network. In addition to linear and non-linear loads and finally an SVC, the mentioned model can be seen in Figure 5 [3].

The controller is subjected to simulations to obtain a detailed model of the plant through the use of state spaces, the simulation process yields a plant of the SVC controller. The proposed method is tested with the occurrence of non-malicious sensing failures of incipient and abrupt type in the primary of the control system, the fault tolerant controller designed by means of the H_∞ methodology is implemented within of the SVC.

3.2. Results

The controller that is obtained through the design process proposed in this document yields the parameters for the controller according to what is shown by expression (3), where A , B , C and D represent the arrays that form the state space that describes the voltage controller region of the SVC.

$$\begin{aligned}
 A &= \begin{bmatrix} -2.85e^{-3} & -437.52 & -200.38 \\ -189.32 & -108.03 & -119.03 \\ -31.96 & 10.56 & -21.65 \end{bmatrix} \\
 B &= \begin{bmatrix} -2.25e^{+3} \\ -9.54e^{+3} \\ -2.56e^{+3} \end{bmatrix} \\
 C &= [-2.68e^{-17} \quad -6.32e^{-17} \quad 3.62e^{-19}] \\
 D &= 0
 \end{aligned} \tag{3}$$

On the other hand, the implemented neural network is designed to work with 2 inputs, each layer has a total of 10 neurons in its hidden layer while each one has 3 output neurons. There are 2 NARX type systems available and each one is used independently to work with the primary and secondary signals. Based on what was stated in the previous chapters, the simulations corresponding to the faults are developed. The occurrence of the fault is planned with an occurrence time of 0.4 seconds of the simulation. Once the MR has already found stability at its point of operation. The faults occur according to what is explained by different factors that trigger alterations in the signals acquired from the primary, the faults tested are incipient according to what is shown in figure 6 and 9, another of an abrupt type that is displayed in figure 7.

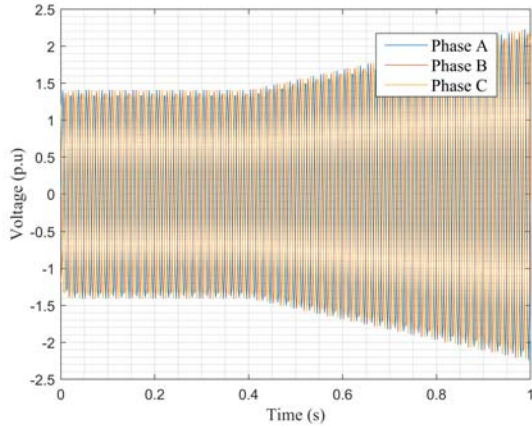


Figure 6. Incipient failure in primary

It can be seen that the abrupt failure that occurs at 0.4 seconds of simulation causes an output with a value of 0, which suggests a disconnection of the voltage sensor involved.

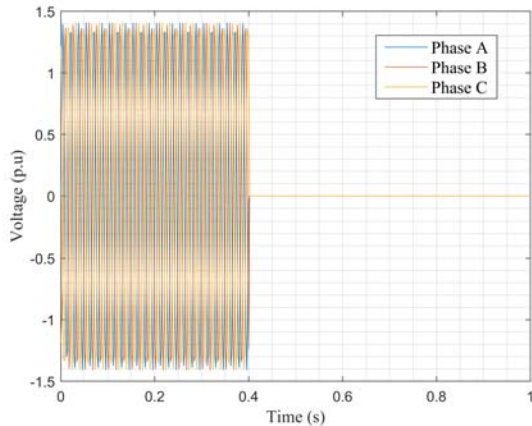


Figure 7. Abrupt failure in primary

The signals shown above were tested in order to verify how a sensing failure can cause undesired changes in the control signals of devices linked to said signals. In this specific case the control signal that triggers the triggering of the detection devices power involved in the operation of SVCs. The signals were introduced in the controller with a PI method and also with the robust controller.

3.3. Incipient failure

Figure 8 shows a comparison of the performance of both control methods and how they develop before the occurrence of the incipient failure.

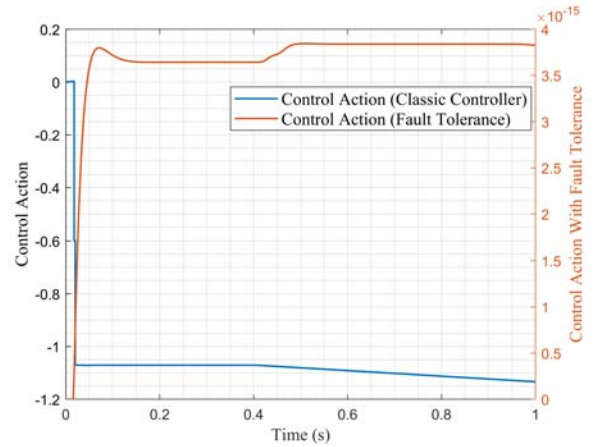


Figure 8. Control action: incipient failure

It can be seen that the control action resulting from both methods is completely different in form and magnitude. The control action resulting from the PI controller has a magnitude that varies between 0 and -1.2 approximately, while the control action resulting from the designed controller with H_∞ varying between 0 and 4×10^{-15} . These magnitudes are altered by the reference points to which the system is subject prior to 0.4 seconds of occurrence of the fault and once the fault occurs immediately the control action is modified.

For a better understanding of the behavior, Figure 9 is presented, which illustrates the error value that occurs with each control action, which should be minimized. It is observed that when the fault occurs, the behavior of the control action of the controller PI tends to a constantly growing divergence, while in the case of the controller built in the present investigation, the error tends to change but the change is minimal compared to the more traditional control action.

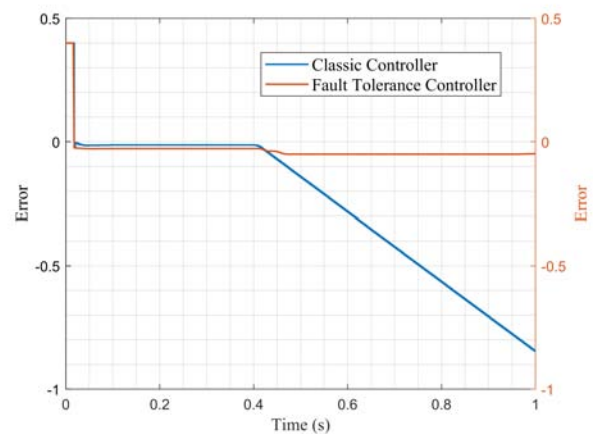


Figure 9. Error: incipient failure

Figure 10 shows the behavior of the output voltage (p.u) in phase A after the signal is processed by the controller H_∞ and a stage composed of an artificial

neural network. Once the fault occurs, the voltage tends to have a fluctuation as an expected effect without this modification being significant, since it has a variation of 0.02 units with respect to the pre-fault condition.

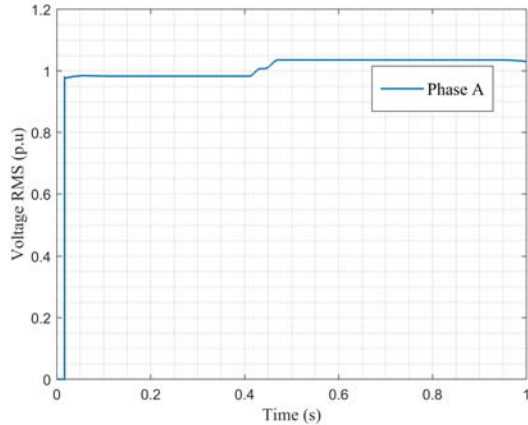


Figure 10. Voltage RMS (p.u), phase A: incipient fault

3.4. Abrupt failure

In a similar way to what was reviewed with the incipient failure, the results obtained are presented for the case in which the failure is of the abrupt type, Figure 11 shows the behavior of the control action subject to the abrupt failure.

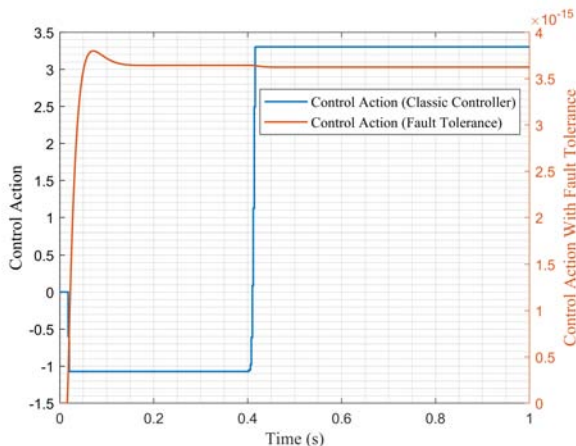


Figure 11. Control action: abrupt failure

It can be visualized again that the control action with a traditional controller has a variation between -1.2 and 3.5 units, having a sudden change at 0.4 seconds in the occurrence of a fault. On the other hand, the control action with the use of the H_∞ system is maintained in the interval between 0 and 4×10^{-15} with a behavior similar to that obtained in the previous fault studied, the controller even shows a lower fluctuation after 0.4 seconds from incipient failure.

Figure 12 corresponding to the error produced as an effect of the control action with both controllers is also presented. Once again it is evident that the error caused by the controller H_∞ is much lower than that produced by the PI controller after the occurrence of the fault, the PI controller again causes a divergence in the error, although in this case the error stabilizes in a short period of time.

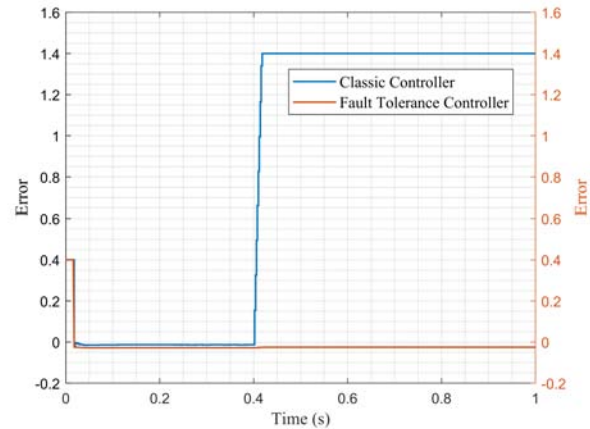


Figure 12. Error: abrupt failure

As previously reviewed, the RMS voltage value in phase A is plotted as an effect of the implementation of the robust controller, the result is shown in Figure 13.

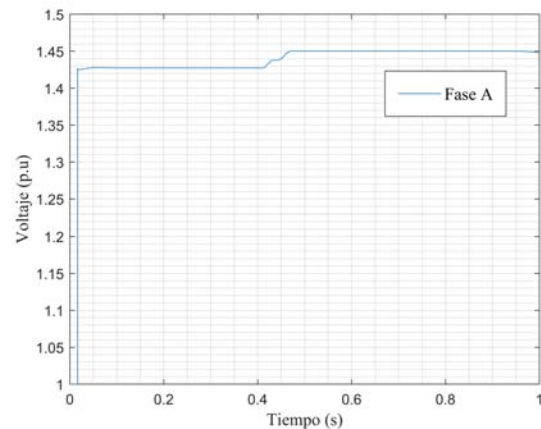


Figure 13. Voltage RMS (p.u), phase A: abrupt failure

Since the error produced by the control action is small the variation that occurs in the voltage is also small which validates the robustness of the controller in the event of sensing failures.

4. Conclusions

It is verified that implementing a fault tolerant controller designed by means of H_∞ improves the capacity

of the controllers to support alterations produced by failure events in the controller input, the performance is much better than a conventional PI type controller. The new controller strategy is effective to maintain the stability action without significant changes.

The operation of the controller designed by means of simulation in software specialized in simulation of dynamic systems Simulink/Matlab is successfully tested. The software allowed to carry out simulations in order to carry out the identification of the system in addition to the controller design and its validation in a Microgrids implemented by means of a Benchmark system.

The designed passive sensing fault-tolerant control system shows better performance in the event of an abrupt fault compared to an incipient fault, the designed parameters of the controller were successfully calculated, although in both cases it is significantly better than a traditional controller.

The correct performance of an artificial neural network is achieved as a previous step to the introduction of a measured signal in the controller involved, the signal that is produced by a sensing error is processed by an artificial neural network to later introduce the signal in the controller.

It is proposed to introduce the methodology of this academic article for the development of robust controllers that can withstand malicious failures and the occurrence of other types of failures as well as in different types of devices that require a robust control action. On the other hand, it is proposed to carry out comparative research with selection algorithms that allow selecting the best control action that is the result of different methodologies to improve its performance.

References

- [1] L. Ortiz, J. W. González, L. B. Gutierrez, and O. Llanes-Santiago, "A review on control and fault-tolerant control systems of AC/DC microgrids," *Heliyon*, vol. 6, no. 8, 2020. [Online]. Available: <https://doi.org/10.1016/j.heliyon.2020.e04799>
- [2] Á. J. Pérez Pazmiño and L. Ortiz Matos, "Despliegue óptimo de redes de distribución y generación distribuida para microrredes eléctricas híbridas CA aisladas usando método heurístico," *Serie Científica de la Universidad de las Ciencias Informáticas*, vol. 15, no. 1, pp. 80–96, 2022. [Online]. Available: <https://bit.ly/3Oj9FP0>
- [3] L. Ortiz, R. Orizondo, A. Aguila, J. W. Gonz, I. Isaac, and J. L. Gabriel, "Hybrid AC / DC microgrid test system simulation : grid-connected mode," *Heliyon*, vol. 5, no. August, p. 21, 2019. [Online]. Available: <https://doi.org/10.1016/j.heliyon.2019.e02862>
- [4] F. Chishti and B. Singh, "Hybrid control of renewable based microgrid synchronized to 3p4w ac distribution network," in *2021 4th Biennial International Conference on Nascent Technologies in Engineering (IC-NTE)*, 2021, pp. 1–6. [Online]. Available: <https://doi.org/10.1109/ICNTE51185.2021.9487755>
- [5] M. Zolfaghari, G. B. Gharehpetian, M. Shafiekhah, and J. P. Catalão, "Comprehensive review on the strategies for controlling the interconnection of AC and DC microgrids," *International Journal of Electrical Power & Energy Systems*, vol. 136, no. October 2021, p. 107742, 2022. [Online]. Available: <https://doi.org/10.1016/j.ijepes.2021.107742>
- [6] M. Ortiz and E. M. Garcia Torres, "Pronóstico de la demanda eléctrica residencial basado en el modelo de regresión adaptativa multivariante spline (MARS)," p. 32, 2015. [Online]. Available: <https://bit.ly/3yewXQw>
- [7] H. Yu, S. Niu, Z. Shao, and L. Jian, "A scalable and reconfigurable hybrid AC/DC microgrid clustering architecture with decentralized control for coordinated operation," *International Journal of Electrical Power and Energy Systems*, vol. 135, p. 107476, 2022. [Online]. Available: <https://doi.org/10.1016/j.ijepes.2021.107476>
- [8] K. Beleño, J. Berrio, A. Pardo, and G. Oscar, "Diseño de una smart grid para un sistema híbrido de energía," *Prospectiva*, vol. 11, no. 2, pp. 94–101, 2013. [Online]. Available: <https://doi.org/10.15665/rp.v11i2.44>
- [9] E. Baneshi, S. M. H. kalali, and A. B. Dehkordi, "Microgrid optimal planning in two functional modes grid connected and the intentional islanding," in *2019 5th Conference on Knowledge Based Engineering and Innovation (KBEI)*, 2019, pp. 857–863. [Online]. Available: <https://doi.org/10.1109/KBEI.2019.8735048>
- [10] D. Carrión and L. Ortiz, "Generación distribuida a partir de bicicletas estáticas y sistemas híbridos," *Ingenius*, no. 10, pp. 44–48, 2013. [Online]. Available: <https://doi.org/10.17163/ings.n10.2013.05>
- [11] L. O. Matos, L. B. Gutiérrez, J. W. Sánchez, and A. A. Téllez, "An arx-petri nets algorithm for active identification of an ac/dc microgrid simulation," in *2019 IEEE 4th Colombian Conference on Automatic Control (CCAC)*, 2019, pp. 1–6. [Online]. Available: <https://doi.org/10.1109/CCAC.2019.8921191>

- [12] J. R. Collaguazo Solís and L. Ortiz Matos, “Control de voltaje óptimo para sistemas de almacenamiento de energía de batería (BESS) acoplados a microrredes de AC utilizando algoritmos LQG.” [Online]. Available: <https://bit.ly/3OBT48Z>
- [13] S. X. Garrido Jácome and L. Ortiz Matos, “Estrategia activa de tolerancia a fallas para el control Buck-Boost de micro-redes eléctricas en DC,” 2019. [Online]. Available: <https://bit.ly/3bo7D1r>
- [14] S. P. Quishpe Guamantica and L. Ortiz Matos, “Detección de fallas de sensado en convertidores CA/CC para micro-redes híbridas usando análisis de componentes principales (PCA),” 2021. [Online]. Available: <https://bit.ly/3QKPKdJ>
- [15] M. Hosseinzadeh and F. R. Salmasi, “Fault-Tolerant Supervisory Controller for a Hybrid AC/DC Micro-Grid,” *IEEE Transactions on Smart Grid*, vol. 9, no. 4, pp. 2809–2823, 2018. [Online]. Available: <https://doi.org/10.1109/TSG.2016.2620803>
- [16] G. X. Álvarez Yanchapanta and H. I. Vaca Vallejo, “Diseño de una microrred híbrida a base de energía fotovoltaica y energía térmica diesel para reducir la contaminación ambiental,” *Universidad de las Fuerzas Armadas. ESPE*, pp. 1–5, 2013. [Online]. Available: <https://bit.ly/3xN2Eiw>
- [17] A. F. Falcón Ayala and L. Ortiz Matos, “Confiabilidad en microrredes eléctricas AC/DC usando control robusto H_∞ y estrategias de tolerancia a fallas,” 2019. [Online]. Available: <https://bit.ly/3bqDOO5>
- [18] S. Jadidi, H. Badihi, and Y. Zhang, “Passive fault-tolerant control of pwm converter in a hybrid ac/dc microgrid,” in *2019 IEEE 2nd International Conference on Renewable Energy and Power Engineering (REPE)*, 2019, pp. 90–94. [Online]. Available: <https://doi.org/10.1109/REPE48501.2019.9025123>
- [19] B. N. Alhasnawi, B. H. Jasim, and B. E. Sedhom, “Distributed secondary consensus fault tolerant control method for voltage and frequency restoration and power sharing control in multi-agent microgrid,” *International Journal of Electrical Power and Energy Systems*, vol. 133, no. August 2020, p. 107251, 2021. [Online]. Available: <https://doi.org/10.1016/j.ijepes.2021.107251>
- [20] A. Vargas-Martínez, L. I. M. Avila, Y. Zhang, L. E. Garza-Castañón, and E. R. C. Ortiz, “Model-based fault-tolerant control to guarantee the performance of a hybrid wind-diesel power system in a microgrid configuration,” *Procedia Computer Science*, vol. 19, no. Seit, pp. 712–719, 2013. [Online]. Available: <https://doi.org/10.1016/j.procs.2013.06.094>
- [21] Y. Xu, S. Tong, and Y. Li, “Adaptive fuzzy fault-tolerant control of static var compensator based on dynamic surface control technique,” *Nonlinear Dynamics*, vol. 73, no. 3, pp. 2013–2023, 2013. [Online]. Available: <https://doi.org/10.1007/s11071-013-0919-3>
- [22] F. Rafael and S. Sevilla, “Fault-tolerant Wide-area Control of Power Systems,” Ph.D. dissertation, 2013. [Online]. Available: <https://bit.ly/3tXSNW6>
- [23] A. Alexander, L. Ortiz, R. Orizondo, and G. López, “Optimal location and dimensioning of capacitors in microgrids using a multi-criteria decision algorithm,” *Heliyon*, vol. 7, no. 9, p. e08061, 2021. [Online]. Available: <https://doi.org/10.1016/j.heliyon.2021.e08061>
- [24] L. Ortiz-Matos, A. Aguila-Tellez, R. Hincapié-Reyes, and J. González-Sanchez, “Multi-criteria optimization of the deployment of a grid for rural electrification based on a heuristic method,” *IOP Conference Series: Earth and Environmental Science*, vol. 73, p. 012020, jul 2017. [Online]. Available: <https://doi.org/10.1088/1755-1315/73/1/012020>
- [25] K. Wang, Y. Ma, P. Ding, R. Mu, and R. Sun, “Operation control strategy for photovoltaic/battery micro-grid,” in *2018 China International Conference on Electricity Distribution (CICED)*, 2018, pp. 821–824. [Online]. Available: <https://doi.org/10.1109/CICED.2018.8592593>
- [26] U. Akram, M. Khalid, and S. Shafiq, “Optimizing a grid-connected micro-grid with optimal renewable generation and battery energy storage,” in *2017 9th IEEE-GCC Conference and Exhibition (GCCCE)*, 2017, pp. 1–9. [Online]. Available: <https://doi.org/10.1109/IEEEGCC.2017.8448232>
- [27] Y.-G. Lv, C.-Y. Long, and T.-Q. Cai, “Research on coordinated operating control of micro-grid power system including wind power, photovoltaic system and battery storage,” in *2014 International Conference on Machine Learning and Cybernetics*, vol. 1, 2014, pp. 181–187. [Online]. Available: <https://doi.org/10.1109/ICMLC.2014.7009114>
- [28] K. Gurney, *An Introduction to Neural Networks*. CRC Press, 2018. [Online]. Available: <https://doi.org/10.1201/9781315273570>

- [29] S. Bharti, S. Dewangan, and S. Ram, "Performance of wind farm distribution system under balanced and unbalanced condition with svc & statcom," in *2016 International Conference on Electrical Power and Energy Systems (ICEPES)*, 2016, pp. 182–187. [Online]. Available: <https://doi.org/10.1109/ICEPES.2016.7915927>
- [30] J. Aho and J. Turunen, "Power quality support for industrial load using hybrid svc," in *22nd International Conference and Exhibition on Electricity Distribution (CIRED 2013)*, 2013, pp. 1–4. [Online]. Available: <https://doi.org/10.1049/cp.2013.1049>
- [31] X. Yang, W. Wang, and W. Jin, "The influence and control measures of distributed photovoltaic generation on the voltage in distribution system," in *2012 China International Conference on Electricity Distribution*, 2012, pp. 1–4. [Online]. Available: <https://doi.org/10.1109/CICED.2012.6508538>
- [32] D. Jacome and A. Águila, "Localización y dimensionamiento óptimo de dispositivos SVC para la compensación de potencia reactiva en SEP," pp. 1–17, 2017. [Online]. Available: <https://bit.ly/3bhLlyx>
- [33] H. Ebrahimirad, A. Choobdar, and G. Dehnavi, "A new control approach for voltage quality improvement in distribution power system by means of an svc," in *2008 4th IET Conference on Power Electronics, Machines and Drives*, 2008, pp. 583–586. [Online]. Available: <https://doi.org/10.1049/cp:20080588>
- [34] Y. Y. Ojeda-Rebolledo, L. D. Pabón-Fernández, E. Caicedo-Peñaranda, J. L. Díaz-Rodríguez, and A. Pardo-García, "Compensador estático var para sistemas de distribución," *Mundo Fesc*, vol. 11, no. 21, pp. 70–86, 2021. [Online]. Available: <https://bit.ly/39LZFiv>
- [35] K. Tsunedomi, Y. Imazu, S. Tamura, T. Sodeyama, T. Omori, D. Cheung, M. Parr, and S. Gough, "Effectiveness of d-svc on rural networks," in *22nd International Conference and Exhibition on Electricity Distribution (CIRED 2013)*, 2013, pp. 1–4. [Online]. Available: <https://doi.org/10.1049/cp.2013.1020>
- [36] N. Demirovic, "Impact of statcom and svc to voltage control in systems with wind farms using induction generators (ig)," in *Mediterranean Conference on Power Generation, Transmission, Distribution and Energy Conversion (MedPower 2016)*, 2016, pp. 1–6. [Online]. Available: <https://doi.org/10.1049/cp.2016.1069>
- [37] R. Gitibin and F. Hoseinzadeh, "Comparison of d-svc and d-statcom for performance enhancement of the distribution networks connected wecs including voltage dependent load models," in *2015 20th Conference on Electrical Power Distribution Networks Conference (EPDC)*, 2015, pp. 90–100. [Online]. Available: <https://doi.org/10.1109/EPDC.2015.7330479>
- [38] W. Tian, Y. Wang, W. Deng, and L. Li, "H-infinity control for a class of multiple time delay fuzzy descriptor systems," in *2013 6th International Conference on Intelligent Networks and Intelligent Systems (ICINIS)*, 2013, pp. 115–118. [Online]. Available: <https://doi.org/10.1109/ICINIS.2013.36>
- [39] D. N. Abara and A. Lanzon, "H-infinity-pid controller for an open-loop unstable system," in *2017 IEEE 3rd International Conference on Electro-Technology for National Development (NIGERCON)*, 2017, pp. 134–138. [Online]. Available: <https://doi.org/10.1109/NIGERCON.2017.8281886>



DESIGN AND VALIDATION OF IoT MEASUREMENT SYSTEM FOR PHOTOVOLTAIC GENERATION

DISEÑO IoT Y VALIDACIÓN DE SISTEMA DE MEDIDA PARA GENERACIÓN FOTOVOLTAICA

Thiago Angelino dos Santos^{1,*} , Filipe Gomes de Freitas¹ ,
 Diego Lima Carvalho Gonçalves¹ , Luis Miguel Fernández-Ramírez² 

Received: 14-05-2022, Received after review: 13-06-2022, Accepted: 18-06-2022, Published: 01-07-2022

Abstract

Use photovoltaic (PV) systems for electricity generation is constantly growing in Brazil. With the reduction in the price of PV modules and the implementation of the electric power compensation system by the power distributor, the consumer is investing in PV microgeneration to reduce the power bill. This article aims to develop an embedded system in the context of the Internet of Things (IoT). Having an IoT monitoring system applied to a grid-connected PV system in an educational institution helps teach IoT and PV generation concepts. The system is based on the ESP32 development board for acquiring DC voltage and current generated by a 1.35 kWp photovoltaic system connected to the grid and installed at the IFCE. This proposal offers a low-cost educational solution using open source and programmable hardware, which sends the data to a database in the cloud, allowing remote access worldwide. Then, using the data analysis methodology, it was possible to validate the values measured with the inverter installed with an error of less than 1% for the voltage and current acquired during one day. With this result, it is concluded that the designed IoT system can be used for measurement in PV systems.

Keywords: ESP32, IoT, measurement, photovoltaic, energy, generation

Resumen

El uso de sistemas fotovoltaicos (FV) para la generación de electricidad está en constante crecimiento en Brasil. Con la reducción del precio de los módulos FV la implementación del sistema de compensación de energía eléctrica por parte del distribuidor de energía, el consumidor está invirtiendo en microgeneración FV para reducir la factura de energía. El objetivo del presente artículo es desarrollar un sistema embebido en el contexto de Internet de las cosas (IoT). Tener un sistema de monitoreo IoT aplicado a un sistema FV conectado a la red en una institución educativa ayuda a enseñar conceptos tanto de IoT como de generación FV. El sistema se basa en la placa de desarrollo ESP32 para la adquisición de tensión y corriente continua generada por un sistema FV de 1,35 kWp conectado a la red e instalado en el IFCE. Esta propuesta ofrece una solución educativa de bajo costo, utilizando código abierto y hardware programable, que envían los datos a una base de datos en la nube, lo que permite el acceso remoto en todo el mundo. Utilizando metodología de análisis de datos, fue posible validar los valores medidos con el inversor instalado con un error inferior al 1% para la tensión y la corriente adquiridas durante un día. Con este resultado se concluye que el sistema IoT diseñado puede ser utilizado para la medición en sistemas FV.

Palabras clave: ESP32, IoT, medida, fotovoltaica, energía, generación

^{1,*} Academic Master's Degree in Renewable Energy (PPGER). Federal Institute of Ceará (IFCE). Maracanaú Campus, Ceará, Brazil. Corresponding author ✉: thiagoangelinos@gmail.com

²Research Group in Electrical Technologies for Sustainable and Renewable Energy. Department of Electrical Engineering, University of Cadiz (UCA). Escuela Politécnica Superior de Algeciras, Cádiz, Spain

Suggested citation: Dos Santos, T. A.; De Freitas, F. G.; Carvalho Gonçalves, D. L. and Fernández-Ramírez, L. M. "Design and validation of IoT measurement system for photovoltaic generation". *Ingenius, Revista de Ciencia y Tecnología*. N.º 28, (july-december). pp. 44-52. 2022. DOI: <https://doi.org/10.17163/ings.n28.2022.04>.

1. Introduction

The first modern solar cell, measuring just two square centimeters in area, was introduced in 1954 with 6% efficiency and five mW of power, as described in [1]. A significant advance in the development of the PV market, identified in [2], was observed from the increase in Chinese production. For the eighth consecutive year, Asia eclipsed all other regions for new installations, accounting for nearly 58% of global additions; even excluding China, Asia was responsible for around 23% of new capacity in 2020. Asia was followed by the Americas (18%), which moved ahead of Europe (16%). China continued to dominate the global market (and solar PV manufacturing), with a share of nearly 35% (up from 27% in 2019). In 2021 the estimated global capacity was 760 Gigawatts, as shown in [3].

In addition to reducing the cost of PV modules, distributed generation in Brazil has become an attractive investment in solar energy. Currently, the consumer can generate electricity and use the compensation system to reduce the cost of energy consumed directly on the bill. Compensation allows the energy exceeding consumption for that month to be used within a maximum period of up to five years. The conditions for connection to the conventional electricity distribution structure were established on April 17, 2012, by the National Electric Energy Agency [4].

Knowing how much the PV system will generate per month is one of the first concerns of the final consumer. The engineer designs the system, but external factors such as dirt, system failures, material wear, and weather conditions can alter the energy generation estimated in the original design. With a monitoring system applied to the PV generation system, it can monitor the production and consumption of electricity. This way, it is possible to identify non-standard behaviors for that system: the faster this identification, the minor damage to the final consumer.

Regarding data monitoring via the Internet, the number of devices connected to the cloud is increasing, and, consequently, the volume of data has grown substantially. Our daily lives are surrounded by constantly updated information. When a status on a social network is changed, there is an information feed, which generates updates to the user's database. This dynamic way to get information quickly, accessible, and up-to-date does not just apply to social media or journalism. Considered the fourth industrial revolution, Industry 4.0 has been gaining prominence and promises to have a more profound and exponential impact than previous industrial revolutions. One of the industry's pillars 4.0, according to Vitalli [5] is the Internet of Things (IoT, English Internet of Things). Among the devices available on the market for IoT applications are the ESP32 and ESP-WROOM (model used in this work), which are constantly used in academic research because of

their easy programming.

IoT systems are applied to facilitate communication between equipment and human beings in various areas, such as hospitals [6], manufacturing processes [7], waste management [8], as well as renewable energies [9] - [10].

The ESP32 development platform has been used in IoT projects around the world. Then, to enable multimedia data transmission via Wi-Fi, this device was used to compose a hybrid communication system and data transmission system in IoT networks [11]. In addition to Wi-Fi communication, the ESP32 also features Bluetooth communication. A vehicle window control system was developed in [12] using Bluetooth communication.

ESP32 was also used in a data center's temperature, humidity, and air quality monitoring network to automate the activation and deactivation of the cooling, ventilation, and air filtration system [13].

1.1. Related Works

The ESP32 and ESP8266 were used to build an IoT network to measure weather data and the temperature of PV modules in [14]. The communication used between the ESP32 and the ESP8266 was Wi-Fi.

A comparative analysis and practical application of the ESP32 microcontroller module for IoT was illustrated in [15]. The article demonstrated that ESP32 is an excellent option for IoT systems, as it presents advantages in performance and price compared to the others analyzed. Its performance reflects its reliability, ensuring the system is always up and running. Thus, they can be used in critical systems such as the one proposed in [16] for monitoring liquefied petroleum gas (LPG) leakage.

In PV systems, ESP32 was used in a water pumping control system powered by a solar generator [17]. A web server using ESP32 was developed in [18] to monitor and collect data from a PV system. Data was stored in a text file and saved directly to the SD memory card. The data can be retrieved, and the text file downloaded onto a web page.

It was possible to verify the real behavior of the PV modules using low-cost components, as can be seen in the tracking system of IV (Current-Voltage) and PV (Power-Voltage) curves built-in [19]. It is also possible to monitor the PV system using low-cost equipment [20] - [21]. This work proposed the development and validation of IoT system didactic with programmable and open-source hardware, aiming at greater flexibility in data collection and submission to a database. Validation was done from a commercial inverter with IoT technology. Just as the software was used in [22] to support teaching, the system designed in this research can be used in the classroom to teach embedded systems, the internet of things, or renewable

energy as an example of a didactic monitoring system.

Some articles that used monitoring systems, applied or not to PV generation, were gathered in Table 1. The use of internet connection through different devices for data communication, processing, and sending was observed. Most of the articles presented (67%) did not use a validation system for the data collected, especially in systems for measuring electrical variables (voltage and current, for example), as in the case of this work, showing the contribution of this paper in this area.

Table 1. Comparison of monitoring articles similar to this

Article	Device	Validation method
[23]	SamD21G	Not applicable
[24]	Arduino Mega 2560 + ESP8266	Not applicable
[25]	ESP32	By commercial equipment
[26]	34970A	Not applicable
[20]	Raspberry Pi	Not applicable
[21]	SanUSB + Wi-Fi modem	VA6510 temperature sensor

Alves et al. [27] analyzed a situation using Didactic Training Engineering (DTE) and found that this structure facilitates didactic mediation and learning. The proposal system can be used for DTE in renewable energy, programming, or embedded system. Another application for this project is in Professional Didactics (PD). Alves [28] accentuated the use of technology to provide an understanding of the notions discussed in the class. Similarly, the teachers could iterate with the students using the proposed system in this work.

This research aims to design, develop and validate a didactic IoT system for monitoring the voltage and current generated by the PV modules. The focus of this research is to develop a didactic system, easy to reproduce to disseminate knowledge in this area of research, facilitating the acquisition of data in photovoltaic solar generation plants. Low-cost sensors for measuring PV system current and voltage are applied. The data obtained were compared with the data collected by the installed PV inverter, checking the error between the systems to validate the developed system.

The system developed in this research can be applied to verify the real power generated for PV plants in [29], for example.

2. Materials and methods

2.1. Problem and Methodology

This section presents the project development stages, exposing the materials and methods used. The proposed system can be divided into 5 (five) parts:

1. Embedded system with Wi-Fi connection
2. Cloud data storage
3. Sensing

4. Data provided by the inverter
5. Embedded system programming.

2.1.1. Embedded system with Wi-Fi connection

Several low-cost devices can provide internet connection and perform pre-programmed actions. With these devices, it is possible to transform a local data acquisition system into an IoT system that constantly feeds a cloud database.

The Raspberry Pi family of devices, developed in the UK by the Raspberry Pi Foundation, has hardware built into a single card and card slot memory, USB interface, HDMI, input/output pins, serial interface, and built-in Wi-Fi modem [30]. These devices can be easily integrated into an IoT network. A Raspberry was used in [31] to monitor current and voltage in a PV pumping plant.

Some devices from the Arduino platform [32], such as the ARDUINO UNO Wi-Fi REV2, are specially designed for IoT applications. These devices have a user-friendly programming platform (Arduino IDE) in C++ with minor modifications.

Other devices widely used due to their low cost are the microcontrollers manufactured by Espressif [33]. These controllers, like the ESP32, allow microcontrollers to connect to a wireless network. The manufacturer provides some hardware versions for use as needed.

A comparison between ESP32 and a previous version of Espressif IoT modules (2014) ESP8266 is shown in Table 2.

Table 2. Comparison between ESP32 and ESP8266

ITEM	ESP32	ESP8266
<i>Clock</i>	160 MHz	80 MHz
<i>Wi-Fi</i>	Yes	Yes
<i>Bluetooth</i>	Yes	No
RAM	512 KB	160 KB
<i>FLASH</i>	16 Mb	16 Mb
ADC	18	1
DAC	2	0

ADC – Analog/Digital
DAC – Digital/Analog Converter

Note that ESP32 has more excellent processing and storage power compared to ESP8266. So, in this research, ESP32 was used for the proposed monitoring system in order to connect the monitoring system the Internet.

2.1.2. Cloud data storage

Some solutions available on the market are AWS IoT Services (Amazon Web Services), CloudMQTT, and Ubidots. AWS IoT is a specialized service, from the edge to the cloud, in IoT technology offered by the company Amazon [34].

CloudMQTT is a service that aims to facilitate sending messages through the MQTT protocol between devices in an IoT system. 24/7 support offers free connection for five users at a speed of 10 Kbit/s [35].

Ubidots is a platform that allows it to connect hardware and/or digital data services to the cloud with its easy-to-integrate API. It has an editable platform for the project's needs and a free mobile application. It has an educational license with the right to connect up to twenty devices with up to ten sensors each [36].

This work, however, proposes the creation of a system like the one used in [7]. But without the use of local storage on an SD card. All data is sent to a cloud server for comparison with data provided by the inverter installed in the PV system.

ThingSpeak™ [37] is a free and configurable analytics platform service often used for prototyping IoT systems that allow you to aggregate, visualize and analyze real-time data streams with cloud storage. ThingSpeak provides instant views of data posted by its devices in ThingSpeak's database through a web platform made available to users. Therefore, this work used the ThingSpeak platform for data storage in the cloud.

2.1.3. Sensing

For power analysis, two variables are essential: voltage and current. The PV system used in this work comprises a set (string) of five PV modules in series, totaling 1.35 kWp. Some technical characteristics of the Jinkosolar PV modules (2019) used can be seen in Table 3.

Table 3. Electrical characteristics of the PV module used in this work

ITEM	STC	NOCT
Maximum Power ()	270 Wp	200 Wp
Maximum power voltage (Vmp)	31.7 V	29.4 V
Maximum power current	8.52 A	6.80 A
Open circuit voltage (Voc)	38.8 V	35.4 V
Current short circuit current	9.09 A	7.38 A
Maximum Series Fuse Rating	15 A	15 A

STC - Standard Test Conditions
 NOCT - Nominal Operating Cell Temperature

The voltage measurement of the modules was made at the DC input of the inverter. The open-circuit voltage, the highest voltage supplied by the system, can be calculated by Equation (1):

$$V_{OUTPUT(max)} = 5 * 38.8 = 194V \quad (1)$$

The voltage difference generated by the string in the PV panel (V_{FV}) is measured by the voltage divider. Knowing that the analog input ESP32 is up to 3.3 V (V_{OUT}), we can calculate the resistors for voltage divider using Equation (2):

$$R_1 = \frac{(V_{FV}V_{OUT})}{V_{OUTPUT(max)}}R_2 \quad (2)$$

For this case, $R_1 = 57.78 * R_2$. R_1 and R_2 are resistors for the voltage divider shown in Figure 1.

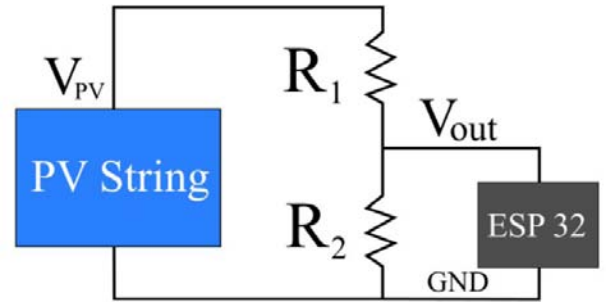


Figure 1. Schematic of the voltage divider used in the system for reading PV voltage

The V_{out} is connected directly to the ESP32 pin to measure a voltage proportional to the voltage of the PV module's string. The ratio between them is $V_{PV} = 58.79 * V_{out}$.

The current measurement is made with the 20A ACS712 current sensor module. This module is shown in Figure 2, highlighting the pin connections. The arrangement chosen for the sensor is between the inverter's DC input and the circuit-breaker box so that the measurement is made parallel to the inverter and as close as possible. Therefore, the proposed project's sensing system measures the power that the PV string provides, comparing it with that registered by the inverter for system validation.

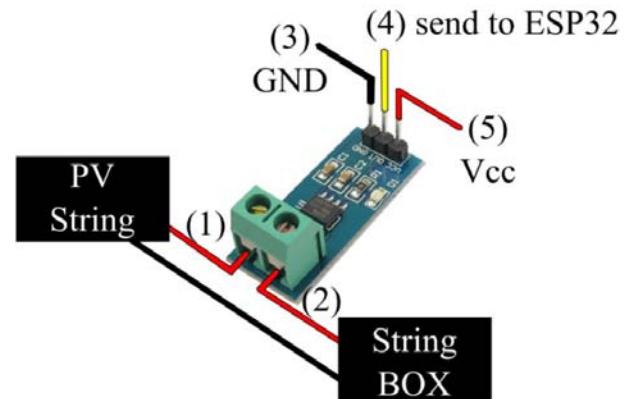


Figure 2. Installation schematic of the 20 A ACS712 current sensor module

This sensor has a 66 mV/A proportional analog output that can be read from the module output pin indicated by number four (4) in Figure 2. The operating voltage of the module is 5VDC (5). Pins one (1) and two (2) correspond to the inverter's DC input and the string box circuit breaker. Pin three (3) corresponds to the source's zero references (gnd) that supply the sensor.

2.1.4. Data provided by the inverter

The inverter used for comparing and validating the system with hardware in this work is model PHB1500-NS from the manufacturer PHB (2020). This equipment has a Wi-Fi monitoring system with real-time data available to users on the manufacturer's page via login and password. Some characteristics of this inverter grid-tie are shown in Table 4.

Table 4. PHB1500-NS inverter characteristics

DESCRIPTION	VALUE
Maximum Power	1950 W
Maximum Voltage	450 V
Generation Start Voltage (DC)	80 V
Current (DC) maximum	10 A
MPPT	1/1
AC power	1500 W
AC output voltage	60 Hz; 220 V
interface	Wi-Fi, USB and RS485

Note that this model has, in addition to interfaces for operation configuration, a Wi-Fi interface used in the monitoring system, which sends the collected data to the manufacturer's server. The manufacturer provides a page web for accessing the generation data collected by the inverter.

With the system proposed in this work, it is possible to program the protocol of how data is collected and sent to the cloud, enabling integration of this data with the user's preferred server. In this way, the user can program the time interval he/she wants and send this data to any server, for example, to research fault detection with intelligent algorithms or any research where data acquisition is necessary.

2.1.5. Embedded system programming

The use of programmable hardware (ESP32) allows the choice of this time according to the user's need and the server for sending the data, enabling future research. The firmware developed and recorded in ESP32 consists of a routine to send the average of the measurements every minute. It is shown in the diagram in Figure 3.

It can be seen from the flowchart in Figure 3 that the program starts by connecting the device to the internet via Wi-Fi to access the NTP server where they have access to local time and later sends the

average value of the measurements to a server in the cloud, which in this case is the Thing Speak, every one minute.

The use of ESP32 also makes it possible to report information about the generation and eventual failures in real-time in a customized way. However, this work focuses on validating the system through comparison with the inverter data, leaving this functionality for future work.

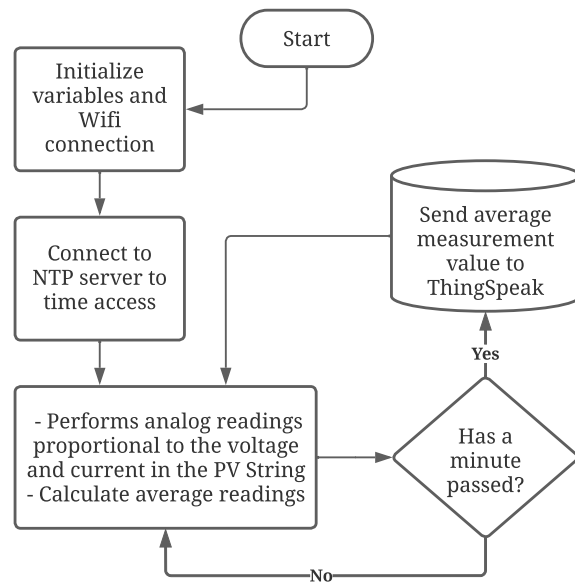


Figure 3. Flowchart of source code (firmware)

3. Results and discussion

In order to ensure the correct measurement of electrical variables, voltage, and current, tests were carried out to calibrate the sensors with the ESP32 with a digital multimeter, as seen in Figure 4.

The current sensor and the divider voltages generate voltages proportional to the current and voltage value of the string PV, respectively. The tests aim to calibrate the current sensor and voltage divider with resistors to ensure the correct proportionality between the value sent to the ESP32 and the value of current and voltage generated by the string PV. Once calibrated, this data is compared with the voltage and current values read and stored by the commercial Inverter of the PV system.

The assembly recorded in Figure 4 shows the current sensor (3) in series with a multimeter (5) between the DC input (2) of the Inverter (1) and the protection box (4), containing circuit breakers and main switch. The current, generated by the string PV, passes through the protective box and is read by the sensor, which, in turn, sends a voltage proportional to the current to one of the analog input ports of the

ESP-WROOM-32 development board (6). It will be installed in a protection frame fixed to the wall (7) to house the system developed in this work. This assembly consists of an initial prototype for laboratory testing. Subsequently, a plate was assembled to extend the ESP-WROOM-32 connections to the voltage divider and current sensor, as seen in Figure 5.

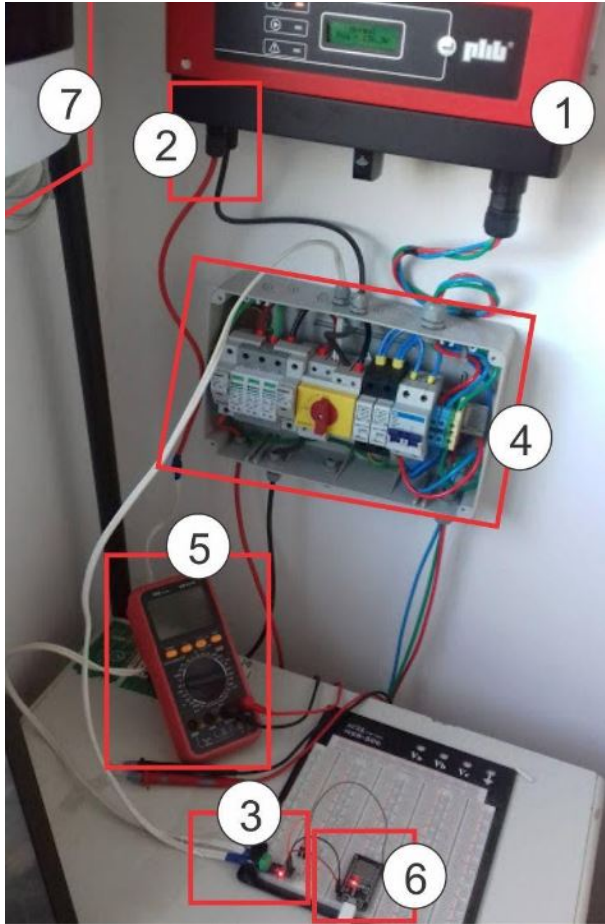


Figure 4. Installation schematic of the 20 A ACS712 current sensor module

This extension board (Figure 5 (b)) was developed to connect the voltage divider to acquire the voltage string PV and the current sensor to acquire the current generated by the string PV to the ESP32. The power to the board comes from an external 5V source (Figure 5 (a)) connected to the ESP-WROOM-32 development board. The voltage divider and the current sensor were installed inside the protection box and the main switch presented in item 4 of Figure 4 and connected to the connection board with ESP32 via network cable (Figure 5 (b)).

With the low-cost IoT system developed in this work, it is possible to obtain current and voltage data generated by the string of five PV modules in series for comparison with the data sent to the cloud by the Inverter installed in the PV plant. The comparative

graph between the current values acquired by the Inverter and the IoT system developed in this work can be seen in Figure 6.

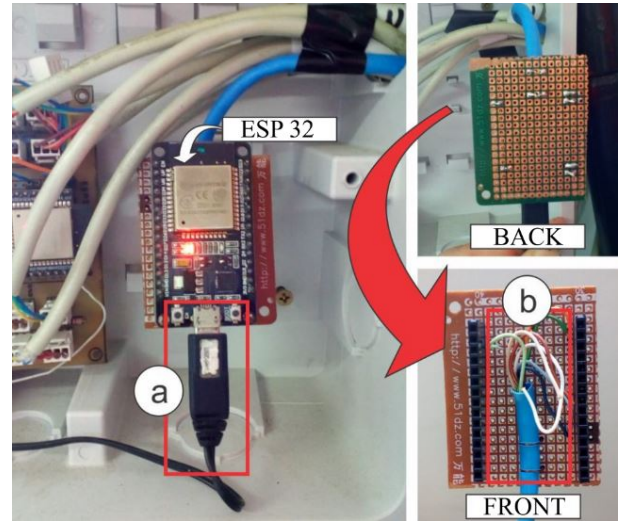


Figure 5. ESP32 and extender plate

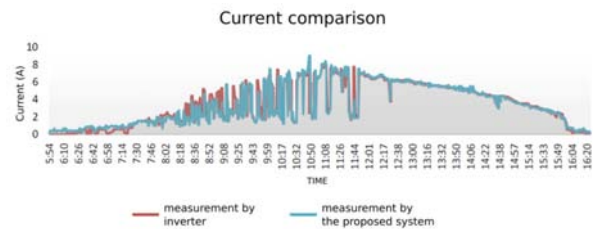


Figure 6. Comparison of current between the inverter and the proposed system

Similarly to the current, the voltage comparison can be seen in Figure 7.

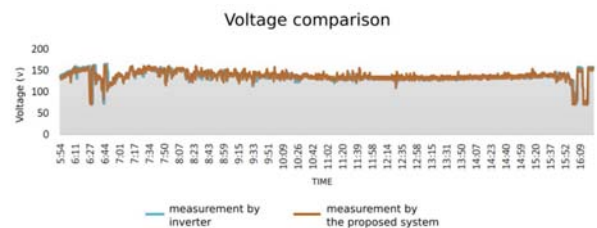


Figure 7. Comparison of voltage between the inverter and the proposed system

From the data collection by the Inverter and the low-cost system, in addition to generating the graphs shown in Figure 6 and Figure 7, the error was calculated by the sum of a defined amount of data collected by each system in the same time interval. A percent error throughout the day of less than 1% for current and voltage was obtained. On the day shown in the graphs in Figure 6 and Figure 7, an error of 0.26% for voltage and 0.56% for the current was observed.

4. Conclusions

IoT monitoring systems applied to PV micro-generation are being increasingly researched and applied, and their development is needed as PV systems continue to become a viable form of electricity generation. Modern PV inverters have IoT technology to send generation data to the manufacturer's server. However, with the system proposed in this work, it is possible to configure how this information is collected and where it is published in the cloud, generating flexibility in data collection for future research.

A low-cost didactic system using the ESP32 microcontroller development board, the ACS712 20A current sensor, and the voltage divider resistors was implemented in this work. With the system in operation, the collected data were compared with the data provided by the PV inverter, enabling the validation of the proposed system.

From the results obtained, considering that the validation showed an error was less than 1%, it can be concluded that the low-cost didactic system using ESP32 can be used to measure PV plants similar to this one. This proposed system helps teach concepts of both IoT and PV generation and encourages the academic community to research renewable energies in technical and university courses.

For future works, artificial intelligence can be applied to the data to detect failures. In addition, the proposed project can help measure and report to users and maintainers, in real-time and customized ways, the performance and any failures in the electrical generation of the analyzed PV systems.

Finally, it can be concluded that it is possible to develop and apply a didactic monitoring system with proper calibration and validation to assist academic research and teaching purposes related to IoT monitoring systems applied to installed PV plants.

References

- [1] A. M. Vallêra and M. C. Brito, "Meio século de história fotovoltaica," *Gazeta de Física*, vol. 1, no. 2, p. 17, 2006. [Online]. Available: <https://bit.ly/2WgwXgP>
- [2] J. T. Pinho, M. A. Galdino *et al.*, *Manual de engenharia para sistemas fotovoltaicos*. CEPEL - CRESESB, 2014, vol. 1. [Online]. Available: <https://bit.ly/3OAYu3Z>
- [3] H. E. Murdock, D. Gibb, T. Andre, J. L. Sawin, A. Brown, L. Ranalder, U. Collier, C. Dent, B. Epp, C. Hareesh Kumar *et al.*, "Renewables 2021-global status report," *Global ENR Report 2022*, 2021. [Online]. Available: <https://t.ly/PW1K>
- [4] B. Rubim, "Tudo o que você precisa saber sobre a revisão da ren 482," *Ecori Energia Solar*, vol. 20, p. 12, 2018. [Online]. Available: <https://bit.ly/3btlyTZ>
- [5] R. Vitalli, "Os 10 pilares de indústria 4.0 - artigos - indústria 4.0," 2018, accessed: 2022-05-14. [Online]. Available: <https://t.ly/J9i6>
- [6] A. Prudenzi, A. Fioravanti, and M. Regoli, "A low-cost iot solution for power availability improvement in hospitals," in *International Conference on Renewable Energies and Power Quality (ICREPQ'18), Salamanca (Spain), 21th to 23th March*, 2018. [Online]. Available: <https://doi.org/10.24084/repqj16.389>
- [7] C. Gamarra, M. Ortega, E. Montero, and J. Guerrero, "Innovative planning synergies between manufacturing processes and microgrids," *Renewable Energy and Power Quality Journal*, vol. 1, no. 14, pp. 939–944, 2016. [Online]. Available: <https://doi.org/10.24084/repqj14.526>
- [8] N. S. Kumar, B. Vuayalakshmi, R. J. Prarthana, and A. Shankar, "Iot based smart garbage alert system using arduino uno," in *2016 IEEE region 10 conference (TENCON)*. IEEE, 2016, pp. 1028–1034. [Online]. Available: <https://doi.org/10.1109/TENCON.2016.7848162>
- [9] F. T. Brito, S. C. Jucá, and P. C. Carvalho, "Controllogger: A remote monitoring system for decentralized renewable energy sources," *Renewable Energy and Power Quality Journal*, vol. 10, p. 432, 2012. [Online]. Available: <https://doi.org/10.24084/repqj10.432>
- [10] R. I. Pereira, P. C. Carvalho, and S. C. Jucá, "Wifi data acquisition system and online monitoring applied to thermoelectric microgeneration modules," *Renewable Energy and Power Quality Journal*, no. 13, pp. 1–6, 2015. [Online]. Available: <https://doi.org/10.24084/repqj13.370>
- [11] A. Saveliev, D. Malov, M. Tamashakin, and V. Budkov, "Service and multimedia data transmission in iot networks using hybrid communication devices," in *MATEC Web of Conferences*, vol. 113. EDP Sciences, 2017, p. 02010. [Online]. Available: <https://doi.org/10.1051/mateconf/201711302010>
- [12] J. Purba and D. Wahyudin, "Bluetooth low energy (ble) based power window system," in *IOP Conference Series: Materials Science and Engineering*, vol. 384, no. 1. IOP Publishing, 2018, p. 012029. [Online]. Available: <https://doi.org/10.1088/1757-899X/384/1/012029>

- [13] J. I. Vega-Luna, F. J. Sánchez-Rangel, G. Salgado-Guzmán, J. F. Cosme-Aceves, V. N. Tapia-Vargas, and M. A. Lagos-Acosta, "Red de monitorización para automatizar el sistema de enfriamiento de un centro de datos," *Ingenius. Revista de Ciencia y Tecnología*, no. 24, pp. 87–96, 2020. [Online]. Available: <https://doi.org/10.17163/ings.n24.2020.09>
- [14] R. I. Pereira, S. C. Jucá, P. C. Carvalho, and C. P. Souza, "Iot network and sensor signal conditioning for meteorological data and photovoltaic module temperature monitoring," *IEEE Latin America Transactions*, vol. 17, no. 06, pp. 937–944, 2019. [Online]. Available: <https://doi.org/10.1109/TLA.2019.8896816>
- [15] A. Maier, A. Sharp, and Y. Vagapov, "Comparative analysis and practical implementation of the esp32 microcontroller module for the internet of things," in *2017 Internet Technologies and Applications (ITA)*. IEEE, 2017, pp. 143–148. [Online]. Available: <https://doi.org/10.1109/ITECHA.2017.8101926>
- [16] A. H. Abdullah, S. Sudin, M. I. M. Ajit, F. S. A. Saad, K. Kamaruddin, F. Ghazali, Z. A. Ahmad, and M. A. A. Bakar, "Development of esp32-based wi-fi electronic nose system for monitoring lpg leakage at gas cylinder refurbish plant," in *2018 international conference on computational approach in smart systems design and applications (ICASSDA)*. IEEE, 2018, pp. 1–5. [Online]. Available: <https://doi.org/10.1109/ICASSDA.2018.8477594>
- [17] I. Allafi and T. Iqbal, "Design and implementation of a low cost web server using esp32 for real-time photovoltaic system monitoring," in *2017 IEEE electrical power and energy conference (EPEC)*. IEEE, 2017, pp. 1–5. [Online]. Available: <https://doi.org/10.1109/EPEC.2017.8286184>
- [18] S. B. Biswas and M. T. Iqbal, "Solar water pumping system control using a low cost esp32 microcontroller," in *2018 IEEE Canadian conference on electrical & computer engineering (CCECE)*. IEEE, 2018, pp. 1–5. [Online]. Available: <https://doi.org/10.1109/CCECE.2018.8447749>
- [19] V. Leite, J. Batista, F. Chenlo, and J. L. Afonso, "Low-cost instrument for tracing current-voltage characteristics of photovoltaic modules," *International Conference on Renewable Energies and Power Quality (ICREPQ'12)*, 2012. [Online]. Available: <https://doi.org/10.24084/repqj10.565>
- [20] R. I. Pereira, I. M. Dupont, P. C. Carvalho, and S. C. Jucá, "Iot embedded linux system based on raspberry pi applied to real-time cloud monitoring of a decentralized photovoltaic plant," *Measurement*, vol. 114, pp. 286–297, 2018. [Online]. Available: <https://doi.org/10.1016/j.measurement.2017.09.033>
- [21] R. I. S. Pereira, S. C. S. Juca, and P. C. M. de Carvalho, "Online monitoring system for electrical microgeneration via embedded wifi modem," *IEEE Latin America Transactions*, vol. 14, no. 7, pp. 3124–3129, 2016. [Online]. Available: <https://doi.org/10.1109/TLA.2016.7587611>
- [22] E. Perge, "Practical application of computer software in visual education." *Acta Didactica Napocensia*, vol. 1, no. 2, pp. 50–55, 2008. [Online]. Available: <https://bit.ly/39Nx4sZ>
- [23] M. Muttillio, T. de Rubeis, D. Ambrosini, G. Barile, and G. Ferri, "Sensor monitoring system for pv plant with active load," in *2019 IEEE 8th International Workshop on Advances in Sensors and Interfaces (IWASI)*. IEEE, 2019, pp. 124–127. [Online]. Available: <https://doi.org/10.1109/IWASI.2019.8791248>
- [24] N. Rouibah, L. Barazane, A. Mellit, B. Haggi, and A. Rabhi, "A low-cost monitoring system for maximum power point of a photovoltaic system using iot technique," in *2019 International conference on wireless technologies, embedded and intelligent systems (WITS)*. IEEE, 2019, pp. 1–5. [Online]. Available: <https://doi.org/10.1109/WITS.2019.8723724>
- [25] R. I. Pereira, S. C. Jucá, and P. C. Carvalho, "Iot embedded systems network and sensors signal conditioning applied to decentralized photovoltaic plants," *Measurement*, vol. 142, pp. 195–212, 2019. [Online]. Available: <https://doi.org/10.1016/j.measurement.2019.04.085>
- [26] F. Harrou, A. Dairi, B. Taghezouit, and Y. Sun, "An unsupervised monitoring procedure for detecting anomalies in photovoltaic systems using a one-class support vector machine," *Solar Energy*, vol. 179, pp. 48–58, 2019. [Online]. Available: <https://doi.org/10.1016/j.solener.2018.12.045>
- [27] F. R. V. Alves, R. C. de SOUSA, and F. C. F. Fontenele, "Didactical engineering of the second generation: A proposal of the design and a teaching resource with the support of the geogebra software in brazil." *Acta Didactica Napocensia*, vol. 13, no. 2, pp. 142–156, 2020. [Online]. Available: <https://doi.org/10.24193/adn.13.2.10>
- [28] F. R. V. Alves, "The professional didactics (pd) and didactics of sciences (ds) in brazil: some implications for the professionalization of the science teacher." *Acta Didactica Napocensia*,

- vol. 11, no. 2, pp. 105–120, 2018. [Online]. Available: <https://doi.org/10.24193/adn.11.2.9>
- [29] W. Pavon, E. Inga, and S. Simani, “Optimal distribution network planning applying heuristic algorithms considering allocation of PV rooftop generation,” *2020 Ieee Andecon, Andecon 2020*, 2020. [Online]. Available: <https://doi.org/10.1109/ANDESCON50619.2020.9272062>
- [30] RASPBERRY, “Buy a Raspberry Pi - Raspberry Pi,” accessed: 2022-06-16. [Online]. Available: <https://t.ly/66e0>
- [31] I. Costa, J. R. Sousa, S. C. Jucá, R. Pereira, and A. Alexandria, “Monitoramento iot de planta de bombeamento fotovoltaico utilizando sistema embarcado linux,” *Enciclopedia Biósfera*, vol. 18, no. 37, pp. 349–363, 2021. [Online]. Available: https://doi.org/10.18677/EnciBio_2021C30
- [32] ARDUINO, “Arduino hardware | arduino,” 2022, accessed: 2022-06-16. [Online]. Available: <https://t.ly/2qmR>
- [33] ESPRESSIF, “Development boards | espressif systems,” accessed: 2022-06-16. [Online]. Available: <https://t.ly/mIGV>
- [34] AWS, “Aws iot - internet of things - amazon web services,” 2022, accessed: 2022-05-02. [Online]. Available: <https://t.ly/gyWf>
- [35] CLOUDMQTT, “Cloudmqtt - hosted message broker of internet of things,” accessed: 2022-05-02. [Online]. Available: <https://t.ly/FTrN>
- [36] UBIDOTS, “Iot platform | internet of things | ubidots,” accessed: 2022-05-02. [Online]. Available: <https://t.ly/RyIE>
- [37] THINGSPEAK, “Iot analytics - thingspeak internet of things,” accessed: 2022-05-02. [Online]. Available: <https://t.ly/tnqU>



PLATFORM FOR DISTANCE LEARNING OF MICROCONTROLLERS AND INTERNET OF THINGS

PLATAFORMA DE ENSEÑANZA A DISTANCIA DE MICROCONTROLADORES E INTERNET DE LAS COSAS

Renata Pereira^{1,*} , Cleonilson de Souza² , Darwin Patino³ , Juan Lata⁴ 

Received: 06-06-2022, Received after review: 14-06-2022, Accepted: 21-06-2022, Published: 01-07-2022

Abstract

Due to the increasing technological development in embedded systems and the Internet of Things (IoT), devices based on microcontrollers are increasingly applied in various areas of knowledge. In this context, online educational platforms and products are considered virtual remote laboratories because students can access the physical devices anywhere as long as they have an Internet-connected computer system. In this sense, this work describes the design and development of a platform with four online educational products for teaching microcontrollers and IoT. These educational products are based on open-source software, allowing their free online distribution and can be accessed from a cloud server. The open-source and multiplatform (Linux, Windows®, and Mac OSX) approach allows more significant user interaction and accessibility. The online educational products make possible the programming of ESP32 firmware remotely via OTA (over the air) and Linux embedded systems based on Raspberry Pi (Rpi), enabling virtual microcontroller laboratory applications. In addition, online educational products allow the manipulation of GPIO pins via the Internet through a graphical interface of the ESP32 and ESP8266 microcontrollers and the Rpi. In this context, the proposed online platform, running on a cloud server, was tested, and the four online educational products of distance learning and actual application of microcontrollers and the Internet of Things have been validated and worked as designed.

Keywords: platform, distance learning, microcontroller, Internet of Things, embedded systems, virtual laboratory

Resumen

Debido al creciente desarrollo tecnológico de los sistemas embebidos y el internet de las cosas (IoT), los dispositivos basados en microcontroladores se aplican cada vez más en diversas áreas del conocimiento. En este contexto, las plataformas y productos educativos online se consideran laboratorios virtuales remotos, ya que los estudiantes pueden acceder a los dispositivos físicos en cualquier lugar siempre que dispongan de un sistema informático conectado a internet. En este sentido, este trabajo describe el diseño y desarrollo de una plataforma con cuatro productos educativos online para la enseñanza de microcontroladores y IoT. Estos productos educativos están basados en software de código abierto, lo que permite su distribución gratuita en línea y se puede acceder a ellos desde un servidor en la nube. El enfoque de código abierto y multiplataforma (Linux, Windows® y Mac OSX) permite una mayor interacción y accesibilidad del usuario. Los productos educativos en línea hacen posible la programación del firmware de ESP32 de forma remota a través de OTA (over the air) y de sistemas embebidos Linux basados en Raspberry Pi (Rpi). Además, los productos educativos en línea permiten manipular los pines a través de la interfaz gráfica de los microcontroladores ESP32 y ESP8266, así como del Rpi. Como resultado, se prueba la plataforma en línea propuesta, ejecutada en un servidor en la nube, y se validaron los cuatro productos educativos de aprendizaje a distancia y la aplicación real de microcontroladores e IoT se encuentran operativos tal como fueron diseñados.

Palabras clave: plataforma, educación a distancia, microcontrolador, internet de las cosas, sistemas embebidos, laboratorio virtual

¹ Electronics, Federal Institute of Alagoas, Alagoas, Brazil. Corresponding author ✉: renata.pereira@ifal.edu.br

² Electrical Engineering, Federal University of Paraíba, Paraíba, Brazil.

³ Electrical Engineering, Universidad de Guayaquil, Guayaquil, Ecuador.

⁴ Electrical Engineering, Universidad Politécnica Salesiana, Guayaquil, Ecuador.

1. Introduction

The COVID-19 pandemic demonstrated that the teaching-learning process in educational institutions was hampered by the lack of and need for face-to-face classes. Several strategies are implemented for schools and universities to reduce the negative impact on students' learning and continuity of education [1,2]. Adopting distance practices has become a crucial part of teaching, especially in Engineering, Science, and Technology courses [3]. Thus, this paper describes a didactic tool that allows the implementation of online practices of microcontrollers and the Internet of things.

Due to the increasing technological development in the areas of embedded systems and the Internet of things (IoT), microcontroller-based devices are increasingly applied in various areas of knowledge such as motor control, security systems, elevator control systems [4], power generation monitoring [5] and in applied scientific research [6]. Therefore, teaching embedded systems, microcontrollers, and IoT topics becomes more and more relevant in Science and Engineering courses. Since online educational products based on microcontrollers and IoT are used over the Internet, remote teaching practices of these teaching resources are possible. In this way, online educational platforms and products are considered remote laboratories since students can access physical devices from anywhere as long as they have a computer system with Internet access [7,8].

1.1. Related Works

The single-board computer, called Raspberry Pi (Rpi), used in the distance education teaching platform proposed in this work, was developed by the Raspberry Pi Foundation to help children and adults learn in the computational area. It is a low-cost portable computer based on free software and interfaces for various peripherals. Other features are 1 GB RAM shared with a GPU (Graphics Processing Unit), VideoCore IV 3D graphics core, 40 general-purpose input/output (GPIO) pins, four ports with USB 2.0 interface for connecting keyboard and mouse used in desktop computers, HDMI (High Definition Multimedia Interface) port, Ethernet port with RJ-45 interface, 56 micro SD (Secure Digital) card interface, camera and monitor interface, as well as 5V power supply and audio output [9].

For developing online educational products based on RPi, a set of libraries and packages are used to ensure communication between all system components. Then, to access Rpi, SSH (Secure Shell) and VNC (Virtual Network Computing) protocols are tested to allow console and graphical environment access, respectively. SSH is a protocol that enables secure communication between two systems using a client/server architecture

and allows users to connect to a remote host. Unlike other remote protocols such as FTP (File Transfer Protocol) or Telnet, SSH encrypts the login session, making it virtually impossible for intruders to collect unencrypted passwords [10].

To ensure interconnection between computers running Microsoft Windows and Linux operating systems and to share files and folders, the Samba package, an open-source implementation of the SMB (Server Message Block) protocol, was installed and configured [11].

For Rpi's C language programs, the WiringPi C library was used, which can be used to program and configure the GPIO pins [12]. Thus, to compile language programs written in C, the GCC (GNU Compiler Collection) compiler is used, accessible, integrated distribution of compilers for programming languages such as C, C++, C#, and Java [13]. The CURL library was also used as an open-source command-line tool for URL syntax construction and data transfer to the cloud [14].

The ESP32 IoT microcontroller was released by the Chinese company Espressif Systems, a manufacturer of embedded wifi antennas and IoT modules with free software and hardware [15]. ESP32 is a low-power, dual-core, dual-mode 32-bit wifi/Bluetooth microcontroller (MCU). The ESP32 MCU has a frequency of 240 MHz and a processing power of 600 DMIPS (Dhrystone million instructions per second).

On the other hand, compared to the latest model, the 32-bit ESP8266 NodeMCU IoT microcontroller with wifi antenna is an earlier and more simplified version, also released by Espressif [16].

The PIC microcontroller (PIC - Peripheral Interface Controller) is an integrated circuit that contains all the circuitry necessary to realize a complete programmable digital system in a single device. This teaching platform also uses the 8-bit PIC18F2550 microcontroller produced by Microchip Technology. The analog-to-digital converter (ADC) module of the PIC18F2550 has ten inputs and is capable of measuring the analog voltage on each channel and converting the measured voltage into a 10-bit digital value [17]. In this context, IoT technology enables the communication between devices without human intervention [18,19] and understands that each device is an autonomous device connected to the Internet. Such devices can interact and communicate automatically, maximizing modularization, comfort, convenience, security, and energy savings, [20]. A database is typically used to store data in the cloud to implement IoT systems. For this purpose, Cloud Computing provides access to a shared pool of configurable computing resources, such as non-relational databases, without needing in-depth knowledge of management technologies [21,22]. The cloud model simplifies the installation, operation, and maintenance of information systems, increasing system efficiency and reliability and reducing costs.

Cloud systems can be classified according to the development or service model. Cloud development models are: public, private, community, or hybrid; Cloud service models are: Platform as a Service (PaaS), software as a Service (SaaS), or Infrastructure as a Service (IaaS). In this work, PaaS is used, which consists of the use of tools and resources to provide services to end-users who are students. Since end-users share information on the same server in the cloud, data privacy and confidentiality are the primary concerns. Thus, the educational products of the learning platform make it possible for the stored data to be secure and encrypted, allowing only the student owner to manage it.

Thus, to write and read variable data in the cloud, the proposed distance learning platform uses Firebase Realtime Database, which is a NoSQL database, i.e., it does not have as standard the system of tables and relationships between data and where data are stored as JSON objects, [23]. In addition, the online didactic platform for distance learning of microcontrollers allows real-time remote use by multiple users.

2. Materials and methods

2.1. Problem and Methodology

IoT devices increasingly require rapid intervention to update libraries and functionality and maintain the security of online environments. To this end, quickly updating the firmware of these IoT devices is an effective way to ensure data security. Thus, the proposed distance learning instructional platform uses IoT firmware updates via Over-The-Air (OTA). The OTA firmware update is performed via HTTP, which allows downloading a binary file from a cloud server to update the firmware of the microcontrollers remotely. OTA update over the Internet is typically implemented in two ways: (i) If a newer firmware version is available, the device periodically queries the server containing the compiled binary file (pull) or another online activation service, such as Firebase. ii) the device receives a notification of a new firmware version via the cloud (push), e.g., via MQTT, and performs the update. The server stores the latest firmware version in binary, and then the time-varying URL of the binary file, which is more secure and flexible than a predefined fixed address, is sent to the microcontroller for download [24]. In this topic, the online educational products of the microcontroller and Internet of things distance learning didactic platform are presented.

3. Results and discussion

The paper demonstrates an educational product to update ESP32 and ESP266 microcontroller codes with the same generic firmware using

<http://sanusb.org/espupdate>. The free version of Firebase (Google's JSON object database) has been implemented to generate an asynchronous update trigger in the cloud for .bin files, as illustrated in Figure 1.

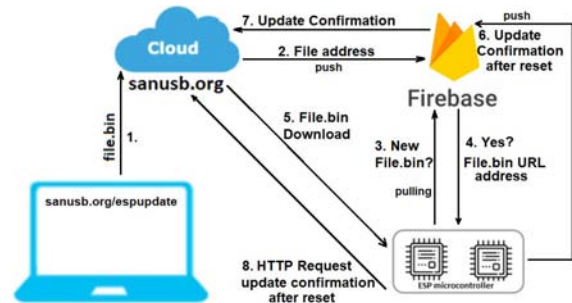


Figure 1. Illustration of the operation of the Espupdate environment

The update (OTA) transmits the compiled binary .bin files to a remote computer over the Internet, enabling microcontroller virtual lab applications. To perform this firmware update in the cloud, users must type in the firmware only the SSID, password, and the same name as the profile entered on the website <http://sanusb.org/espupdate> and by uploading the .bin to the website, the firmware of the ESP microcontrollers is updated remotely over the Internet. The user profile name entered at sanusb.org/spupdate can be alphanumeric.

It is possible to test this webcast educational product on different networks by accessing the website <http://sanusb.org/espupdate/> through the lab or home network and the ESP32 or ESP8266 microcontroller attached to the smartphone connected to the 4G mobile network, or vice versa.

It is worth considering that, through tests performed, .bin files compiled with the same name and sequential downloads for the update in the cloud, it may happen that the last .bin file sent for the update is not downloaded by the ESP microcontroller but a previously uploaded .bin File, since they have the same name and download URL. For this reason, in this project, the name of the .bin files uploaded to the site have names based on the time of upload, consequently, the download URL as well; this prevents a previously uploaded file or another file with the same name from being downloaded, generating a unique and unmatched URL. In this case, for the version of the .bin file name and download URL, the following are used: year, month, day, time, and the cyclic order of upload [25].

Once the .bin file update is completed and the microcontroller automatically restarts, the new verification code is sent to http://sanusb.org/espupdate/*Profile/ to confirm the update on the website. It is important to note that

to use EspUpdate, it is not necessary to open ports on the router or enable firewall permissions.

3.1. ESPGpio Educational Product

The educational product, called ESPGpio, allows changing the logic level of the ESP32 and ESP266 microcontroller pins that can be programmed with open source firmware [26], illustrated in Figure 2 through the graphical access available at sanusb.org/esp. The user profile name entered at sanusb.org/espgpio can be alphanumeric.

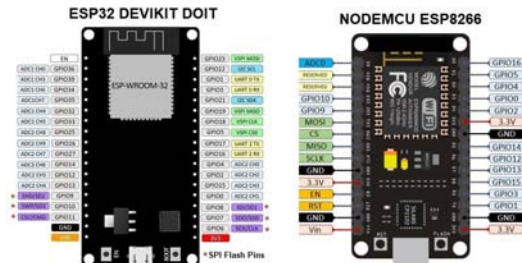


Figure 2. Illustration of ESP32 and ESP8266 GPIO pins

Figure 3 shows an illustration of the automatic operation of the ESPGPIO environment. In this case, a firebase cell is used to share between the microcontroller and the user’s graphical environment. An even integer is represented by the sum of 2. It is raised to the power of the number of activated pins.

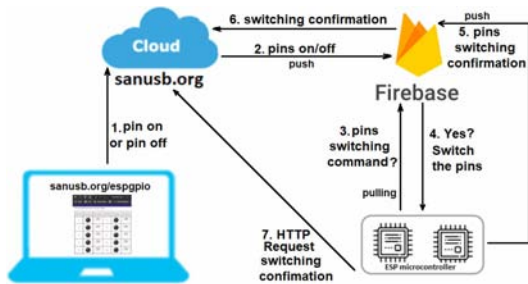


Figure 3. Illustration of the GPIO pins of an ESP32 or ESP8266

The graphical environment generated at sanusb.org/espgpio, illustrated in Figure 4, has 30 GPIO pins that the user must select to load switching through relays or electronic devices such as LEDs. It is important to note that if there is a power failure or voltage drop, the state of the last pins when the voltage drop is restored returns to normal, as the state of the pins is updated and queried in Firebase, which is a persistent database.

After completing the change of the pin states, the new pin state is indicated with green color in the graphical environment http://sanusb.org/espgpio/*Profile*/, if it is at a high logic level, as illustrated in Figure 4, where *Profile* is the profile given by the user.



GPIO	Status	Action	GPIO	Status	Action
1		On	2		Off
3		On	4		Off
5		Off	6		On
7		On	8		On
9		On	10		On

Figure 4. Illustration of the graphical environment of the ESP32 and ESP8266 GPIO pins

It is important to note that it is recommended to avoid using Gpio pin one on the ESP8266 Nodemcu, which is the Tx pin, as it prevents serial communication of program debugging by the serial monitor, and Gpio pins 06 to 11 on the ESP32 Devkit, as they are used for flash recording.

3.2. Educational product RPI GPIO

The educational product RPI GPIO is similar to ESPGpio but is used to change the state of the logic pins on the Raspberry Pi board. Figure 5 shows the illustration of the staples of a RaspberryPi.

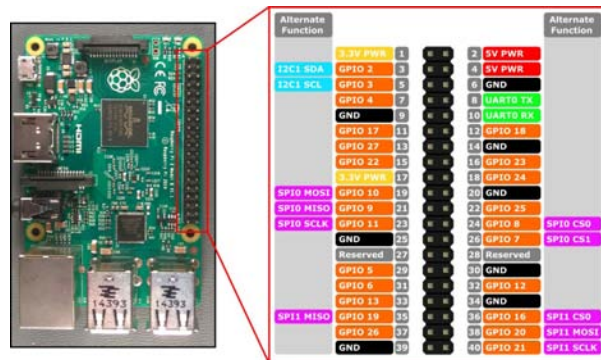


Figure 5. Illustration of the GPIO pins of a Raspberry Pi

After creating the profile at sanusb.org/gpio, a page is generated with links to pages to access the Rpi pins and firmware buttons for the extraction application and the insertion application in bash Shell language, as illustrated in Figure 6.



Figure 6. Link to pages with pin buttons and programs for Rpi

For both the complete application and the push application, it is necessary, after downloading the programs, to grant permission in the terminal as superuser (sudo su) and execute permission with the commands `chmod 755 SgpioInstall.sh`, for the pull application and `chmod 755 Sgpiopushmqtt.sh`, for push application [27]. Clicking on the profile link generates a page with buttons representing each of the I/O pins of a Rpi, as illustrated in Figure 7.

In the pull case, clicking on the button for a given physical pin sends a command to a file contained in the online profile periodically queried by the `Sgpioinstall.sh` script that is operating on the Rpi. In the case of push MQTT, clicking the button sends a publish command to the broker `mqtt.eclipse.org` on the topic with the same name as the user's profile; in the case of the example, lease and downloads this command to the Rpi that is operating the `Sgiopushmqtt.sh` script with subscription (subscribe) to the same topic.

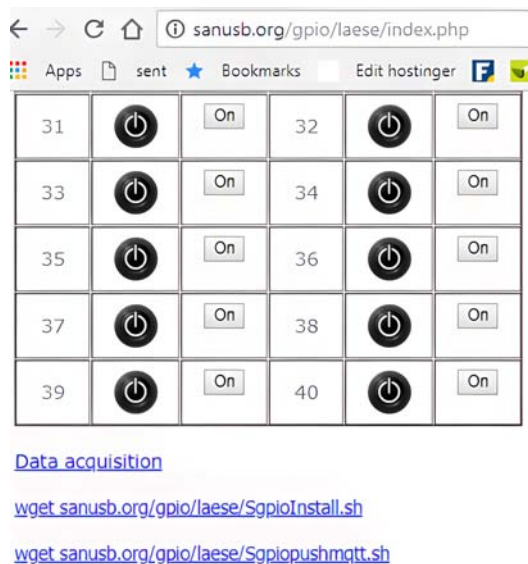


Figure 7. Illustration of the graphical environment of Raspberry Pi GPIO pins

With the RPI GPIO environment, it is possible to create an IoT application using a laptop or smartphone to, for example, control the activation of household appliances via the Internet, such as a fan via a relay, as illustrated in Figure 8. In this case, a Raspberry Pi Zero, also accessible via the Internet, is used. As can be seen, to use the `sanusb.org/gpio` environment, it is

necessary to create a profile initially. After completing the profile, a link is generated to access a page with buttons, and each button corresponds to a pin of the Raspberry Pi IoT device [27].

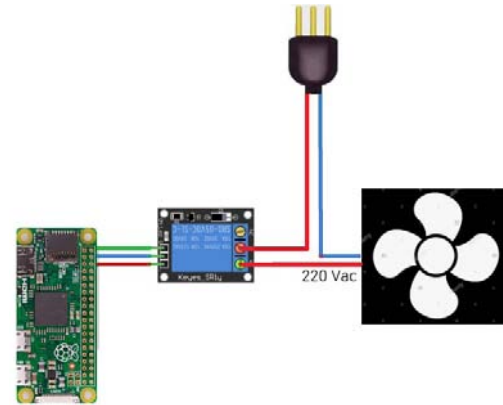


Figure 8. Illustration of a circuit for IoT operation of a fan with Raspberry Pi

3.3. IOTUS educational product

The educational product IOTUS (IoT update system) is a PaaS, i.e., a platform as a service in which the user can create a profile and update scripts in C, python, or shell language on the Rpi-based Linux embedded system and also update the firmware in hexadecimal of the PIC family microcontroller through the USB port of the RPI [28], as illustrated in Figure 9.

Thus, IOTUS consists of three main parts, namely: 1) Raspberry Pi-based Linux embedded system (ELS), 2) Analog-to-digital converter embedded system (ADCES), which uses a SanUSB microcontroller, based on a free software and hardware tool with the PIC18Fxx5X family, including the native USB interface; and 3) WEB page for automatic real-time update (upload) of scripts.

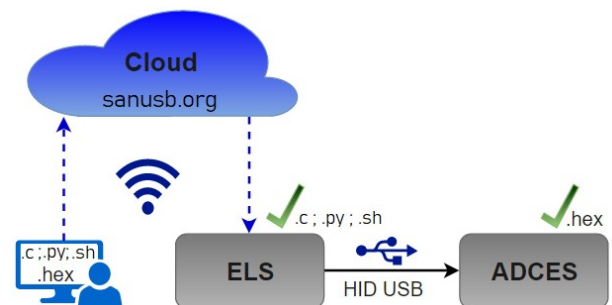


Figure 9. Remote firmware and script upgrade

ADCES consists of the open-source development tool SanUSB illustrated in Figure 9. SanUSB is composed of open-source software and hardware of the PIC18Fxx5x family with a native USB interface. This

free tool is efficient in project development because removing the microcontroller to update the firmware is unnecessary, unlike other development systems that typically use specific recording hardware and require a wired connection. In addition, the SanUSB tool is cross-platform, i.e., it can be used on Windows®, Mac OSX, and Linux, as well as being plug and play, i.e., it is automatically recognized by the operating systems without the need to install any driver [29].

Thus, this tool allows the compilation, recording, and emulation of a program to be performed quickly and efficiently by connecting the microcontroller to a computer system via USB. Its application is an RPi. The ELS RPi-based computer system can directly implement electronic designs, mainly due to its general-purpose input/output (I/O) pins (GPIO) with support for digital sensors, actuators, and I²C and SPI protocols to perform communications with peripherals [30]. The communication variety allows the RPi to communicate with a broader range of peripherals, and the Wiring Pi pin access library, written in C, facilitates programming and configuring the GPIO pins through a command-line utility "gpio." This work has two ways of communication between ADCES and RPi: serial communication and USB interface. To realize serial communication between a PIC microcontroller and the RPi pins of the ELS, the ground (GND), GPIO 14 (TX), and GPIO 15 (RX) pins are used. In this work, the computer system used to register the PIC microcontroller (ADCES) is the RPi (ELS), whose connection pins for USB and serial communication are shown in Figure 10.

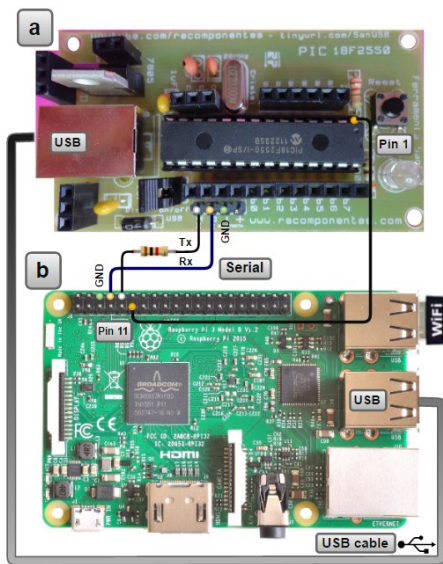


Figure 10. Serial connection between ADCES (SanUSB board) (a) and RPi (b)

Therefore, a graphical interface and recording software was developed to directly transfer the embedded Linux system interface firmware to the ADCES PIC

using the Human Interface Device (HID) communication protocol through the USB port. The proposed ADCES is an embedded RISC system and allows on-line firmware updates from the cloud. Files can be uploaded remotely to update ADCES firmware (.hex files) and update RPi scripts (.c, .py or .sh files). A physical connection between pin 11 of the RPi and pin 1 of the ADCES is required to update ADCES. The PaaS profiles (PaaS A, B, or N) illustrated in Figure 11 are free and automatically generated by the online server after registering the user profile, where it is possible to debug and/or test an IoT application. Thus, any user (A, B, or N) can create and configure an IoT profile in the cloud in real-time and update firmware and scripts over the Internet.

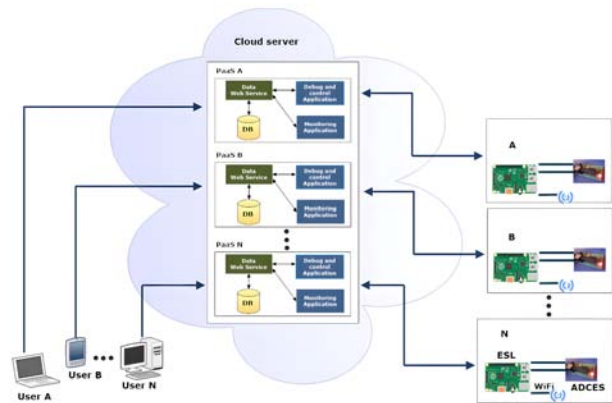


Figure 11. Proposed PaaS profile of IOTUS

Accessing the web page at <http://sanusb.org/iotus/sanusb.php>, illustrated in Figure 12, allows sending and updating scripts in ELS with language extensions in C (.c), Python (.py), Shell scripts (.sh), and hexadecimal (.hex) in ADCES through the server. Due to network latency, the address of the files uploaded to ELS and ADCES are variable and are renamed with the user's profile along with the updated version, which starts with "0" and at each upload is incremented. Considering the shape "ingenious," if the first file is Python, it will be automatically renamed to "ingenious0.py" and "ingenious1.py" will be the name of the script and, consequently, of the new URL that is used to download by ELS.

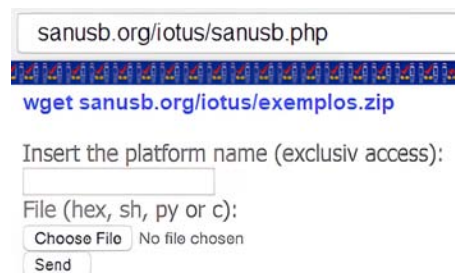


Figure 12. IoT scripts update the WEB page

IOTUS has been programmed to upload files to the server through the <http://sanusb.org/iot/sanusb.php> page by following these steps: 1. Insertion of the profile used by the student and by ELS to download the file; 2. Browse for the firmware (.c, .py, .sh or .hex) that will be sent for automatic update. Sample scripts are downloaded from sanusb.org/iotus/examples.zip. 3. The 'Submit' button executes the file transfer to the server, which is then renamed and automatically transferred to the ELS. IOTUS is programmed to operate decentralized and distributed, allowing multiple users and multiple simultaneous communications using the same cloud server. After entering a profile name and submitting any firmware, as illustrated in Figure 13, SloderInstall.sh is automatically generated and available for download.

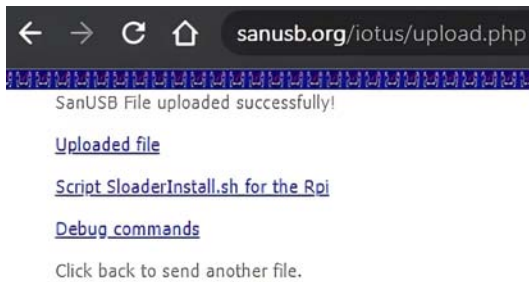


Figure 13. The website with a link to download the SloderInstall.sh script

Therefore, to update the firmware (.c, .py, .sh, or .hex) via the cloud, it is necessary to previously run the SloderInstall.sh script in ELS to check for new firmware updates at user-defined time intervals, download the updated firmware and perform a specific task according to the file extension. The SloderInstall.sh script checks at startup whether the libraries required for this educational product are installed and, if not, install them in Rpi. If a "hexadecimal" file is sent, ELS writes the file to ADCES over the cable connection between RPi pin 11 and ADCES pin 1. If a ".c" file is sent, ELS compiles the script and then executes the compiled file. In the case of a shell script or a file created in Python, ELS directly runs the file in the background. Figure 14 illustrates the flowchart of the SloderInstall.sh verification operation.

Another feature of the proposed IOTUS PaaS is that when using this online educational product, there is no need to unblock router and/or firewall ports.

As an application for the developed IOTUS, a Photovoltaic (PV) module supplying a 50 W load is used, with the following specifications: Model YL95P-17b 2/3, Maximum Power 95 WP, Efficiency 14.3%, open circuit voltage (Voc) 22.5 V and short circuit current (Isc) 5.59 A.

The sunshine hours for Fortaleza, in Brazil, where the system was implemented, are from 6 am to 4 pm.

Local meteorological conditions allow stable solar irradiance from 8 am to 2 pm (between 800 and 1250 W/m²). However, in this period high PV module temperatures are measured, which reduces the PV module efficiency. Using data from January as an example, Figure 15 shows that PV module temperature can reach values from 49 °C at 8 am to 62 °C at noon [31].

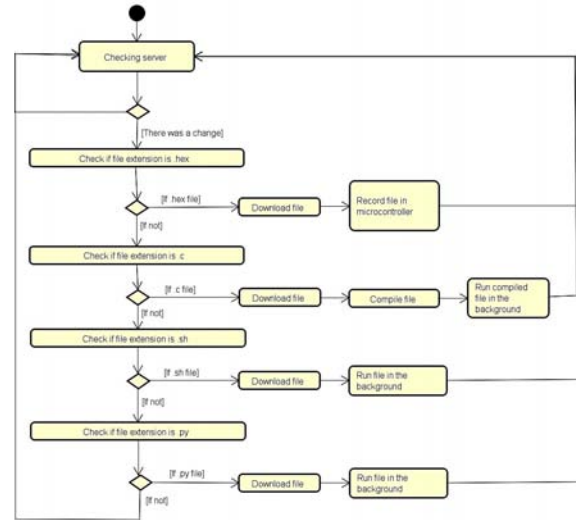


Figure 14. SloderInstall.sh operation flowchart

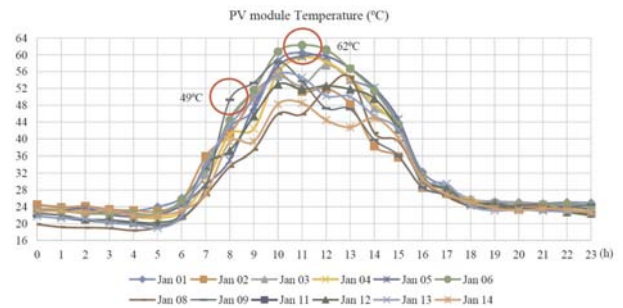


Figure 15. PV Temperature on January in Fortaleza-BR

As a second application, IOTUS ESP32 system is validated using a Programmable Logic Controller (PLC) with 12-bit resolution AD channel [32]. Figure 16 shows the monthly average curve of the PV module temperature measured. For temperature values above 52 °C, the error between the proposed IoT monitoring using ESP32 and the PLC increases, about 2 °C; for lower temperature values, the measurement follows the reference value. Figure 17 shows the correlation between the PV module temperature measured by the proposed IoT monitoring and PLC reference value for the average measurements. Using the Root Mean Square Error (RMSE), the correlation is about 0.9989.

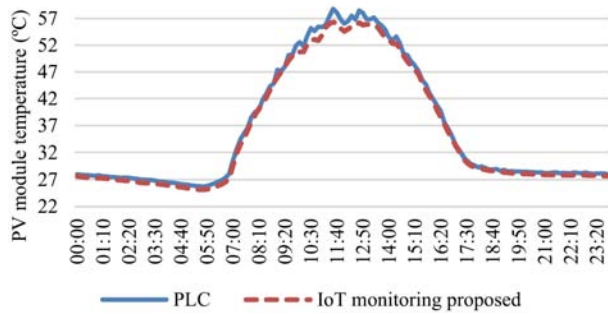


Figure 16. PV module temperature measured by the proposed IoT monitoring and PLC

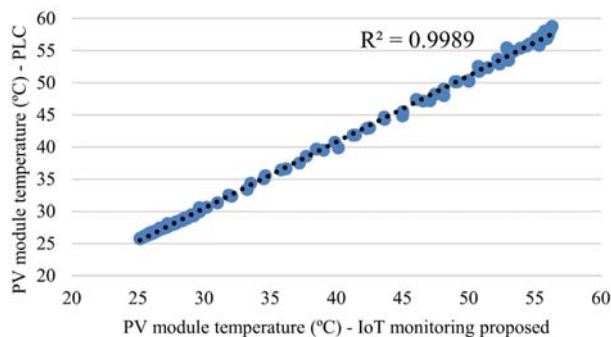


Figure 17. Correlation between PV module temperature measured by the proposed IoT monitoring and PLC reference value

4. Conclusions

This work described the design and development of four educational products in an online platform for distance learning of microcontrollers and IoT, which were tested, validated, and worked as designed. Specifically, the proposed ESP UPDATE educational product allows the update of the ESP32 and ESP266 microcontroller codes in the cloud, and it is possible to use it through the Internet anywhere and on any device (computer, smartphone), and this allows virtual microcontroller lab applications. The educational product ESPGPIO for ESP32 and ESP8266 and the RPI GPIO for Rpi allow IoT applications from a laptop or smartphone to control the activation of home appliances through the Internet intuitively and interactively.

IOTUS enables online recording of ADCES developed with a PIC microcontroller and firmware update on a Raspberry Pi-based embedded Linux system (ELS). Using open-source and cross-platform software (Linux, Windows®, and Mac OSX) for online teaching allows for more significant user interaction and accessibility due to the possibility of free distribution. Another advantage of the four proposed educational products is that there is no need to unblock ports and/or firewalls when using the cloud service.

Finally, this paper also presented the main features and advantages of the microcontrollers used in the online platform: low cost and the use of accessible hardware and software. The use of Rpi simplified the processing and provided a portable size circuit using Linux as the operating system and C as a programming language. The development of programs for the various functionalities demonstrated the possibility of building an effective and low-cost solution where the user can add functionalities and configurations according to his needs. In addition, the proposed educational products eliminate the need to install software on the computer that will access the distance education platform server.

References

- [1] C. Y. Yeh, Y. M. Cheng, and S. J. Lou, “An internet of things (IoT) maker curriculum for primary school students: Develop and evaluate,” *International Journal of Information and Education Technology*, vol. 10, no. 12, pp. 889–896, 2020. [Online]. Available: <https://doi.org/10.18178/ijiet.2020.10.12.1475>
- [2] P. Jacko, M. Bereš, I. Kováčová, J. Molnár, T. Vince, J. Dziak, B. Fecko, Š. Gans, and D. Kováč, “Remote IoT Education Laboratory for Microcontrollers Based on the STM32 Chips,” *Sensors*, vol. 22, no. 4, 2022. [Online]. Available: <https://doi.org/10.3390/s22041440>
- [3] D. Sarpong, G. Ofori, D. Botchie, and F. Clear, “Do-it-yourself (DiY) science: The proliferation, relevance and concerns,” *Technological Forecasting and Social Change*, vol. 158, no. May, 2020. [Online]. Available: <https://doi.org/10.1016/j.techfore.2020.120127>
- [4] D. De Roeck, K. Slegers, J. Criel, M. Godon, L. Claeys, K. Kilpi, and A. Jacobs, “I would DiYSE for it! A manifesto for do-it-yourself internet-of-things creation,” *NordiCHI 2012: Making Sense Through Design - Proceedings of the 7th Nordic Conference on Human-Computer Interaction*, pp. 170–179, 2012. [Online]. Available: <https://doi.org/10.1145/2399016.2399044>
- [5] J. L. Victor, S. C. Jucá, R. I. Pereira, P. C. Carvalho, and L. M. Fernández-Ramírez, “IoT monitoring systems applied to photovoltaic generation: The relevance for increasing decentralized plants,” *Renewable Energy and Power Quality Journal*, vol. 17, no. September, pp. 536–545, 2019. [Online]. Available: <https://doi.org/10.24084/repqj17.368>
- [6] R. I. Pereira, M. M. Camboim, A. W. Villarim, C. P. Souza, S. C. Jucá, and P. C. Carvalho, “On

- harvesting residual thermal energy from photovoltaic module back surface,” *AEU - International Journal of Electronics and Communications*, vol. 111, p. 152878, 2019. [Online]. Available: <https://doi.org/10.1016/j.aeue.2019.152878>
- [7] A. Morris and N. Lessio, “Deriving Privacy and Security Considerations for CORE,” *Internet of Things and Cloud-based Services Conference*, vol. 1, no. 1, pp. 2–11, 2018. [Online]. Available: <https://doi.org/10.1145/3267357.3267363>
- [8] D. Mijailovic, A. Dordevic, M. Stefanovic, D. Vidojevic, A. Gazizulina, and D. Projovic, “A Cloud-Based with Microcontroller Platforms System Designed to Educate Students within Digitalization and the Industry 4.0 Paradigm,” *Sustainability*, vol. 13, no. 22, 2021. [Online]. Available: <https://doi.org/10.3390/su132212396>
- [9] RaspberryPi Foundation, “Raspberrypi.” [Online]. Available: <https://bit.ly/3tXNSUY>
- [10] Red Hat, “Red Hat Enterprise Linux: Manual de referencia.” [Online]. Available: <https://bit.ly/3xSVdpV>
- [11] Red Hat-, “Red Hat SSH.” [Online]. Available: <https://bit.ly/3NpD2OI>
- [12] Wiringpi, “Wiring Pi.” [Online]. Available: <https://bit.ly/39QkERe>
- [13] GCC, “GCC online documentation.” [Online]. Available: <https://bit.ly/3Oi0UFb>
- [14] CURL, “Command line tool and library for transferring data with URLs.” [Online]. Available: <https://curl.se/>
- [15] ESP, “ESP32 Series Datasheet,” *Espressif Systems*, pp. 1–65, 2021. [Online]. Available: <https://bit.ly/2E6qqIt>
- [16] ESP8266EX, “ESP8266EX Datasheet,” *Espressif Systems*, p. 31, 2020. [Online]. Available: <https://bit.ly/2E6qqIt>
- [17] M. Technology, “USB Microcontrollers with nanoWatt Technology,” *Technology*, 2006. [Online]. Available: <https://bit.ly/3OEOKpk>
- [18] A. Kevin, “That ’ Internet of Things ’ Thing,” *RFiD Journal*, p. 4986, 2010. [Online]. Available: <https://bit.ly/3OdZmvI>
- [19] E. Inga, J. Inga, and A. Ortega, “Novel approach sizing and routing of wireless sensor networks for applications in smart cities,” *Sensors*, vol. 21, no. 14, pp. 1–17, 2021. [Online]. Available: <https://doi.org/10.3390/s21144692>
- [20] A. Peralta, E. Inga, and R. Hincapié, “Optimal Scalability of FiWi Networks Based on Multistage Stochastic Programming and Policies,” *Journal of Optical Communications and Networking*, vol. 9, no. 12, p. 1172, 2017. [Online]. Available: <https://bit.ly/3zZJicE>
- [21] H. Tabrizchi and M. Kuchaki Rafsanjani, *A survey on security challenges in cloud computing: issues, threats, and solutions*. Springer US, 2020, vol. 76, no. 12. [Online]. Available: <https://doi.org/10.1007/s11227-020-03213-1>
- [22] E. Inga, M. Campaña, R. Hincapié, and O. Moscoso-zea, “Optimal Deployment of FiWi Networks Using Heuristic Method for Integration Microgrids with Smart Metering,” *Sensors*, vol. 18, no. 8, pp. 1–21, 2018. [Online]. Available: <https://doi.org/10.3390/s18082724>
- [23] Firebase, “Firebase.” [Online]. Available: <https://bit.ly/3blnhLa>
- [24] S. E. Ooi, R. Beuran, and Y. Tan, “Secure iot development: A maker’s perspective,” *2021 IEEE International Conference on Omni-Layer Intelligent Systems, COINS 2021*, 2021. [Online]. Available: <https://doi.org/10.1109/COINS51742.2021.9524205>
- [25] Github, “SanUSB / EspCloudUpdate.” [Online]. Available: <https://bit.ly/3Nj8azh>
- [26] J. I. Vega Luna, F. J. Sánchez-Rangel, G. Salgado-Guzmán, J. F. Cosme-Aceves, V. N. Tapia-Vargas, and M. A. Lagos-Acosta, “Red de monitorización para automatizar el sistema de enfriamiento de un centro de datos,” *Ingenius, Revista de Ciencia y Tecnología*, no. 24, pp. 87–96, 2020. [Online]. Available: <https://doi.org/10.17163/ings.n24.2020.09>
- [27] S. Jucá and R. Pereira, “Aplicações práticas de sistemas embarcados Linux utilizando Raspberry Pi,” *PoD Editoria*, 2018. [Online]. Available: <https://bit.ly/3negu8Q>
- [28] Github, “SanUSB / IOTUS.” [Online]. Available: <https://bit.ly/3zWHxgx>
- [29] S. C. Jucá, P. C. Carvalho, and F. T. Brito, “A low cost concept for data acquisition systems applied to decentralized renewable energy plants,” *Sensors*, vol. 11, no. 1, pp. 743–756, 2011. [Online]. Available: <https://doi.org/10.3390/s110100743>
- [30] I. M. Dupont, P. C. Carvalho, S. C. Jucá, and J. S. Neto, “Novel methodology for detecting non-ideal operating conditions for grid-connected photovoltaic plants using Internet of Things architecture,” *Energy Conversion*

- and Management*, vol. 200, no. September, p. 112078, 2019. [Online]. Available: <https://doi.org/10.1016/j.enconman.2019.112078>
- [31] R. Pereira, I. Dupont, P. Carvalho, and S. Jucá, “IoT embedded linux system based on Raspberry Pi applied to real-time cloud monitoring of a decentralized photovoltaic plant,” *Measurement Journal*, vol. 114, pp. 286–297, 2018. [Online]. Available: <https://doi.org/10.1016/j.measurement.2017.09.033>
- [32] R. Pereira, S. Jucá, and P. Carvalho, “IoT embedded systems network and sensors signal conditioning applied to decentralized photovoltaic plants,” *Measurement*, vol. 142, pp. 195–212, 2019. [Online]. Available: <https://doi.org/10.1016/j.measurement.2019.04.085>



STRUCTURAL ANALYSIS OF A LONG-DISTANCE DOUBLE-DECKER BUS DURING CRASHES

ANÁLISIS ESTRUCTURAL DE UN BUS DE DOS PISOS DE LARGA DISTANCIA DURANTE COLISIONES

Jimmy Brito Morocho¹ , Marco Amaya Pinos^{1,*} , Luis López López¹ ,
Fabricio Espinoza Molina¹

Received: 13-05-2021, Received after review: 18-10-2021, Accepted: 26-11-2021, Published: 01-07-2022

Abstract

This study presents an analysis of frontal impact and lateral overturn collisions of a double-decker bus, carried out in accordance with Regulations 66 and 29 of the United Nations Economic Commission of Europe (UN/ECE), and the Ecuadorian Standardization Service Institute (INEN) with its regulation 1323:2009. The INEN is on charge of regulating the buses for transportation of Ecuadorian passengers. The continuous improvement of active and passive safety of buses with respect to accidents, is currently a topic with great social impact. In this context, the present paper applies the finite element method (FEM) to analyze the behavior of a double-decker bus subject to different collision scenarios, such as frontal impact and lateral overturn, with the purpose of studying the effects of an accident of this type of structure, considering that the existing regulations are not specific for this kind of vehicles. The obtained results enable taking into account different considerations when designing these elements.

Keywords: Collisions, rollover, frontal impact, regulation, energy, bus

Resumen

Este estudio presenta un análisis de colisiones de impacto frontal y volcamiento lateral de un autobús de dos pisos, conforme al Reglamento 66 y 29 de la Comisión Económica de las Naciones Unidas para Europa (UN/ECE), y el Servicio Ecuatoriano de Normalización (INEN) con su normativa 1323:2009, encargado de regular los autobuses para el transporte de pasajeros en el Ecuador. En la actualidad la mejora constante de la seguridad activa y pasiva de los autobuses con respecto a los accidentes es un tema de gran impacto social. En este contexto se analiza la colisión de un autobús de dos pisos aplicando el método de elementos finitos (MEF), el cual es sometido a diferentes escenarios de colisión como es de un impacto frontal y un volcamiento lateral, con la finalidad de estudiar los efectos de un accidente de este tipo de estructuras donde la normativa no es específica para esta clase de vehículos. Los resultados obtenidos permiten tener en cuenta consideraciones importantes al momento del diseño de estos elementos.

Palabras clave: colisiones, volcamiento, impacto frontal, reglamentación, energía, autobús

^{1,*}Universidad Politécnica Salesiana, Cuenca-Ecuador. Corresponding author ✉: mamaya@ups.edu.ec.

Suggested citation: Brito Morocho, J.; Amaya Pinos, M.; López López, L. and Espinoza Molina, F. "Structural Analysis of a Long-distance Double-decker Bus During Crashes". *Ingenius, Revista de Ciencia y Tecnología*. N.º 28, (july-december). pp. 63-70. 2022. DOI: <https://doi.org/10.17163/ings.n28.2022.06>.

1. Introduction

The bus is one of the main transportation means in Ecuador, due to its efficiency, flexibility in service routes and costs for the user; however, in 2018 this transportation mean was responsible for 8 % of the road crashes, significantly contributing to the accident rate and to the number of victims [1]; therefore, there is a great interest in improving both active and passive safety of passengers since the most frequent accidents are frontal impacts and overturns, which are considered the most serious and generate a great social impact due to both human and economic losses.

In 2015, the States Members of the United Nations adopted the 2030 Agenda, which states different sustainable objectives; it is intended to «make cities and human settlements inclusive, safe, resilient and sustainable» [2], and with the goal for 2030 of «providing access to transportation systems that are safe, affordable, accessible and sustainable for all and improving road safety, particularly through the expansion of public transportation, paying special attention to the needs of vulnerable people, women, children, people with disabilities and older people» [2].

International initiatives and regulations developed by government organizations that are sustained on the safety of human beings and which guarantee their integrity, should be considered when generating new public transportation systems and optimizing the existing ones. For example, double-decker buses have a large mass and their center of gravity is located at a point very high with respect to the floor, which significantly reduces its stability and resistance to a collision or to an overturn. If it is taken into account that these passenger transportation units travel long distances, it is relevant to consider all aspects related to the safety in the event of a collision [3].

Among the different types of accidents in which buses may be directly involved, frontal impacts and lateral overturns are deadliest. A study conducted by Transport Canada shows that frontal impacts represent 70 % of all bus accidents. In addition, it is considered one of the collisions that produce more deaths and serious injuries than any other accident. In general, when two vehicles that approximate at a high speed are involved in these impacts, the front structure of the vehicle is involved [4].

A study presented by Ramírez *et al.* [1] also indicate that traffic accidents that occur in roads involving public passenger transportation systems are mainly frontal collisions. Similarly, they state that the difference between the masses and configurations of the vehicles during the impact, generate critical material damages and serious injuries or even loss of life of the occupants.

The resistance to collisions is the capability of the structure to absorb the kinetic energy of the overturn

or frontal impact, which should provide an appropriate protection to the vehicle occupants during the traffic accident. This criterion is especially important in passenger transportation vehicles such as buses [5]. This is the reason why, the purpose of the simulations performed in the bus superstructure is to analyze the amount of energy absorbed during a frontal impact or lateral overturn collision in a double-decker bus. Such structure should be deformed as little as possible and should avoid any element to get into the bus survival space [6], according to regulations 29 [7] and 66 of the UN/ECE [8] and regulation NTE INEN 1323:2009 [9].

2. Materials y methods

The study of interest starts with a 3D modeling considering all the details and dimensions of the structure of the double-decker bus. CAD tools were used with the purpose of obtaining the final model for the simulation stages using the FEM; Solidworks was used for the preprocessing stage, while Ansys – LS DYNA [10] was used for the processing and post-processing stages.

The overturn study of the bus structure using the FEM was based on the NTE INEN 1323:2009 regulation [9] and on regulations 29 and 66 of the UN/ECE [7, 8]. The latter is pioneer in increasing the safety of public transportation year after year, implementing regulations that enable guaranteeing the safety of the occupants when a bus experiences a collision and no invasion of the structure to the passenger survival space occurs during an overturn.

In the application domain, regulation 66 of the UN/ECE states that it only applies to single deck vehicles, rigid or articulated, belonging to categories M2 or M3; according to regulations NTE INEN 1323 [9] and 2656 [11], double-decker buses belong to category M3; for these reasons, the overturn test of a double-decker bus may be carried out according to regulation 66, which supports the application of the regulation indicated in this study [8].

Once the overturn analysis was carried out, it was studied a frontal collision of the structure, which enabled visualizing the effect of this type of collision on structure deformation and how it invades the survival space [12].

2.1. Delimitation of the survival space

The survival space shows the geometrical features stated in regulation 66 of the UN/ECE considering the bus dimensions, and it should be located along its entire length as observed in Figure 1. Passengers and operators are in this space; during a collision, this space must not be invaded by the bodywork structure or any accessory that may affect the physical integrity of the occupants [8].

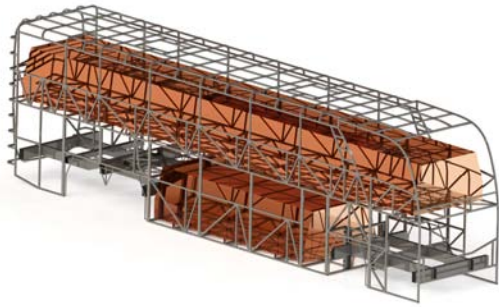


Figure 1. 3D modeling of the survival space within the bus passenger compartment

The location of the center of gravity of the bus structure must be clearly defined, as shown in Figure 2.

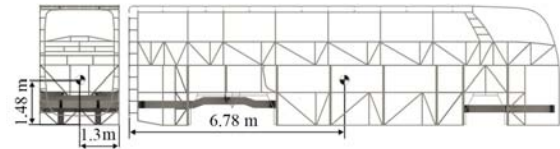


Figure 2. Location of the center of gravity of the bus structure

2.2. Conditions of the bus superstructure

Annex 4 of regulation 66 of the UN/ECE presents the perspectives of the structural description of the bus superstructure; the profiles and structural materials should comply with national and international standards [8].

The structural profiles used in the bus bodywork are shown in Table 1.

Table 1. Bus structural profiles

Profile	Quality	Regulation
R 80 × 40 × 2 mm	ASTM A-500	NTE INEN 1623
R 60 × 40 × 3 mm	ASTM A-500	NTE INEN 1623
R 60 × 40 × 3 mm	ASTM A-500	NTE INEN 1623
R 40 × 20 × 2 mm	ASTM A-500	NTE INEN 1623
C 50 × 50 × 3 mm	ASTM A-500	NTE INEN 1623

Paragraph 1.3 of annex 9 of regulation 66 of the UN/ECE [8] indicates that the data necessary to carry out the test must be met, where the values of mass, center of gravity and moments of inertia of the bus structure must be obtained in advance.

The values of mass, moments of inertia and center of gravity of the bus structure are shown in Table 2, and were obtained during the modeling process.

Table 2. Data sheet of the bus structure

Parameter	Value
Mass	3632,73 kg
Longitudinal position of the COG	6,78 m
Transverse position of the COG	1,30 m
Transverse height of the COG	1,48 m
I _{xx}	7,30179 × 10 ⁷ mm ⁴
I _{xy}	-7221,14 mm ⁴
I _{xz}	48267,2 mm ⁴
I _{yy}	7,09992 × 10 ⁷ mm ⁴
I _{yz}	-1,68985 × 10 ⁶ mm ⁴
I _{zz}	7,86809 × 10 ⁶ mm ⁴
I ₁₁	7,3018 × 10 ⁷ mm ⁴
I ₂₂	7,10443 × 10 ⁷ mm ⁴
I ₃₃	7,82286 × 10 ⁶ mm ⁴

2.3. Analysis using finite elements

The accuracy of finite elements models depends on the number of nodes and elements, as observed in Figure 3, which depends on the size and the types of components of the mesh; hence, the smaller the size and the larger the number of elements in a mesh, more precise will be the results of the analysis [13].

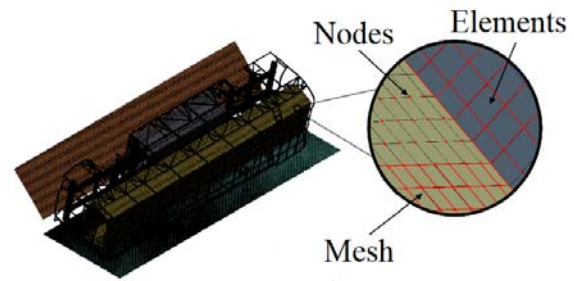


Figure 3. Nodes and elements of a mesh

Important aspects, such as the quality and type, should be taken into account to generate the mesh of the bus structure; these aspects are related with the density and type of the mesh used, which for this case study is a 20 mm hexahedral mesh [14, 15].

2.4. Computer simulation of the overturn test of a vehicle as equivalent homologation method

The bus overturn test is a quite fast and dynamic process with well differentiated stages; this should be considered when planning the test. The bus will tilt without balancing and without dynamic effects until it reaches an unstable equilibrium and starts to overturn, as specified in Figure 4 [8].

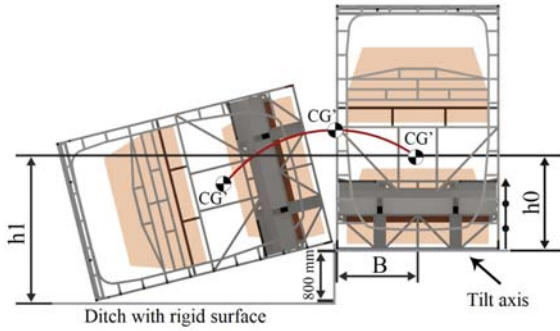


Figure 4. Specification of the overturn test of a vehicle at initial position in the platform

Annex 9 of regulation 66 of the UN/ECE, is applied through the finite element method for computer simulation of the overturn test of a double-decker bus structure. The mathematical values entered in the software to simulate the overturn correspond to the bus turning speed with respect to an axis located in the tilting platform and the gravity, in order to simulate the movement of the structure with respect to the platform.

Equation (1) gives the value of angular speed to be applied.

$$\omega = \sqrt{\frac{2 \cdot m \cdot g \cdot \Delta h}{I}} = 3,3953 \text{ rad/s}^2 \quad (1)$$

Where:

m = mass (kg)

g = gravitational constant (m/s^2)

Δh = height variation (m)

I = rotational inertia ($\text{kg} \cdot \text{m}^2$)

The contacts between the master surface and a set of slave nodes are defined for the simulation. The master surface is defined through the rigid elements used to establish the surface on which the structure of the bus impacts, as seen in Figure 5.



Figure 5. Bus in position of first contact with the rigid impact surface

2.5. Computer simulation of the frontal collision

Recent statistics of traffic accidents demonstrate that almost two thirds of the collisions are frontal, and half

of them show a coverage between 30 and 50 % of the front surface [16]. Computer simulation tests are conducted according to regulation 29 of the UN/ECE [8], to assess the effects of this type of collision.

Computer simulation tests of frontal impacts against stationary objects, enable observing the behavior of the vehicle during a collision; it is also an inexpensive method, compared to a real Crash Test [10], [17,18].

The frontal impact is analyzed at 64 km/h, considering that the bus has a frontal impact against a centered stationary barrier (Figure 6). This impact intends to simulate the most frequent type of collisions in roads that result in serious or deadly injuries, since most frontal crashes in double-decker buses directly involve the operators' cabin [19].

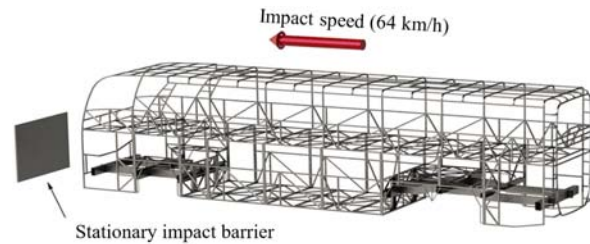


Figure 6. Specifications for simulating the bus frontal impact

It is important to indicate that the speed limit for this type of vehicles in straight roads is 90 km/h, according to the Ecuadorian National Transportation Agency, situation which is considered in other research works that analyze the frontal impact of a single-deck bus [20].

3. Results and discussion

3.1. Bus overturn

The application of the overturn test of the double-decker bus structure using the finite element method, works well until the structure reaches its maximum deformation at time instant $t = 0.621s$ after impacting the rigid surface.

3.1.1. Energies

The values of height obtained for the centers of gravity during the overturn, shown in Table 3, are used to find the difference between the heights (Δh) of the center of gravity, equation 3, which is a variable required in equation 2 that gives the total energy (E_T) that will be absorbed by the bus superstructure in the overturn test.

Table 3. Centers of gravity

Parameter	Value
Point of instability (H)	2284,8 mm
Point of contact (HC)	632 mm

$$E_T = 0,75 \cdot m \cdot g \cdot \Delta h \tag{2}$$

$$\Delta h = H - HC \tag{3}$$

$$E_T = 4,42 \times 10^7 \text{ J}$$

According to the equations of regulation 66, the total energy absorbed by the bus is $4,42 \times 10^7 \text{ J}$, and the maximum value of total energy absorbed obtained in the simulation (Figure 7) is $4,56 \times 10^7 \text{ J}$. When comparing the total energy calculated and the one obtained in the simulation there is a difference of 3.32 %, which is due to the fact that the center of gravity is not exact because not all mechanical and finishing components, such as glasses, seats, etc., are considered in the modeling process. Although this difference exists between the values obtained in the calculation and in the simulation, it may be considered that they are coherent and acceptable.

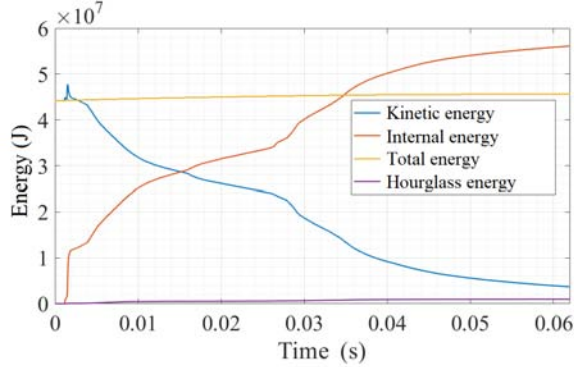


Figure 7. Energies obtained from the simulation of the bus overturn test

The maximum value of Hourglass energy during the overturn test is $0,0966 \times 10^7 \text{ J}$, which represents 2 % of the total energy. According to annex 9 of regulation 66, this value should not exceed 5 % for the simulation to be accepted; therefore, this requirement is fulfilled.

3.1.2. Survival spaces

Considering that regulation 66 states that the structure should never invade the survival space or vice versa during the overturn, when the bus structure reaches maximum deformation, it does not fulfill such regulation.

Figure 8 shows the displacement of the structure with respect to the survival space. The lower deck of the bus is not affected by the structure deformation since it is rigid enough to withstand an overturn collision; however, the survival space of the upper deck is invaded by the structure in 48 mm when reaching the maximum deformation during the overturn; thus, it does not fulfill the requirement of regulation 66 of the UN/ECE.

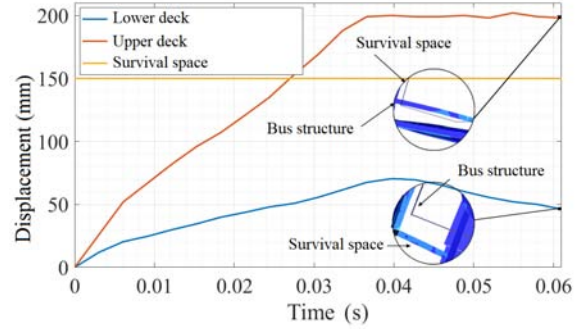


Figure 8. Displacement of the double-decker bus structure with respect to the structure

3.1.3. Speed

The bus speed is high until it impacts on the rigid surface, and after this instant the speed decreases progressively (Figure 9); however, the most important time interval is when the bus impacts on the surface, since our interest is the contact between the two surfaces during the overturn test; the speed value does not decrease to zero, because the overturn simulation is carried out until the maximum deformation of the bus structure according to the regulation.

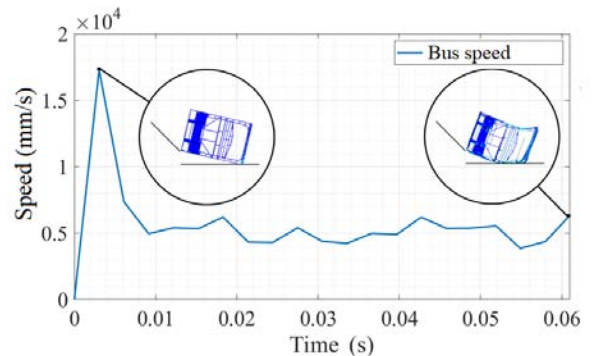


Figure 9. Behavior of the speed during the bus overturn test

3.2. Frontal impact

The bus speed prior to the collision is given by the speed change (ΔV) that the vehicle experiences and by the deceleration, which is a function of the mass and the rigidity of the objects that collide.

The impact zone of the bus with the barrier covers the entire vehicle width; therefore, the bus frame absorbs most of the kinetic energy during the collision, and moreover, the mathematical model was adjusted to obtain the same conditions of a real physical test.

3.2.1. Energies

The maximum total energy generated in the simulation of the bus frontal impact is $4,56 \times 10^8 J$, which remains constant, i.e., is the same before and after the collision; this indicates that the energy produced in the collision is dissipated through the deformation, better known as internal energy (Figure 10).

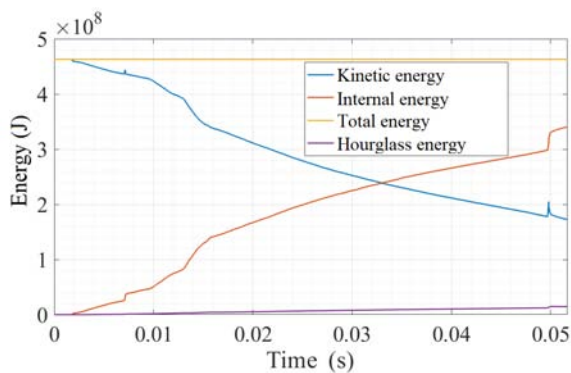


Figure 10. Energies obtained from the simulation of the bus frontal impact

During the bus impact, the maximum value reached by the Hourglass energy is $0,106 \times 10^8 J$ (Figure 11), which represents 2.3 % of the total energy; thus, it fulfills the regulation which indicates that this value should not exceed 5 % of the total energy.

3.2.2. Deformation

The cabin of the driver reaches a deformation of 250 mm, as can be observed in Figure 11, due to the impact with the wall. The structure profiles with greater deformation are those that impact directly with the surface; moreover, the chassis wings behave as an underrun bar, which prevents the cabin of the driver from experiencing an excessive deformation, but this does not prevent that structure debris may damage the integrity of the controllers of the transportation unit.

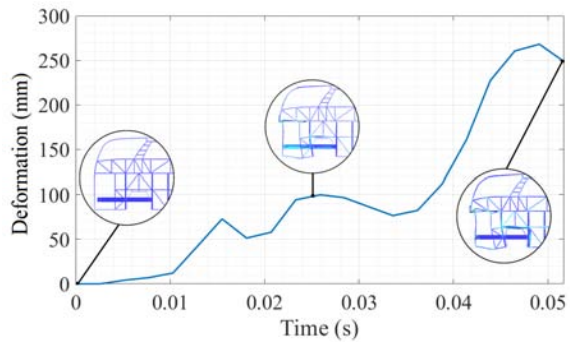


Figure 11. Bus deformation during the frontal impact on the stationary surface

3.2.3. Speed

The bus starts with a speed of 17 800 mm/s (64 km/h), which then decreases continuously due to the impact on the stationary barrier; thus, the cabin of the driver is deformed in a short time interval until reaching a standstill, and the most affected parts are the ones that impact directly on the surface (Figure 12).

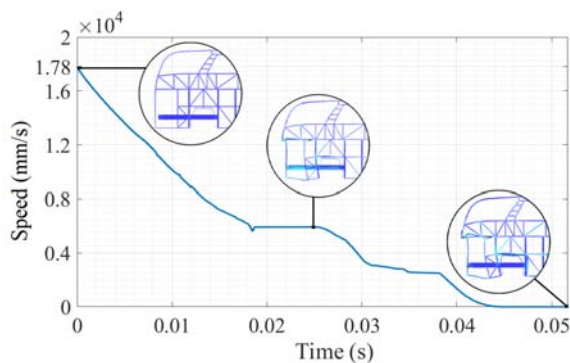


Figure 12. Behavior of the speed during the simulation of the bus frontal impact

4. Conclusions

This study set up two computer simulation processes, namely lateral overturn and frontal impact, of a double-decker bus, according to regulations R66 and R29 of the UN/ECE [8] and regulation NTE INEN 1323:2009 [9]. This enabled to estimate the resistance of the vehicle superstructure during a collision, and also to observe the behavior of the structure with respect to the survival space and the deformation modes of the vehicle.

The collision analysis enables to evaluate the elastoplastic behavior of the steel that makes up the structure of the double-decker buses used in interprovincial transportation, through the computer simulation based on explicit dynamics.

The upper part of the structure was affected during the overturn, since there was a deformation that generated an invasion of 48 mm of the survival space; this can be observed in Figure 8.

Since the center of gravity is not exact, there is a percentage error of 3.32 % between the value of total energy obtained in the overturn simulation and the one calculated using the formulas suggested by regulation 66 of the UN/ECE [8]. It is important to indicate that this numerical error is considered small, and therefore the results obtained for the bus overturn are valid.

The forces generated by the frontal impact of the bus structure on a stationary surface produce high deformation, especially in the cabin of the driver where it reaches values of 250 mm in a very short period of time. This is because the most critical parts are the profiles that receive the impact directly. The bus superstructure is one of the main passive safety components in these vehicles, and therefore design optimization is essential for minimizing the damages that may be caused to passengers and operators of the transportation unit.

In general, the frontal part of the bus structures does not have any protection system to safeguard the life of the cabin occupants during a frontal impact. These elements of the bodywork structure are not capable of totally dissipating the kinetic energy, which should be considered in the design of these elements.

References

- [1] B. del Valle Arenas Ramírez, F. E. Molina, A. Arenas, E. Donnet, and F. A. Izquierdo, “Metodología de estudio de accidentes de transporte colectivo de personas en países con carencia de información de calidad = methodology for the study of traffic accident with buses and coaches in countries with lack of quality information,” in *XIV Congreso Iberoamericano de Ingeniería Mecánica (XIV CIBIM)*, 2019, pp. 1–10. [Online]. Available: <https://bit.ly/3CUEqDo>
- [2] United Nations. (2021) Objective 11: Make cities more inclusive, safe, resilient and sustainable. United Nations. Sustainable Development Objectives. [Online]. Available: <https://bit.ly/3nPicP8>
- [3] N. Çolak, U. Şahin, A. Candaş, and C. İmrak, “Desing and analysis of the protective structure of an intercity bus during a rollover accident,” *Trans Motauto World*, vol. 3, pp. 62–65, 2018. [Online]. Available: <https://bit.ly/3re5dIK>
- [4] W. T. Gardner, *Evaluation of occupant protection in buses*. RONA Kinetics and Associates Ltd., 2002. [Online]. Available: <https://bit.ly/30XY3xo>
- [5] ENNOMOTIVE. (2019) Choque de vehículos: ¿Cómo se absorbe la energía mecánica? [Online]. Available: <https://bit.ly/3CMviko>
- [6] B. D. Palacios, “Análisis mediante el mef de la protección de los conductores en autobuses,” 2016. [Online]. Available: <https://bit.ly/3HVFFWU>
- [7] UN/ECE, *Regulation No 29 of the Economic Commission for Europe of the United Nations (UN/ECE) – Uniform provisions concerning the approval of vehicles with regard to the protection of the occupants of the cabin of a commercial vehicle*. Economic Commission for Europe of the United Nations (UN/ECE). [Online]. Available: <https://bit.ly/3FOFJ96>
- [8] —, *Regulation No 66 of the Economic Commission for Europe of the United Nations (UN/ECE) – Uniform technical prescriptions concerning the approval of large passenger vehicles with regard to the strength of their superstructure*. Economic Commission for Europe of the United Nations (UN/ECE), 2011. [Online]. Available: <https://bit.ly/3r7Y391>
- [9] INEN, *NTE INEN 1323. Vehículos Automotores, Carrocerías de Buses, Requisitos*. Servicio Ecuatoriano de Normalización, 2009. [Online]. Available: <https://bit.ly/3oU82Mo>
- [10] E. A. Fazio, F. A. Izquierdo, R. G. Pastoril, and Á. L. M. López, “Aplicación de técnicas de ensayo virtual a ensayos de vuelco de superestructuras de autobuses y autocares.” in *Actas del IX Congreso de Ingeniería del Transporte, CIT 2010*. Madrid, España: Universidad Politécnica de Madrid, 2010. [Online]. Available: <https://bit.ly/314TI5y>
- [11] INEN, *NTE INEN 2656: Clasificación Vehicular*. Servicio Ecuatoriano de Normalización, 2016. [Online]. Available: <https://bit.ly/3lbTpDd>
- [12] A. Garcia, M. Sanchez, E. Alcalá, and A. Carretero, “Diseño estructural de autobuses y autocares,” *DYNA-Automoción y Transporte*, vol. 73, no. 3, 1998.
- [13] O. C. Zienkiewicz, *El método de los elementos finitos*. Editorial Reverté, 1981. [Online]. Available: <https://bit.ly/3DWiVUf>
- [14] C. H. A. Arroba, M. A. C. Suárez, C. G. S. Espín, and G. E. C. O. na, “Simulación de vuelco con ANSYS y LS-DYNA de una superestructura de un autobús y su incidencia en el área de supervivencia,” *Ciencia Digital*, vol. 6, no. 4.2, pp. 86–99, 2019. [Online]. Available: <https://doi.org/10.33262/cienciadigital.v3i4.2.1011>

- [15] G. Núñez Milán, “Simulación de un ensayo de vuelco de un autobús mediante ls-dyna,” B.S. thesis, 2016. [Online]. Available: <https://bit.ly/3CUzK0A>
- [16] D. D. Illescas Pérez, “Simulación de un choque frontal de un vehículo automóvil contra diferentes tipos de barrera,” 2009. [Online]. Available: <https://bit.ly/3HZn77U>
- [17] E. Acar, B. Yilmaz, M. A. Güler, and M. Altin, “Multi-fidelity crashworthiness optimization of a bus bumper system under frontal impact,” *Journal of the Brazilian Society of Mechanical Sciences and Engineering*, vol. 42, no. 9, p. 493, Aug 2020. [Online]. Available: <https://doi.org/10.1007/s40430-020-02572-3>
- [18] M. A. Güler, M. E. Cerit, S. K. Mert, and E. Acar, “Experimental and numerical study on the crashworthiness evaluation of an intercity coach under frontal impact conditions,” *Proceedings of the Institution of Mechanical Engineers, Part D: Journal of Automobile Engineering*, vol. 234, no. 13, pp. 3026–3041. [Online]. Available: <https://doi.org/10.1177/0954407020927644>
- [19] Latin NCAP. (2021) Impacto frontal. Latin NCAO. Para autos mas seguros. [Online]. Available: <https://bit.ly/2ZpTDPc>
- [20] D. Cárdenas, J. Escudero, S. Quizhpi, and M. Amaya Pinos, “Propuesta de diseño estructural para buses de carrocería interprovincial,” *Ingenius. Revista de Ciencia y Tecnología*, no. 11, pp. 42–52, 2014. [Online]. Available: <https://bit.ly/3xtnjYr>



IMPROVEMENT OF THE LACTOSE GRINDING PROCESS FOR A COMPANY MANUFACTURING DAIRY PRODUCTS

MEJORA DEL PROCESO DE MOLIENDA DE LACTOSA PARA UNA EMPRESA FABRICANTE DE PRODUCTOS LÁCTEOS

Darío J. Pinguil Loja¹ , Víctor R. Lojano Pillco¹ ,
Nelson G. Jara Cobos^{1,*} , Fran Z. Reinoso Avecillas¹

Received: 08-09-2021, Received after review: 30-11-2021, Accepted: 11-03-2022, Published: 01-07-2022

Abstract

This research presents results obtained after the implementation of an improvement in the lactose grinding process of a company which manufactures dairy products. The current situation of the process was determined identifying that a lactose particle size of 40.23 μm is obtained in a grinding time of 48 continuous hours. After theoretical and experimental research processes, it was obtained as the best option a fine grinding with an average particle size of 22 μm in a grinding time of 5 continuous hours, using a drum mill with a volume of grinding elements of 25% and an operating velocity of 61 rpm, and the Cylpebs as specified in this research work; this generates savings in raw material (lactose), energy consumption and operation time of the grinding process.

Keywords: Lactose, particle size, granulometric analysis, cylpebs distribution

Resumen

Esta investigación presenta resultados obtenidos luego de haber implementado una mejora en el proceso de molienda de lactosa de una empresa fabricante de productos lácteos. Se determinó la situación actual del proceso, identificando que, en un tiempo de molido de 48 horas continuas, se obtiene un tamaño de partícula de lactosa de 40,23 μm . Posterior a los procesos de investigación teórica y experimental se estableció que con el uso de un molino de tambor con un volumen de elementos molientes del 25 %, una velocidad de operación de 61 rpm y el uso de cylpebs especificados en este trabajo, representan la mejor opción para obtener una molienda fina con un tamaño promedio de partículas de 22 μm en un tiempo de molido de 5 horas continuas, lo que genera principalmente un ahorro por materia prima (lactosa), consumo energético y tiempo de operación del proceso de molido.

Palabras clave: lactosa, tamaño de partícula, análisis granulométrico, distribución de cylpebs

^{1,*}Grupo de Investigación y Desarrollo en Simulación, Optimización y Toma de Decisiones GID - STD, Universidad Politécnica Salesiana, Ecuador. Corresponding author ✉: njara@ups.edu.ec .

Suggested citation: Pinguil Loja, D. J.; Lojano Pillco, V.R.; Jara Cobos, N. G. and Reinoso Avecillas, F. Z. "Improvement of the lactose grinding process for a company manufacturing dairy products," *Ingenius, Revista de Ciencia y Tecnología*, N.º 28, pp. 71-79, 2022, DOI: <https://doi.org/10.17163/ings.n28.2022.07>.

1. Introduction

The quality policies and the global market in general demand industries that they produce better quality products, i.e., the market becomes more competitive, making the task more difficult for many industries that want to remain in the market and, especially, open new niches.

This project develops a proposal for improving the lactose grinding process, used as raw material for producing condensed milk; in this sense, it has been sought to purely achieve the reduction of the particle size, with the purpose of obtaining a better consistency in the final product.

At the initial stage, it is determined the results of the current situation of the grinding process parameters such as, operating time, grinding velocity, volume of raw material (lactose) and particle size. The aim of this is to set the goals necessary to fulfill the attainment of an average size of the particle of 25µm, feature required to manufacture condensed milk in the company. Afterwards, an experimental analysis was carried out to determine the best type of mill that enables to reduce the size of the particles and the grinding time.

The improved particle size is determined by means of the macroscopic measuring process.

The results obtained prove that the size of the lactose particle as raw material significantly improves the quality of the condensed milk texture, as one of the dairy products that employs this raw material.

The work of analysis, proposals for improvement, experimental development and measurements is found in a comprehensive manner in the final report of the work by Lojano Pillco *et al.* [1].

1.1. Parameters that influence the grinding process

There is a series of parameters that influence the lactose grinding process [2], some of which are presented below:

- Critical velocity
- Mill operating velocity
- Relationship between the variable elements of the mills
- Size of the grinding elements
- Load volume
- Distribution of the material to be grinded
- Power
- Mill types

1.1.1. The critical velocity

Is the one that occurs when the centrifugal force cancels the influence of gravity on the balls. The following equation (1) determines this critical velocity [3].

$$V_c = \frac{42,3}{\sqrt{D}} \text{ Metric system} \quad (1)$$

Where:

$$\begin{aligned} V_c &= \text{Critical velocity in rpm} \\ D &= \text{Mill diameter [m]} \end{aligned}$$

1.1.2. The mill operating velocity

Should be smaller than the critical velocity; the operating range of the ball mills or cyppebs is chosen between 65% and 80% of V_c [4]. Figure 1 shows the movement of the mill with its cascade and waterfall effects, respectively.

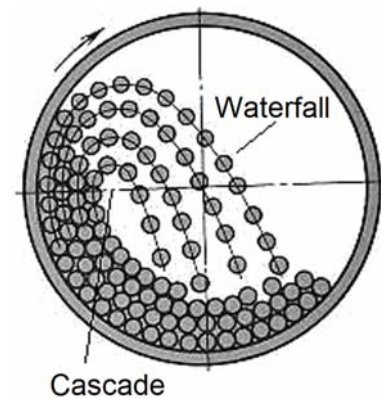


Figure 1. Movement of the load in a ball mill [5]

Equation (2) is presented for calculating the operating velocity [5].

$$V_{op} = V_c \times \%V_c \quad (2)$$

Where:

$$\begin{aligned} V_{op} &= \text{Operating velocity} \\ V_c &= \text{Critical velocity in rpm} \\ \%V_c &= \text{Percentage of critical velocity} \end{aligned}$$

1.1.3. The relationship between the variable elements of the mills

Considers mill variables such as critical velocity, mill internal diameter and grinding bodies [2].

1.1.4. Maximum size of the grinding elements

Should not present a unique uniform size, but a distribution of the grinding elements is made from the maximum diameter, but at lower sizes. The maximum size of the grinding elements is obtained from the percentage distribution and the corresponding dimensions of the components to obtain an effective grinding.

1.1.5. The load of the grinding bodies

Makes reference to the fact that the mills do not operate totally full. The volume occupied by the grinding elements and the material to be grinded referred to the total volume of the mill cylinder is known as the load of the grinding bodies, which is calculated using equation (3) [2].

$$B = V_m \times b \times 0,6 \times \delta_b \quad (3)$$

Where:

- B = Weight of the grinding bodies [kg]
- b = constant (0,2 - 0,4)
- V_m = Volume of the material in dm^3
- δ_b = density of the cylpebs 7,8 kg/dm^3
- D = nternal diameter of the mill cylinder
- L = nternal length of the mill

The degree of filling in the lactose grinding using cylpebs typically comprises a load between 25 and 33% of the total volume, and is constituted by the grinding bodies and the material to be grinded [3].

1.1.6. The distribution of size of the grinding material, balls or cylpebs

It may be determined through various methods, of which two were used in this research:

Method 1. According to the diameter. Once the initial load of the grinding material is known, the diameters of the balls that are planned to be used are added. The sum corresponds to 100%. Afterwards, the percentage corresponding to the value of each diameter is determined. The result obtained corresponds to the percentage in weight of the initial load, which corresponds to each size of cylpebs.

Method 2. According to the diameter with Bond formula. Once the initial load of the grinding material and their maximum size is known, the distribution percentage corresponding to each ball size is determined using: $Y = 100(X/B)^{3/2}$; this is taken to the graph to determine the percentage in weight corresponding to each commercial size of cylpebs that should be fed.

Regarding the percentage distribution of the grinding means as a function of the diameter, it is applied Bond formula given by equation (4) [6].

$$y = 100 \left(\frac{x}{B} \right)^m \quad (4)$$

Where:

- y = % weight of grinding means with diameter below x
- B = aximum ball diameter [in] or [mm]
- x = diameter of the ball to be distributed [in] or [mm]
- m = constant, its values are:
(3,2 for rod mills or cylpebs)
(3,84 for ball mills)

1.2. Lactose

The lactose appears as white crystalline particles or powder. They are traditionally used in manufacturing pills, and it is considered a sugar of great importance in the food processing industries. It is an excellent excipient of tablets and pills, among many other applications.

The solubility of lactose is ten times smaller than that of sucrose, if sugars added are summed, the immediate problem will be to avoid the saturation of the solution, since when the saturation limit is reached the excess of sugars will precipitate as crystals forming lumps, physical defect that commonly appears in commercial sweets [7]. In this sense, using a lactose with a particle size around 30 μm results very convenient to improve the quality of dairy products such as condensed milk.

1.3. Methods for measuring the particle size

The methods of granulometric analysis by sieving and microscopic visualization were used in this project.

1.3.1. Granulometric analysis by sieving

It is one of the most ancient techniques for classifying powders through sieving. It is among the most commonly used and less costly techniques for determining the particle size distribution in a wide range of sizes, from little more than 100 μm to approximately 20 μm [8] (Figure 2).



Figure 2. Sieve and sieving process

A complete granulometric analysis consists in passing a material, in general 100 grams representative of the original sample, through a series of sieves, starting with a lower number of meshes and ending with the one with the higher number.

Table 1 presents the sieve designation according to what is established in the ASTM E-11 standard.

Table 1. ASTM sieve designation and corresponding aperture openings [9]

ASTM Sieve Designation					
Aperture Opening	Designation	Aperture Opening	Designation	Aperture Opening	Designation
125 mm	5.00 in.	9.50 mm	3/8 in.	425 µm	No. 40
106 mm	4.24 in.	8.00 mm	5/16 in.	355 µm	No. 45
100 mm	4 in.	6.70 mm	0.265 in.	300 µm	No. 50
90 mm	3 ½ in.	6.30 mm	¼ in.	250 µm	No. 60
75 mm	3 in.	5.60 mm	No. 3 ½	212 µm	No. 70
63 mm	2 ½ in.	4.75 mm	No. 4	180 µm	No. 80
53 mm	2.12 in.	4.00 mm	No. 5	150 µm	No. 100
50 mm	2 in.	3.35 mm	No. 6	125 µm	No. 120
45 mm	1 ¾ in.	2.80 mm	No. 7	106 µm	No. 140
37 mm	1 ½ in.	2.36 mm	No. 8	90 µm	No. 170
31.5 mm	1 ¼ in.	2.00 mm	No. 10	75 µm	No. 200
26.5 mm	1.06 in.	1.70 mm	No. 12	63 µm	No. 230
25 mm	1 in.	1.40 mm	No. 14	53 µm	No. 270
22 mm	7/8 in.	1.18 mm	No. 16	45 µm	No. 325
19 mm	¾ in.	1.00 mm	No. 18	38 µm	No. 400
16 mm	5/8 in.	850 µm	No. 20	32 µm	No. 450
13.2 mm	0.53 in.	710 µm	No. 25	25 µm	No. 500
12.5 mm	½ in.	600 µm	No. 30	20 µm	No. 635
11.2 mm	7/16 in.	500 µm	No. 35		

1.3.2. Microscopy analysis

It is a technique that enables quickly visualizing the size and nominal shapes of the particles in a sample, and obtain a representative micrography of the region analyzed; in addition, it enables enlarging details of the shape and surface of the particles [1] (Figure 3).

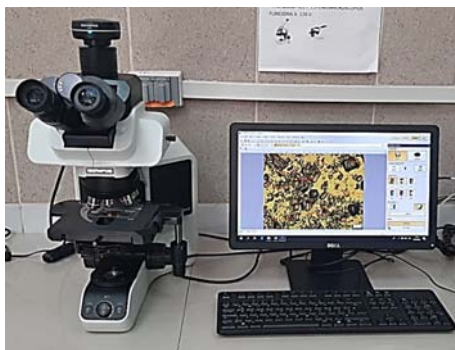


Figure 3. OLYMPUS BX43 Microscope

2. Materials and methods

For the research, it was carried out at first instance an evaluation of the current situation of the lactose grinding process carried out at the company manufacturer of dairy products, establishing the fundamental variables of the process such as velocity, distribution of the grinding material and grinding time. The samples were subject to sieves and microscopy to know the current

size of the particle and, based on this information, a proposal was made for improving the lactose grinding process with the optimal operating parameters.

2.1. Description of the current lactose grinding equipment

It is used a horizontal rotating mill with a diameter of 20 cm and a length of 30 cm, capacity of 2 kg, power of 1 hp and a rotating velocity of 61.7 rpm; it employs stainless steel washers as grinding elements (see Figure 4).



Figure 4. Horizontal rotating mill

3. Operating parameters

Table 2 presents the parameters used for the lactose grinding process.

Table 2. Operating conditions

Operating conditions	
Grinding time [h]	48
Lactose weight [kg]	2,5
Tricalcium Phosphate weight [g]	100
Velocity [rpm]	61
Grinding material	washers

Regarding the washers used for the grinding process, these are placed in a volume of approximately 12%, in a number of 40 units, whose distribution is made according to their internal and external diameter (see Table 3 and Figure 5).



Figure 5. Grinding material – Stainless steel washers

Table 3. Distribution of sizes of washers

Int. Diam. (mm)	Ext.m Diam. (mm)	Weight (kg)	Number
42	75	2,9322	37
22	50	0,1585	2
13	38	0,07925	1
TOTAL		3,17	40

As it has been mentioned, the material to be grinded is lactose, which provides sweetness to the milk. This product is commercialized in sacks of 50 kg (see Figure 6), generally with an initial granulometry of 150 μm , value determined by the manufacturer.



Figure 6. Lactose: sack and sample

With the purpose of verifying the particle size set in the raw material, it was determined the distribution of the particle size using the sieving method, considering a sample of 100 g and a stirring time of 30 min [10].

Once such procedure has been carried out [11], the previous results of the sieving process are seen in Figure 7, where the curve of % of passing accumulated represents the percentage of sample with its equivalent size, and the curve of % of retained accumulated represents the percentage of material with a larger size (x).

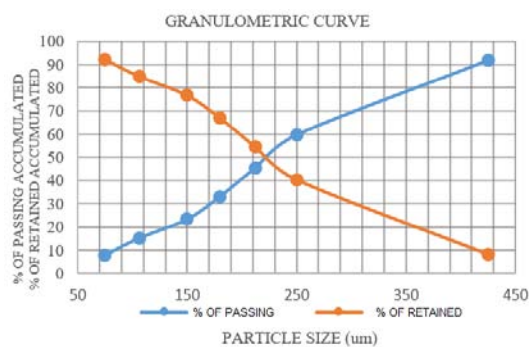


Figure 7. Percentage of passing accumulated and retained accumulated vs. particle size

With what has been determined and making average estimations of the particle sizes, based on the sieve distribution and relating it to the mesh size in μm and the weight of the retained fraction, values are presented to estimate the characteristic average

of the distribution of lactose grain sizes as 241 μm (Table 4). This value differs from the certified size of the lactose particle size, which is 150 μm , setting the need of choosing another procedure for measuring the particle size.

The microscopic analysis enabled to quickly visualize the nominal size and shape of the particles of a sample, and obtain a representative micrograph of the region analyzed; in addition, details of the shape and surface of the particles are obtained through enlargement [1].

According to the aforementioned procedure and an augmentation factor of 4x, it may be observed that the lactose particles have heterogeneous and random shapes, with different dimensions (Figure 8).

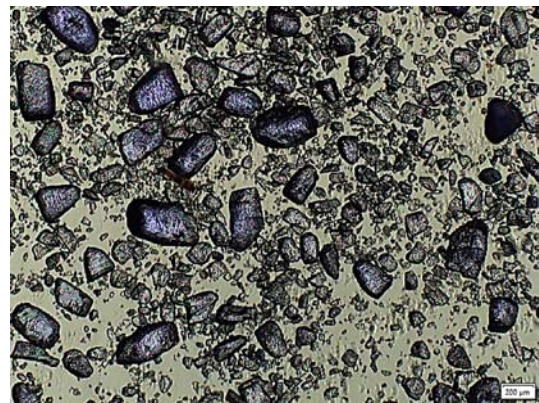


Figure 8. Lactose particles before grinding

3.1. Particle size obtained – current lactose grinding process

Once the lactose has been subject to the current grinding process, it is obtained the microphotograph of a sample, in order to determine the average size and shape of the resulting particle (see Figure 9).

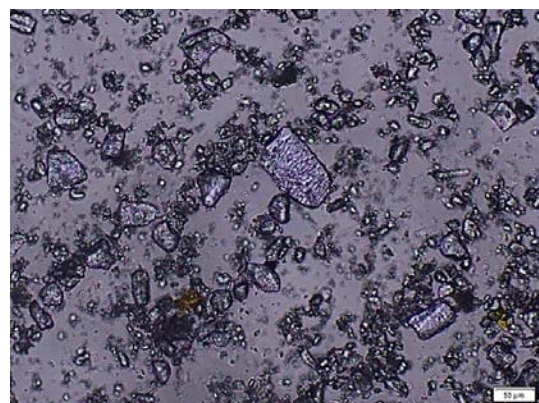


Figure 9. Lactose particles after 48 h of grinding

After 30 measurements were performed, it was obtained a minimum particle size of 19.99 μm , a maximum size of 108.67 μm , which resulted in an average

of 40.23 μm and a standard deviation of 17.24 μm . In the sense, it has been possible to determine that the current process reduces the size of the particle, but, due to the heterogeneity of the particle sizes and to the larger number of grinding hours (which causes that the lactose sticks on the grinding elements), this raw material results inadequate to obtain condensed milk with the consistency required by the company.

3.2. Improvement alternatives

According to the research works, the following parameters are considered for selecting the mill type:

- Grain size to be obtained
- Grinding time
- Grinding type
- Required power
- Cost

After analyzing the weighting of the parameters applied to the four types of mills that may be employed for the lactose grinding process, namely planetary mill, attritor mill, drum mill and high energy mill, the drum mill resulted the best option, achieving the highest weighting value (see Table 4). Therefore, for the development of the present improvement project, the horizontal rotating drum mill was used, to mainly determine the optimal time, velocity and size distribution of the grinding material.

Table 4. Weighting of results – selection of the best alternative

Mill type	Cost	Weighting				Total
		Power required	Grinding time	Grain size	Type type	
Planetary	3	3	5	5	1	17
Attritor	3	3	3	3	5	17
Drum	5	3	3	3	5	19
High energy	1	1	5	5	1	13

3.3. Experimental grinding tests

Three grinding parameters were taken into account for the improvement process: size distribution of the grinding material, grinding time and velocity; for this purpose, preliminary tests were carried out with different types of grinding material: balls and cylpebs.

Filling. The optimal filling of the mills is determined according to equation (5) and Figure 10 [1].

$$h = 0,16D \quad (5)$$

Where:

h = distance from the central axis of the drum

D = drum internal diameter

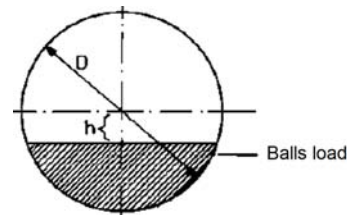


Figure 10. Filling of grinding material [1]

Critical velocity. After performing the corresponding calculations, it is determined a critical velocity of 94.5 rpm; thus, the operating velocity should be in a range from 65 to 80%, which corresponds to values between 61.425 rpm and 75.6 rpm.

Grinding material. Two types of grinding materials, balls and cylpebs, were used for the tests, with dimensional, weight and size distribution features as specified in Tables 5 and 6; for both cases it was kept constant a filling degree of 25% and a velocity of 61.4 rpm.

Table 5. Size distribution of balls

Diameters (in)	% Weight	Weight (kg)	Unit weight (kg)	Number of balls
1 ¼	55,55	3,57	0,132	27
1	44,44	2,85	0,0671	42
2 ¼	100%	6,43		69

Table 6. Size distribution of cylpebs

Diam. (mm)	Length (mm)	% Of weight	Weight (kg)	Unit weight (kg)	Number
1 ½	29,28	26,66	1,82	0,262	7
1 ¼	29,19	22,22	1,52	0,183	8
1	22,44	17,77	1,21	0,089	14
¾	23,01	13,33	0,91	0,051	18
05-ago	18,18	11,11	0,76	0,028	27
½	19,15	8,88	0,6	0,02	30
45/8		100%	6,85		104

4. Results and discussion

Table 7 shows the results of the five tests with different grinding times using balls as grinding elements; the particle sizes were measured using the microscopy technique, in which three samples of each test performed were taken and, similarly, thirty measurements for each sample were performed, giving as result the maximum and minimum sizes of the lactose particles.

In the different tests performed, it was also observed that a larger grinding time implies larger product losses, mainly due to the agglomeration of the

lactose in the mill walls and in the grinding bodies, as a result of the increment in the operating temperature [1].

Table 7. Results obtained with balls as grinding material

Losses (g)	Time (h)	Particle size (um)	
		Maximum	Minimum
100	1	102,6	26,45
110	2	96,89	19,85
119	3	85,42	17,25
150	4	60,07	12,08
200	5	59,04	6,82

The test was performed with 1050 grams of lactose and 100 grams of tricalcium phosphate, with a minimum grinding time of one hour, because at that time the reduction in the particle size of the product begins to be noted, and a maximum grinding time established at five hours, because at that time a larger agglomeration of the product in the mill walls and in the grinding bodies begins to be noted. In this way, a good reduction in particle size was obtained according to the microscopy images (see Figures 11 and 12).

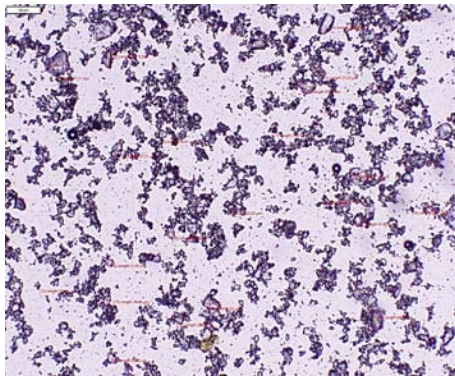


Figure 11. Lactose particles grinded for 1 h – Scale 100 μm

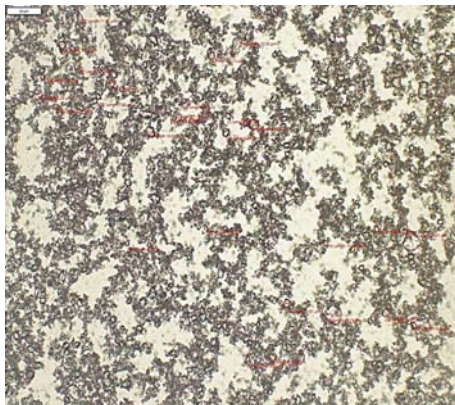


Figure 12. Lactose particles grinded for 5 h – Scale 50 μm

Table 8 presents the results of the five tests performed at different grinding times, similarly using 1050 grams of lactose and 100 grams of tricalcium phosphate; the measurement of the particle sizes is carried out using the microscopy technique, in which 30 measurements of each sample are carried out.

Table 8. Results obtained with cylpebs as grinding material

Losses (g)	Time (h)	Particle size (um)	
		Maximum	Minimum
80	1	100,85	15,56
120	2	92,62	12,23
132	3	78,45	10,81
290	4	65,48	9,89
359	5	54,29	5,78

Figures 13 and 14 display a difference in the sizes of the lactose particles, for grinding times of one and five hours, where the sizes of the lactose particle may be appreciated.

One of the factors that are established for improving the lactose grinding process is the grinding material; in this case it is proposed to use cylpebs (stainless steel cylinders), because this shape has a larger surface area to reduce the size of the lactose particle through impact, enabling to obtain a larger number of fine particles in less time.

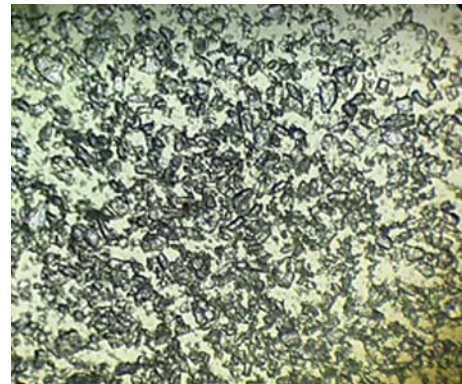


Figure 13. Lactose particles grinded for 1 h – Scale 100 μm

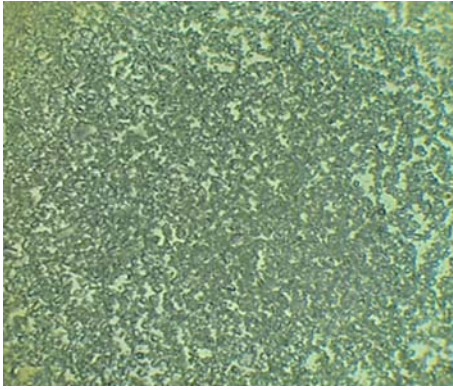


Figure 14. Lactose particles grinded for 5 h – scale 100 μm

Operating parameters such as the time, velocity and size distribution of the cylpebs, should be controlled for the grinding to be effective. These improved parameters are presented in Table 9, which are compared with the results of the current situation of the company.

Table 9. Improved operating parameters

Parameters						
% Load volume	Velocity [rpm]	Grinding time [h]	Grinding material	Weight (kg)	Number	Size [μm]
12	61	48	washers	3,174	40	40,23
25	61	5	cylpebs	6,85	104	22

5. Conclusions

The variables identified that have influence on the lactose grinding process are the size distribution of the grinding material, the grinding times and the velocity, which impact the size of the lactose grain.

Through the grinding tests performed in the drum mill, it was possible to determine the adequate operating parameters for the grinding process. Consequently, the cylpebs were selected as the most efficient grinding material for the grinding process in fine products, with an effective grinding time of 5 hours.

The selection of the cylpebs as grinding elements is because they offer a larger surface area for breaking the lactose particles through impact, thus being more effective in less time with larger number of fine particles, enabling to obtain a grain size of 22.075 μm in a grinding time of 5 h.

The lactose load applied to the grinding was optimized, because with less operating hours the raw material does not stick on the internal walls of the drum nor on the grinding bodies, significantly reducing the losses.

With a particle size of 22 μm , it was possible to qualitatively determine (through touch) the improvement of the condensed milk texture, which represents

for the company an improvement in the product quality.

References

- [1] V. R. Lojano Pillco, D. J. Pinguil Loja, and N. G. Jara Cobos, *Propuesta de mejora para el proceso de molienda de lactosa en empresas láctea*. Universidad Politécnica Salesiana, Ecuador. [Online]. Available: <https://bit.ly/3a4IusB>
- [2] A. O. Venegas Tomalá, *Diseño y construcción de un molino de bolas para aplicaciones de pulvimetalurgia en los laboratorios de Ingeniería Mecánica de la Facultad de Ingeniería Civil y Mecánica de la Universidad Técnica de Ambato*. Universidad Técnica de Ambato, Ecuador. [Online]. Available: <https://bit.ly/3R0Ewlm>
- [3] J. R. Alcántara Valladares, *Diseño práctico de un molino de bolas*. Instituto Politécnico Nacional, México, vol. 7, no. 2. [Online]. Available: <https://bit.ly/3acXvIG>
- [4] O. A. Gutiérrez Gutiérrez, *Estudio para calibración de molinos*. Universidad de Chile, vol. 158. [Online]. Available: <https://bit.ly/3bH0Ujm>
- [5] M. S. Altamirano Peralta and D. J. Sacoto Rivera, *Evaluación experimental del proceso de molienda de crudo de UCEM planta industrial Guapán*. Universidad del Azuay, Ecuador, vol. 1, no. 1. [Online]. Available: <https://bit.ly/3xZFupi>
- [6] G. A. Villablanca Robles, *Estudio de prefactibilidad para la construcción y operación de una minicentral hidroeléctrica (MCH) en la subcuenca del río Palora*, vol. 22. [Online]. Available: <https://bit.ly/3NxFJxx>
- [7] C. D. Char, *HACCP, Microbiología predictiva y factores en combinación para mejorar la calidad de productos lácteos: dulce de leche: aplicación del concepto de factores en combinación y de la microbiología predictiva en el mejoramiento de la calidad del dulce de leche*. Universidad de Buenos Aires, Argentina. [Online]. Available: <https://bit.ly/3yy46qz>
- [8] R. C. Rowe, P. Sheskey, and M. Quinn, *Handbook of pharmaceutical excipients, Six Edition*. Pharmaceutical Press. [Online]. Available: <https://bit.ly/3xZGIgw>
- [9] A. Jillavenkatesa, L.-S. H. Lum, and S. Dapkunas, “Nist recommended practice guide: Particle size characterization.” [Online]. Available: <https://doi.org/10.6028/NBS.SP.960-1>

- [10] E. J. Montes Montes and R. Torres Gallo, “Determinación de los factores de forma de área (α) y volumen (β), de cristales de α -lactosa utilizando microscopía óptica,” vol. 13, no. 2, pp. 17–24. [Online]. Available: <https://doi.org/10.21897/rta.v13i2.666>
- [11] E. A. Luna Méndez and F. T. Valencia Guaricela, *Elaboración de guías prácticas de procesos metalúrgicos para el laboratorio de minas de la Universidad del Azuay*. Universidad del Azuay, Ecuador. [Online]. Available: <https://bit.ly/3Ai7fw8>



MATHEMATICAL MODEL OF A RESISTIVE OVEN FOR THERMOFORMING POLYPROPYLENE SHEETS

MODELO MATEMÁTICO DE UN HORNO RESISTIVO PARA TERMOFORMADO DE LÁMINAS DE POLIPROPILENO

Lidia Castro-Cepeda^{1,*} , José Cortés-Llanganate^{1,2} 

Received: 03-05-2022, Received after review: 06-06-2022, Accepted: 13-06-2022, Published: 01-07-2022

Abstract

A mathematical model of a resistive oven for the production of thermoformed sheets is developed in this paper; such oven is located in a production plant in the city of Riobamba. The objective of the research is to achieve temperature stability and that the plates have a homogeneous dimension when going through the thermoforming process, to guarantee customer satisfaction. For this purpose, the physical variables that govern the heat transfer phenomena, namely radiation, convection and conduction, are analyzed, to obtain a mathematical model that predicts the temperature profile of the oven in the thermoforming process, from which a controller is designed using various control techniques that are efficiently coupled to the system. A theoretical study of the physical phenomena and of the mathematical equations that represent them is proposed in the first stage of the research. Then, they are solved through computational techniques using Simulink to obtain the temperature profile. Finally, this model is validated by comparing it with those obtained in previous works through statistical techniques, and a new controller that guarantees minimum temperature variability is proposed. As a result of the simulation, a variation of ± 1 mm in the width of the plate is achieved.

Keywords: heat transfer, modelling, polypropylene, temperature, thermoforming

Resumen

En el presente trabajo se desarrolla un modelo matemático de un horno resistivo para la producción de planchas termoformadas, localizado en una planta de producción de la ciudad de Riobamba. El objetivo de la investigación es conseguir la estabilidad de la temperatura y que, al pasar por el proceso de termoformado, las planchas tengan una dimensión homogénea que garantice la satisfacción del cliente. Para ello se analizan las variables físicas que rigen los fenómenos de transferencia de calor; radiación, convección y conducción, y así obtener un modelo matemático que prediga el perfil de temperatura del horno en el proceso de termoformado, a partir del cual se diseña un controlador utilizando varias técnicas de control que se acoplen al sistema de forma eficiente. En la primera etapa de la investigación se plantea un estudio teórico de los fenómenos físicos y las ecuaciones matemáticas que los representan. Luego son resueltas a través de técnicas computacionales usando Simulink para conseguir el perfil de temperatura. Por último, se valida este modelo comparándolo con aquellos ya obtenidos en trabajos anteriores a través de técnicas estadísticas; finalmente, se propone un nuevo controlador que garantice la variabilidad mínima de la temperatura. Como resultado de la simulación se consigue una variación de ± 1 mm del ancho de la plancha.

Palabras clave: modelado, polipropileno, temperatura, termoformado, transferencia de calor

^{1,*}Facultad de Mecánica, Escuela Superior Politécnica de Chimborazo - Ecuador. Corresponding author ✉: lidia.castro@esPOCH.edu.ec.

²Jefe de Planta Prefabricados Riobamba, Unión Cementera Nacional UCEM S.A - Ecuador.

Suggested citation: Castro-Cepeda, L. and Cortés-Llanganate, J. "Mathematical model of a resistive oven for thermoforming polypropylene sheets," *Ingenius, Revista de Ciencia y Tecnología*, N.º 28, pp. 80-91, 2022, DOI: <https://doi.org/10.17163/ings.n28.2022.08>.

1. Introduction

The worldwide plastics industry has grown in recent years. Besides the virgin raw material production data, this is also evidenced in the percentage of plastic that is currently recycled in the countries of the world. Regarding recycling, the plastic had an increase of 80 % in 10 years in European countries [1].

In Ecuador, the plastic is used in various production fields, such as: food industry (drinks packages, snacks, etc.), construction industry (translucent roofs, plastic tiles, curtains, etc.), kitchen utensils in general [2]. Specifically, there is an industry in the city of Riobamba devoted to manufacturing translucent polypropylene sheets that are used as a complement of fiber cement roofs.

The plant has three production lines that have been assembled with recycled technology, coming from countries such as Spain; they are acquired at lower prices for reuse after they have completed their useful life cycle. Then, it is repowered in local industries making some adjustments and even mechanizing parts and pieces that are coupled to the system so that they operate with the greatest possible efficiency. The process for transforming the polypropylene is summarized in Figure 1.

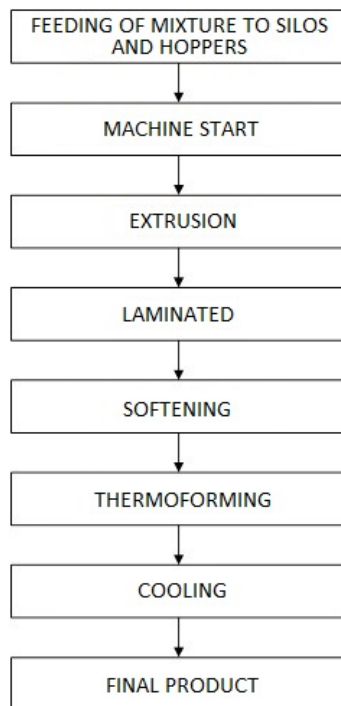


Figure 1. Process for transforming the polypropylene

The main machine of this line is a thermoforming machine that produces type P7 polypropylene sheets. This research work has been carried out on the input oven of such plastic thermoforming machine. Previous works were conducted to control and improve the production of the thermoforming oven.

The first work consisted in setting up a SCADA system for temperature control. It was based on a hysteresis control system, where the resistances of the machine were turned on and then turned off when they reached the desired value of temperature [3]. At present, the described system is being used in the area of extrusion, distribution and output ovens. Figure 2 shows the architecture of the network used in the SCADA system.

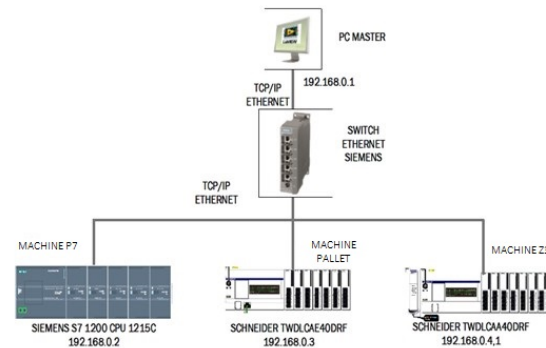


Figure 2. Architecture of the local area network of the machines [3]

The second work consisted in the design of a controller for the input oven, based on system identification. This enabled obtaining the transfer function of the oven. Once such function was identified, a PI controller was calculated for its control [4]. This system is being currently used in the production plant to control the input oven.

Up to this moment, the system has not been modeled mathematically, and thus the real behavior of its variables is unknown. Therefore, it has been considered necessary to find this mathematical model, which will be compared with the existing models. Based on them, modifications that improve the product quality will be suggested in the controllers. At present, the product meets the current regulations of the country, but it is observed that its width is not completely uniform. When it is stacked for distribution and sale, the customer has the sensation and perception that the plates do not meet the regulation, due to the variability of their dimensions. Therefore, the main problem of this oven is that it produces plates with a very variable width that causes that some clients do not accept the product.

Among the research works analyzed, [5–8], Neacă and others use the heat transfer phenomena to quantify the temperature through the mathematical model found, which is similar for this case study. However, each publication is distinguished because its entire system is in accordance with the particular features of each oven. In contrast, the study by Throne [9], [10] is based on two variables, namely the molar absorptivity and the emissivity, emphasizing that they are fundamental in the development of the model. Following

the recommendation of this author, the appropriate data will be used in the radiation analysis, which are detailed in the solution statement.

Meanwhile, Khan [11], Erdogan [12] and Chy [13] include in their research work specific properties such as density, thermal diffusivity, thickness, specific heat and thermal conductivity, data that are also considered in the development of this research work, for the conduction and convection analysis, considering the accessibility to the equipment and the features detailed in the description of the oven structure.

On the other hand, Schmidt [14] and Ajersch [15] use infrared sensors and thus their study is aimed at radiation analysis; these publications reach results that fit the reality, but due to the experimental conditions of the oven under study it is not possible to replicate this technique. However, it will be useful to compare and discuss the results at the end of this research. This is similar to Chy and Boulet [16], who divide in layers the material to be heated, and then interpret the results as a single element through numerical techniques; it is not possible to carry out this condition in this study, but it will be useful to contrast such results when formulating the conclusions.

Even though all these researchers developed acceptable mathematical models of the oven, especially for the heating phase, there are still some discrepancies between the simulation, the experimental results and the variables used by each author in his/her research work; in addition, such mathematical models fit the particular features of each oven.

Therefore, this research is intended to develop an improved model for the oven under study that fits its features. It is taken into account that the process is mainly executed through trial and error, based on the intuition and experience of the machine operator. Consequently, it arises the initiative of understanding the oven heating process, specially emphasizing on the features typical of its construction knowing that it is an oven manufactured empirically. With this mathematical model it is sought to establish a more precise way to predict the temperature profile inside the oven, in order to use it in the future for a better control of the process.

There is a study carried out previously about the oven under analysis. In 2017, Cortés implemented a temperature control system for the thermoforming oven of the machine known as P7. It briefly describes the oven, stating that «it consists of metallic plates, that constitute a chamber. Such chamber has a glass wool insulation to reduce heat irradiation to the outside. S-type and U-type resistances (known as such due to their shape) of different electric power are located inside» [3]. The author obtains a model of the oven through system identification graphical techniques, as a step prior to the design of the corresponding controller. Various techniques are applied, and compared

with each other. At the end of the corresponding validation, it is chosen the Analytical without Delay graphical method, which yielded the highest percentage of 90.95%.

Regarding the model obtained by means of system identification, Cortés [4] performed the associated calculations to obtain a system controller, which yielded acceptable results with respect to the temperature variability. Nevertheless, there is still the issue of the width of the plates. The purpose of obtaining the mathematical model of the oven of interest seems simple, but putting it into practice is much more complex, since it largely depends on the data available. The aim is to provide a system model that shows the real dynamic behavior of the oven, thus enabling to calculate different controllers that finally optimize its operation.

2. Materials and methods

The methodology to develop this research work is summarized in the diagram of Figure 3.

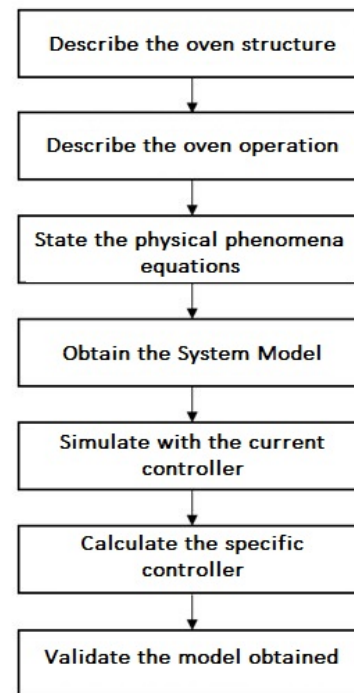


Figure 3. Working methodology

2.1. Description of the oven structure

The oven under study, which is shown in Figure 4, was constructed locally, with ohmic electric resistances that heat up by Joule effect and release their heat. The oven has been constructed with recycled elements, machine pieces and equipment, which are coupled to each other to fulfill the requirements of the production process. For this specific case, the industrial production

of thermoformed plates is used nationally in different applications. The oven is constituted by metallic plates. It is parallelepiped-shaped, constituted by two boxes, one inside and another outside made up of 2 mm galvanized steel sheets. Such boxes are separated 5 cm with respect to each other, and insulation is placed between plates. For this design it was used fiberglass manufactured from a mixture of sands, borates and silicates, thus fulfilling the parameters recommended by various authors mentioned in the state of the art. For this reason, from this point on it will be supposed that the oven has the insulation necessary to avoid significant losses that modify the temperature profile of this oven.



Figure 4. Thermoforming oven of machine P7

2.2. Description of the oven physical phenomena

To take measurements about the real operation of the oven under study, two J type thermocouples were placed with the purpose of measuring the temperature at the center of the oven and in a lateral wall every second, during the time necessary to reach stability, approximately 5000 seconds. The oven has a built-in data acquisition system, and these data were stored in a computer connected to the equipment, and will be used to obtain the mathematical model. To make the oven study simpler and more practical, the oven operation has been divided into the three stages that are detailed in Figure 5.

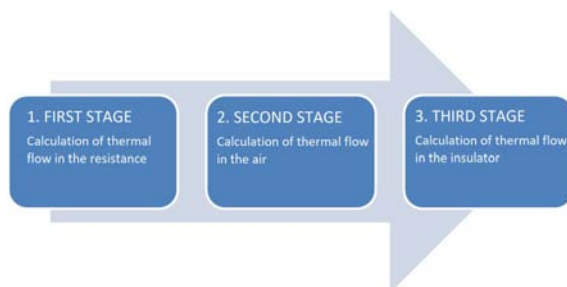


Figure 5. Oven operation diagram

Table 1 shows the nomenclatures to be used in the different sections of the present paper.

Table 1. Nomenclature used in the different equations

Abreviatura	Significado
$i(t)$	Electric current that circulates through the conductor.
$u(t)$	Voltage to which the electrical resistance is connected.
$R(T)$	Resistance of the conducting cable as a function of the temperature.
ρ	Resistivity of the resistance as a function of temperature.
L	Length of the resistance cable.
A	Area of the conductor cross section.
$p(t)$	Electric power.
\dot{Q}_{sto}	Thermal flow stored in the resistance.
\dot{Q}_{rad}	Heat thermal flow by radiation.
\dot{Q}_{conv}	Heat thermal flow by convection.
m	Mass.
$C_c(T)$	Specific heat of the conductor as a function of temperature.
ΔT_w	Heating of the resistance (temperature difference).
T_0	Initial temperature (Ambient temperature of the place, initially $T_w = T_0$).
ε	Emissivity constant.
C_n	Stefan-Boltzmann constant.
S_w	Surface of the resistance cable.
T_1	Temperature inside the oven surface.
T_w	Temperature of the cable.
α	Convection coefficient of the air inside the resistance.
T_a	Temperature of the air inside the oven.
$\dot{Q}_{conv\ t-a}$	Total thermal flow produced by the resistances in the air.
$\dot{Q}_{conv\ a-p}$	Thermal flow produced by the air on the wall.
$\dot{Q}_{sto\ a}$	Thermal flow stored in the air.
$a_p(T)$	Convection coefficient of the air and the oven wall as a function of the temperature.
S_p	Internal surface of the oven walls.
m_{a1}	Mass of the air inside the oven.
$c_a(T)$	Specific heat of the air as a function of temperature.
T_a	Temperature of the air inside the oven with no load.
$\dot{Q}_{out\ cond}$	Thermal flow transferred to the outside by conduction.
$\dot{Q}_{sto\ insul}$	Thermal flow stored in the insulation.
k	Thermal conductivity of the material.
A	Area through which the heat flows.
ΔX	Insulation thickness.
ΔT	Temperature difference.
P	Density.
V	Volume.
y_{model}	Values obtained from the model.
$y_{observed}$	Values observed in the experiments.
N	Number of data.

2.2.1. Calculation of heat flow in the resistance

It starts with the transformation of electric energy into thermal energy in the resistance. It is fundamentally based on the basic Ohm's law given by equation (1).

$$u(t) = i(t) * R(T) \quad (1)$$

The only element in the oven that takes part in this energy transformation is the resistance, whose calculation is fundamental because it is unknown when constructed manually. Equation (2) is used for this purpose, which involves the resistivity, a function of temperature, the length and the cross section of the

resistance, data that can be easily obtained through measurements, tables and knowing the material of which it is made of.

$$R = \rho * \frac{L}{A} \quad (2)$$

Then, it is applied the energy conservation law in thermodynamics, which states that the amount of heat received by the system is transformed and performs work against external forces, as shown in equation (3).

$$p(t) = \dot{Q}_{sto} + \dot{Q}_{rad} + \dot{Q}_{conv} \quad (3)$$

The thermal flow stored in the resistance is expressed through equation (4).

$$\dot{Q}_{sto} = \frac{d(Q_{sto})}{dt} = \frac{d(m * C_C(T) * \Delta T_w)}{dt} \quad (4)$$

The heating by radiation is verified in equation 5.

$$\dot{Q}_{rad} = \varepsilon * C_n * S_w * (T_w^4 - T_1^4) = K_1 * (T_w^4 - T_1^4) \quad (5)$$

2.2.2. Calculation of thermal flow in the air

After carrying out the corresponding calculation of resistance, it is continued with the equations for the air inside the oven, with the purpose of relating the heat transfer phenomena and developed the desired mathematical model. The total thermal flow, presented in equation (6), is obtained from the equation that relates the thermal flow produced by the resistance and the thermal flow by the air on the wall.

$$\dot{Q}_{conv\ t-a} = \dot{Q}_{conv\ a-p} + \dot{Q}_{sto\ a} \quad (6)$$

The thermal flow produced by the air on the wall is expressed using again the convection phenomenon. Afterwards it is calculated the thermal flow stored in the air, which is expressed in (7).

$$\dot{Q}_{sto\ a} = \frac{d}{dt}(Q_{sto\ a}) = \frac{d}{dt}(m_{a1}c_a(T)(T_a - T_0)) \quad (7)$$

2.2.3. Calculation of thermal flow in the insulator

After the study of heat transfer in air has been completed, it is carried out the insulation analysis. Equation (8) is used for this purpose, which defines the heat flow on the wall due to the air movement, which is equal to the sum of the thermal flow transferred to the outside by conduction and the heat stored in the insulator itself.

$$\dot{Q}_{conv\ a-p} = Q_{conduction\ ext} + Q_{sto\ insul} \quad (8)$$

The oven has an insulating wall made of fiberglass, and hence it is necessary to quantify it, and the thermal conduction phenomenon is used for this purpose. The mathematical expressions and definitions that will be used in the solution of the mathematical model has been explained in a general manner, and the following section details the most important calculations that will be fed to the system.

2.3. Solution statement

After presenting in detail the physical phenomena supported on classical theory that appear during the heating of the oven for the thermoforming production process, it is proceeded with the mathematical calculation with the purpose of obtaining the differential equations that will enable finding the desired mathematical model. The Simulink mathematical tool was used with the aim of implementing computationally the solution to the problem, since it is visual programming environment that operates on Matlab.

The data in the technical sheet of the material is used to start with the calculations of resistance. These data were found in the company catalogs to specifically verify that the correct information supplied by the provider is used. The conductor used in this case is Nikrothal 70 [17]. Appropriate calculations are carried out that lead to equation (9).

$$T_w = \int \left(\frac{\left(\frac{u^2(t)}{R} - K_1 * (T_w^4 - T_1^4) - \alpha * S_w * (T_w - T_a) \right)}{m * C_c} \right) dt + T_0 \quad (9)$$

This equation is implemented in Simulink, and the scheme of inputs and outputs may be visualized in Figure 6.

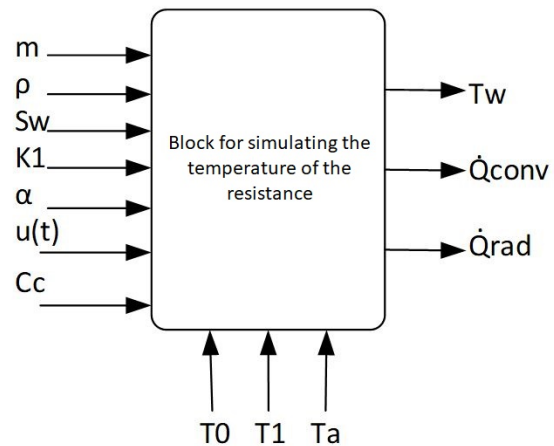


Figure 6. Scheme of inputs and outputs for calculating the temperature of the resistance

Then, the behavior of the resistance as a function of the temperature is obtained, and with it the heat that

transforms through the physical phenomena already described. Such implementation may be observed in detail in Figure 7, which corresponds to equation (9).

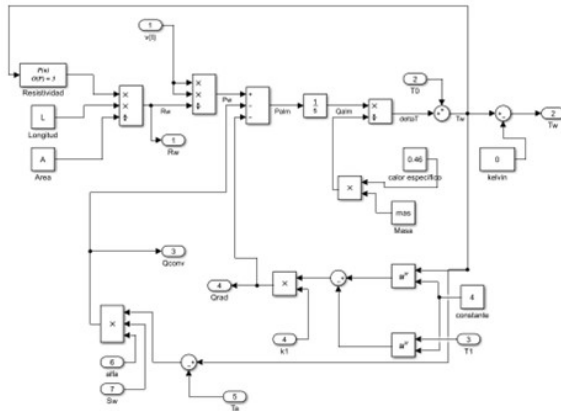


Figure 7. Implementation of equation (9)

Figure 8 shows the response of the resistance temperature as a function of time when it is connected to a voltage of 440 VCA; such temperature profile will be used in the model of the thermoforming oven.

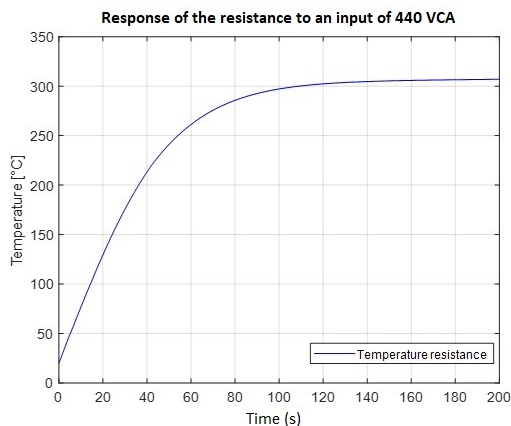


Figure 8. Resistance temperature along time

Finally, the temperature of the oven is calculated, resulting in equation (10) that is implemented in Simulink. Such equation is the result of the mathematical calculations of the fundamental equations of thermodynamics.

$$T_a = \frac{\int (\dot{Q}_{conv\ t-a} - a_p(T) S_p(T_a - T_1)) dt}{m_{a1} c_a(T)} + T_0 m_{a1} c_a(T) \quad (10)$$

Figure 9 shows the basic scheme that describes the inputs and outputs of the Simulink implementation of equation (10).

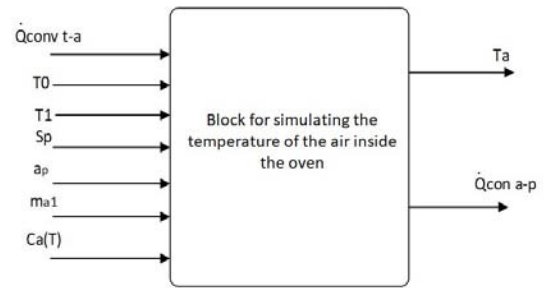


Figure 9. Scheme of inputs and outputs for calculating the temperature of the air inside the oven

The calculation of the temperature of the air inside the oven, equations and data obtained through tables and calculations are implemented in Simulink. Such implementation may be observed in detail in Figure 10, which corresponds to equation (10).

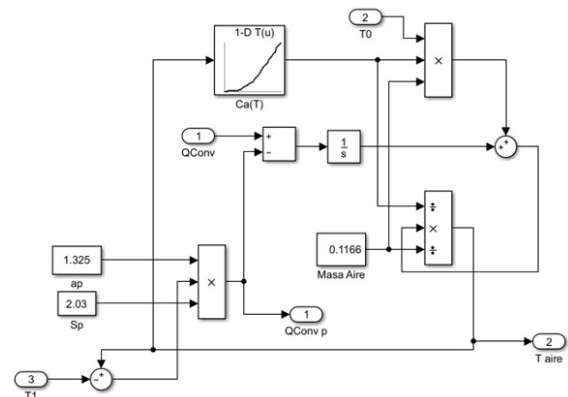


Figure 10. Implementation of equation (10)

After the calculation of the thermal flow of the resistance and the air of the oven is available, the subsequent step is to calculate the temperature lost in the insulation to obtain the temperature of the oven wall. The temperature of the air can be obtained relating all these calculations, data that should be known for its further processing in the calculation of the control systems. The data obtained through the oven data acquisition system is used in the case of the wall temperature. Figure 11 shows the total implementation for calculating the temperature of the air inside the oven. The blocks defined in previous steps have been used for this purpose.

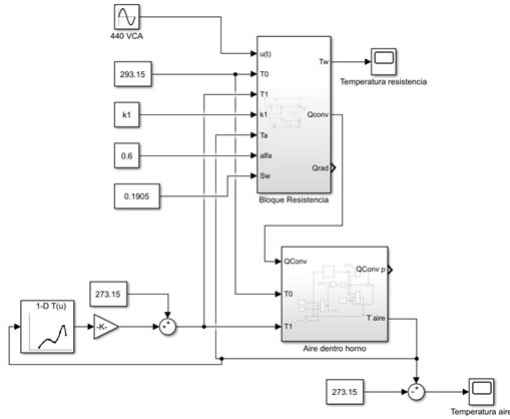


Figure 11. Total implementation of temperature calculation in the air of the oven

Figure 12 shows the response of the mathematical model comparing it with the response of the oven obtained through data acquisition. As it is observed, the model fits very well the real performance curve. This enables to predict that the validation of the mathematical model will be better than the validation of the model obtained by means of graphical identification techniques published by Cortés [4].

A step input has been applied to both the real system and the mathematical model for obtaining Figure 12. For the real system, a voltage of 440 VCA has been applied to the resistances. A similar value of voltage has been applied to the mathematical model. The data acquisition in the oven is carried out reading the type J thermocouple, which is sampled at a period of 1 second.

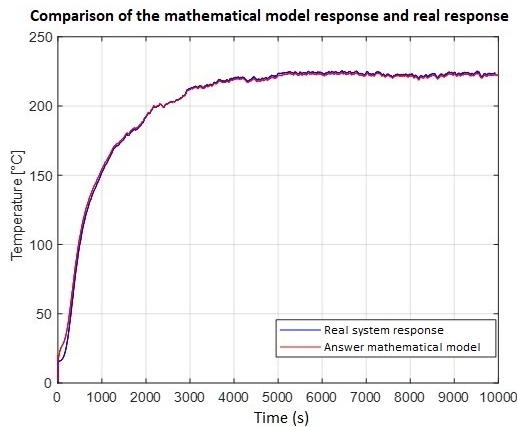


Figure 12. Comparison of the response of the mathematical model *vs* the real response

3. Results and discussion

3.1. Validation of the model obtained

The mathematical obtained is validated using mathematical techniques that enable quantifying it. This

section considers various points of view, as explained below.

3.1.1. Comparison of the root mean square error of the mathematical model *vs* the current model

Figure 13 is similar to Figure 12. All the curves shown are the responses to a step input of 440 VCA. The behavior of the real system is shown in blue, whose data were taken experimentally through the data acquisition system and processed in MATLAB. The response of the mathematical model obtained through the calculations described in previous sections is shown in red. The difference is in the green curve, which corresponds to the response of the model obtained by graphical identification to a step input of 440 VCA; this response is currently used in the plant for calculating the controller. It may be visually inferred in this plot that the mathematical model is similar to the profile of real temperatures, and so it is expected that this error is smaller when it is quantified.

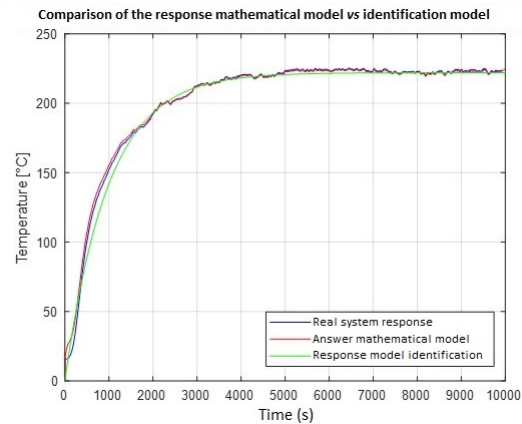


Figure 13. Comparison of the responses of the mathematical model *vs* the model calculated by graphical identification

The root mean square error (RMSE) [18], whose mathematical expression is represented by equation (11), is calculated for the first validation.

$$RMSE = \sqrt{\frac{\sum_{I=1}^N (y_{model} - y_{observed})^2}{N}} \quad (11)$$

The values of 2 RMSEs of the responses to a step input of 440 VCA were calculated:

- RMSE between the model obtained by graphical system identification, which is currently used for calculating the controller, and the real system, whose result is represented in equation (12).

- RMSE between the mathematical model found in this research work and the real system, whose result is represented in equation (13).

In the statement of the solution, it has been obtained the curve that represents the real mathematical model, but it is necessary to compare it with the experimental data, and at the same time with the model currently used for controlling the thermoforming machine.

$$RMSE_{current-model} = 4,3354 \text{ } ^\circ C \quad (12)$$

$$RMSE_{mathematical-model} = 2,3395 \text{ } ^\circ C \quad (13)$$

From the comparison of the errors calculated it is evident that the error of the mathematical model is smaller than the error of the current model; therefore, the mathematical model found in this research work fits the real curve of the thermoforming oven with greater precision.

3.1.2. Comparison of control responses to a step input

Starting from the original control system shown in Figure 14, the mathematical model is inserted in the current control system with the purpose of analyzing its response to a step value (input signal) of 140 °C.

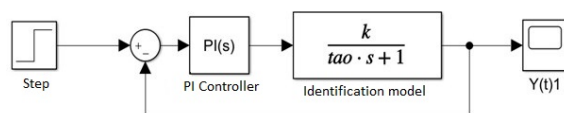


Figure 14. Temperature control system using the identification model

Figure 15 shows the comparison of the response of the control system with the identification model (blue line) versus the response of the control system with the mathematical model (red line), and the step of 140 °C (black line). It is observed that the responses are different despite using the same controller, and thus it is interpreted that it is not the appropriate one for the mathematical model and, therefore, it becomes necessary to find one that fits better to the features typical of the mathematical model; in this way, it is expected that there is a greater stability in the temperature and this implicitly leads to improve the final product avoiding the mismatches in the width of the thermoformed plates.

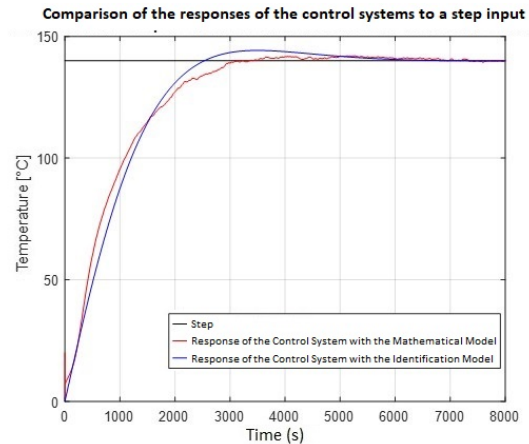


Figure 15. Comparison of the responses of the control systems

3.1.3. Calculation of a new controller that fits to the conditions of the mathematical model, to simulate and verify its response

The classical Ziegler-Nichols control method is applied to calculate the new controller and simulate the response of the system. This is one of the most well-known methods for tuning the parameters of PID controllers, and its rules come from an experimental response according to the dynamics of the process and without assuming any previous knowledge of the plant to be controlled [19–21].

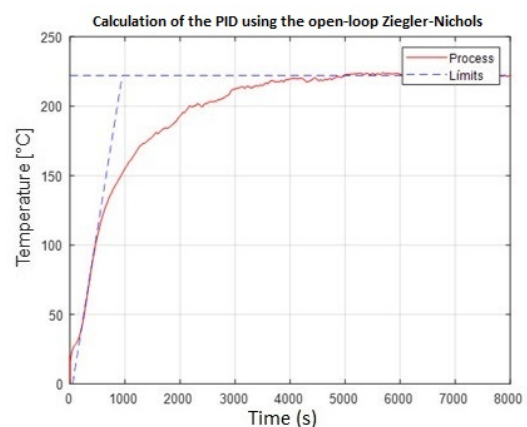


Figure 16. Calculation of the PID parameters by means of the open-loop Z-N for the mathematical model

Figure 16 shows the limits used to obtain the data required, and thus apply the open-loop Ziegler-Nichols method.

As it is observed in Figure 17, the response of the PID controller using the Ziegler-Nichols method does not show improvements compared to the current system. This is because the stabilizing time (time to reach the set-point value) is high and the temperature

variation does not decrease. Due to this it is necessary to calculate the PID controller through using method.

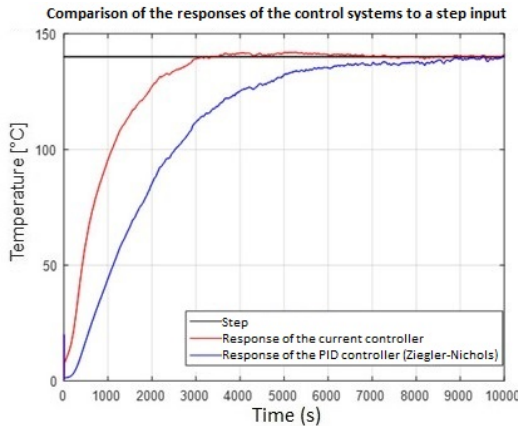


Figure 17. Comparison of the response of the PID controller applying Ziegler-Nichols *vs* the current PI controller

The Simulink PID Tuner tool provides a single-loop PID tuning method of fast and wide application for the PID controller blocks. The parameters of the PID controller may be tuned with this method to achieve a robust design with the desired response time.

Figure 18 shows the responses of the control system, comparing the one obtained through the Simulink PID Tuner tool (shown in blue), with the response of the current controller (shown in red). It is verified that this controller generates a better system response reaching temperature stability in the smallest time possible, it adjusts much better resulting in a smaller temperature variability. It should be taken into account that the data used for the subsequent analysis are the data obtained after 4000 seconds, since it is there when the system remains stable.

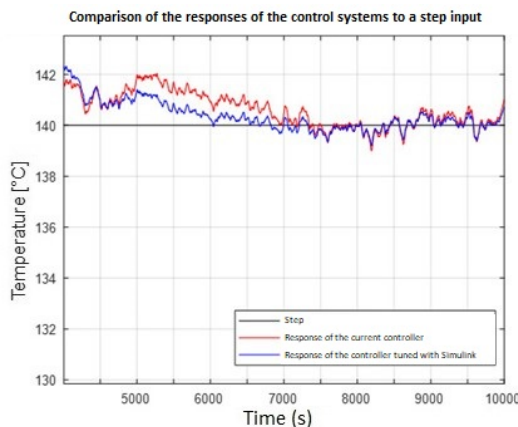


Figure 18. Detailed visualization of the responses of the control systems *vs* controllers tuned

The behavior of the data is verified through statistical analysis techniques to compare them with the current ones, to quantify the improvement that would

be produced if this controller is applied in the production process. The mean temperature of the current controller is 140.62 oC, whereas the mean temperature with the controller proposed in this work is 140.35 oC, so it is evidenced quantitatively that there is a greater temperature stability applying this controller that uses the mathematical model developed. In addition, this is reflected in the error of the standard deviation, which is smaller for the new controller. The 72.81% of the data simulated with the new controller are normal with respect to their mean, whereas only 65.55% of the data of the current controller are normal with respect to their mean, but if the data of the current controller are compared with respect to the standard deviation of the new controller, only 54.41% of the data are normal. Hence, it is identified that the new controller provides better results to the system, which guarantees a greater stability of the temperature if it is implemented.

It is conducted a linear regression analysis with data provided by the quality department, with measurements of the temperature and the width of the thermoformed plates, with the purpose of obtaining an equation and verifying the correlation between temperature and width, where A represents the width and T the temperature of the oven, as shown in equation (14). With this mathematical model it is calculated the width of the plates with the temperatures obtained in the system with the current controller, and the corresponding statistical analysis is conducted.

$$A = -1,20 + T + 1088,62 \quad (14)$$

Figure 19 shows the histogram of the plates measured, and there is a variation of ± 2 mm; in addition, it is clearly seen that the data are quite disperse. Hence, the plates are heterogeneous with respect to their width, and when stacked it gives the sensation that the regulation is not met.

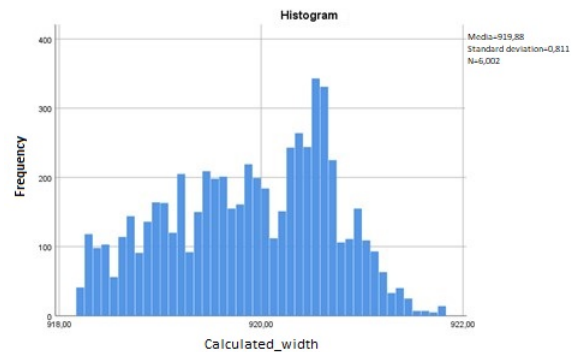


Figure 19. Histogram of the measured width of the thermoformed plates

On the other hand, Figure 20 shows the histogram of the plates calculated with the linear regression model using the system with the proposed controller, and it

is clearly observed that there is smaller dispersion of the data and there is a variation of ± 1 mm; thus, it is assumed that they will look more homogeneous when stacked, providing security to the client regarding the product quality. Although it would be important to have experimental data to verify the data obtained in this research work.

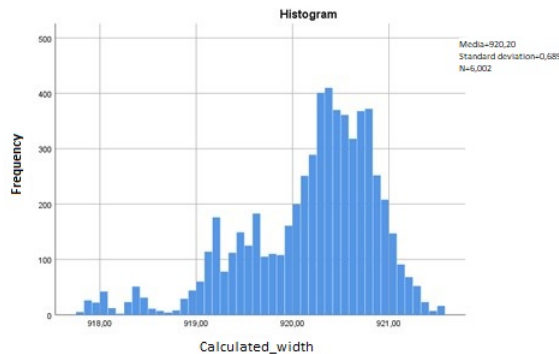


Figure 20. Histogram of the calculated width of the thermoformed plates

In this way, it is validated the mathematical model and in turn the new proposed controller, which is expected to be applied in the production plant to have access to these data; this confirms the effectiveness of what has been detailed in this document.

4. Conclusions

It was obtained the mathematical model of the resistive oven for producing thermoformed sheets, from which it was calculated a new controller for the system. Its behavior was simulated and the variability of the plate width was projected as ± 1 mm, as opposed to the variation of ± 2 mm with the current controller. Such results show the effectiveness of the new controller.

It was found the mathematical model of the oven. For this purpose, its operation was divided in three parts. First, the equations that have influence on resistance heating were formulated. Then, the equations that have incidence on oven heating through radiation and convection were expressed. At last, the equations that have influence on the heating of the oven wall temperature were used. However, the last part was not calculated since the specific information of the insulator on the oven walls is not available. Instead, the data acquired by means of the equipment data acquisition system was used.

It was found the mathematical model that best fits the real behavior of the oven. This is evidenced when calculating the root mean square error of the mathematical model, which is smaller compared to the model obtained by system identification. Therefore, it is concluded that the mathematical model obtained in

this work has a better validation than the one obtained with the current control system.

It was simulated a system that uses the current oven controller coupled to the mathematical model found. It was evident that the operation dynamics of the oven is slower with respect to the simulation of the current control system. This is due to the fact that the mathematical model takes into account different phenomena that occur, such as the loss of heat in the oven walls. For this reason, it was necessary to calculate a new controller that fits the mathematical model in a better way.

Another controller was calculated that improved the final behavior of the system. However, it was not obtained by means of traditional calculations of PID controllers. Instead, automatic tuning techniques available in Simulink (PID tuner tool) were used. The main difference is that the controller is not calculated in terms of the initial behavior desired by the user (2% overshoot, stabilization time of 3600 seconds).

In this case, the overshoot is approximately 3.5% and the stabilization time is 4000 seconds. The mathematical model obtained analyzing the data of the polypropylene plates' width was validated. For this purpose, it was necessary to calculate a function that relates the temperature with the width of such plates. After comparing the results of the two systems (current and new), it is concluded that the new control system has a variation of ± 1 mm, whereas the current control system has a variation of ± 2 mm.

To obtain a better validation of the systems with respect to the width of the plates, it is necessary to design better methods for recording information, that store the temperature together with the specific dimension features in real time. In other words, knowing the width of the plate at the instant at which the oven has a particular value of temperature. For this purpose, it would be necessary to implement a more complex data acquisition system that would have direct incidence on the production costs, which for the moment is not feasible in the production plant.

References

- [1] European Parliament. (2014) Plastic garbage: from waste to resource. [Online]. Available: <https://bit.ly/3xwkPJ6>
- [2] A. Méndez Prieto, "Reciclado de plásticos de uso agrícola," *Integra. Revista de la Asociación Ecuatoriana de Plásticos*, no. 58, pp. 24–26, 2019. [Online]. Available: <https://bit.ly/3aVgjMF>
- [3] M. E. Olivo Silva and J. L. Cortés Llanganate, "Diseño e implementación de un sistema SCADA para el monitoreo de máquinas del proceso de producción de traslúcido para Techoluz de

- Tubasec CA,” Escuela Superior Politécnica del Chimborazo, Ecuador. 2013. [Online]. Available: <https://bit.ly/3zzQgVx>
- [4] J. L. Cortés-Llanganate, “Diseño de un sistema de control de temperatura para los hornos de termoformado de la máquina de láminas P7 de Techoluz en Tubasec CA,” Escuela Superior Politécnica del Chimborazo, Ecuador. 2017. [Online]. Available: <https://bit.ly/3Qq8iQ3>
- [5] M. I. Neacă and A. M. Neacă, “Modeling and simulation of the transient heating regime in an electrical oven,” in *2010 IEEE International Conference on Automation, Quality and Testing, Robotics (AQTR)*, vol. 3, 2010, pp. 1–6. [Online]. Available: <https://doi.org/10.1109/AQTR.2010.5520672>
- [6] —, “Mathematical model for resistive tubular heater,” in *2016 International Conference on Applied and Theoretical Electricity (ICATE)*, 2016, pp. 1–6. [Online]. Available: <https://doi.org/10.1109/ICATE.2016.7754676>
- [7] M. I. Neacă, “Simulink model for resistive tubular heater,” in *2018 International Conference on Applied and Theoretical Electricity (ICATE)*, 2018, pp. 1–6. [Online]. Available: <https://doi.org/10.1109/ICATE.2018.8551453>
- [8] —, “Comparative simulation of the dynamic regimes of resistive heating elements,” in *2019 International Conference on Electromechanical and Energy Systems (SIELMEN)*, 2019, pp. 1–6. [Online]. Available: <https://doi.org/10.1109/SIELMEN.2019.8905842>
- [9] J. L. Throne, “Heating semitransparent polymers in thermoforming,” *Thermoforming Quarterly*, vol. 8, 1999.
- [10] J. L. Throne and P. J. Mooney, “Thermoforming: Growth and evolution,” *Thermoforming Quarterly*, vol. 50, no. 11, p. 113, 2005.
- [11] S. A. Khan, P. Girard, N. Bhuiyan, and V. Thomson, “Improved mathematical modeling for the sheet reheat phase during thermoforming,” *Polymer Engineering & Science*, vol. 52, no. 3, pp. 625–636, 2012. [Online]. Available: <https://doi.org/10.1002/pen.22125>
- [12] E. S. Erdogan and O. Eksi, “Prediction of wall thickness distribution in simple thermoforming moulds,” *Strojniški vestnik - Journal of Mechanical Engineering*, vol. 60, no. 3, pp. 195–202, 2014. [Online]. Available: <https://doi.org/10.5545/sv-jme.2013.1486>
- [13] M. Chy, “Estimation and control of plastic temperature in heating phase of thermoforming process,” Ph.D. dissertation, McGill University. 2014. [Online]. Available: <https://bit.ly/39s46Pe>
- [14] F. M. Schmidt, Y. Le Maout, and S. Monteix, “Modelling of infrared heating of thermoplastic sheet used in thermoforming process,” *Journal of Materials Processing Technology*, vol. 143–144, pp. 225–231, 2003, proceedings of the International Conference on the Advanced Materials Processing Technology, 2001. [Online]. Available: [https://doi.org/10.1016/S0924-0136\(03\)00291-7](https://doi.org/10.1016/S0924-0136(03)00291-7)
- [15] M. Ajersch, “Modeling and real-time control of sheet reheat phase in thermoforming,” mthesis, McGill University. 2004. [Online]. Available: <https://bit.ly/3zEJWMK>
- [16] M. I. Chy and B. Boulet, “Development of an improved mathematical model of the heating phase of thermoforming process,” in *2011 IEEE Industry Applications Society Annual Meeting*, 2011, pp. 1–8. [Online]. Available: <https://doi.org/10.1109/IAS.2011.6074343>
- [17] KANTHAL. Podemos electrificar cualquier proceso de calentamiento. Sandvik AB. [Online]. Available: <https://bit.ly/3MKUKfb>
- [18] D. S. Mendoza, J. Solano, and R. Correa, “Modelo de operador fraccional para describir la dinámica de los supercondensadores,” *Revista UIS Ingenierías*, vol. 19, no. 3, pp. 79–86, 2020. [Online]. Available: <https://doi.org/10.18273/revuin.v19n3-2020008>
- [19] M. A. Moreno, *Apuntes de control PID*. Unviersidad Mayor de San Andres, La Paz - Bolivia, 2001, vol. 8.
- [20] V. V. Patel, “Ziegler-nichols tuning method,” *Resonance*, vol. 25, no. 10, pp. 1385–1397, Oct 2020. [Online]. Available: <https://doi.org/10.1007/s12045-020-1058-z>
- [21] M. D. I. Putri, A. Ma’arif, and R. D. Puriyanto, “Pengendali Kecepatan Sudut Motor DC Menggunakan Kontrol PID dan Tuning Ziegler Nichols,” *Techno (Jurnal Fakultas Teknik, Universitas Muhammadiyah Purwokerto)*, vol. 23, no. 1, 2022. [Online]. Available: <http://dx.doi.org/10.30595/techno.v23i1.10773>



STRUCTURAL AND MODAL ANALYSIS OF ADAPTER PLATES FOR HYDRAULIC HAMMERS AND SKID STEERS UNDER REAL WORK CONDITION

ANÁLISIS ESTRUCTURAL Y MODAL DE LAS PLACAS ADAPTACIÓN PARA MARTILLOS HIDRÁULICOS Y MINICARGADORES EN CONDICIONES REALES DE OPERACIÓN

Yuri Villa^{1,*} , Trevor Vook¹ , Jorge L. Villa² , Pablo Carbajal³ ,
Leonardo Barrera⁴ , Max Florez⁵ 

Received: 16-05-2022, Received after review: 13-06-2022, Accepted: 15-06-2022, Published: 01-07-2022

Abstract

In Perú the need for utility projects such as gas network installation for residents has increased the demand for the use of Hydraulic Hammers (HH) with mini-loaders, due to the low investment required compared to other machinery equipment and to the versatility. The easiness to interchange hydraulic hammers with buckets to complete the demolition and cleaning stages offers for contractors a higher productivity than manual operations. For that reason, the virtual design software Inventor Professional was used to design a suitable adapter plate with adequate resistance and durability, which has a direct impact on the structure of the hydraulic hammer and the hydraulic arm of the skid steers. Simultaneously, a basic animation was developed to explain the effect of the operation style over the hydraulic hammers and the adapter plates. Finally, for this development, it was considered the construction of an adapter plate as a fuse in the system, in case operators exceed the resistance capacity of the hydraulic hammer structure.

Keywords: Design, hydraulic hammer, skid steer, adapter plate, Inventor Professional, Ansys

Resumen

En Perú, la necesidad de proyectos de servicios como la instalación de redes de gas para los residentes, ha incrementado la demanda del uso de martillos hidráulicos (HH) con cargadores compactos debido a la baja inversión en comparación con otros equipos de maquinaria y la versatilidad. La facilidad para intercambiar martillos hidráulicos con cucharones para completar las etapas de demolición y limpieza ofrecen para los contratistas una alta productividad en comparación con una operación manual. Por esa razón, el software de diseño virtual Inventor Professional fue usado para diseñar una placa de adaptación con la resistencia y durabilidad adecuadas, lo cual tiene un impacto directo sobre la estructura del martillo hidráulico y el brazo hidráulico del cargador compacto. Simultáneamente, se desarrolló una animación básica para explicar el efecto del estilo de operación sobre los martillos hidráulicos y las placas de adaptación. Finalmente, para este desarrollo, se consideró la construcción de la placa de adaptación como un fusible en el sistema, en caso de que los operadores excedan la capacidad de resistencia de la estructura del martillo hidráulico.

Palabras clave: diseño, martillo hidraulico, mini-cargadores, platos adaptadores, Inventor Profesional, Ansys

^{1,*}Department of Biological and Agricultural Engineering, North Carolina State University, United States. Corresponding author ✉: yvillar@ncsu.edu.

²École Nationale Supérieure Agronomique de Toulouse, Institut National Polytechnique de Toulouse, France.

³Departamento de Gestión empresarial, Universidad Nacional Agraria la Molina, Lima.

⁴Facultad de Ingeniería y Arquitectura, Universidad de San Martín de Porres, Lima.

⁵Facultad de Ciencias e Ingeniería, Pontificia Universidad Católica del Perú, Lima.

Suggested citation: Villa, Y.; Vook, T.; Villa, J. L.; Carbajal, P.; Barrera, L. and Florez, M. "Structural and Modal Analysis Of Adapter Plates For Hydraulic Hammers And Skid Steers Under Real Work Condition," *Ingenius, Revista de Ciencia y Tecnología*, N.º 28, pp. 92-99, 2022, DOI: <https://doi.org/10.17163/ings.n28.2022.09>.

1. Introduction

In South America, it is common to build roads without service nets installed because the executed facility projects are limited by investment capital. The necessity to improve the quality of life and to expand services for residents opened a huge market for demolition products such as hydraulic hammers [1].

Projects such as gas pipe installations require building trenches, beginning with the cutting of hard surface concrete pavement or asphalt to create, on average, 20 cm wide openings. For demolition, hydraulic hammers mounted on a compact skid steer are used, which can also be utilized to clean the removed waste material and for restoration [2].

In Peru, for natural gas massification construction projects, a Case Skid Steer model SR220 and Hydraulic Hammer SB202 were used. The hammer has special features such as a solid body structure, a grease refilling valve located on the top of the body, and the narrowest box section width of 17 cm, which reduces the energy invested over kilometers of gas pipe installation [3].

At the same time, the demand for new operators and contractors to install gas pipes boosted the demand for systems of skid steer- adapter plate- hydraulic hammer. Due to dealer's market strategies, the focus on the importance of the adapter plate and their potential impact on the performance and useful time of hydraulic hammers were lost. The demand for training, new strategies and different solving proposals increased when the rate of claims rose from 5% to 35%, particularly for irreparable damages in hydraulic hammers [4].

Independent research using advanced virtual analysis was made by the major local adapter plate manufacturer "Soluciones Barrera EIRL", which had a participation of 60% of products in the closed market of Atlas Copco SB202 and Case SR202. This company is one of the most innovative ones in the Peruvian market.

After evaluation of the nature of the failure and the recurrence, a relation was detected between poor operation skills, the extreme resistance and hardness of the adapter plate, and the presence of other manufacturers of adapter plates without adhering to engineering standards. Similarly, the focus was not on the evaluation and the control of damaging effects [5].

As a result, an objective was set to build the adapter plate as a fuse in the system. Static and dynamic virtual simulation were used to design a new adapter plate with Inventor Professional. Afterward, Ansys analysis confirmed the behavior. Complimentary with the registration of performance and claim records, a group of adapter plates was made to improve the building process, product quality, and finally cost reduction.

2. Materials and Methods

2.1. General overview

In 2004 the Camisea Gas project, which cost 3.9 billion dollars (USD), began a gas massification process in Peru. Due to the intensiveness of this activity, a method was set to install pipelines in the soil in a depth of 30 cm. This depth created the technical recommendation to build trenches with a depth of 70 cm. Some work was in streets paved with concrete or asphalt and for that reason, it was necessary to demolish the hard road surfaces that were previously cut in widths of 20 cm [6, 7] (Fig 1).



Figure 1. Trench building, demolition and excavation [8]

Historical reference sales from 2014 for a group of 15 new skid steer, adapter plate, and hydraulic hammer systems showed a high number of warranty claims resulting from failures on the solid body of the hydraulic hammers. After a thorough evaluation using a penetrant liquid, the formation of cracks on hydraulic hammers was detected.

An investigation was performed to understand the failure origin, which was related to the overload on the hammer. A possible explanation was extrapolated due to other failures in moil points, bushings, and pistons. At the same time, 4 skid steers showed initial microcrack formation in their arms. Consequently, a hypothesis was established considering the system of skid steer - adapter plate - hydraulic hammer as a single unit where vibration and resonance generated during the demolition process traveled through the system and produced cracks in the least tough part of the system. As a second part of the method, a new prototype considering the adapter plate as a fuse was established and is explained in this research [9].

2.2. Skid-steers a multipurpose machine

Skid-steers are used in different industries as multipurpose compact carriers for construction, handling materials vehicles, and agriculture equipment [10]. In

combination with hydraulic hammers, some methods of demolition can be made, using as a recommendation the specification of hydraulic flow rate, static pressure, and the hammer weight resistance detailed as a reference [11].

Additionally, the decision of the size of the bucket was in relation to the density of material handled, in this case, old concrete or asphalt 5-20 cm thick and compacted soil was lifted from the surface into trucks as waste material. In this experience, the model SR220 from Case was mounted with 240 kg heavy-duty buckets with a capacity of 0.44 m³ reported by customers and supported by the brochure [12].

2.3. Selection of hydraulic hammer for operation condition

Boundary conditions were the minimum width of the trench, the depth of 70 cm and, as operations were inside the trench, the hammer lubricator nipple located by its design on the top of the hammer. A hammer with higher resistance for overload and built with minimum internal parts were used under endurance conditions. For that reason a Case Skid Steer model SR220, equivalent to Caterpillar model 236B was selected with a hydraulic breaker Atlas Copco SB202 with a solid body [13] (Fig. 2).

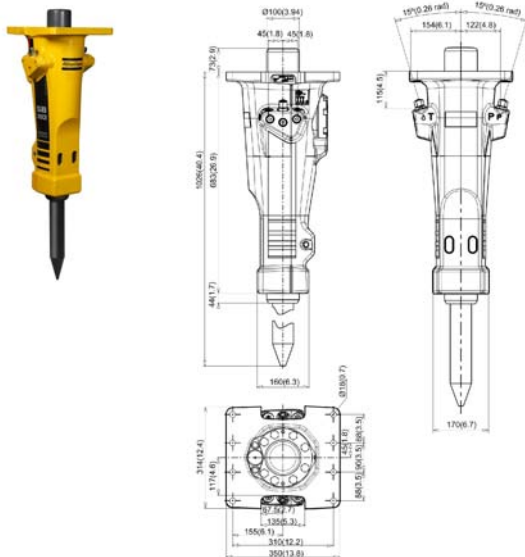


Figure 2. Hydraulic Hammer SB202 Atlas Copco [3]

2.4. Impact on the skid steer and hydraulic breaker durability

Good maintenance and adequate design of the adapter plate for Hydraulic hammer allows to obtain the maximum result. Diagnostic tests were made to detect minor failures in order to fix them, which is an important part of a preventive maintenance program.

Contractors reported an operative availability between 61% and 81% after a strategic plan was applied to improve it [14].

The standard configuration was the use of SB202 due to its special features its patent design, resistance for overloads and higher location of the lubrication valve. The reliability of the hammer was not measured but was reported by contractors as higher than other products that they used.

2.5. Real work conditions

Crack formation as a result of the use of the hydraulic hammer was reported by Li *et al.* (2019) [15] using Ansys Workbench which showed the behavior in the arm structure in an articulate system, when a hydraulic hammer is used. Fundamental parameters about the potential impact and crack formation were taken referentially from the registered real operations. The hypothesis was to test the adapter plate as a fuse to protect the hammer and skid steer integrity, considering the maximum overload condition when operators use excessive hydraulic pressure with the arms-hammer over the surface for demolition, and in a non-aligned 90° angle of operation (between the hammer and the surface). This can be considered the most extreme operation condition and, for that reason, a line of research was open to optimize the adapter plate (Fig. 3).



Figure 3. Skid Steer working with Hydraulic Hammer SB202 [16]

2.6. Fabrication of adapter plate

Physical measurements were taken from the hydraulic hammer Atlas Copco SB202 and the top mounting region of the arm, taking into consideration the tridimensional measurements to connect both machines and, afterwards a tridimensional drawing was developed using the software Inventor Professional and Ansys to analyze the static structural and dynamic behavior under maximum impact frequency of 1800 blows per

minute (BPM). For the analysis, the adapter plate was made independent from the system of the skid steer arm and the hydraulic hammer. Boundary conditions such as gravity, the weight of 16,750 N applied to the adapter plate and hydraulic force in contact regions with the hammer and the skid steer arm were applied.

2.7. Criteria for adapter plate redesign

The redesign of the adapter plate was made considering a soft material in the first stage of analysis, and following the results of the first six months, those were redesigned using a reinforcement which increased the lifetime to over one year of standard operation. The system skid steer-adapter plate-hammer was used for the demolition of road hard cover (old asphalt, concrete) and to break the compacted soil structure (Table 1).

Table 1. Boundary operational conditions for the system Skid steer-adapter plate – hydraulic hammer

Boundary conditions (Used for Inventor and Ansys simulation)	
Operation	Demolition
Machine weight Skid steer Case model SR220	33752 N
Coupling system	Mechanical
Material use for adapter plate	Carbon Steel ASTM A-36
A shift in a common Labor Day	12 h
Effective percussion time per shift	1-3 h
Total time used by month	30-90 h

3. Results and discussion

3.1. Static Analysis

Loaded static analysis was performed using Autodesk 2020 Inventor Professional, considering the weight of Skid Steer with attachments of 33,752 N (Table 1); as a result of the operation observed a weight of 16,750N was considered (Fig. 2). Due to the two contact regions between the arm and the adapter plate, a force of 8,375 N was applied to each contact area and a force of 16,750 N was applied to the contact surface between the adapter plate and the hydraulic hammer. (Fig. 4).

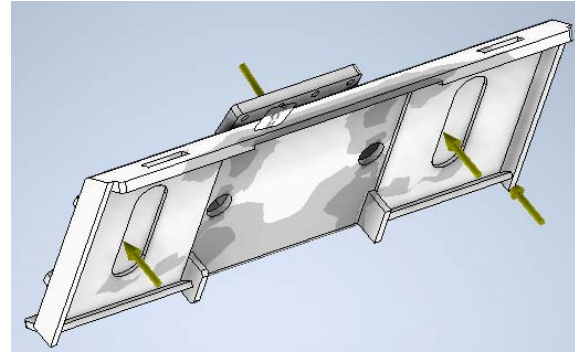


Figure 4. Adapter Plate built in Inventor

For the meshing analysis in Autodesk Inventor 2020 (Fig. 5), the average size element used was 0.05, the minimum size element 0.1, the grading factor 1.5 and the maximum turn angle 30 deg. Geometrically the adapter plate was designed considering flat shapes reducing the presence of curvatures. Referential recommendations are detailed in Table 2.

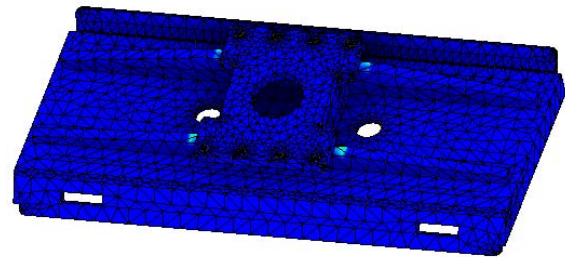


Figure 5. Adapter Plate Meshing

Table 2. Boundary operational conditions for the system Skid steer-adapter plate – hydraulic hammer

Parameters	
Element Average Size	0.1 - 0.05
Element Minimum Size	0.1 - 0.2
Grading Factor	1.5 - 3.0
Maximum Turn Angle degrees	30 - 60

For the static analysis, the tensile yield stress of carbon steel ASTM A36 (Table 3) used is 250 MPa., with Young’s modulus = 199.959 GPa, and Poisson ratio = 0.3. (Fig. 6). Assuming a maximum Von Mises Stress of 31.33 MPa (Fig. 6) and a deflection limitation of 0.25 mm, a maximum result of displacement of 0.09856 mm (Fig. 7) was obtained.

Table 3. Carbon Steel ASTM A36 Properties [17]

Material		
Name	Steel ASTM 36	
General	Mass Density	7.85 g/cm3
	Compressive Yield Strength	250 Mpa
	Yield Strength	152 Mpa
	Ultimate Tensile Strength	400 Mpa
	Young's Modulus	19.959 Gpa
Stress	Poisson's Ratio	0.3 ul
	Shear Modulus	76.9073 Gpa

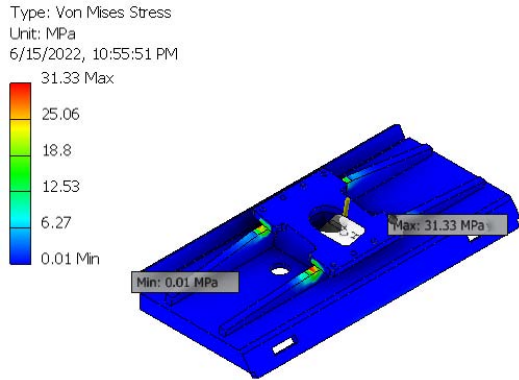


Figure 6. Von Mises Stress Static Analysis in Inventor

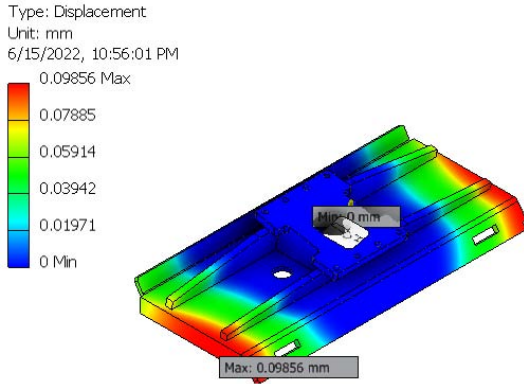


Figure 7. Displacement Static Analysis in Inventor

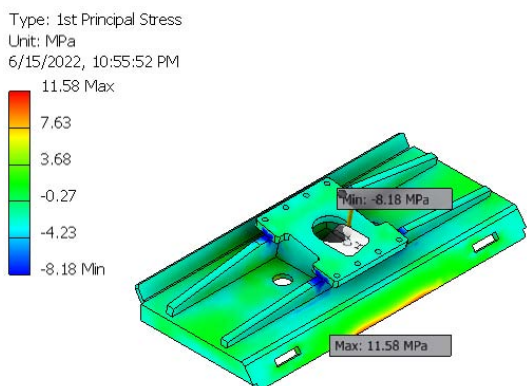


Figure 8. Maximum Tensile Stress Static Analysis

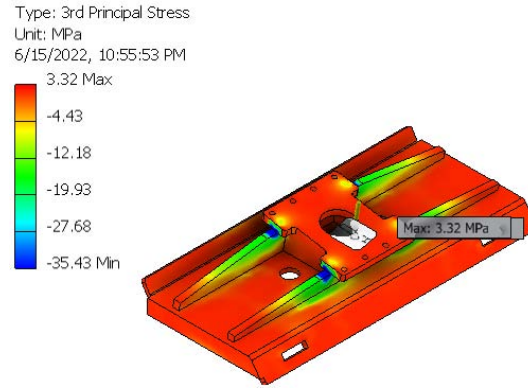


Figure 9. Maximum Compressive Stress Static Analysis

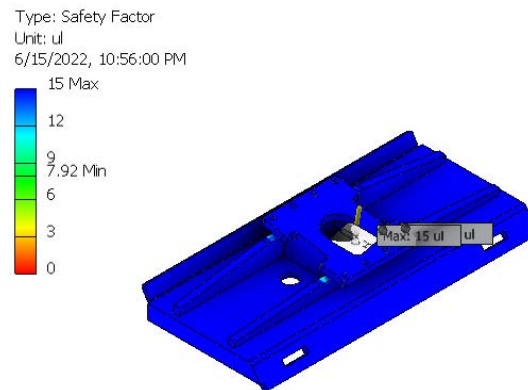


Figure 10. Safety factor Static Analysis

The maximum tensile stress of 11.58 MPa (Fig.8) is below the Von-Mises condition (32.38 MPa) (Fig. 7), because the stress was distributed throughout the whole structure. The maximum compressive stress was 3.32 MPa (Fig. 9), which was observed in the support structure interfaces between the hammer base plate and the skid-steer base plate. The maximum compressive stress of ASTM A36 carbon steel used is 152 MPa [18]. The minimum safety factor was 7.92 (Fig. 7) which means that we achieve a high factor of safety with this design [19] Table 4.

Table 4. Comparison Static and Dynamic Analysis

Type	Static Stress (Mpa)	Dynamic Excluding Prestress (Mpa)	Dynamic Including Prestress (Mpa)	Percentage Difference
Max. Principle Stress	11.58	12.37	23.95	48.34%
Min. Principle Stress	3.32	4.55	7.87	42.19%

3.2. Modal Analysis

The impact frequency of using one SB202 was in a range of 850-1800 blows/min (max 30 Hz). The total maximum deformation was 3.0405×10^{-6} mm in the contact region between the adapter plate and hammer and in the central region of the adapter plate areas with 0.098 mm (Fig. 7).

A stress drop for harmonic analysis was performed in Ansys Modal and Harmonic Response. As a first analysis, it is usual to evaluate where the stress relaxations and prestress removal took place in the adapter plate. Static stress was 11.58 MPa (Table 4) in the initial stage. As dynamic action starts, this situation gets relaxed first. Dynamic stress analysis was used to compensate for the static compression and to bring down the static effect to zero in order to reverse the resistance developed inside the material.

The Dynamic stress excluding prestress was 12.37 MPa (Fig. 11) and the total dynamic stress was 23.95 MPa (Table 4). Maximum principal stress and minimum principal stress percentage difference values of the static and dynamic results are 48.34% and 42.19% which is less than 50% (Fig. 12).

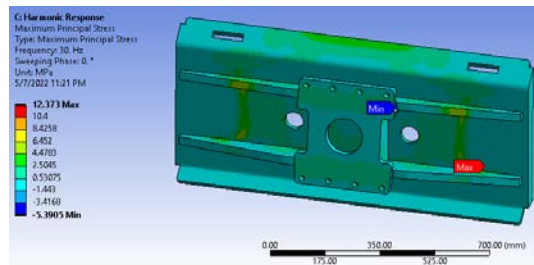


Figure 11. Harmonic Analysis in Ansys Max Frequency of 30Hz

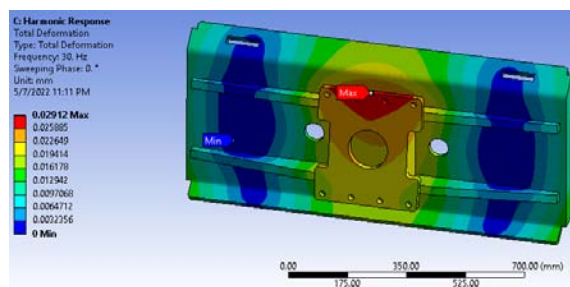


Figure 12. Maximum Principal Stress in Harmonic Analysis

3.3. Fatigue Analysis

Table 5 shows the resulting fatigue life analysis reported by Ansys, we had 1.00×10^8 cycles up to structural failure (Fig. 13). For that reason, using the hydraulic hammer and its operational performance of 600

and 1800 BPM and correlating with the operational hours per day, which results in a range of 308.64 to 925.93 days of operation before failure.

Table 5. Fatigue analysis per operation cycles

Item	Value	Units	Value	Units
Cycles before fatigue (one blow= one cycle)	1.00E+08		1.00E+08	
Hammers Blows Per Minute	1800	BPM	600	BPM
Considering one hour	60	min	60	min
Operational effective hours per day	3	hours	3	hours
Number of days	308.64	days	925.93	days

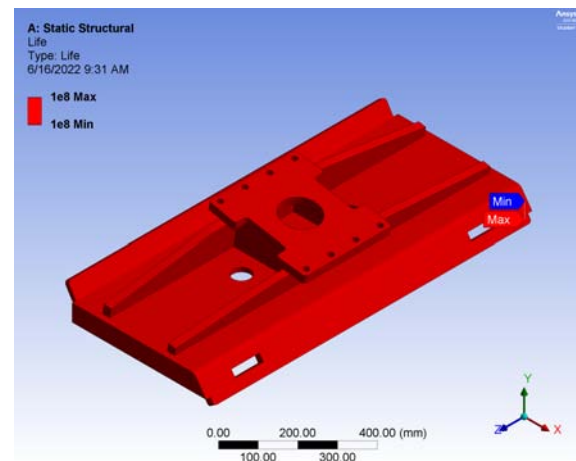


Figure 13. Fatigue Life Analysis in cycles

Similarly, the safety factor resulting from the fatigue analysis reported a minimum number of 4.3599 (Fig. 14) which is over 1 and we can consider this a reliable design.

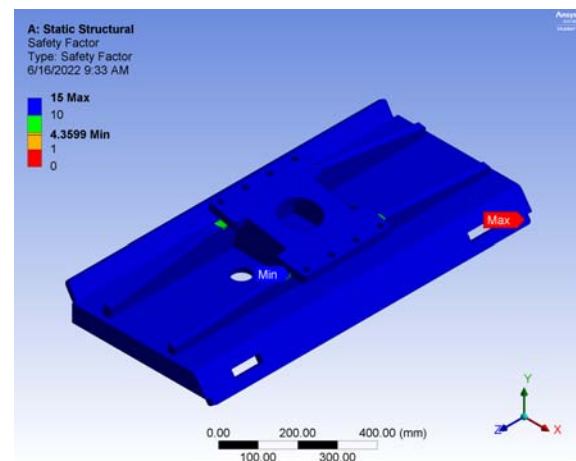


Figure 14. Fatigue Analysis – Safety factor

Due to the maximum stress of 31.33 Mpa (Fig. 6) with a safety factor of 7.92 (Fig. 10), this sustains up to 1.00×10^8 cycles (Fig. 13) before structural failure.

This performance supports the goal of this design attaining the maximum durability while also acting as a fuse protecting the hammer and skid steer structure if an overload happens. With the stress load reported it is still under the endurance limit, because despite the 1.00×10^8 cycles before fatigue, the safety factor is over 1 which means we have space for future optimization.

3.4. Building and welding process

The adapter plate was built using carbon steel ASTM-A36, with welding 6011 and 7018 with 5/32" size and for the final product an electrostatic paint RAL9005 was used, and each final product was registered with a progressive registration number for the product quality control and warranty management (Fig. 15).

3.5. Standard product for the market

As a marketing strategy, the supplier offered six months as a standard warranty and included a constantly updated optimization for final users with high reliability using new adapter plates as a backup in case of quality problems with the presence of cracks in the structure (Table 2).

Table 6. Record of adapter plates and qualitative performance

Plate	Fabrication	Time use (month)	Warranty (month)	Observation
1	15-Jan-15	6	12	Normal Wear
2	15-Jan-15	4	12	Normal Wear
3	15-Jan-15	8	12	Normal Wear
4	15-Jan-15	7	12	Normal Wear
5	15-Jan-15	12	12	Normal Wear
6	15-Jan-15	16	12	Small cracks
7	15-Jan-15	6	12	Normal Wear
8	15-Jan-15	8	12	Normal Wear
9	15-Jan-15	12	12	Normal Wear
10	15-Jan-15	14	12	Small cracks

After 14 months of use, a group of 10 adapter plates built simultaneously were physically evaluated along with their warranty claims. The results confirmed normal wear during operation and the presence of cracks after the warranty period of 12 months. (Table 6) At the same time, no cracks were observed in the solid structure of hammers or skid steer boom structure, and complementary animation and training videos were developed to explain the effect of inappropriate operation to customers [16]. Proper training and operation contributed to reducing damage to hydraulic hammers.

Finally, this product has been a probed solution from 2015 up to current date for skid-steers-hammers system for demolition application in Peruvian market; however, its price represents 20% of acquisition price, for that reason, it is recommendable to start an optimization research to reduce production costs. This adapter plate was standardized to be used by the majority of brands which work with Atlas Copco

hammers and the serial production surpasses 500 units up to date with reliable performance and having, as a result, lower warranty claims and side effects over hydraulic hammers.



Figure 15. Adapter plate as final product

4. Conclusions

Stress applied during the demolition of hard road covers, pavement and asphalt, across the system including skid steer-adapter plate-hydraulic hammer was identified as the main concern of this study and the style of operation. For that reason, as part of an optimized product development, training videos were developed to improve operational skills.

Complementary to that, a warranty claim strategy was established to reestablish confidence in the products and an exclusive supplier was appointed including a reliable warranty response, which contributed to reintroducing the product reducing the warranty claims of failures in hydraulic hammers to a 99% during the following 12 months.

There is space for the optimization process because the safety factor obtained is higher than 7.95 and the difference percentage between static and dynamic results are lower than 50%, and in the industry, a reference of 20% is used to obtain the maximum resistance. However, the peaks of stress do not exceed the maximum tensile yield stress of ASTM A36 carbon steel which was 250 MPa, and the maximum compressive stress of ASTM A36 carbon steel was 152 MPa. The strategy confirmed the use of the adapter plate as an element to protect the hammer and skid-steer from deformation.

The adapter plate was demonstrated to act as a fuse protecting the hammer and skid steer arm, confirming our hypothesis. Continual innovation is recommended to improve the adaptor reliability and performance on job sites which will increase the product's reputation in the marketplace.

References

- [1] N. Montes de Oca and S. Velut, "Energy modernisation and regional reorganisation of the southern andes: The unexpected materialities of the southern peruvian gas pipeline," *Journal of Alpine Research / Revue de géographie alpine*, pp. 1–16, 2022. [Online]. Available: <https://doi.org/10.4000/rga.9465>
- [2] S. Maroye and A. Aerssens, "Natural gas distribution network of lima and callao, peru," 2005. [Online]. Available: <https://bit.ly/3A4d6ox>
- [3] Atlas Copco, *Safety and operating instructions Hydraulic breakers*. Construction Tools PC AB, 2015. [Online]. Available: <https://bit.ly/3u2XyxL>
- [4] ITM, *Manual de Seguridad y Bioseguridad para los Laboratorios de Química del ITM*. Instituto Tecnológico Metropolitano, 2012. [Online]. Available: <https://bit.ly/3btbhqS>
- [5] T. Yalçın, "Design of a skid steer loader," 2012. [Online]. Available: <https://bit.ly/3ngsjv0>
- [6] L. Leung and G. P. Jenkins, "An economic evaluation of peru's liquefied natural gas export policy," vol. 74, pp. 643–654. [Online]. Available: <https://doi.org/10.1016/j.enpol.2014.06.028>
- [7] Cálidda, "Instrucciones y recomendaciones técnicas para obras que impliquen trabajos sobre o cerca de instalaciones de gas natural." [Online]. Available: <https://bit.ly/3HWp19R>
- [8] —, "Guía del plan de prevención de daños (ppd)," 2022. [Online]. Available: <https://bit.ly/3noe47r>
- [9] *Synthesis of Dynamical Structure of the Hydraulic Breaker With a Vibration-Free Handle*, ser. International Design Engineering Technical Conferences and Computers and Information in Engineering Conference, vol. Volume 1: 21st Biennial Conference on Mechanical Vibration and Noise, Parts A, B, and C, 09 2007. [Online]. Available: <https://doi.org/10.1115/DETC2007-34667>
- [10] D. A. Ashcroft, E. H. Priepke, and W. J. Sauber, "Design and development of new generation skid steer loaders," *SAE Transactions*, vol. 103, pp. 252–258, 1994. [Online]. Available: <http://www.jstor.org/stable/44473342>
- [11] Wheeler CAT, "Caterpillar performance handbook," 2018. [Online]. Available: <https://bit.ly/3u20ISq>
- [12] CASE, "Skid steer loadertier 4 interim certified," 2013. [Online]. Available: <https://bit.ly/3bv1nVV>
- [13] Epiroc, "Spare parts list hydraulic breakers sb 202," 2022. [Online]. Available: <https://bit.ly/3xY5PE4>
- [14] A. Palomino-Valles, M. Tokumori-Wong, P. Castro-Rangel, C. Raymundo-Ibañez, and F. Dominguez, "TPM maintenance management model focused on reliability that enables the increase of the availability of heavy equipment in the construction sector," *IOP Conference Series: Materials Science and Engineering*, vol. 796, no. 1, p. 012008, 2020. [Online]. Available: <https://doi.org/10.1088/1757-899x/796/1/012008>
- [15] J. Li, Y. Wang, K. Zhang, Z. Wang, and J. Lu, "Design and analysis of demolition robot arm based on finite element method," *Advances in Mechanical Engineering*, vol. 11, no. 6, p. 1687814019853964, 2019. [Online]. Available: <https://doi.org/10.1177/1687814019853964>
- [16] Y. Villa, "Esplicación práctica de uso de martillos hidráulicos," 2014.
- [17] P. Preedawiphat, N. Mahayotsanun, K. Sa-ngoen, M. Noipitak, P. Tuengsook, S. Sucharitpwatskul, and K. Dohda, "Mechanical investigations of astm a36 welded steels with stainless steel cladding," *Coatings*, vol. 10, no. 9, 2020. [Online]. Available: <https://doi.org/10.3390/coatings10090844>
- [18] Matweb, "Matweb-astm a36 steel, bar," 2015. [Online]. Available: <https://bit.ly/3OJ0Uh2>
- [19] K.-l. Lu, W.-g. Zhang, Y. Zhang, H. Huang, Y.-s. Chen, W.-y. Li, and C. Wang, "Crack analysis of multi-plate intersection welded structure in port machinery using finite element stress calculation and acoustic emission testing," *International Journal of Hybrid Information Technology*, vol. 7, no. 5, pp. 323–340, 2014. [Online]. Available: <https://doi.org/10.14257/ijhit.2014.7.5.30>



COMPARATIVE ANALYSIS OF THERMAL COMFORT OF A SINGLE-FAMILY HOUSE IN LSF AND BRICK MASONRY

ANÁLISIS COMPARATIVO DE CONFORT TÉRMICO DE VIVIENDA UNIFAMILIAR EN LSF FRENTE A MAMPOSTERÍA

Rodrigo Brito-Peña^{1,*} , Daniel Villa-Enderica¹ , Esteban Zalamea-León¹ 

Received: 16-05-2022, Received after review: 17-06-2022, Accepted: 20-06-2022, Published: 01-07-2022

Abstract

Residential construction in Ecuador has recently grown a 35.6%. The typical construction system for housing envelopes is concrete block or brick; construction in Light Steel Framing (LSF) or galvanized steel frames is emerging. To solve the housing demand, the thermal comfort inside a two-story one-family home in the city of Cuenca is evaluated considering both construction systems, to know the comfort standards offered by homes in accordance with the Ecuadorian Construction Standard (NEC, Norma Ecuatoriana de la Construcción). The research was carried out with Design Builder and Therm, where the parameters that influence the energy performance of homes are analyzed. Under local conditions, the predominant system reaches annual hourly thermal comfort values of 51%, but the LSF system reaches 62%. However, with improvement strategies in the overall envelope, the LSF reaches 86%. The variables in decreasing order of thermal influence were: air infiltrations, envelope construction system and housing deployment. In Cuenca it is feasible to use the LSF with minimum insulation to reach acceptable levels of comfort, being an adequate alternative to be promoted for building one-family housings.

Keywords: Housing, Light Steel Framing, Thermal comfort, Simulation

Resumen

La construcción residencial en Ecuador ha crecido un 35,6 %. El sistema constructivo típico para envolvente de viviendas es de bloque de concreto o de ladrillo, la construcción en LSF (Light Steel Framing) o marcos de acero galvanizado (LSF) está en surgimiento. Para solucionar la demanda habitacional se evalúa el confort interior térmico de una de vivienda unifamiliar de dos plantas en la ciudad de Cuenca con ambos sistemas constructivos para conocer los estándares de confort que ofrecen las viviendas en concordancia con la Norma Ecuatoriana de la Construcción (NEC). La investigación se realizó con Design Builder y Therm donde se analizan los parámetros que influyen en el desempeño energético de las viviendas. Con las condiciones locales, el sistema predominante alcanza valores de confort térmico horario anual del 51 %, pero el sistema LSF alcanza un 62 %. Sin embargo, con estrategias de mejoramiento en la globalidad de la envolvente, el LSF alcanza el 86 %. Las variables en orden de mayor a menor influencia térmica resultaron: infiltraciones de aire, sistema constructivo de la envolvente e implantación de la vivienda. En Cuenca es posible el uso del LSF con aislamiento mínimo para alcanzar niveles aceptables de confort, siendo una alternativa adecuada a promover para edificar viviendas unifamiliares.

Palabras clave: vivienda, *steel frame*, confort térmico, simulación

^{1,*}Dirección de Investigación de la Universidad de Cuenca, Universidad de Cuenca, Ecuador.
Corresponding author ✉: jrodrigo.britop@ucuenca.edu.ec.

Suggested citation: Brito-Peña, R.; Villa-Enderica, D. and Zalamea-León, E. "Comparative analysis of thermal comfort of a single-family house in LSF and brick masonry," *Ingenius, Revista de Ciencia y Tecnología*, N.º 28, pp. 100-124, 2022, DOI: <https://doi.org/10.17163/ings.n28.2022.10>.

1. Introduction

For each particular context it is important to establish comparative analyses of different construction technologies, to set capabilities in terms of security, durability, quality, thermal comfort, among other aspects. It has been evidenced that the thermal performance of dry construction systems such as Lightweight Steel Framing (LSF) may reach conditions similar to those of masonry [1], and it is possible to define insulation levels appropriate for the context.

According to the American Institute of Architects (AIA, 2007), 50% of the worldwide emissions of greenhouse gases were produced by the construction industry. To a large extent, this is a consequence of the high consumption of buildings and the lack of comfort in them. An impact is generated from the manufacturing, transportation execution, use and maintenance of the building up to the end of its life cycle [2]. Likewise, construction is placed as the second industry with the highest energy demand worldwide, and most of such consumption is used for achieving indoor environmen-

tal quality [3,4]. Therefore, it is important to determine the capability of the construction materials to achieve quality in thermal comfort with high degree of construction efficiency [5,6]. In the last fifteen years, the construction sector in Ecuador has grown 35.6% due to the economic and population development. Among the total number of construction permissions granted in 2018, 84.1% correspond to residences, 56.9% correspond to one-family housings and 88.1% are new housings.

The predominant materials for housings in Ecuador are reinforced concrete for foundations, structure and roof, concrete block or brick masonry for walls and envelopes, structured in steel for constructive speed. The introduction of alternative construction systems is minimum, and very little consideration is given to the affectations due to the materials selected. The housing in LSF dry construction has a share of only 2.9 % in Ecuador [7], as seen in Figure 1 [7]. The systems that enable prefabrication are an opportunity to reduce the construction cost, but the comfort levels should be also considered [8].

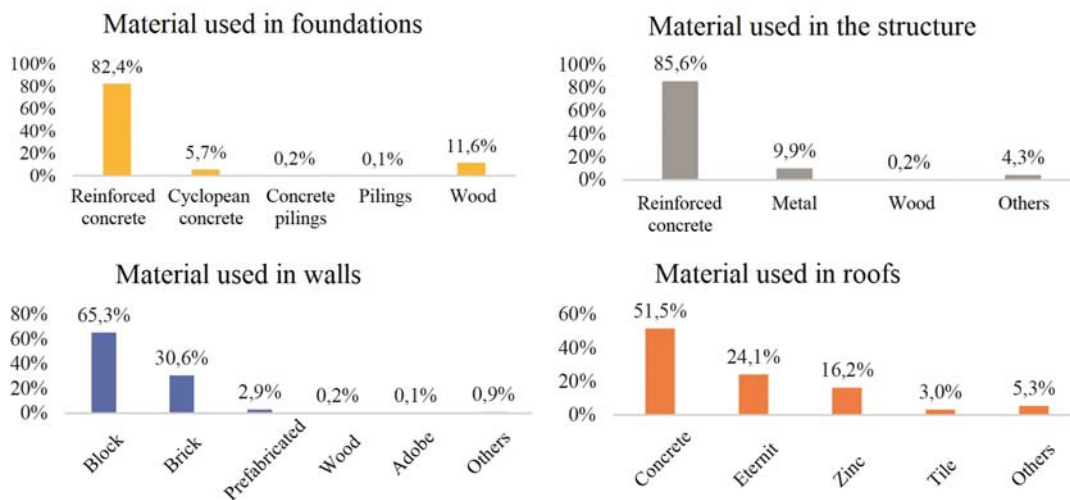


Figure 1. Main materials that predominate in the construction in Ecuador

The implementation of the LSF dry system may result less offensive with the environment, and offers great advantages compared to traditional wet systems regarding its *in situ* impact [9]. Various constructive advantages are typical of this system, such as the potential prefabrication and speed, durability, seismic-resistant capability, convenient prices, among others [10]. The LSF has a good thermal performance since it enables including the insulation required and calibrated according to the local conditions; it has the capability of reaching high levels of thermal insulation, even in extreme weather [11,12].

In addition, according to [9,13], the main deficit regarding the thermal capacity in the LSF is in the thermal bridges as a consequence of the light steel

structural frames which should not be more than 0.60 m apart. With respect to structural capacity, the LSF has appropriate conditions due to the lower rigidity and weight, which implies that the seismic response is adequate in regions of high seismicity, such as the Andean zone [14,15]. Likewise, it responds favorably to accidental loads [16].

In terms of safety in the event of fire, the LSF is recommended over other flame-retardant technologies [17]. At the same time, it is capable of integrating all components necessary to construct a building. The construction methods are manufacturing on-site, by prefabricated panels and, finally, the modular construction [18]. The LSF tends to be more expensive compared to masonry housings typical in Ecuador, due

to the reduced penetration of the material. However, it may result a convenient system due to the advantages of industrialization and market economy [19]. It reduces the labor costs between 62.5% and 73%, and improves management of consumables, operations and logistics at the construction sites [20]. In Ecuador, the deficit in housings together with the difficult economic situation causes the construction of low-budget buildings using handcrafted materials, and those housings do not fulfill the appropriate levels of thermal comfort, and thus, new buildings should meet NEC standards [21].

1.1. Climatic conditions of the surroundings of the housing under study

Ecuador is divided in six climatic zones, according to what is established by the ASHRAE 90.1 and Miduvi [22]. The reference housing is located in climatic zone 3 of Ecuador, determined as a region of rainy continental mountains. Figure 2 shows a diagram

of the climatic conditions 3). The zone is very close to the Equator, at an altitude of 2550 m above sea level; due to these conditions, it is a temperate and stable climate all year round. The temperature varies between maximum and minimum averages of 7 and 25 °C; however, extremes of -1.7 °C and 28.9 °C are recorded, with an average of 15.6 °C. March is the hottest month and August the coldest one, but the extreme conditions of cold or hot normally do not last more than a few hours. Due to the Equatorial conditions, seasonal climatic variations are minimal. The duration of the day is also stable all year round, with the dawn occurring between 05:50 and 6:30 and the dusk between 18:05 and 18:35, depending on the season. The wind is low, with preponderance from the Northeast. Consequently, it is about a temperate weather with greater incidence of excessive cooling, but with a weather benign for habitability; most buildings lack active conditioning systems. However, this aspect implies that out of comfort moments are usual.

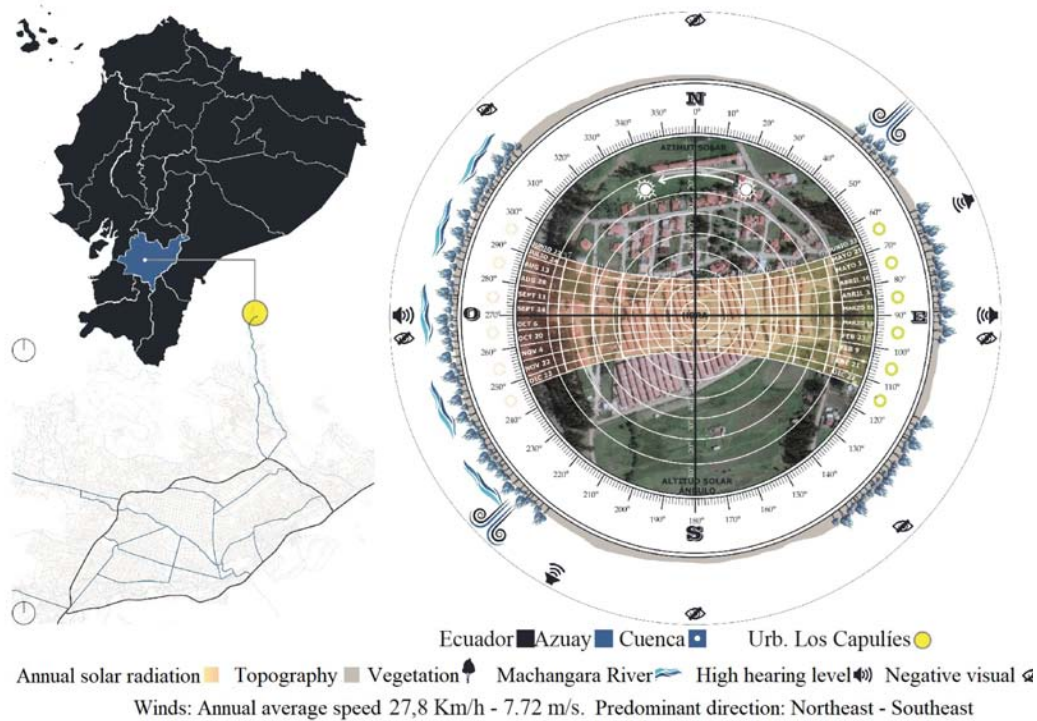


Figure 2. Location and scheme of the climatic conditions of the surroundings

It will be analyzed a housing with spatial and morphological features that are recurrent in the country, with the most frequently used construction system consisting of masonry and concrete, with the objective of determining the base environmental conditions. On that basis, variations are compared according to the change of envelope in the LSF construction system. For this purpose, simulations are programmed to contrast

the thermal behavior of the same housing materialized in two different construction systems and envelopes, LSF system vs. traditional system, assuming the same functional and spatial conditions. It is analyzed the type II model of one-family housing found at the residential area Los Capulies, located at Cuenca, which was developed by the Housing Ministry (Miduvi, Ministerio de la Vivienda) of Ecuador. These housings

are arranged in high-density settings, paired on both sides to achieve a maximum leverage of the piece of land. The distance between the fronts is only five meters, whereas the backs are three meters apart. This arrangement reduces solar incidence, and also causes

visualization and privacy problems. Figure 3 shows the configuration of the housings (based on documents of the Emuvi EP). Even though it has aspects regarding design conditions, this work analyzes the influence of envelope materials.

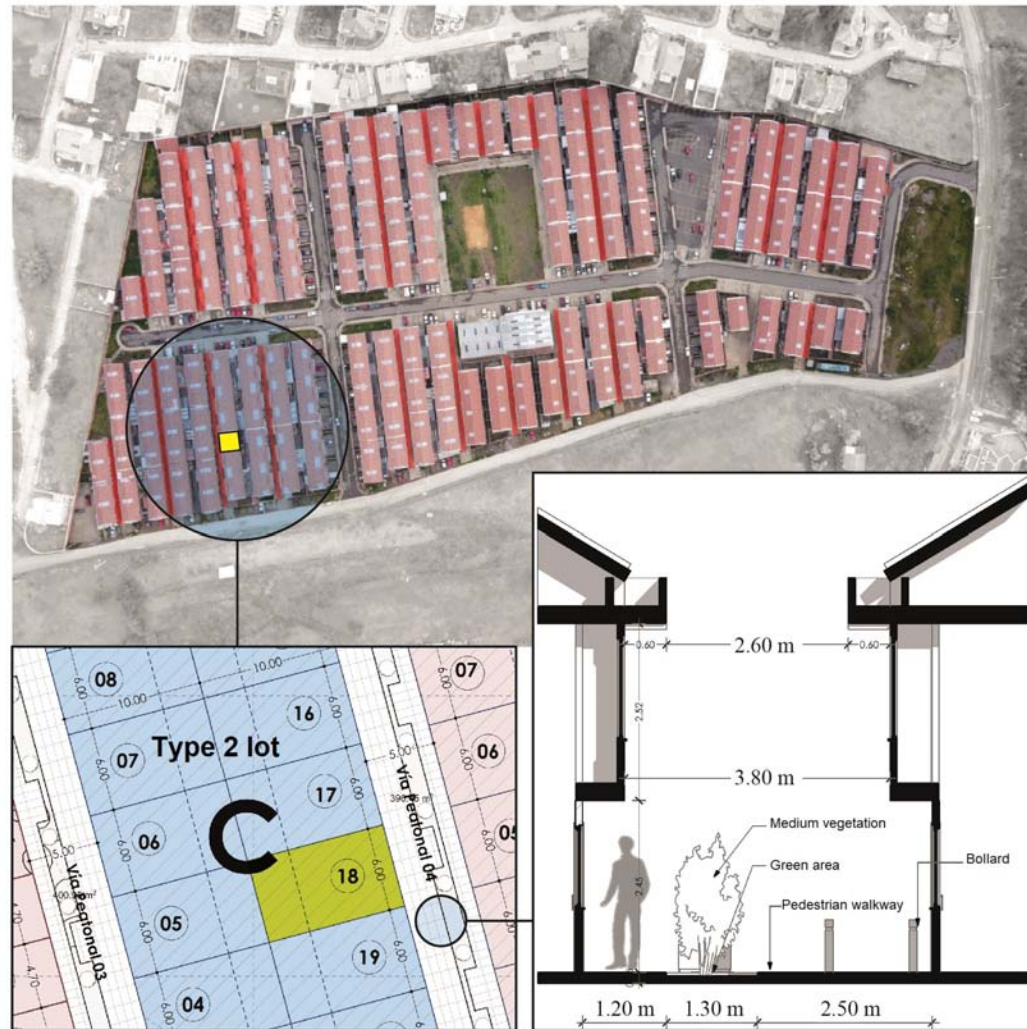


Figure 3. Housing under study together with the remaining housings in the residential area Los Capulíes

2. Materials and methods

At first instance, the parameters and features that have influence on energy performance were established, and analyzed with respect to the levels of thermal comfort of the regulation that dictates that the indoor temperature should be maintained between 18 and 26 °C [23]; it is considered that excesses or deficits imply being out of the range of thermal comfort. With this precedent, the following parameters were determined for studying energy performance:

Deployment: It is determined by the position of the housing within the block, corresponding to a corner, middle or isolated housing. Weather: It is deter-

mined by means of the climatological archive of the Cuenca region. Internal thermal gains: It is referred to the amount of energy as heat within the housing, contributed by electric appliances and users. Air infiltrations: Make reference to the air exchanges per hour at a pressure of 50 Pa, i.e., to the levels of air renewal inside a housing.

These parameters will be studied in three variations of the same housing, according to its location within a block: isolated, middle and corner.

Eighty-five models were constructed for the analysis, from virtual variations of the materials. The indoor operating temperature (OT) is considered the variable for the analysis of results; the dry bulb external tem-

perature (ET) only represents the temperature that affects the housing envelope and enables reflecting the level of conditioning reached by the housing. Regarding the levels of infiltration of this type of structures, indicators found in Chile [24] are considered since there are no local studies. Lower levels of air infiltration (10 ACH50) are expected in the masonry envelope, compared to the 25 ACH50 expected in the LSF. However, when the LSF is constructed with greater insulation, materials of better thermal performance and high construction quality, with emphasis on the constructive joints, the air exchanges decrease [25].

At a second instance, digital models of the one-family housing to be studied were made in two groups. The recurrent configurations and materials for the region, i.e., the traditional wet system, were modeled in the first group. The models with the LSF system were made in the second group. Finally, the indoor thermal comfort of the two construction systems was analyzed at a third instance. Virtual models were studied with the Design Builder [26] and Therm [27] energy simulators, fed by 2016 climatic information of the region under study. The climatic file (.tmy) (typical average climate) was not used, because it implies to lose days and hours with extreme temperatures; hence, it was used climatic data corresponding to one year (2016) in the epw file.

The evaluation was performed in sequential stages, due to the interaction of different factors that have influence on the indoor thermal comfort. The first stage seeks to determine the incidence of orientation, a diffuse aspect in the equatorial weather. Prior to analyzing the thermal comfort of the housing, in the second stage it is intended to determine with Design Builder the energy performance of the housing with LSF, without including thermal insulation. The model is fed by envelope coefficients from the thermal anal-

ysis of the materials carried out in Therm, tool that enables to determine in detail the insulation capacity considering affectations implied by thermal bridges. In the third stage it is sought to know if there are improvements in the thermal levels with minimal insulations in the LSF system. Finally, in the fourth stage it is sought to improve the materials used in the LSF system, with the purpose of knowing if the thermal increase is significant; thus, the Therm tool is used again to analyze the configurations of the different carpentries.

The frequency Thermal Discomfort (FDT) is the percentage of time in which the operating temperature does not reach the required standards [28]. Therefore, in this research the results will be analyzed as percentages referred to a year in its 8760 associated hours. Likewise, the parameters or variables with higher or lower incidence on the thermal performance of the housing will be established in the final instance.

2.1. Original features and materials of the housings under study

The reference housing is a two-story one-family housing of 86.40 m² which, according to the INEC, is a recurrent typology in the country. It is a housing with average size and condition to accommodate four inhabitants. The housing is constructed with steel structure, masonry brick walls for the envelope, with plaster only in the interior and fiber cement roof with a false plaster ceiling parallel to the fiber cement. The bottom and mezzanine floors are made of concrete, with porcelain coating in wet areas and floating flooring in dry environments. Finally, the carpentries are made of steel with simple glass. As a basis for comparison, the indoor thermal quality is simulated with these conditions; Figure 4 shows the reference housing.



Figure 4. Status of the housing under study in 2020

The LSF proposal adopts the same conditions of the base model. The structural dimensions are provided by the engineering department of the local distribution company. The recommended components are the following: Stud profiles (columns) of 90×0.93 mm in walls and trusses, Track (beams) of 90×0.93 mm in walls and trusses, Stud of 200×1.8 mm in mezzanine floor and Track 200×1.8 mm in mezzanine

floor. However, the use and configuration of the layers of insulation and coating materials are not determined according to the thermal performance, due to the minimum use of this technology nationwide. Both suppliers and consumers choose the components and materials based on various criteria to build the housing. Figure 5 shows the plans of the housing adapted to LSF.

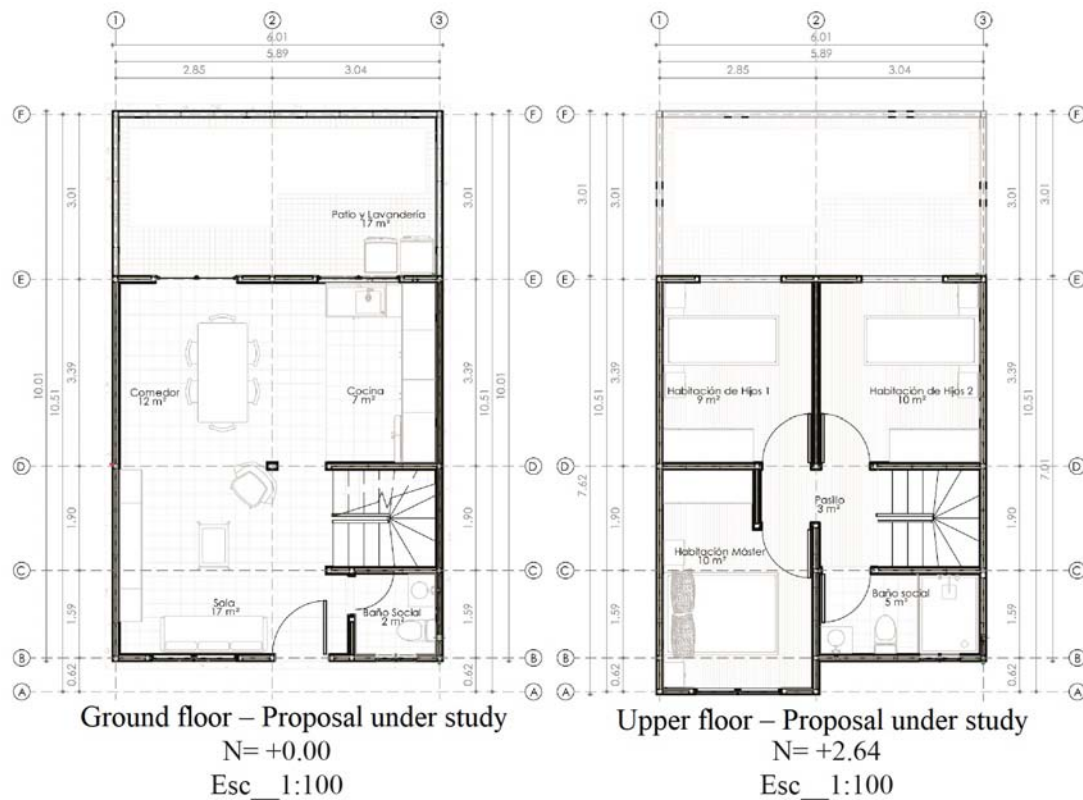


Figure 5. Proposal materialized with LSF

2.2. General conditions for the indoor thermal comfort study

The aspects and features of the envelope are identified as input data for the indoor thermal comfort analy-

sis, and the parameters for the digital evaluation are established categorized in six groups (Table 1).

Table 1. General conditions and parameters

N.°	Parameter	Code	Variables	Variable description	Comments
1	Housing typology	V01	V. brick middle	Current status	Middle
2		V02	V. brick corner	Current status	corner
3		V03	V. brick isolated	Current status	isolated
4		V04	V. LSF middle	Proposal	Middle
5		V05	V. LSF corner	Proposal	corner
6		V06	V. LSF isolated	Proposal	isolated
7	Deployment	I01	Current east facade	Orientation of main facade	Current status
8		I02	Current west facade	Orientation of main facade	Current status
9		I03	North facade	Orientation of main facade	North
10		I04	South facade	Orientation of main facade	South
11		I05	East facade	Orientation of main facade	East
12		I06	West facade	Orientation of main facade	West
13	Weather	C01	Annual	Annual average	Average
14		C02	Coldest month	Monthly average	Average
15		C03	Warmest month	Monthly average	Average
16		C04	Coldest day	Coldest day in the year	All day long
17		C05	Warmest day	Warmest day in the year	All day long
18	Internal gains	GI1	Users	3.7	average [29]
19		GI2	Appliances and equipments	13.31 W/m ²	W/m ²
20	Air infiltrations of the construction system	SC1	10 in all stages	Brick and steel mixed system	Source: [30]
21	(Levels ACH at 50 Pa)	SC2	25 in stages 1 and 2, 10 in stages 3 and 7 in stage 4.	LSF System	Source: [30]

3. Results and discussion

3.1. First stage: Base thermal performance of the reference housing, current status

Twenty digital models were made in the first stage, divided in two groups according to the construction system. The first group analyzes the mixed system con-

stituted by brick in a steel structure of the housings in their current deployment; this is the base situation. The second group is focused on LSF. Table 2 describes in detail the evaluation parameters for all simulations, considering infiltration levels in air replacements per hour (ACH) at a pressure of 50 Pa, under different orientations of the front facade through which the housing is accessed.

Table 2. Variation parameter in the First stage

N.º	Construction system		Housing typology	Deployment
	Type	Features		
E1_01	Brick and steel mixed system	10 ACH50 Traditional masonry housing	Middle	East
E1_02				West
E1_03	Corner		Este	
E1_04			West	
E1_05	Isolated		North	
E1_06			South	
E1_07			Este	
E1_08			West	
E1_09	LSF System	LSF housing without insulation	Middle	North
E1_10				South
E1_11	25 ACH50		Este	
E1_12			West	
E1_13	Esquinera		North	
E1_14			South	
E1_15	Isolated		Este	
E1_16			West	
E1_17			North	
E1_18			South	
E1_19		Este		
E1_20		West		

The models with the orientations of the front and back facades with the main openings, doors and windows, are considered favorable when they face east and west (higher solar incidence) and unfavorable when facing north and south (minimum incidence of irradiation as a consequence of the equatorial latitude). The

predominant orientation of the winds is demonstrated in Figure 2. It is found that the average thermal variation is minimal due to the orientation, as shown in Figure 6. For the subsequent stage, only scenarios with unfavorable orientations will be studied, to visualize the results in the most extreme temperatures.

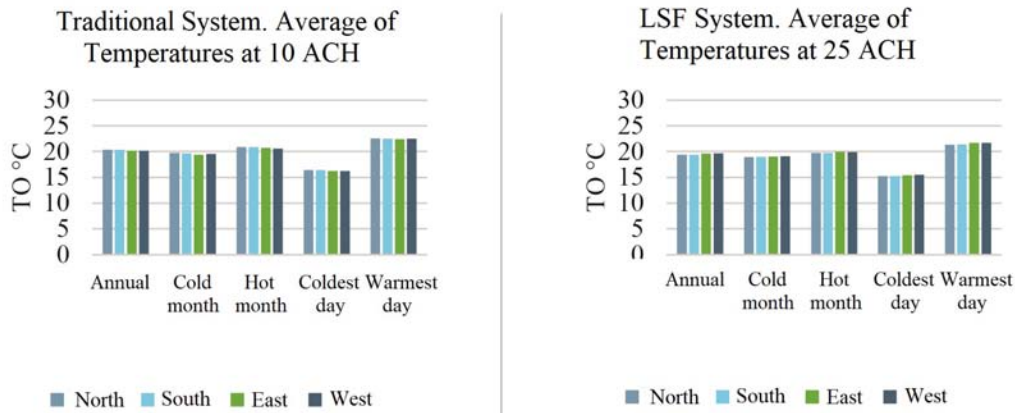


Figure 6. Average OT as a function of the Deployment parameter

3.1.1. Analysis of the thermal performance of the construction systems through the envelope section by means of THERM

The thermal transmittance of each envelope material of the construction systems under study, is analyzed in this section. The steel profiles that constitute the structure of the entire housing are added to the traditional system; such profiles are exposed in the original

model. Likewise, the LSF is considered with a simple insulation through a 50 mm thick single layer of stone wool, with which there is a 40 mm remnant air layer in the envelope section. The variable of study is the influence of the metallic structure in each construction system. It is found the influence of the thermal bridges on the housings. The most unfavorable cases of each orientation are analyzed, as shown in Figure 7.

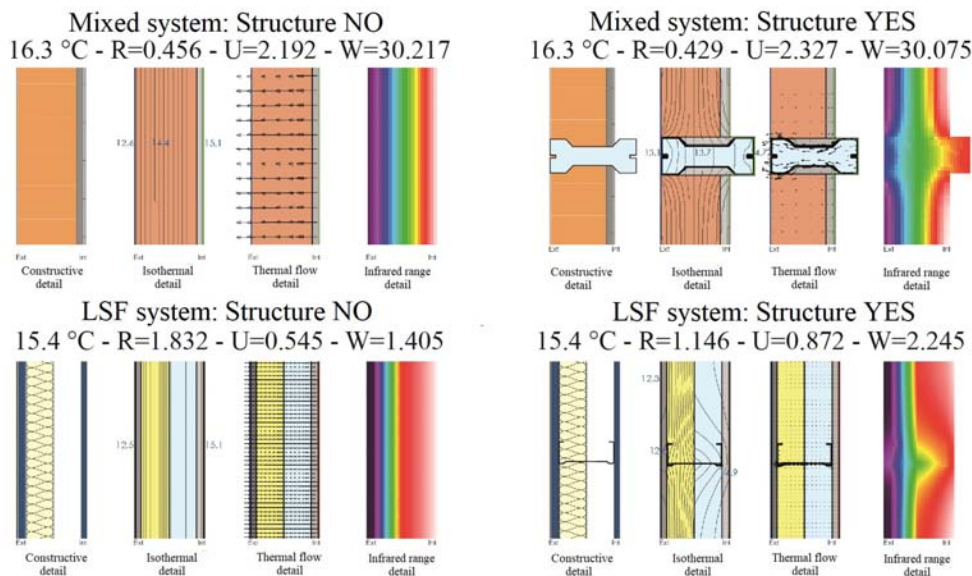


Figure 7. Thermal analysis of the section of both construction systems in THERM and conductivity determined

High values of thermal transmittance are evidenced in all the walls of the envelope, the thermal bridges are important in both construction systems, which significantly influences the insulation capacity. In the mixed construction system constituted by bricks in steel porticoes, higher values of thermal transmittance are observed in the zones in which structural elements

meet. However, in the LSF, the thermal transmittance is spread and mitigated by the fiber cement and plaster cardboard coating.

3.2. Second stage: Thermal analysis with incidence of the thermal bridges in unfavorable orientations

At this stage (Table 3), the digital models are configured again in Design Builder, entering in the simulator the new values of the Thermal resistance parameter or

R Factor of each material, values that are reduced to 67.78% of the original value according to the study by means of THERM. In this section, the housings are analyzed again with the condition of the Deployment parameter, referred in this case to the most unfavorable orientations, i.e., without direct solar incidence on facades.

Table 3. Second stage

N.º	Construction system		Housing typology	Facade orientation
	Type	Features		
E2_01	Brick and steel mixed system	Traditional masonry housing	Middle	North
E2_02				South
E2_03	10 ACH50		Corner	North
E2_04				South
E2_05			Isolated	North
E2_06				South
E2_07	LSF System		Middle	North
E2_08				South
E2_09	25 ACH50	LSF housing without insulation	Corner	North
E2_10				South
E2_11			Isolated	North
E2_12				South

With the brick and steel envelope, in the case of the coldest day the housing is in comfort only at noon, whereas in the case of the warmest day, the comfort occurs in the morning and in the afternoon. An important peak in high temperatures is observed at noon.

Consequently, the housing experiences overheating, since there is no insulation in the roof; specifically, overheating in the upper floor, as observed in Figure 8.

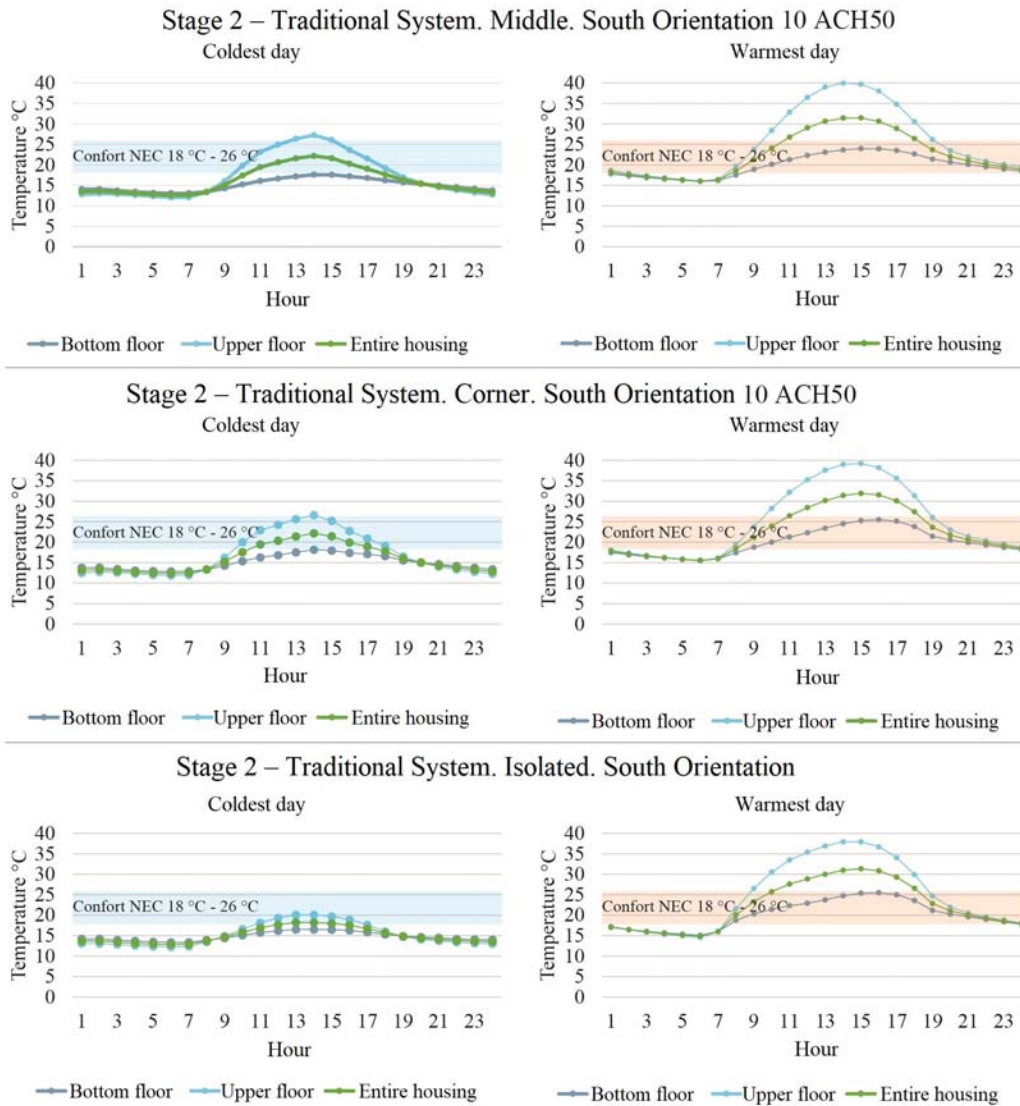


Figure 8. Thermal comparison, traditional system, second stage

For the coldest day in the LSF system, there is comfort after noon. However, in the warmest day the comfort extends for almost all day long. It is observed that the thermal curve tends to reduce the oscillation

during the 24 hours of the day. The maximum and minimum peaks are less pronounced than in the reference system, as it is seen in Figure 9. Figure 10 shows the general thermal comparison of the second stage.

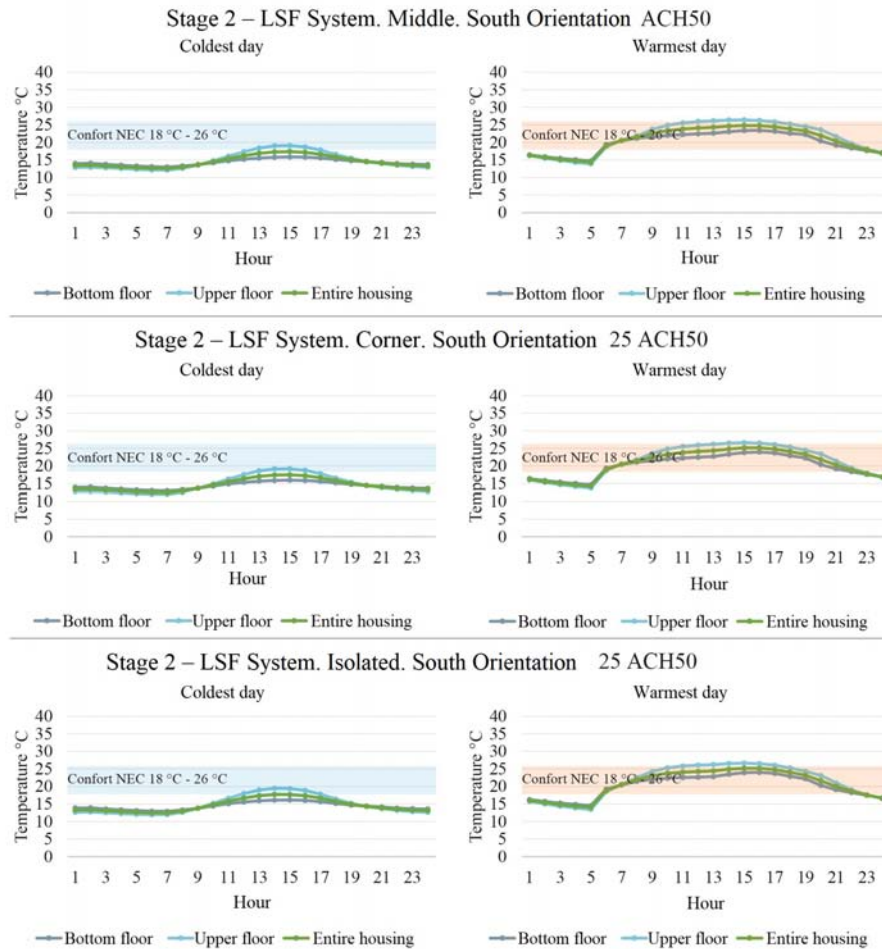


Figure 9. Thermal comparison, LSF system, second stage

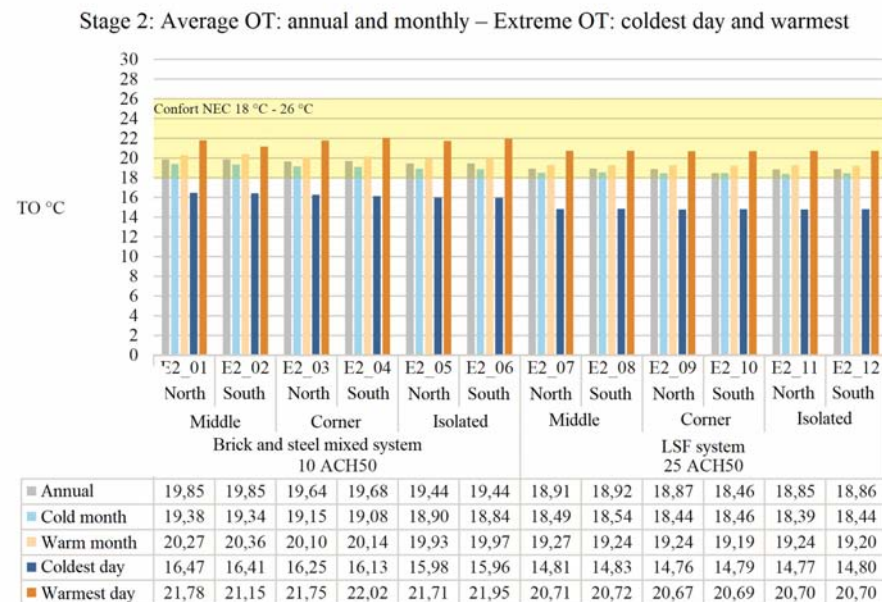


Figure 10. General thermal comparison for the second stage

3.2.1. Analysis of the different inclusions of thermal insulation in the housings with LSF

For the climatic features of the Andean region in Ecuador, the «cold wall» [9] typology is used in the

LSF analysis, as it is observed in Figure 11 [9]. This wall typology with the insulation in the internal side retains the heat in the interior in a better way, according to the analysis with THERM. In addition, it is the simplest and the most economical.

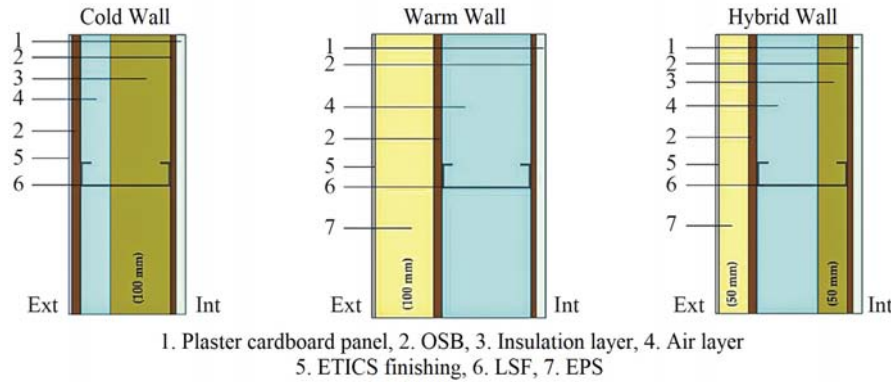


Figure 11. Wall typologies: warm, cold and hybrid

It is also analyzed the incidence of the infiltrations estimated for the constructive topology; according to the construction system, it has been considered an ACH50 of 25, and from it, the consequent thermal performance of the housing. The base housing (A01) shows the worst performance in average. The A02 and A03 cases (A03 interior insulation is recommended by acoustic conditions) are similar. However, the A03 housing implies a more hermetic one, due to a better configuration of the surfaces of the envelope thermally insulated in a more uniform manner. The air chamber produced between the roof and the false ceiling of the upper floor provides better results with respect to the

base configuration, considering that these housings are currently not constructed with false ceiling and, much less, with insulation; hence, it is usual the overheating in the presence of direct equatorial irradiation, as well as important thermal losses at night. It is observed that the A04 and A05 cases are critical with respect to the previous ones. This implies that it is necessary insulation in the roof to a larger extent and in the floor to a lesser extent. From the 24 hours of the day, the results are quantified only at the hours that reach the NEC comfort range (18 and 26 °C), as seen in Figure 12.

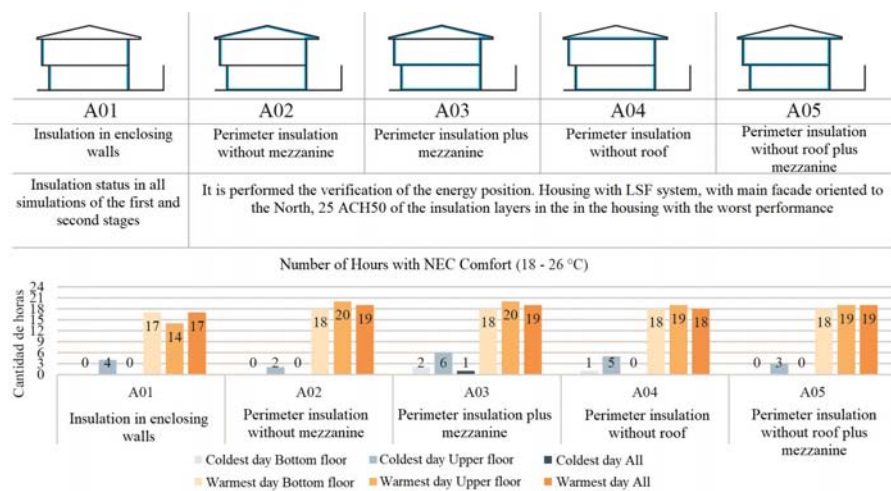


Figure 12. Types of insulation and energy performance in number of comfort hours

3.2.2. Analysis of the energy performance of the different configurations of carpentries by means of THERM

The thermal bridges in the carpentries are also analyzed; the cases to be studied are presented in Table 4. Simulating only the glass panels without the influence

of a carpentry, the insulation capacity of the double glass panel (C14) is consistently higher compared to the simple glass panel (C13). Therefore, a window with double glass and air chamber is an improvement. With respect to the carpentry materials, wood or PVC are adequate alternatives with good insulation features, as observed in Figure 13.

Table 4. Simulations of carpentries

N.º	Type	Material	Climatic condition	Configuration of glass panels	Comments
C01	Window	Aluminum	Warm day	simple	Slidigns.
C02			Cold day	double	Profile
C03			Warm day	simple	commercial
C04			Cold day	double	Standard
C05	Window	Wood	Warm day	simple	Sliding.
C06			Cold day	double	Carpentry
C07			Warm day	simple	Handcrafted
C08			Cold day	double	
C09	Window	PVC	Warm day	simple	Sliding.
C10			Cold day	double	Profiles
C11			Warm day	simple	commercial
C12			Cold day	double	Standard
C13	Ninguna	Glass	Indiferente	simple	Exclusive
C14				double	glass panels
C15	Door	Wood	Warm day	simple	Door with
C16			Cold day	simple	simple MDF wood sheet
C17	Door	Steel	Warm day	simple	Door with
C18			Cold day	simple	simple steel plate

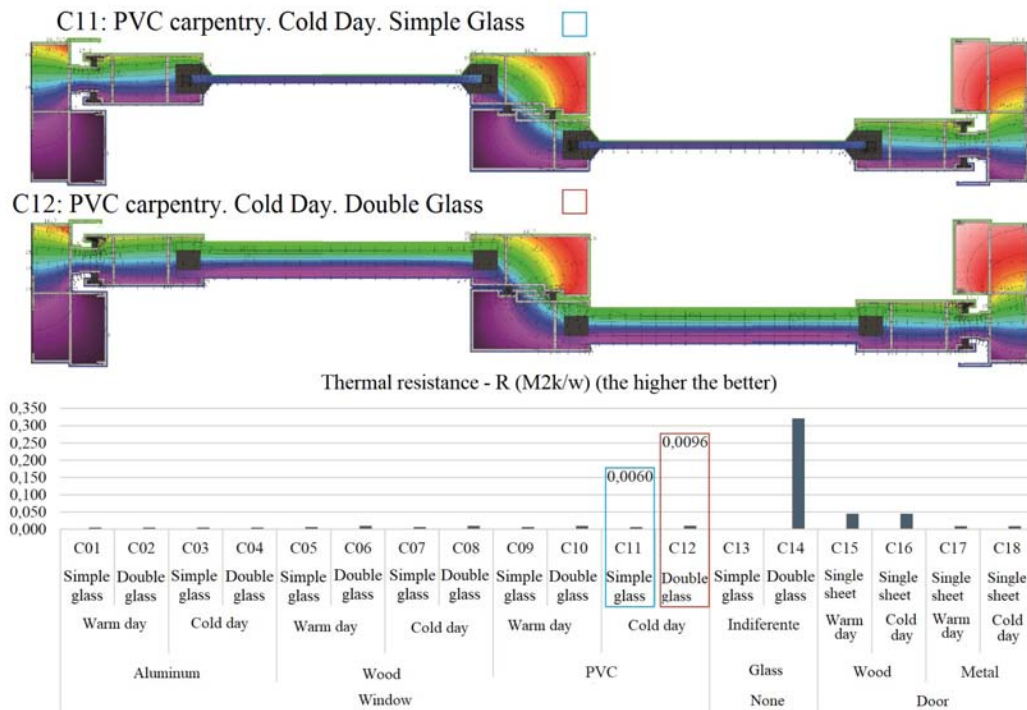


Figure 13. Results of the carpentries in days of extreme cold

3.3. Third stage: Thermal analysis of a housing with traditional materials vs. a housing with LSF with insulation

At this stage, the indoor temperature under normal use conditions is checked through simulations. In addition, the deployment with the orientations; favorable (east) and unfavorable (south). In the case of LSF

with the following variations: Configuration of insulation, minor air infiltrations and carpentries. Table 5 shows the simulations. The housing with LSF uses the simulation solution A03 (perimeter insulation plus mezzanine). Therefore, the level of air infiltrations decreases from 25 to 10 ACH50, data taken from the study by (Madrid; Opazo; Parada, 2012).

Table 5. Conditions for Stage 3 of simulations

N.º	Construction system		Housing typology	Orientation of front facade
	Type	Features		
E3_01	Mixed system: brick and steel		Middle	South
E3_02		Traditional		East
E3_03	10 ACH50	masonry	Corner	South
E3_04		housing		East
E3_05	3,7 users		Isolated	South
E3_06	13,31 W/m ²			East
E3_07	LSF System		Middle	South
E3_08		Standard LSF construction.		East
E3_09	10 ACH50	Thermal isolation of the envelope:	Corner	South
E3_10		EPS in Slab, 50 mm stone wool in walls,		East
E3_11	3,7 users	mezzanine and roof.	Isolated	South
E3_12	13,31 W/m ²			East

The general result of every simulation indicates better thermal levels for both construction systems. However, it should be remarked that the thermal gains have been included. In this way, these are the thermal levels of the housing with traditional system for daily

use of its occupants. In the case of the LSF system the values are much better, as observed in Figure 14. With respect to the number of comfort hours, Figure 15 shows detailed results.

Stage 3: Average OT: annual and monthly – Extreme OT: coldest day and warmest day

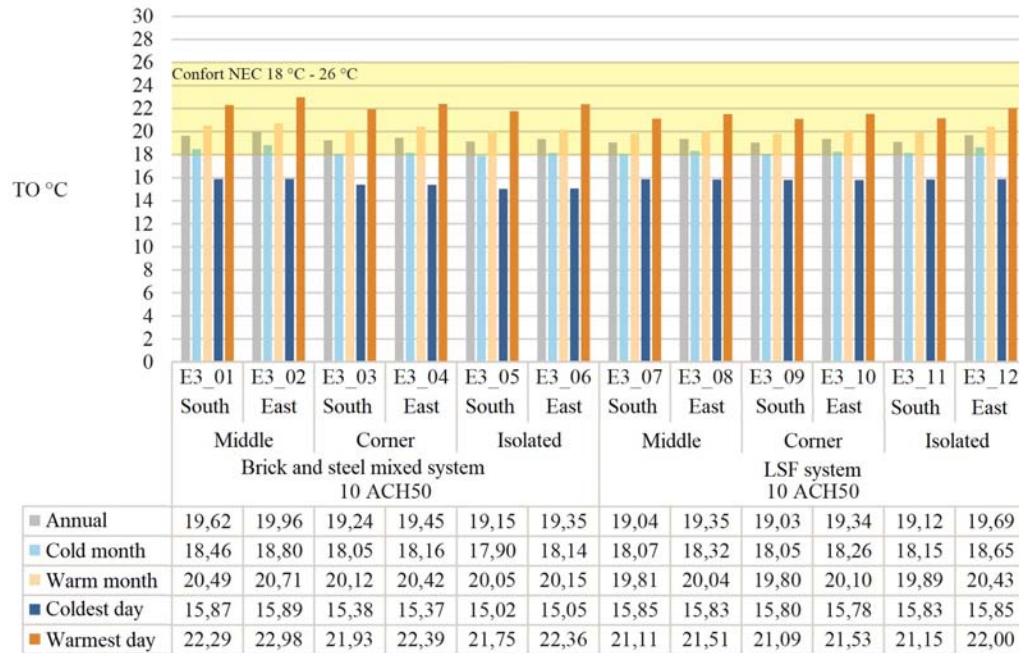


Figure 14. General thermal comparison for the third stage

Number of comfort hours. Third stage. NEC Comfort Range (18 °C - 26 °C)

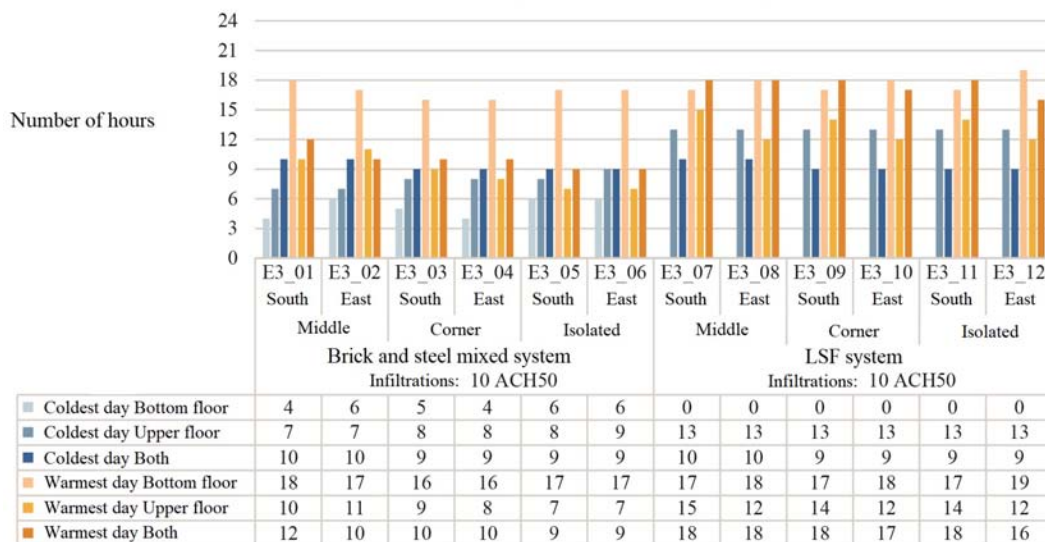


Figure 15. Comparison of number of comfort hours for the third stage

A comparison of the thermal levels of this simulation with the previous stage for the most extreme cases leads to the following comments. In the traditional system, the actual one, the housing shows adequate indoor thermal comfort 38 % of the time in a cold day,

whereas low temperatures occur at night and early morning. This percentage slightly raises to 42 % for the hottest day, with overheating occurring from 10:00 to 18:00; this is mainly due to the minimum insulation capacity of the roof, as observed in Figure 16.

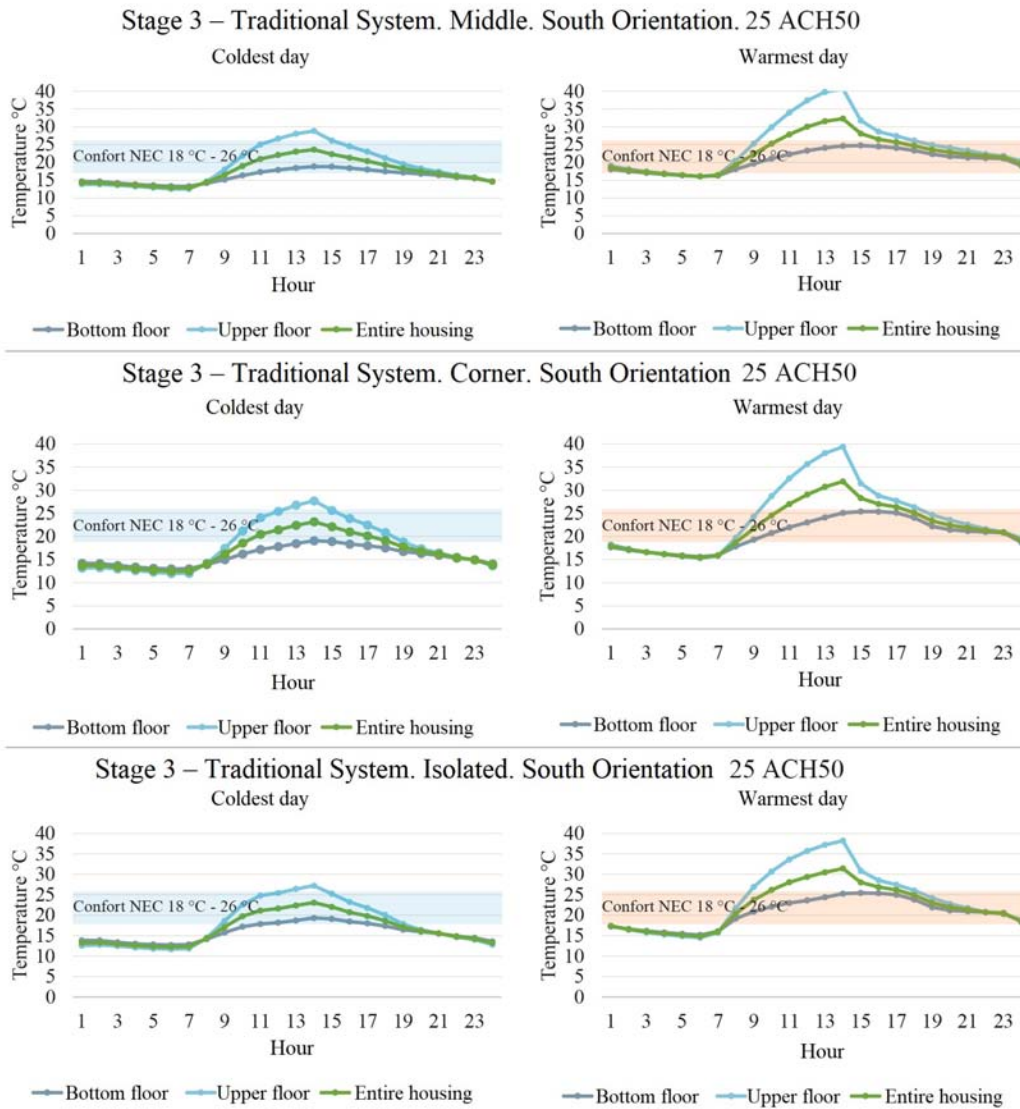


Figure 16. Thermal comparison, traditional system, third stage

In the LSF system, with the standard construction features established in Table 5, during the day the housing reaches indoor thermal comfort 38% of the time, with temperature values between 13.47 °C and 19.52 °C. In the scenario of the day with highest temperature, the housing reaches indoor thermal comfort

in 67% of the hours, with a temperature range between 16.53 °C and 26.89 °C. In the coldest and warmest day, the percentage of daily comfort hours practically does not exceed 50% for both construction systems, as it is observed in Figure reffigura17.

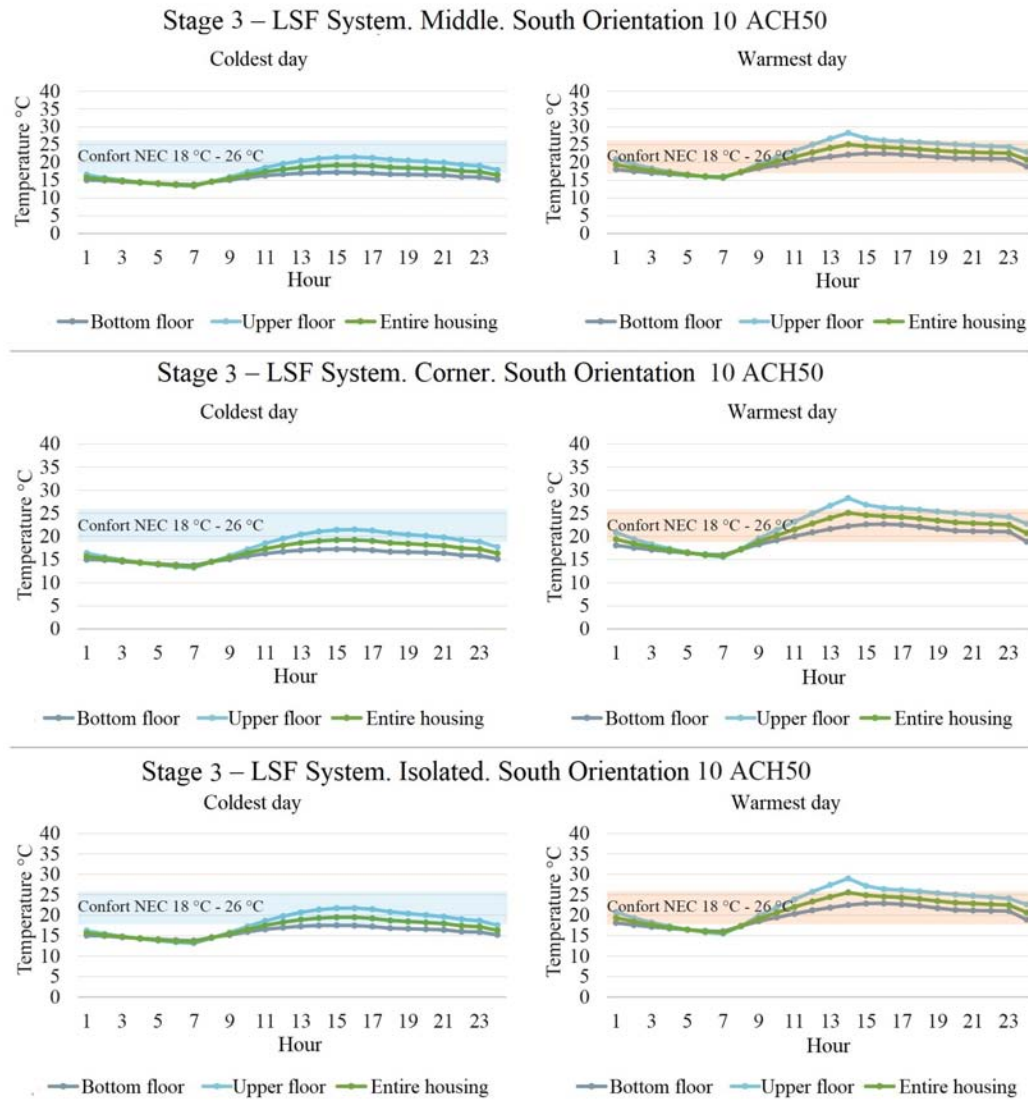


Figure 17. Thermal comparison, LSF system, third stage

3.4. Fourth stage: Analysis of the housing with LSF with the recommended construction features, with emphasis on constructive quality and air infiltrations

Once it is known the real performance of the reference housing with masonry and steel structure construction system (third stage), the LSF system is analyzed measuring the possibility of increasing the annual comfort

hours, adapting the system to improve the constructive quality and the hermeticism of the housing with high performance construction strategies (Table 6). In this stage, an envelope adjustment to reduce infiltrations is considered, assuming to reach 7 ACH50 (Table 6). Previous studies with LSF and wood framework have established a reachable value of 7.47 ACH50 [31]. In parallel, the International Energy Conservation Code (IECC) considers a value of 7 ACH50.

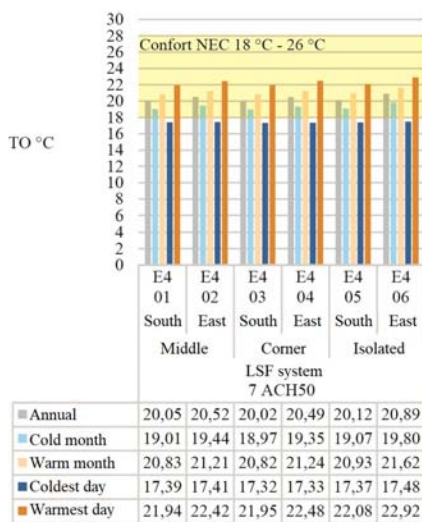
Table 6. Conditions for the stage 4 of simulations

No.	Construction system		Housing typology	Orientation access facade
	Type + ACH	Features		
E4_01	LSF system	Construction with high insulation. Thermal isolation of the envelope: EPS in Slab, 50 mm stone wool in walls,	Middle	South
E4_02				East
E4_03	7 ACH50	mezzanine and roof.	Corner	South
E4_04				East
E4_05	3,7 users	y cubierta.	Isolated	South
E4_06	13,31 W/m ²			East

The results point out that for the coldest day, as shown in Figures 18 and 19, the values of Operating Temperature oscillate between 15.92 and 18.55 °C. The differences between maximum and minimum values are minor. Consequently, it is found that the fluctuations are minor. The increase in comfort hours, with respect to the previous stage, goes from 38 to 46%, with infiltrations of 7 ACH50 with double glass windows. In the analysis of the warmest day, the val-

ues of operating temperature are between 20.53 and 25.77 °C. The difference between the maximum and minimum thermal values is considerably smaller than the reference housing. The increase in comfort hours, with respect to the previous stage, goes from 67 to 100%. In the warmest day, an overheating is observed at the time of direct solar incidence, which may be counteracted with natural ventilation due to the lower external temperature.

Etapa 4: TO Promedio: anual y mensual
TO Extrema: día cálido y día frío



Number of comfort hours. Fourth stage.
NEC Comfort Range (18°C - 26°C)

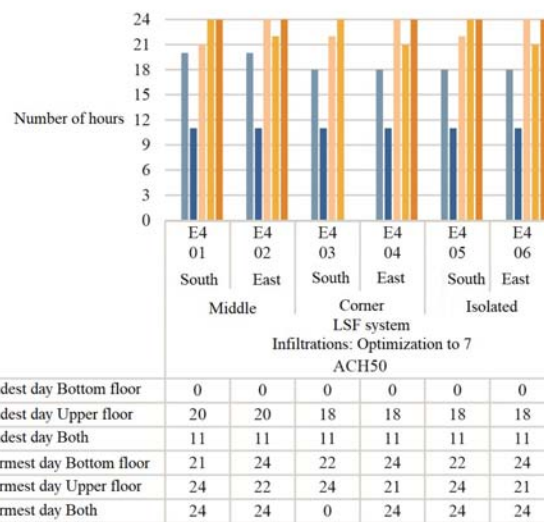


Figure 18. Comparison of the thermal performance and of the number of comfort hours for the fourth stage

Figure 19 shows the housing with LSF in all orientations, where it is seen that the thermal curve oscillates less throughout the day. The thermal variations are not very pronounced, as it is evidenced in previous stages. With the recommended construction strategies,

considering the materials with the purpose of reducing the levels of ACH exchanges, the thermal behavior of the housing is more stable in temperature, without the need of using active heating systems.

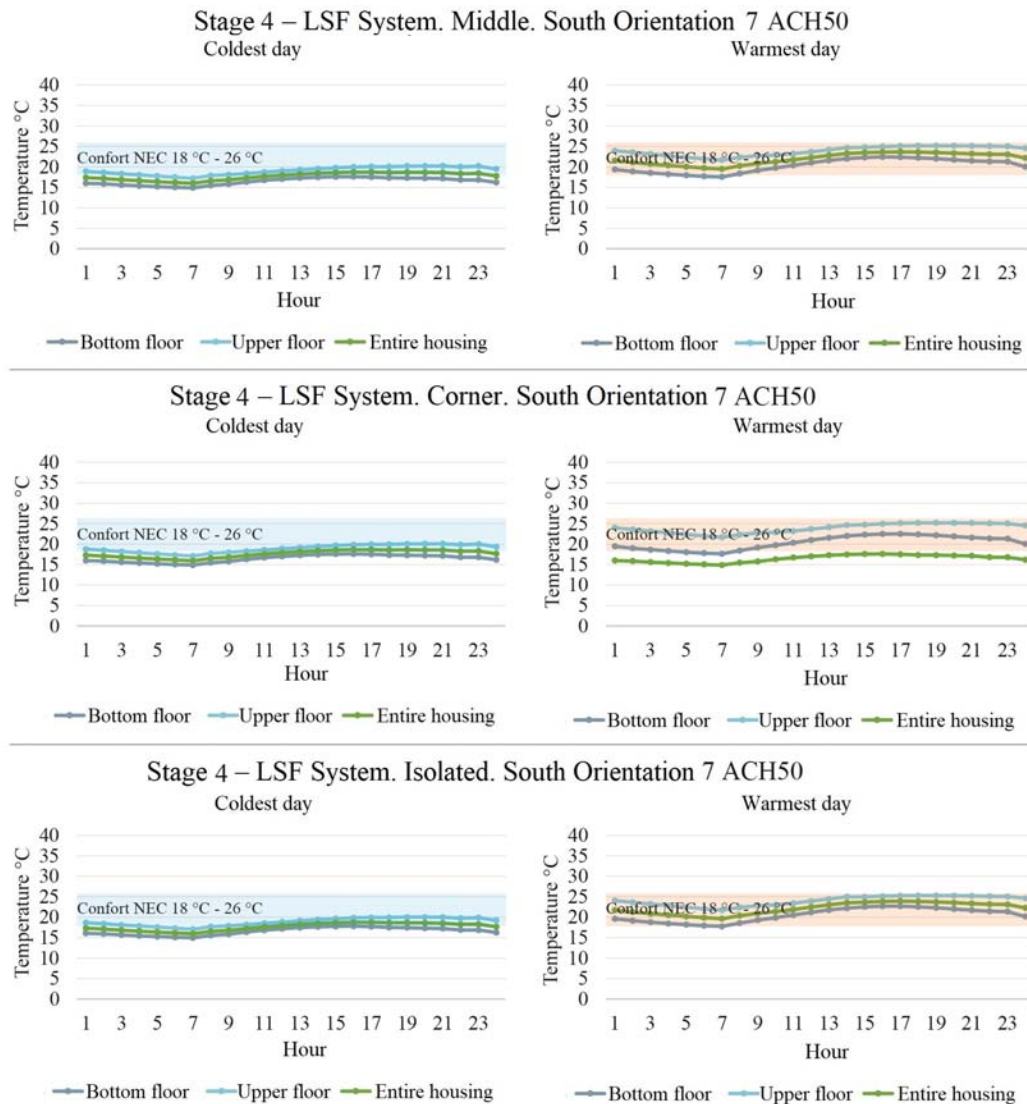


Figure 19. Thermal comparison, LSF system, fourth stage

3.5. Discussion

In the first stage, it is only determined the most favorable and most unfavorable results, with respect to the orientation of the housings. The orientation of the main facade with openings of doors and windows facing towards the east and west is better regarding thermal performance. However, the thermal variation is not considerably smaller in the north-south orientation due to the dimensions of the housing.

In the second stage, the results of unfavorable orientations (north-south) are observed on the reference housing, where indoor thermal comfort is reached in only 27% of hours throughout the year. The housing with LSF, without insulations in subfloor and ceilings,

always in the same orientations, reaches indoor thermal comfort 42% of the time. In the third stage, for the housings in their current status the average percentage (under all orientations) of hours in a year in indoor thermal comfort is 51%. This mainly occurs due to the steel structure exposed both internally and externally, and by the important losses in the roof without false ceiling. In addition, doors and windows typically metallic also imply considerable thermal bridges. The housings with LSF and standard optimization strategies to 10 ACH50 improve to 62% the number of comfort hours with respect to the base housing. In stage 4, in Figures 20 and 21, for the housings with LSF with high optimization strategies and infiltrations in 7 ACH50, the percentage of comfort time is 86%.

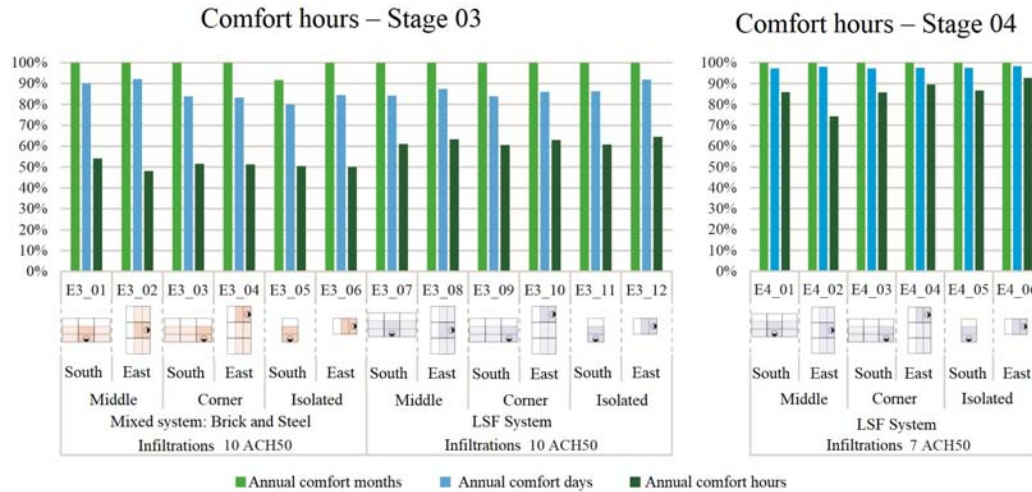


Figure 20. Comparison of the number of comfort hours

The results indicate that the reference housing with traditional construction system has an average minimum temperature of 15.38 °C and an average maximum temperature of 27.68 °C, both out of the NEC comfort range. However, when the housing has an envelope in LSF with standard optimization strategies and with basic features and isolation materials, the average minimum temperature improves slightly to 15.55 °C, without reaching the minimum of the standard, and the average maximum temperature is 26.38 °C, slightly above the maximum of the standard. Finally, for the housing in LSF with high optimization strategies, features recommended by the analysis, the

average minimum temperature is 17.19 °C, close to the 18 °C established by the standard, and temperatures above 26 °C are not observed. At last, it is found that the parameter with highest thermal incidence is the control of air infiltrations.

Figure 21 shows an average comparative chart of the three housing typologies in a unique monthly, daily and hourly average value. In this way, results are shown as a function of the percentage of average time in which the housings are in comfort. Average values are used, since it was demonstrated in each of the stages that thermal variations of the housing typologies in minimal, without exceeding 1 °C in most cases.

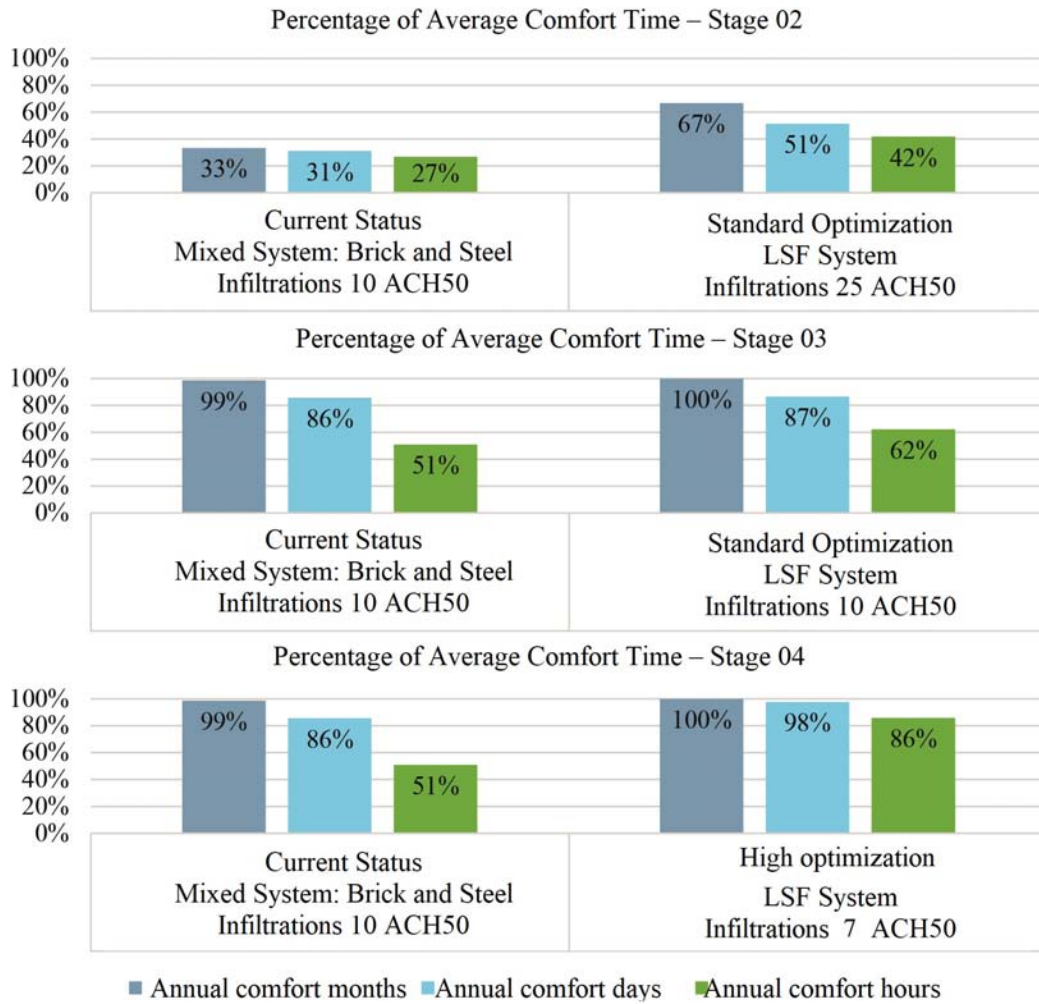


Figure 21. Comparison of the number of comfort hours of all stages

It is evidenced that the dimensions of the LSF section, stated according to the structural analysis, are more than enough to integrate the necessary insulation: 50 mm in stone wool placed between the studs, attached to the external side, leaving an air chamber of 50 mm between the studs, in a cold wall scheme. Then,

the other parameters analyzed arranged in decreasing order of importance include air infiltrations, material of carpentries and, to a lesser extent, the orientation. Figure 22 shows a scheme of the housing recommended with the new LSF system for the Andean region.

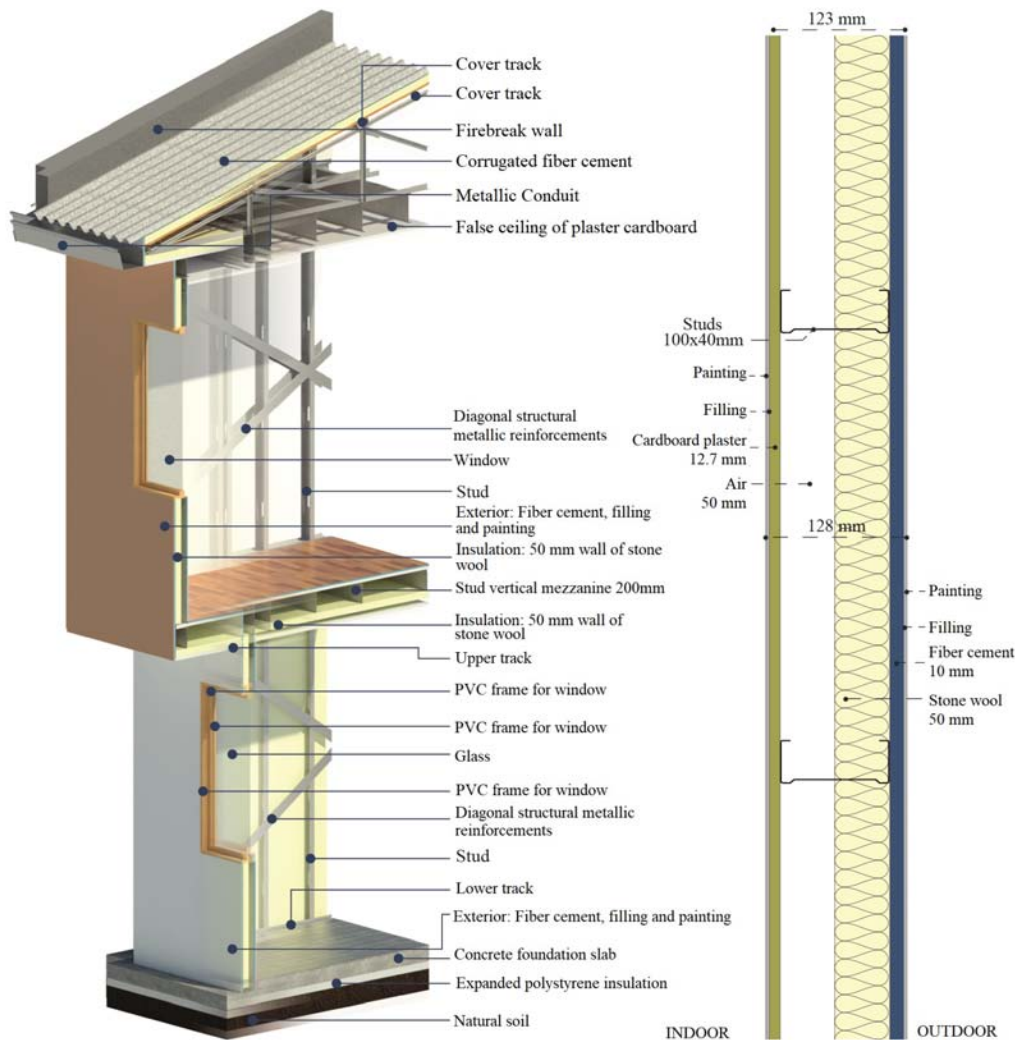


Figure 22. Scheme of the proposal of the housing built with LSF

4. Conclusions

This work carries out an analysis with widely validated simulators, to detect comfort conditions and mismatches in housings when changing and modifying the construction system, as well as the comfort parameters. Once it is analyzed the modification of the envelope from the traditional construction system using steel with brick envelope, it is also analyzed the implications of the modification of the envelope and other parameters such as orientation, infiltration and material of carpentries. Even though these are simulations, it is the fastest way to be able to analyze the different parameters in equal circumstances with the modifications required.

The comfort levels of the housings built with LSF are higher, compared to the reference housing built with the mixed construction system of brick masonry and structure with steel porticoes (traditional construction methodology). With the change in construction

system, the number of comfort hours in the housing increases 11%, but a work with hermeticism, change of material in carpentries, insulation in slabs, mezzanines and ceilings, enables to reach 35% more hours within the comfort range. Although the brick block as envelope material has better thermal inertia, the LSF reaches appropriate levels of the envelope, even in the simple configuration in sandwich wall.

The most important variables for environmental performance, according to this study, arranged in decreasing order of thermal influence are: insulation in roof, mezzanine and foundation slab, the results indicate that horizontal insulations increase the percentage of comfort from 42 to 64%. Then, the parameter of air infiltrations through the hermeticism increases thermal comfort from 62 to 86%. Third, considering the housing material in general, together with the type of carpentries, the improvement of one system with respect to the other goes from 51 to 86%. The variables with lower incidence correspond to the deployment

and typology of the housings. These factors are due to the configuration and size of the housings, since the dimensions are not big. The orientation, normally a factor of great thermal incidence in other latitudes, for equatorial locations the solar route causes that the irradiation incidence lasts few hours.

The results of the analyses by orientation show that, in average, the indoor temperature is only 1 °C higher in the north – south orientation, and even well-oriented housings receive little direct solar radiation on the facades due to the minimal separation between housings because of the grouping conditions.

With the proposed configuration of materials, it is feasible to build a housing in the city of Cuenca with habitability conditions within the thermal comfort range between 18 °C and 26 °C. Consequently, it is adaptable to various cities in Colombia, Ecuador and Peru that are in equatorial conditions at a height close to 2500 m above sea level. However, for more extreme weather it is necessary to check the envelope adaptability.

The change of materials not only seeks to generate housing that are comfortable for final users, but it also seeks, as indicated by sources consulted, to reduce the environmental and ecological impact generated by the construction industry with handcrafted processes, many of them with no control, avoiding unnecessary wastes and saving resources that are increasingly scarce, before, during and after the construction.

References

- [1] V. Arengo Piragine, J. Cruz Breard, and C. Pilar, “Anteproyecto de viviendas sociales con steel framing en corrientes. comparación con sistema húmedo tradicional,” *Arquitecto*, no. 15, p. 37, 2020. [Online]. Available: <http://dx.doi.org/10.30972/arq.0154386>
- [2] A. O. Venegas Tomalá, *Evaluación de la energía contenida, emisiones de CO2 y material particulado en la fabricación del ladrillo semimecanizado tochano en Cuenca, a través del análisis de ciclo de vida (ACV)*. Universidad de Cuenca, Ecuador, 2018. [Online]. Available: <https://bit.ly/2Soq1IU>
- [3] M. T. Baquero L. and F. Quesada M., “Eficiencia energética en el sector residencial de la ciudad de Cuenca, Ecuador,” *Maskana*, vol. 7, no. 2, pp. 147–165, 2016. [Online]. Available: <https://doi.org/10.18537/mskn.07.02.11>
- [4] M. Manzan, E. Zandegiacomo De Zorzi, and W. Lorenzi, “Numerical simulation and sensitivity analysis of a steel framed internal insulation system,” *Energy and Buildings*, vol. 158, pp. 1703–1710, 2018. [Online]. Available: <https://doi.org/10.1016/j.enbuild.2017.11.069>
- [5] M. Bernardes, S. G. Nilsson, M. S. Martins, and A. Romanini, “Comparativo econômico da aplicação do sistema light steel framing em habitação de interesse social,” *Revista de Arquitetura IMED*, vol. 1, no. 1, pp. 31–40, 2012. [Online]. Available: <https://doi.org/10.18256/2318-1109/arqimed.v1n1p31-40>
- [6] L. M. Lupan, D. L. Manea, and L. M. Moga, “Improving thermal performance of the wall panels using slotted steel stud framing,” *Procedia Technology*, vol. 22, pp. 351–357, 2016. [Online]. Available: <https://doi.org/10.1016/j.protcy.2016.01.108>
- [7] INEC. (2017) Encuesta de edificaciones 2017. Instituto Nacional de Estadísticas y Censos del Ecuador. [Online]. Available: <https://bit.ly/3NsvnyW>
- [8] MIDUVI, *NEC-11. Vivienda De Hasta 2 Pisos Con Luces De Hasta 4.0 M*. Ministerio de Desarrollo Urbano y Vivienda. República del Ecuador., 2011. [Online]. Available: <https://bit.ly/3HU0uCk>
- [9] E. Roque and P. Santos, “The effectiveness of thermal insulation in lightweight steel-framed walls with respect to its position,” *Buildings*, vol. 7, no. 1, 2017. [Online]. Available: <https://doi.org/10.3390/buildings7010013>
- [10] A. M. Sarmanho Freitas and R. C. Moraes de Crasto, *Steel Framing: Arquitectura*. Instituto Latinoamericano del Fierro y el Acero - ILAFA, 2007. [Online]. Available: <https://bit.ly/3QOMYUy>
- [11] J. L. Lamus Rodríguez, “Análisis de viabilidad económica: sistema constructivo light steel framing en Colombia,” Master’s thesis, Universidad de los Andes. Colombia, 2015. [Online]. Available: <https://bit.ly/3HRQfhU>
- [12] E. Rodrigues, N. Soares, M. S. Fernandes, A. R. Gaspar, Álvaro Gomes, and J. J. Costa, “An integrated energy performance-driven generative design methodology to foster modular lightweight steel framed dwellings in hot climates,” *Energy for Sustainable Development*, vol. 44, pp. 21–36, 2018. [Online]. Available: <https://doi.org/10.1016/j.esd.2018.02.006>
- [13] E. de Angelis and E. Serra, “Light steel-frame walls: Thermal insulation performances and thermal bridges,” *Energy Procedia*, vol. 45, pp. 362–371, 2014. [Online]. Available: <https://doi.org/10.1016/j.egypro.2014.01.039>
- [14] B. Schafer, D. Ayhan, J. Leng, P. Liu, D. Padilla-Llano, K. Peterman, M. Stehman, S. Buonopane, M. Eatherton, R. Madsen, B. Manley, C. Moen, N. Nakata, C. Rogers, and

- C. Yu, “Seismic response and engineering of cold-formed steel framed buildings,” *Structures*, vol. 8, pp. 197–212, 2016. [Online]. Available: <https://doi.org/10.1016/j.istruc.2016.05.009>
- [15] T. Tafsirojjaman, S. Fawzia, D. Thambiratnam, and X. Zhao, “Seismic strengthening of rigid steel frame with cfrp,” *Archives of Civil and Mechanical Engineering*, vol. 19, no. 2, pp. 334–347, 2019. [Online]. Available: <https://doi.org/10.1016/j.acme.2018.08.007>
- [16] J. R. da Silva Nogueira, I. J. Apolônio Callejas, and L. Cleonice Durante, “Desempenho de painel de vedação vertical externa em light steel framing composto por placas de madeira mineralizada,” *Ambiente Construído*, vol. 18, no. 3, 2018. [Online]. Available: <https://doi.org/10.1590/s1678-86212018000300282>
- [17] F. Bolina, R. Christ, A. Metzler, U. Quinino, and B. Tutikian, “Comparison of the fire resistance of two structural wall systems in light steel framing,” *DYNA*, vol. 84, no. 201, pp. 123–128, abr. 2017. [Online]. Available: <https://doi.org/10.15446/dyna.v84n201.57487>
- [18] E. Yandzio, R. M. Lawson, and A. G. J. Way, *Light steel framing in residential construction*. SCI. Silwood Par, Ascot, Berkshire, 2015. [Online]. Available: <https://bit.ly/3xXZhoV>
- [19] P. E. Amador Salomão, A. D. Alves Soares, A. L. P. Lorentz, and L. T. Gonçalves de Paula, “Conventional masonry and light steel framing comparative analysis: a case study in unifammary residence in teófilo otoni, mg,” *Research, Society and Development*, vol. 8, no. 9, p. e14891268, Jun. 2019. [Online]. Available: <https://doi.org/10.33448/rsd-v8i9.1268>
- [20] H. OlivieriIvan, I. C. Alves Barbosa, A. C. Da Rocha, A. Denis Granja, and P. S. Pucharelli Fontanini, “A utilização de novos sistemas construtivos para a redução no uso de insumos nos canteiros de obras: Light steel framing,” *Ambiente Construído*, vol. 17, no. 4, 2017. [Online]. Available: <https://doi.org/10.1590/s1678-86212017000400184>
- [21] MIDUVI, *Acuerdo Ministerial: Reglamento para validación de tipologías y planes masa para proyectos de vivienda de interés social*. Ministerio de Desarrollo Urbano y vivienda. República del Ecuador, 2019. [Online]. Available: <https://bit.ly/3HSg3ul>
- [22] —, *Eficiencia energética en edificaciones residenciales NEC-HS-EE*. Ministerio de Desarrollo Urbano y vivienda. República del Ecuador, 2018. [Online]. Available: <https://bit.ly/39U5CtD>
- [23] —, *Eficiencia energética en la construcción en Ecuador*. Ministerio de Desarrollo Urbano y vivienda. República del Ecuador, 2011. [Online]. Available: <https://bit.ly/39QqLoM>
- [24] Intergovernmental Panel on Climate Change, *Summary for Policymakers*. Cambridge University Press, 2014, ch. Climate Change 2013 – The Physical Science Basis, pp. 1–30. [Online]. Available: <https://doi.org/10.1017/CBO9781107415324.004>
- [25] S. A. Navarrete Boutaud, *Impacto de las infiltraciones de aire en el desempeño energético y térmico de las viviendas*. Universidad de Concepción. Chile, 2016. [Online]. Available: <https://bit.ly/3QSwxqg>
- [26] Design Builder. (2022) Design builder software. [Online]. Available: <https://bit.ly/3OnQ8gp>
- [27] Berkeley Lab. (2022) THERM. Windows and Daylighting. [Online]. Available: <https://bit.ly/3HU2iv6>
- [28] J. Roset Calzada, R. A. Vásquez Paredes, and L. M. Barajas Saldaña, “ús eficient de programes informatics en arquitectura: Designbuilder i Dialux,” *JIDA '14. II Jornadas sobre Innovación Docente en Arquitectura*, 2014. [Online]. Available: <https://doi.org/10.5821/jida.2014.5027>
- [29] INEC. (2011) Vii censo de población y vi de vivienda. Instituto Nacional de Estadísticas y Censos. [Online]. Available: <https://bit.ly/3br35Ym>
- [30] H. Madrid, F. Opazo, and O. Parada, “Impacto de las infiltraciones de aire en el desempeño energético y térmico de las viviendas,” *Construcción*, 2012. [Online]. Available: <https://bit.ly/3yn1Gev>
- [31] The U.S. Department of Housing and Urban Development Office of Policy Development and Research, *Steel vs. Wood. Cost Comparison. Beaufort Demonstration Homes*. Partnership for Advancing Technology in Housing, 2002. [Online]. Available: <https://bit.ly/3ngPhCz>

GUIDELINES FOR PUBLICATION IN INGENIUS JOURNAL

1. General Information

INGENIUS is a scientific publication of the *Universidad Politécnica Salesiana* of Ecuador, published since January 2007, with a fixed biannual periodicity, specialized in Mechanical Engineering, Electrical Engineering, Electronics, Computer Science and its integration in what is now known as Mechatronics; these lines of action strengthen areas such as automation, control, robotics, among others..

It is a scientific journal, which uses the peer-review system, under double-blind review methodology, according to the publication standards of the Institute of Electrical and Electronics Engineers (IEEE). Compliance with this system allows authors to guarantee an objective, impartial and transparent review process, which facilitates the publication of their inclusion in reference databases, repositories and international indexing.

INGENIUS is indexed in the directory and selective catalog of the Regional Online Information System for Scientific Journals of Latin America, the Caribbean, Spain and Portugal (Latindex), in the Directory of Journals of Open Access DOAJ, In the Information Matrix for the Analysis of Journals, MIAR, In the Ibero-American Network of Innovation and Scientific Knowledge, REDIB and in repositories, libraries and specialized catalogs of Latin America.

The journal is published in a double version: printed (ISSN: 1390-650X) and digital (e-ISSN: 1390-860X), in Spanish, each work being identified with a DOI (Digital Object Identifier System). The articles sent to INGENIUS magazine must comply with the following criteria:

2. Scope and policy

2.1. Theme

Original contributions in Mechanical Engineering, Electrical and Electronic Engineering, Computer Science and its integration in what is now known as Mechatronics, as well as related areas: Automation, Control, Domotics, Robotics in their different fields of action and all those related disciplines with the same central theme.

All the work carried out by national or foreign researchers may be published once they meet the required scientific quality criteria.

2.2. Contributions

INGENIUS Journal preferably publishes articles related to empirical research, and also reports of technological development, proposals for models and innovations, products for the elaboration of graduate and postgraduate thesis that contribute to the field of science and technology, as well as select revisions of literature. (state-of-the-art).

- **Research:** 5,000 to 6,500 words of text, including title, abstracts, descriptors, charts and references.
- **Reports:** 5,000 to 6,500 words of text, including title, abstracts, charts and references.
- **Reviews:** 6,000 to 7,000 words of text, including charts and references. Current, selective and justified references, would be specially valued from among 40 works

The INGENIUS Journal publishes original and unpublished works written in Spanish and English, they may not have been published

through any printed or electronic media, nor be in the process of arbitration or publication.

Every article will be subjected to a rigorous arbitration process; the evaluation of the article will be made according to criteria of originality, relevance, relevance, contributions, scientific rigor and compliance with established editorial guidelines.

Being an arbitrated publication, the Editorial Board approves its publication based on the concept of specialized pairs. The reception of a document does not imply commitment of publication.

It is essential to present a letter of presentation and grant of rights which can be downloaded from: [urlhttps://goo.gl/ZNkMRD](https://goo.gl/ZNkMRD).

Contributions must be exclusively sent and through the OJS (Open Journal System) <https://goo.gl/JF7dWT>. In which all authors must previously register as a user. For any consultation of the procedure you should contact:

revistaingenius@ups.edu.ec,
jcalles@ups.edu.ec ó
mquinde@ups.edu.ec.

3. Presentation and structure of the manuscripts

For those works that are empirical investigations, the manuscripts will follow the IMRDC structure (Introduction, Materials and Methods, Results and Discussion and Conclusions), being optional the Notes and Supports. Those papers that, on the contrary, deal with reports, studies, proposals and reviews may be more flexible in their epigraphs, particularly in material and methods, analysis, results, discussion and conclusions. In all typologies of works, references are mandatory.

Articles may be written on Microsoft Word (.doc or .docx) or L^AT_EX(.tex). The template to

be used can be downloaded from the journal's website, a, <https://goo.gl/gtCg6m>, while for L^AT_EX in <https://goo.gl/hrHzzQ>, it is necessary that the file be anonymised in Properties of File, so that the author(s) ID is not displayed.

Figures, Graphs and/or Illustrations, as well as Charts shall be numbered sequentially including an explanatory description for each. The equations included in the article must also be numbered; the figures, charts and equations must be cited in the text.

Use space after point, commas and question marks.

Use “enter” at the end of each paragraph and title heading. Do not use `.enter.anywhere` else, let the word processor program automatically break the lines.

Do not center headings or subheadings as they should be aligned to the left.

Charts must be created in the same program used for the document body, but must be stored in a separate file. Use tabs, not spaces, to create columns. Remember that the final size of printed pages will be 21 x 28 cm, so the tables must be designed to fit the final print space.

3.1. Structure of the manuscripts

3.1.1. Presentation and cover letter

1. **Título (español) / Title (inglés):** Concise but informative, in Spanish on the front line and in English on the second, when the article is written in Spanish and vice versa if it is written in English.
2. **Authors and affiliations:** Full name and surname of each author, organized by order of priority and their institutional affiliation with reference to the end of the first sheet, where it must include: Dependency to which belongs within the

institution, Institution to which he/she belongs, country, ORCID. A maximum of 5 authors will be accepted, although there may be exceptions justified by the complexity and extent of the topic.

3. **Abstract (Spanish) / Abstract (English):** It will have a maximum extension of 230 words, first in Spanish and then in English. : 1) Justification of the topic; 2) Objectives; 3) Methodology and sample; 4) Main results; 5) Main conclusions.
4. **Keywords (Spanish) / Keywords (English):** 6 descriptors must be presented for each language version directly related to the subject of the work. The use of the key words set out in UNESCO's Thesaurus will be positively valued.
5. **Presentation (Cover Letter):** A statement that the manuscript is an original contribution, not submission or evaluation process in another journal, with the confirmation of the signatory authors, acceptance (if applicable) of formal changes in the manuscript according to the guidelines and partial assignment of rights to the publisher, according to the format established in: <<https://goo.gl/ZNkMRD>>

3.1.2. Manuscript

1. **Título (español) / Title (inglés):** Concise but informative, in Spanish on the front line and in English on the second, when the article is written in Spanish and vice versa if it is written in English.
2. **Authors and affiliations:** Full name and surname of each author, organized by order of priority and their institutional affiliation with reference to the end of the first sheet, where it must include: Dependency to which belongs within the institution, Institution to which he/she belongs, country, ORCID. A maximum of 5 authors will be accepted, although

there may be exceptions justified by the complexity and extent of the topic.

3. **Abstract (Spanish) / Abstract (English):** It will have a maximum extension of 230 words, first in Spanish and then in English. : 1) Justification of the topic; 2) Objectives; 3) Methodology and sample; 4) Main results; 5) Main conclusions.
4. **Keywords (Spanish) / Keywords (English):** 6 descriptors must be presented for each language version directly related to the subject of the work. The use of the key words set out in UNESCO's Thesaurus will be positively valued.
5. **Introduction:** It should include the problem statement, context of the problem, justification, rationale and purpose of the study, using bibliographical citations, as well as the most significant and current literature on the topic at national and international level.
6. **Material and methods:** It must be written so that the reader can easily understand the development of the research. If applicable, it will describe the methodology, the sample and the form of sampling, as well as the type of statistical analysis used. If it is an original methodology, it is necessary to explain the reasons that led to its use and to describe its possible limitations.
7. **Analysis and results:** It will try to highlight the most important observations, describing, without making value judgments, the material and methods used. They will appear in a logical sequence in the text and the essential charts and figures avoiding the duplication of data.
8. **Discussion and Conclusions:** It will summarize the most important findings, relating the observations themselves to relevant studies, indicating contributions

and limitations, without adding data already mentioned in other sections. It should also include deductions and lines for future research.

9. **Supports and acknowledgments (optional):** The Council Science Editors recommends the author (s) to specify the source of funding for the research. Priority will be given to projects supported by national and international competitive projects.
10. **The notes (optional):** will go, only if necessary, at the end of the article (before the references). They must be manually annotated, since the system of footnotes or the end of Word is not recognized by the layout systems. The numbers of notes are placed in superscript, both in the text and in the final note. The numbers of notes are placed in superscript, both in the text and in the final note. No notes are allowed that collect simple bibliographic citations (without comments), as these should go in the references.
11. **References:** Bibliographical citations should be reviewed in the form of references to the text. Under no circumstances should references mentioned in the text not be included. Their number should be sufficient to contextualize the theoretical framework with current and important criteria. They will be presented sequentially in order of appearance, as appropriate following the format of the IEEE.

3.2. Guidelines for Bibliographical references

Journal articles:

- [1] J. Riess, J. J. Abbas, "Adaptive control of cyclic movements as muscles fatigue using functional neuromuscular stimulation". IEEE Trans. Neural Syst. Rehabil. Eng

vol. 9, pp.326–330, 2001. [Online]. Available: <https://doi.org/10.1109/7333.948462>

Books:

- [1] G. O. Young, "Synthetic structure of industrial plastics" in *Plastics*, 2nd ed., vol. 3, J. Peters, Ed. New York: McGraw–Hill, 1964, pp. 15–64.

Technical reports:

- [1] M. A. Brusberg and E. N. Clark, "Installation, operation, and data evaluation of an oblique–incidence ionosphere sounder system," in "Radio Propagation Characteristics of the Washington–Honolulu Path," Stanford Res. Inst., Stanford, CA, Contract NOBSR–87615, Final Rep., Feb. 1995, vol. 1

Articles presented in conferences (unpublished):

- [1] Vázquez, Rolando, Presentación curso "Realidad Virtual". National Instruments. Colombia, 2009.

Articles of memories of Conferences (Published):

- [1] L. I. Ruiz, A. García, J. García, G. Taiboadá. "Criterios para la optimización de sistemas eléctricos en refinerías de la industria petrolera: influencia y análisis en el equipo eléctrico," IEEE CONCAPAN XXVIII, Guatemala 2008.

Thesis:

- [1] L.M. Moreno, "Computación paralela y entornos heterogéneos," Tesis doctoral, Dep. Estadística, Investigación Operativa y Computación, Universidad de La Laguna, La Laguna, 2005.

Guidelines:

- [1] IEEE Guide for Application of Power Apparatus Bushings, IEEE Standard C57.19.100–1995, Aug. 1995.

Patents:

- [1] J. P. Wilkinson, "Nonlinear resonant circuit devices," U.S. Patent 3 624 125, July 16, 1990.

Manuals:

- [1] Motorola Semiconductor Data Manual, Motorola Semiconductor Products Inc., Phoenix, AZ, 1989.

Internet resources:

- [1] E. H. Miller, "A note on reflector arrays" [Online]. Available. <https://goo.gl/4cJkCF>

3.3. Epigraphs, Figures and Charts

The epigraphs of the body of the article will be numbered in Arabic. They should go without a full box of capital letters, neither underlined nor bold. The numbering must be a maximum of three levels: 1. / 1.1. / 1.1.1. At the end of each numbered epigraph will be given an enter to continue with the corresponding paragraph.

The charts must be included in the text according to order of appearance, numbered in Arabic and subtitled with the description of the content, the subtitle should go at the top of the table justified to the left.

Figures can be linear drawings, maps or black and white halftone or color photographs in 300 dpi resolution. Do not combine photographs and line drawings in the same figure.

Design the figures so that they fit eventually to the final size of the journal 21 x 28 cm. Make sure inscriptions or details, as well as lines, are of appropriate size and thickness so that they are not illegible when they are reduced to their final size (numbers, letters and symbols must be reduced to at least 2.5 mm in height After the illustrations have been reduced to fit the printed page). Ideally, the linear illustrations should be prepared at about a quarter of their final publication size.

Different elements in the same figure should be spelled a, b, c, etc.

Photographs should be recorded with high contrast and high resolution. Remember that

photographs frequently lose contrast in the printing process. Line drawings and maps should be prepared in black.

The text of the figures and maps must be written in easily legible letters.

If the figures have been previously used, it is the responsibility of the author to obtain the corresponding permission to avoid subsequent problems related to copyright.

Each figure must be submitted in a separate file, either as bitmap (.jpg, .bmp, .gif, or .png) or as vector graphics (.ps, .eps, .pdf).

4. Submission process

The manuscript must be sent through the OJS system of the journal, <<https://goo.gl/JF7dWT>>, the manuscript should be uploaded as an original file in .pdf without author data and anonymized according to the above; In complementary files the complete manuscript must be loaded in .doc or .docx (Word file), that is to say with the data of the author (s) and its institutional ascription; Also the numbered figures should be uploaded in independent files according to the corresponding in the manuscript (as bitmap .jpg, .bmp, .gif, or .png or as vector graphics .ps, .eps, .pdf). It is also obligatory to upload the cover letter and grant of rights as an additional file.

All authors must enter the required information on the OJS platform and only one of the authors will be responsible for correspondence.

Once the contribution has been sent the system will automatically send the author for correspondence a confirmation email of receipt of the contribution.

5. Editorial process

Once the manuscript has been received in OJS, a first check by the editorial team of the following points:

- The topic is in accordance with the criteria of the journal.
- Must have the IMRDC structure.
- Must be in the INGENIUS format.
- Must use the IEEE citation format.
- All references should be cited in the text of the manuscript as well as charts, figures and equations.
- The manuscript is original; for this, software is used to determine plagiarism.

The assessment described above can take up to 4 weeks.

If any of the above is not complete or there is inconsistency, an email will be sent to the author to make the requested corrections.

The author will make the corrections and re-send the contribution through an email in response to the notification and will also upload the corrected manuscript into OJS supplementary files.

The editorial team will verify that the requested corrections have been incorporated, if it complies, the manuscript will start the second part of the process that may be followed by the author through OJS, otherwise the author will be notified and the manuscript will be archived.

The second phase of the process consists of the evaluation under the methodology of double-blind review, which includes national and foreign experts considering the following steps:

- The editor assigns two or more reviewers for the article.

- After reviewing the article, the reviewers will submit the evaluation report with one of the following results.

- Publishable
- Publishable with suggested changes
- Publishable with mandatory changes
- Non publishable

- The editor once received the evaluation by the reviewers will analyze the results and determine if the article is accepted or denied.

- If the article is accepted, the author will be notified to make corrections if required and the corresponding editorial process will be continued.

- If the article is denied, the author will be notified and the manuscript will be archived.

- In the two previous cases the result of the evaluation of the reviewers and their respective recommendations will be sent.

The second phase of the process lasts at least 4 weeks, after which they will be notified to the author giving instructions to continue with the process.

6. Publication

The INGENIUS Journal publishes two issues per year, on January 1st and July 1st, so it is important to consider the dates for sending the articles and their corresponding publication. Articles received until October will be considered for the January publication and those received until April for the July publication.

UNIVERSIDAD POLITÉCNICA SALESIANA DEL ECUADOR

Juan Cárdenas Tapia, sdb,
Rector

©Universidad Politécnica Salesiana
Turuhuayco 3-69 y Calle Vieja
Postal code 2074
Cuenca, Ecuador
Teléfono: (+593 7) 205 00 00
Fax: (+593 7) 408 89 58
Email: srector@ups.edu.ec

Exchange

Exchange with other periodicals is accepted.

Address:

Secretaría Técnica de Comunicación
Universidad Politécnica Salesiana
Turuhuayco 3-69 y Calle Vieja
Postal code 2074
Cuenca, Ecuador
Phone: (+593 7) 205 00 00 Ext. 1182
Fax: (+593 7) 408 89 58
Email: rpublicas@ups.edu.ec
www.ups.edu.ec
Cuenca – Ecuador

INGENIUS, Journal Science of Technology,
Special Issue 28: Electric Networks and Smart Cities
january/june 2022

John Calle Sigüencia, Editor in chief
revistaingenius@ups.edu.ec

Thematic Editors

Sandro César Silveira Jucá, PhD
Sandra Céspedes, PhD
Esteban Inga Ortega, PhD

Printed

Centro Gráfico Salesiano: Antonio Vega Muñoz 10-68 y General Torres.
Phone: (+593 7) 283 17 45
Cuenca – Ecuador
Email: centrograficosalesiano@lms.com.ec

OTHER PERIODIC PUBLICATIONS OF THE UNIVERSITY
UNIVERSITAS, Journal of Social and Human Sciences.

LA GRANJA, Journal of Life Sciences.

ALTERIDAD, Journal of Education.

RETOS Journal of Administration Sciences and Economics.

UTOPÍA, University Youth Ministry Magazine.

SOPHIA, Collection of Philosophy of Education.



ABYALA | UNIVERSIDAD
POLITÉCNICA
SALESIANA

